The Gemmological Association of Great Britain

The Journal of Gemmology

Mexican jadeite-bearing rock: a first mineralogical and gemmological approach

Mikhail Ostrooumov and Alfredo Victoria Morales

Abstract: Jadeite-bearing pebbles have been found in secondary deposits overlying Cretaceous sediments in the Vizcaino Peninsula, Sierra San Andres, Baja California Sur, Mexico, the first in the country. These pebbles are probably derived from a blueschist assemblage associated with a serpentinite-matrix mélange complex about 2 km north of Puerto Nuevo. Jadeite is accompanied by omphacite and aegirine, and different associated minerals enable distinction from Californian and Guatemalan jadeites.

Keywords: EPMA, infrared spectra, jadeite, Mexico, Raman spectra, SEM, XRD

Introduction

Jadeite is a well-known but uncommon mineral that is found in rocks associated with fragmental serpentinites. Described occurrences are limited to about a dozen worldwide (Harlow and Sorensen, 2005). Among the few occurrences of jadeite, only two are described from the Americas. The major deposits in serpentinite bodies along the central Motagua Valley in Guatemala served as the source of carved jade for Middle America (Bishop *et al.,* 1993; Breuckner *et al.,* 2005). The minor but well-described occurrence along Clear Creek, New Idria serpentinite, in San Benito County, California (Coleman, 1961) does not appear to have been used as a cultural source of jadeite.

Jadeite rocks from other parts of California have been reported in lapidary literature (Foshag and Leslie, 1955; Foshag, 1957; Castro and Castro, 1979; Pashin, 1995) but observations by Harlow *et al.* (2006) find them to be selvages of

Figure 1: Jadeite-bearing pebble from Baja California Sur State, Mexico.

jadeite-aegirine combined with a variety of other minerals and generally dissimilar to jadeite-rich rocks used for carving.

Panczner (1989) reported the presence of jadeite from Mexico in the state of Guerrero, municipalities of Arcelia and Texco, and in the state of Mexico, municipality of Tejupilco, without any mineralogical analysis, but more recent fieldwork has not confirmed the presence of jadeite in these geological settings (Keeman, 1999). The present authors have not found a description of any

confirmed Mexican jadeite in geological, mineralogical and gemmological literature.

In 2007, Eng. Jorge Diaz de Leon (Mineral Technology Company) presented to the Mexican Mineralogical Society some green rocks which had been found in the Vizcaino peninsula, Baja California Sur, Mexico. Using non-destructive infrared reflection spectrometry we established that these samples (see *Figure 1*) contain jadeite (Ostrooumov, 2007), so this is the first confirmed occurrence of jadeite in Mexico. The purpose of the present work is to characterize the mineralogical and chemical composition, spectroscopic parameters and gemmological characteristics of these jadeite-bearing rocks.

Location

The Vizcaino peninsula is a mountainous region located on the western side of Baja California. The peninsula is underlain by Triassic ophiolite, Jurassic island-arc rocks,

Mexican jadeite-bearing rock: a first mineralogical and gemmological approach
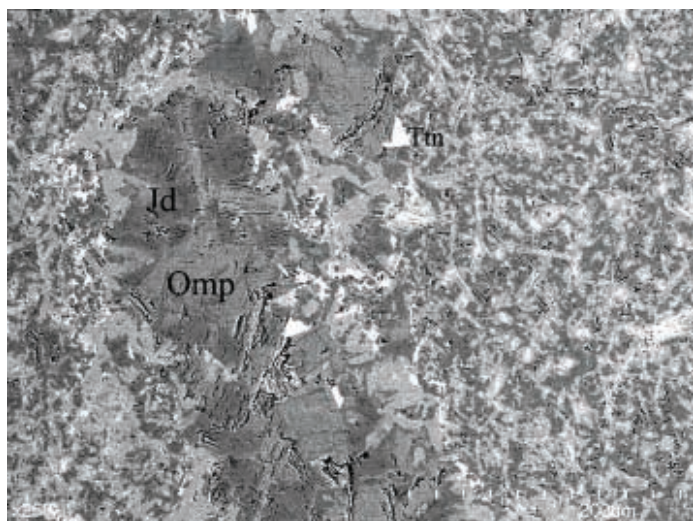

Figure 2: Back scattered electron (BSE) image of jadeite-bearing rock showing larger crystals of jadeite (Jd) and omphacite (Omp) in a finer-grained matrix which contains the same pyroxenes and some titanite (Ttn).

Mesozoic blueschist and Cretaceous submarine-fan deposits (Barnes and Mattison, 1981), overlain by a secondary deposit in which jadeite-bearing pebbles were discovered near 27°31' 40" N, 114°43' 39" W. The jadeite-bearing fragments range from a few cm to as large as 30 cm across. In our opinion, these pebbles were formed by abrasion and transportation of primary metamorphic rocks from their source in the blueschist-bearing serpentinite mélange at Puerto Nuevo. This mélange complex has been described in detail by Moore (1986).

Experimental and technical background

From a range of the green jadeite-bearing rocks three were collected for analysis. They were ground to produce flat surfaces and polished with diamond and alumina abrasives. The polished samples were microscopically imaged using a Hitachi S-4700 Field Emission-Scanning Electron Microscope (SEM) with a back-scattered electron (BSE) detector and PGT-Imix energy-dispersive X-ray spectrometric (EDS) analyser. Electron-microprobe analysis of these samples to determine concentrations of the major constituent elements in the minerals (except O) was carried out using a Cameca SX100 instrument operating at 15 kV and 10 nA sample current, employing a point beam. X-ray diffraction (XRD) analyses were obtained using a Brüker AXS-D8 Advanced diffractometer and a Brüker D8 Discover diffractometer with General Area Detector Diffraction System V4.1.27 (GADDS), both instruments with Cu-Kα monochromatic radiation.

In this study, three polished sections were examined with Raman microprobe (RMP). Their Raman spectra were recorded using the λL=514.5 nm line of an Ar+ laser with a Jobin-Yvon T64000 spectrometer equipped with a multichannel charge-coupled device (CCD) detector cooled at 77K. The samples were analyzed under an Olympus microscope with 50× and 100× objectives giving 2 μm spatial resolution. Infrared spectra were collected using a Tensor 27 FTIR spectrometer (Brüker) with a Hyperion microscope and Variable Angle Specular Reflectance Accesory (VeeMaxII, PIKE Technologies), accumulating 100 scans at a resolution of 4 cm⁻¹. The UV-Visible-NIR absorption spectra were recorded from 200 to 2500 nm using a Perkin-Elmer LAMBDA 900 microspectrometer operating at 1 nm resolution. Regions of 100 μm in diameter with homogeneous colour and nearly free of inclusions were chosen for spectroscopic measurements.

Results and discussion

Mineralogical and chemical composition

The main mineral phases in the Mexican jadeite assemblages are jadeite (pale green), omphacite (dark green), aegirine (green to black) and albite *(Figure 2)*. Also visible under the microscope is a network of very small prisms overgrown by a matrix of impure jadeite. There are sporadic grains of colourless titanite and analcime which are surrounded by overgrowths on omphacite prisms. Some less common minerals present are zoisite, allanite and celsian *(Table I)*.

This mineralogical assemblage differs from that of jadeite rock from Guatemala which commonly contains quartz, white-brown mica (phengitic muscovite, paragonite, phologopite and preiswerkite), amphibole (actinolite, taramite) and some typical accessory minerals (titanite, rutile, zircon, apatite and chlorite), and also from the jadeitites of the New Idria serpentinite (San Benito County, California) which contain quartz, lawsonite and zircon.

Fifty-five pyroxene analyses were obtained and typical compositions are shown in *Table II*; the molecular percentages of end-members jadeite (Jd), diopside (Di, $CaMgSi_2O_6$), hedenbergite (Hd, $CaFe^{2+}Si_2O_6$), aegirine (Ac, $NaFe^{3+}Si_2O_6$), enstatite (En, $Mg_2Si_2O_6$) and ferrosilite (Fs, $Fe_2Si_2O_6$) were then calculated from them. The compositions range from Jd100 to omphacite, nominally Jd50[Di+Hd]50 but could reach as low as Jd40[Di+Hd]60. The aegirine component typically increases with omphacite content. When plotted on the ternary diagram Jadeite–(Diopside + Hedenbergite)–Aegirine *(Figure 3)*, the 55 analyses show extensive isomorphic substitution. All analysed grains of the jadeites contain iron in ferric and ferrous states. At the same time, only five analyses showed traces of Cr. Thus, the Mexican jadeites typically contain little or no chromium.

Although the rocks resemble jadeitites, the order of crystallization of pyroxene shows a trend in composition from jadeite to omphacite to aegirine. There appeared

Mexican jadeite-bearing rock: a first mineralogical and gemmological approach

Table I: Minerals accompanying jadeite in jadeitites from Mexico, California, U.S.A., and Guatemala.

Location	Mexico	California	Guatemala
Mineral			
Omphacite	•	•	•
aegirine	•		
albite	•	•	•
white mica			•
quartz		•	•
analcime	•		•
amphibole		•	•
zoisite			•
lawsonite		•	•
rutile			•
titanite	•	•	•
zircon		•	•
other	allanite celsian	diopside pectolite pumpellyite vermiculite	diopside augite chlorite banalsite nepheline apatite chlorite cymrite hyalophane graphite glaucophane

Table II: Representative compositions of pyroxenes in Baja California Sur jadeite-bearing rocks.

Oxides (wt. %)	Jadeite OM117	Omphacite OM104	Aegirine OM143
SiO_2	54.77	58.85	54.52
TiO_2	0.20	0.11	0.90
Al_2O_3	21.63	6.22	4.78
Cr_2O_3	0.00	0.00	0.06
Fe_2O_3	2.53	5.66	24.72
FeO	0.00	5.43	0.62
MgO	0.87	6.87	1.33
CaO	1.29	13.82	2.85
MnO	0.03	0.81	0.12
BaO	0.03	0.00	0.01
Na_2O	14.83	6.27	12.44
K_2O	0.01	0.01	0.00
Total	99.64	99.71	101.05
Cation numbers based on 6 O			
Si	1.997	2.008	1.972
Al^{iv}	0.003	0.000	0.027
Sum	2.000	2.008	2.000
Ti	0.005	0.003	0.025
Al	0.871	0.270	0.180
Cr	0.000	0.000	0.002
Fe^{3+}	0.065	0.157	0.689
Fe^{2+}	0.000	0.167	0.019
Mg	0.044	0.377	0.074
Ca	0.047	0.545	0.113
Mn	0.001	0.025	0.004
Na	0.986	0.448	0.894
K	0.000	0.000	0.000
Ba	0.000	0.000	0.000
Sum	4.021	4.000	4.000

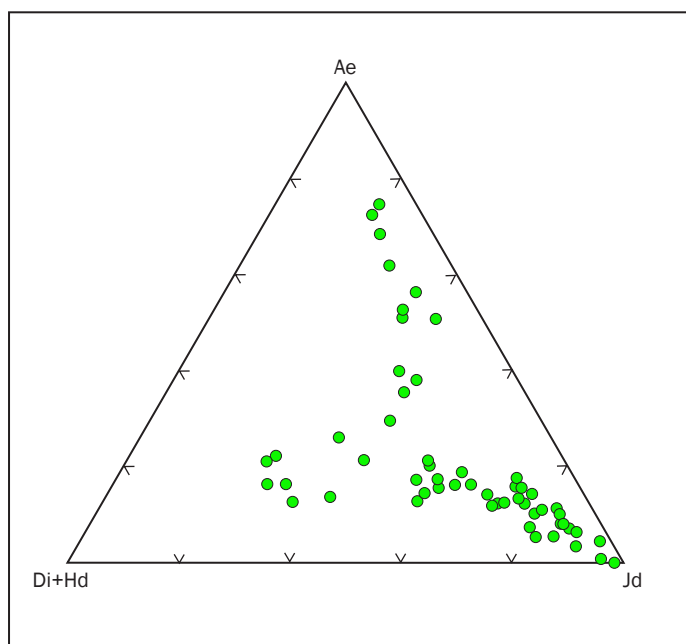

Figure 3: Individual microprobe analyses of pyroxene from jadeite-bearing rocks from Baja California Sur, Mexico, plotted as molecular proportions of diopside + hedenbergite (Di+Hd), aegirine (Ae) and jadeite (Jd) on a ternary diagram. The omphacite analyses lie in the region between jadeite and diopside + hedenbergite, and there appears to be continuous variation between these end-members.

Mexican jadeite-bearing rock: a first mineralogical and gemmological approach

Table III: Raman spectra (wavenumbers, cm^{-1}) of jadeite, omphacite and aegirine from Mexico compared with jadeite from the Urals.

Jadeite from Ural deposit (Ostrooumov, 1986)	Jadeite Jd$_{96}$[Di+Hd]$_4$	Omphacite Jd$_{50}$[Di+Hd]$_{40}$Ae$_{10}$	Aegirine Ae$_{75}$Jd$_{19}$[Di+Hd]$_6$	Assignments (Lazarev, 1995)
1038 m	1041 s	1035 s	1041 m	Si-O str (bridged)
987 m	994 m	979 m	969 s	Si-O str (non-bridged)
699 vs	701 vs	692 vs	678 vs	sym Si-O-Si str
575 m	578 w	558 w	546 m	O-Si-O def
525 m	525 w	518 w	498 w	O-Si-O def
432 m	435 w	435 w	433 vw	O-Si-O def
374 s	376 vs	368 vs	344 s	Al-O str/O-Si-O def
327 m	329 w	322 w	328 w	Al-O str/O-Si-O def
309 m	311 m	307 w	300 w	Al-O str/O-Si-O def
292 w	294 w	282 vw	280 vw	external mode
255 m	257 w	252 vw	250 vw	external mode
223 w	224 w	218 vw	208 w	external mode
204 s	205 w	201 m	183 w	external mode

N.B.: Relative intensities are denoted by: s=strong, m=medium, w=weak, v=very, sh = shoulder; assignments: str =stretch, def=deformation, sym = symmetric.

to be no compositional gaps in this trend, but unfortunately the grain size was generally too small to test whether this continuity was real (*Figure 3*). This zoning trend, exclusive of inclusions in jadeite, has not been recorded from any other jadeite worldwide (Harlow *et al.,* 2006).

In the Mexican jadeite rock X-ray diffraction provides the possibility of precisely determining which pyroxenes are present by means of their d-spacing and intensities of some diffraction peaks. Some early X-ray investigations (Ostrooumov, 1986) have shown that omphacite and aegirine differ from jadeite in having larger d$_{221}$ and d$_{331}$ values and higher ratios of the intensities of these peaks. In this study X-ray diffraction investigations showed that the pale green crystals are pure jadeite with d$_{221}$=2.921–2.95 Å and d$_{331}$=2.817–2.831 Å. The d$_{221}$/d$_{331}$ intensity ratio is 0.81. The diffractogram of dark green pyroxene (omphacite) was distinguished by increases in d values: d$_{221}$=2.931–2.982 Å and d$_{331}$=2.843–2.899 Å; and the ratio of intensities of these peaks increased to 0.96–1.80. The jadeite also has d$_{110}$=6.22–6.23 Å whereas in omphacite, d$_{110}$ is higher at 6.344 Å. The black green pyroxene is characterized by a series of reflections at 3.162, 2.462 and 2.102 Å which confirmed that it is aegirine and thus three different pyroxene species (jadeite, omphacite and aegirine) are present in this rock.

Spectroscopy and gemmological characteristics

The Raman spectrum of a jadeite jade sample from Mexico has been recorded in the wavenumber range 100–1500 cm^{-1}, and shows a very strong band at 700 cm^{-1}, two strong bands of high frequencies near 1000 cm^{-1} (990 and 1040 cm^{-1}), and two bands of low frequencies (376 and 205 cm^{-1}) which are characteristic of jadeite (*Figure 4a*). Omphacite and aegirine show different Raman spectra (see *Table III* for comparisons).

In recent years, Infrared Reflection Spectrometry (IRS) has been widely used (Ostrooumov, 2007) to identify the different monoclinic pyroxenes. The spectra obtained by this technique can be measured from any surface with an area of 0.01–1 mm^2 and the Mexican jadeites did not require special preparation or removal from their matrix. The infrared reflection spectra of jadeite are characterized by typical bands at 1165, 1083 and 954 cm^{-1} (*Figure 4b*) and these are listed with the corresponding bands of omphacite and aegirine in *Table IV*.

Table IV: Infrared reflection spectra (wavenumbers, cm^{-1}) of jadeite, omphacite and aegirine from Mexico.

Jadeite Jd$_{96}$[Di+Hd]$_4$	Omphacite Jd$_{50}$[Di+Hd]$_{40}$Ae$_{10}$	Aegirine Ae$_{75}$Jd$_{19}$[Di+Hd]$_6$	Assignments (Ostrooumov, 2007)
1165 sh	1156 sh	1134 sh	Si-O str (bridged)
1083 vvs	1068 vvs	1062 vvs	Si-O str (bridged)
954 vs	940 vs	955 s	Si-O str (non-bridged)
926 w	912 w	905 s	Si-O str (non-bridged)
852 w	847 w	774 vw	Si-O str (non-bridged)
742 vw	741 vw	660 vw	asym Si-O-Si str
585 s	574 m	522 s	O-Al str
530 s	514 s	480 sh	O-Si-O def
468 s	460 s	454 s	O-Si-O def
433 m	420 vw	415 sh	-

N.B.: Relative intensities are denoted by: s = strong, m = medium, w = weak, v = very, sh = shoulder; assignments: str = stretch, def = deformation, sym = symmetric.

Mexican jadeite-bearing rock: a first mineralogical and gemmological approach

In and near the visible range, the spectrum of green jadeite consists of absorption bands at 370, 382, 430, 437, 540, 575, 600, 830, 880 and 1170 nm. According to Langer *et al.* (1995), UV-visible-near infrared spectroscopy showed some absorption features that are related to Fe^{3+} or Fe^{2+} or to both valencies. The correlated set of bands consisting of those at 370, 382, 430, 437, 540, 600 and 830 nm show a pattern close to that characteristic of a d^5 trivalent ion in octahedral oxygen coordination. Our EPMA analyses of jadeite generally indicate the presence of some divalent iron. Spectra of ortho- and clinopyroxenes have absorption bands in the 900–1000 nm and 1150–1250 nm ranges which are assigned to Fe^{2+}, and corresponding absorption features are observed in the jadeite spectra at about 880 and 1170 nm. The simultaneous presence of both Fe^{3+} and Fe^{2+} means that intervalence charge transfer is possible and in accordance with Burns (1970), the 575 nm band is assigned to an $Fe^{2+} \rightarrow Fe^{3+}$ intervalence charge-transfer band. The typical absorption bands of Cr^{3+} in the visible region between 630 and 690 nm are absent, which is consistent with the EPMA results.

Some idea of the colour range of the Mexican jadeite rock can be obtained using the International Commission of Illumination (ICI) colour measuring system, which is based on the physiological perception of colour. This system has been found useful for describing the colour characteristics of minerals and gems (Ostrooumov, 1987 a,b; Langer *et al.,* 1995) where the colour is specified by three characteristics: (a) hue (nuance) or dominant wavelength - λ, (b) chroma, or saturation - P%, and (c) lightness - Y%.

Preliminary colorimetric calculations show that the colours of Mexican jadeite have very low saturation (P=7%) and lightness (Y=15%). Therefore they are characterized by darker colours in comparison with pure green jadeite from other deposits. The dominant wavelength of Mexican jadeite (λ=543) is a slightly yellowish green. However, this combination of colorimetric parameters

defines a colour which differs from that of chromium-bearing jadeites. To take one example, measurements on the jadeites from the Polyarniy Ural (Russia) deposits yielded colorimetric parameters showing higher values of saturation (P=18-20) and lightness (Y=20-34%) and a purer green hue with λ=518-528 nm (Ostrooumov, 1986). These jadeites consequently have more attraction for the gem trade.

The following properties were determined from three samples of rough jadeite-bearing rocks in the 1–2 cm size range:

Figure 4: Raman (a) and infrared reflection (b) spectra of jadeite sample from Mexico.

colour	green
pleochroism	weak to moderate
RI	α = 1.654–1.668 β =1.643–1.645 γ =1.640–1.652
birefringence	0.012–0.020
hydrostatic SG	3.23–3.52
fluorescence	pale-green under long-wave and white or inert under short-wave UV radiation

Mexican jadeite-bearing rock: a first mineralogical and gemmological approach

Conclusion

X-ray diffraction, and chemical, spectrometric and scanning electron microscopy examinations confirmed the discovery of jadeite in the Sierra de San Andres, Baja California Sur, in northwestern Mexico. The material contains a possible blue schist assemblage and may be worthy of further study as a jadeite variant. The Sierra de San Andres jadeite rocks differ from those in California and from the Guatemalan jadeites in their associated minerals and can be distinguished on this basis. The jadeite discovery could represent an interesting mineralogical and gemmological opportunity and although the full range and economic potential of this jadeite has not been determined, it may well have features that distinguish it from other important jadeite deposits in the world.

Acknowledgements

References

Barnes, D., and Mattison, J.M., 1981. Late Triassic-Early Cretaceous age of eugeoclinal terranes, western Vizcaino Peninsula, Baja California Sur, Mexico. *Geological Society of America. Abstracts with Programs,* **13**, 43

Bishop, R.L., Sayre, E.V., and Mishara, J., 1993. Compositional and structural characterization of Maya and Costa Rica jadeitites. Chap. 2 in: F.W. Lange (Ed.), *Precolumbian Jade: New Geological and Cultural Interpretations,* 30–60. University of Utah Press, Salt Lake City, Utah

Breuckner, H.K., Harlow, G.E., and Chiquin, M., 2005. Two jadeitite belts in the Motagua Valley Fault Zone, Guatemala: Two subduction events or one subduction event with retrogression? *Geol. Soc. Am. Abstr. Program, Annual Meeting,* **37**, 67

Burns, R.G., 1970. *Mineralogical Application of Crystal Field Theory.* Cambridge University Press, Cambridge

Castro, K., and Castro, D., 1979. Jade in Central America. *Gems & Minerals,* **500**, 11–12, 32–6

Coleman, R.G., 1961. Jadeite deposits of the Clear Creek area, New Idria district, San Benito County, California. *Jour. Petrol., 2*, 209–47

Foshag, W.F., 1957. Mineralogical studies on Guatemalan jade. *Smithsonian Miscellaneous Collections,* **135**(5), 60

Foshag, W.F., and Leslie R., 1955. Jadeite from Manzanal, Guatemala. *Am. Antiquity,* **21**, 81–3

Harlow, G.E., Murphy, A.R., Hozjan, D. J., De Mille, C.N., and Levinson, A.A., 2006. Pre-Columbian jadeite axes from Antigua, West Indies: description and possible sources. *Canadian Mineralogist,* **44**(2), 305–21

Harlow, G.E., and Sorensen, S.S., 2005. Jade (nephrite and jadeitite) and serpentinite: Metasomatic connections. *Int. Geol. Rev.,* **47**, 113–46

Keeman, F., 1999. *Geological-Mining Monograph of the State of Guerrero.* Mexican Geological Survey, Mexico.

Langer, K., Platonov, A., and Rossman, G., 1995. Optical Absorption Spectroscopy. Chap. 3.3 in: Marfunin A. (Ed.), *Advanced Mineralogy,* Vol. 2, 109–23. Springer-Verlag, Berlin

Lazarev, A., 1995. *Vibrational spectra and structure of silicates.* Science, Moscow

Moore, T.E., 1986. Petrology and tectonic implications of the blueschist-bearing Puerto-Nuevo mélange complex. Vizcaino Peninsula, Baja California Sur, Mexico. *Bull. Geological Society of America,* **164**, 43–58

Ostrooumov, M., 1986. Spectrometric and crystal chemical investigations of the jadeite from Polyarniy Ural and Kazakhstan deposits. In: Yushkin, N. (Ed.), *Problems of the Ural Mineralogy,* 97–8. Science, Sverdlovsk

Ostrooumov, M., 1987a. Colorimetry of minerals. *Nature, Moscow,* **6**, 43–53 (in Russian)

Ostrooumov, M., 1987b. Colorimetry of the amazonite. *Proceedings of the URSS Mineralogical Society,* **1**, 77–84 (in Russian)

Ostrooumov, M., 2007. *Espectrometría infrarroja de reflexión en Mineralogía Avanzada, Gemología y Arqueometría.* UNAM, Mexico City, Mexico

Panczner, A., 1987. *Minerals of Mexico.* Van Nostrand Reinhold Company, New York

Pashin, A., 1995. The great California jade loop. *Rock & Gem,* **25**(12), 44–5

The Authors

Mikhail Ostrooumov
Metallurgical Institute, Mineralogical Department, University of Michoacan, B.P. 888, C.P. 58000, Morelia, Michoacan, Mexico
Fax: +52 443 322 35 00 ext.4031
Corresponding author: e-mail ostroum@umich.mx

Alfredo Victoria Morales
Department of Earth Sciences, Engineering Faculty, National University of Mexico

New data for distinguishing between hydrothermal synthetic, flux synthetic and natural corundum

Alexei S. Bidny, Olga S. Dolgova, Ivan A. Baksheev and Irina A. Ekimenkova

Abstract: Although the synthesis of coloured corundum became widespread long ago, it may still be difficult to distinguish some natural and synthetic specimens especially if no inclusions are visible. The analysis of oxygen isotopic composition in combination with standard gemmological measurements (especially UV spectroscopy) can prove very useful in the identification of hydrothermal synthetic and flux synthetic corundums and in distinguishing them from natural stones. The indicator of flux synthesis is the presence of a 290 nm line in the photoluminescence spectrum and hydrothermal synthetic corundums contain negative $\delta^{18}O$ values.

Keywords: corundum, EDXRF, isotope analysis, spectroscopy, synthetic corundum

Introduction

Along with diamond and emerald, gem-quality corundum (particularly ruby) commands the highest prices in the world market. Therefore finding criteria to distinguish gem-quality natural stones from synthetics is important. On the other hand, the market price of natural stones can be influenced by their geographical source and genetic type of deposit. For instance, in the early years of the last century, the best quality sapphires from lamprophyre of the Yogo Dike, Montana, U.S.A., were compared with 'Kashmir blue' sapphires, because the price of the latter was much higher (Allen, 1991). The same is true for vivid blue Sri Lankan sapphires, called 'Kashmir blue', although their prices are generally lower than Burmese 'Kashmir blue' sapphires.

The synthesis of coloured corundum became widespread on commercial production of Verneuil boules in the early twentieth century. The most common growth techniques today are Verneuil flame fusion, Czochralski pulling, flux and hydrothermal growth. Each of these methods may be used to grow large crystals of synthetic corundum in various colours, making them readily available and relatively inexpensive for the jewellery industry.

The key diagnostic feature of Verneuil synthetic corundum is the curved growth lines, best seen in dark-field illumination in pale to colourless stones or in bright-field illumination in strongly coloured stones. These lines reflect changes in growth rate, and result from minute differences in distribution of colouring agents and strain between adjacent layers. Locating curved growth lines in cut stones may present difficulties, especially with pale-coloured specimens, or with the yellow, orange and pale red (pink) varieties unless shadowing and polarization techniques are applied.

Czochralski-grown synthetic stones appear similar to Verneuil products. Careful examination reveals features allowing positive distinction from both natural corundum and Verneuil synthetics: gas bubbles, faint curved growth lines and roughly parallel rows of minute particles of unknown identity which resemble the rain-like flux inclusions found in Kashan flux rubies (Hughes, 1997). Overall, however, they are more difficult to recognize than flame fusion stones due to a generally more continuous (i.e. better controlled) growth process.

Flux and hydrothermal synthetics are relatively expensive compared to the products described above. This explains why they are not so widespread in the

New data for distinguishing between hydrothermal synthetic, flux synthetic and natural corundum

Table I: Characteristics and oxygen isotope compositions of studied samples.

Origin	Sample No.	Colour	Shape	Weight (ct)	$\delta^{18}O‰$ (SMOW)
syenitic pegmatite, Umba Valley, Tanzania	1	red	round brilliant	0.43	n/a*
	2	bluish-green	round brilliant	0.58	+9.1
syenitic pegmatite, Madagascar	3	red	rough	0.84	n/a
	4	red	rough	0.48	n/a
	5	red	rough	0.26	n/a
	6	blue	rough	2.45	+6.3
syenitic pegmatite, Potanin Mts, South Urals	7	bluish-grey	rough	1.68	n/a
syenitic pegmatite, Ilmen Mts, South Urals	8	greyish-blue	rough	1.20	+8.8
contact-metamorphic, Koltashi, Middle Urals	9	grey	rough	2.02	n/a
skarn, Pamir	10	pinkish-red	rough	8.36	+8.4
metasomatized gneiss, Khitostrovskoye, Karelia	11	purplish-red	rough	19.28	−14.7
	12	purplish-red	rough	15.34	−11.3
metasomatic margarite veinlets, Emerald mines, Middle Urals	13	blue	rough	4.31	+2.0
metasomatized gabbro, Rai-Iz, Polar Urals	14	red	rough	0.64	+3.1
metamorphic, West Keivs, Kol'skii peninsula	15	bluish-grey	rough	3.39	n/a
metamorphic, Svintsoviy stream, Khybini	16	blue	rough	0.98	n/a
'hydrothermal' breccia, Alabashka, Middle Urals	17	red	rough	1.20	+9.1
hydrothermal, Semizbugu, Kazakhstan	18	light blue	rough	0.86	n/a
skarn, Luc Yen, North Vietnam	19	red	rough	10.34	n/a
flux synthesis, CGL**	20	red	rough	0.43	+7.9
	21	pink	rough	0.35	n/a
flux synthesis, Kashan	22	red	rough	13.38	+4.8
flux synthesis, Ramaura	23	red	rough	14.66	+14.8
flux synthesis, Balitsky	24	dark red	rough	8.15	n/a
	25	dark red	rough	1.40	n/a
hydrothermal synthesis, Balitsky	26	light blue	rough	23.94	n/a
	27	black	rough	18.06	n/a
	28	brown	rough	10.71	n/a
	29	zonal: green on the edge, blue in the centre	rough	9.19	−5.0
	30	greenish-grey	rough	18.98	−0.7
	31	greyish-blue	rough	19.26	n/a
	32	grey	rough	26.06	−3.6
	33	red	rough	7.50	−1.3
	34	blue	rough	3.15	−5.8
	35	red	rough	6.32	−2.1
Summary of results from Giuliani *et al.* (2005)					
flux					+7.5 ... +18.5
Verneuil					+24.4
natural					+4.2 ... +22.7

* Not available

**Crystal Growth Laboratory, Division of Crystallography and Crystallochemistry, Lomonosov Moscow University, Moscow, Russia

New data for distinguishing between hydrothermal synthetic, flux synthetic and natural corundum

jewellery market and their distinctive features have not been completely described.

The problem of separating synthetic and natural corundum is not really very challenging for a laboratory with modern testing methods such as microscopy, FTIR, UV-Vis and EDXRF spectrometry. However, experience in the identification of natural and synthetic corundum indicates that standard gemmological techniques occasionally may not be sufficient to distinguish for certain between natural, flux-grown and hydrothermally grown stones.

Here we consider two additional techniques, excitation spectroscopy and oxygen isotope analysis, to see whether these could contribute to the reliability of the testing procedure. In addition, isotopic study can help in the recognition of the genetic type of the source deposit of a corundum and occasionally in its geographical location.

Oxygen isotope contents in rubies and sapphires from 106 deposits worldwide were published by Giuliani *et al.* (2005), but the study contained no data on corundum from Russian deposits. Isotope data on some flux synthetic corundums were published by Polyakov and Ustinov (1997), but data for hydrothermal synthetic corundum have not been found.

Results and discussion

Microscopic observation of corundum is especially useful when a stone contains foreign inclusions, inhomogeneous coloration or visible growth and strain features. Inclusions in corundums of different genesis are shown in *Figure 2*. While inclusions of minerals are indicators of natural genesis *(Figure 2a)*, flux and platinum or iridium particles indicate flux-grown stones *(Figure 2b)*. The distinctive feature of hydrothermal synthetic corundum is the presence of parallel undulating growth structures within the stone *(Figure 2c)*.

EDXRF data were obtained for 14 natural corundums from different deposits *(Figure 3a)*, five flux synthetic samples and five hydrothermal synthetic samples *(Figure 3b)*. The results show that

Materials and methods

In this study we have used hydrothermal and flux synthetics and natural corundum from Russian deposits *(Figure 1)* in addition to natural corundums from Madagascar, Tanzania and Vietnam.

Thirty-five rough and cut samples of natural corundum from the deposits mentioned above, synthetic corundum grown by the flux method in the laboratories of Ramaura, Kashan, Balitsky and Lomonosov Moscow University (Moscow, Russia), and synthetics grown by the hydrothermal method in the laboratory of Balitsky (IEM, RAS, Chernogolovka, Russia), were studied using optical microscopy, spectroscopic techniques (IR, UV-absorption and photoluminescence analysis) and oxygen isotope analysis. Every specimen was prepared as a transparent slice with two parallel faces parallel to the *c*-axis.

The studied stones are red, blue, grey, green, pink, black and brown, and range in weight from 0.26 to 26.06 ct *(Table I)*. As natural red corundum is the most expensive variety, UV-absorption and photoluminescence data were obtained especially for them, as well as for some sapphires of other colours.

EDXRF analysis was carried out with a Camebax SX50 microanalyser using an accelerating voltage of 15 kV and current of 40 nA.

IR and UV spectra were recorded with a Fourier transform infrared spectrometer FSM 1201 and a UV spectrophotometer Lomo SFL-1 with xenon emission lamp respectively (both at room temperature), in the Gem Research Laboratory of Lomonosov Moscow State University. The wavenumber range of FTIR spectra was 400–4000 cm^{-1} with a resolution of 1 cm^{-1}; for UV spectra the wavelength range was 200–400 nm with a resolution of 0.1 nm.

Oxygen isotope compositions were measured on a mass-spectrometer MAT-250 in GEOCHI RAS, Moscow, Russia. The measuring procedure is standard and described by Faure (1986). Small samples are ground into powder to prepare solutions; to avoid contamination of oxygen values by included phases, microsamples are taken locally from pure corundum areas. After measuring the oxygen isotopes, δ values were calculated as described by Hoefs (1997).
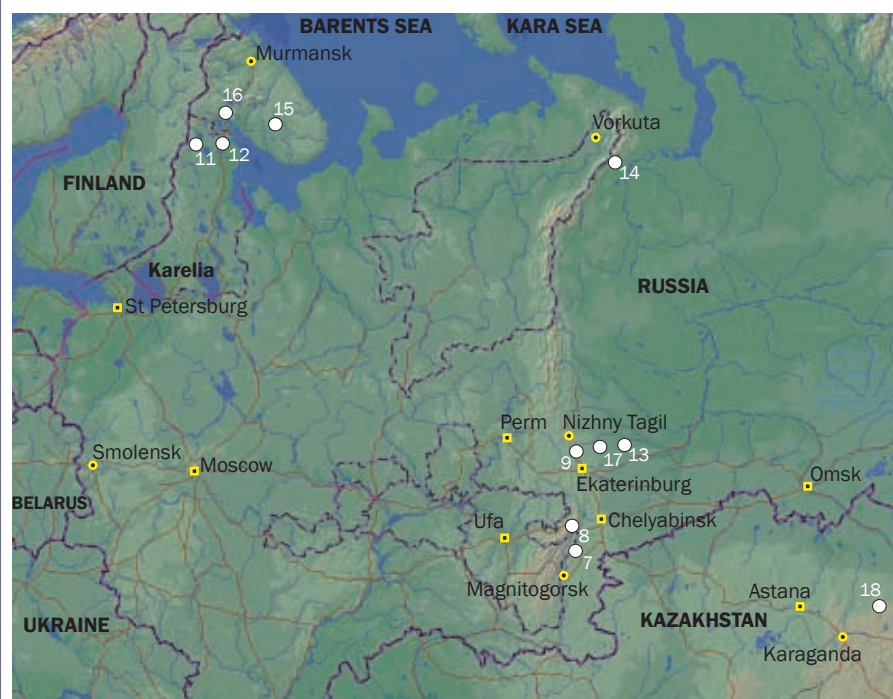

Figure 1: Russian localities of corundum. The numbers correspond to those listed in Table I.

New data for distinguishing between hydrothermal synthetic, flux synthetic and natural corundum
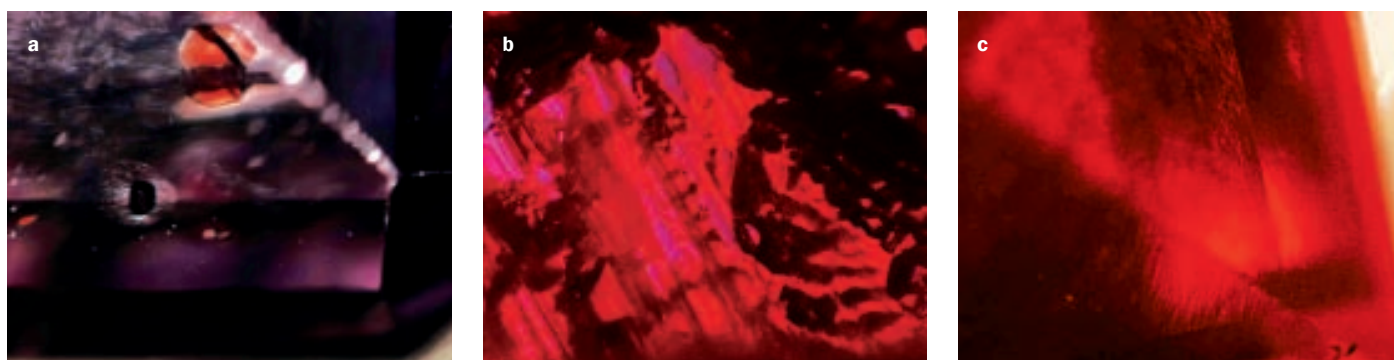

Figure 2: Inclusions in corundums of different genesis: (a) mineral inclusion (possibly rutile) in natural sample No. 1; (b) flux inclusions in flux-grown corundum sample No. 20; and (c) parallel undulating growth features in hydrothermal synthetic-grown corundum (sample 32, partially faceted).

there are three main impurity elements in corundums: chromium, iron and gallium. Their proportions are different in samples from different deposits due to various fluid and host rock compositions. So these proportions can be used to indicate a locality or growth laboratory. The diagrams in *Figure 3* show two genetic groups of natural sapphires: from deposits with syenitic pegmatite (Ilmen and Potanin Mountains, South Urals; Madagascar; Umba Valley, Tanzania) and desilicated and hydrothermal rocks (West Keivs, Kol'skii peninsula; Svintsoviy stream, Khybini; Koltashi, Middle Urals; Emerald mines, Middle Urals). The former appear to have high proportions of iron and low proportions of gallium, while the latter contain less iron and more gallium. The diagram of synthetic specimens shows no distinctive features for hydrothermal synthetics, but low proportions of iron in flux specimens is notable.

The FTIR spectra of the hydrothermal synthetic samples showed relatively strong absorption bands related to OH-complexes in the 3600–3100 cm^{-1} region:
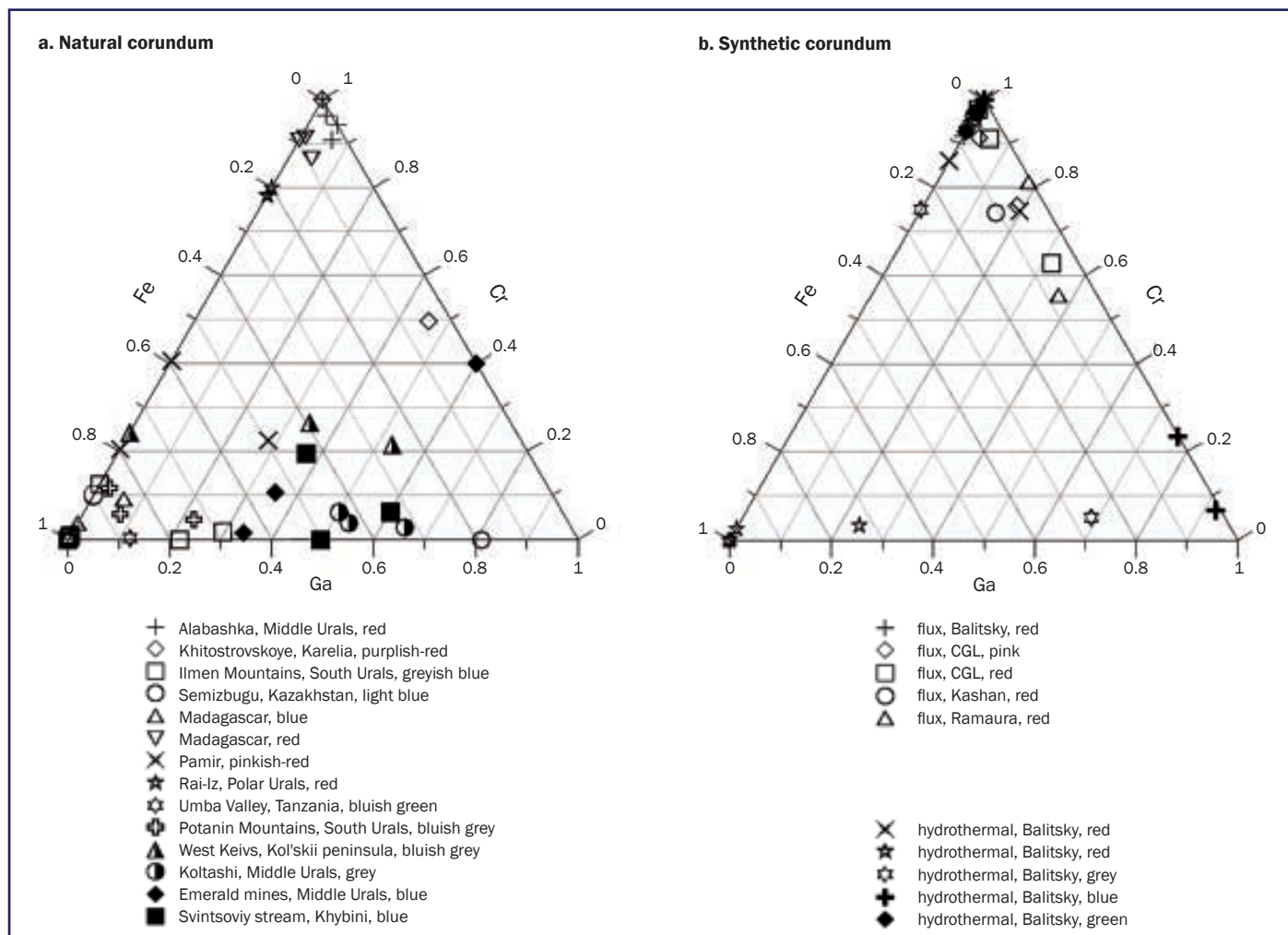

Figure 3: Cr, Ga and Fe proportions in weight percent in (a) natural corundum and (b) synthetic corundum, analysed in this study. See Table I for descriptions of the samples.

New data for distinguishing between hydrothermal synthetic, flux synthetic and natural corundum

3193, 3209, 3233, 3262, 3289, 3304, 3384, 3484, 3564 and 3586 cm^{-1} (Figure 4). The 'water' bands were much less evident in the spectra of the natural stones. In spite of the fact that hydrous components and water in infrared spectra of natural corundum vary greatly from sample to sample and depend on OH incorporated in the corundum structure, hydrous natural inclusions and healed fissures, they are distinctly different in pattern from the spectra of hydrothermal synthetics. The flux synthesis uses pure Al_2O_3 with minor added metals but not water and so 'water' bands are absent from FTIR spectra of flux synthetic corundum.

To distinguish between natural and flux rubies their photoluminescence and UV absorption spectra were studied. The excitation spectra of red chromium photoluminescence (which generates an emission line at 693 nm) showed a series of broad bands with maxima at 380, 390, 450 and 500 nm in all samples. Also there was an excitation band centred at 290 nm that was seen in spectra of synthetic rubies only, with both high and low contents of iron (Figure 5, left). The band at 290 nm is caused by an electron transition due to F$^+$ complexes (anion vacancies with one electron) found in pure single crystals of synthetic corundum (α-Al_2O_3) grown by the Verneuil

method and by the method of directed crystallization (Syurdo et al., 1998). The emission region for the 290 nm excitation in our case lies between 490 and 380 nm, and so may excite red chromium fluorescence.

Distinctive features were revealed in the UV absorption spectra of the investigated stones. In addition to common chromium and iron absorptions, there is a band at 342 nm in the spectra of the flux rubies (Figure 5, right). The
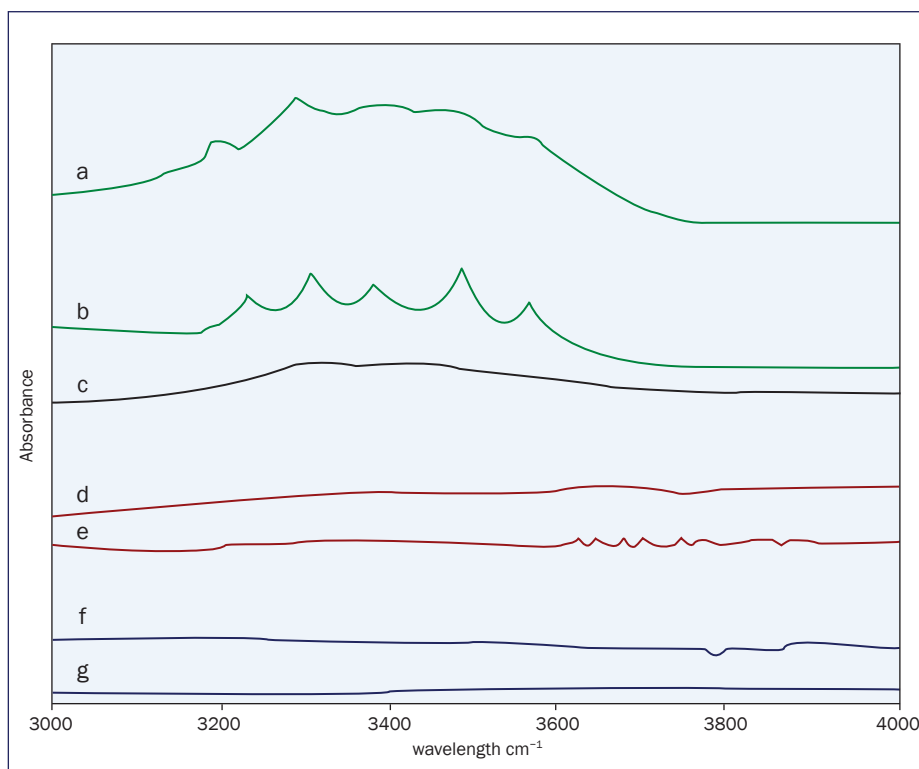
Figure 4: The 'water' bands in the IR spectra of synthetic and natural corundum.
Hydrothermal synthetic: (a) sample No. 30, (b) sample No. 33, (c) sample No. 29.
Natural: (d) sample No. 5, (e) sample No. 10.
Flux synthetic: (f) sample No. 20, (g) sample No. 25.

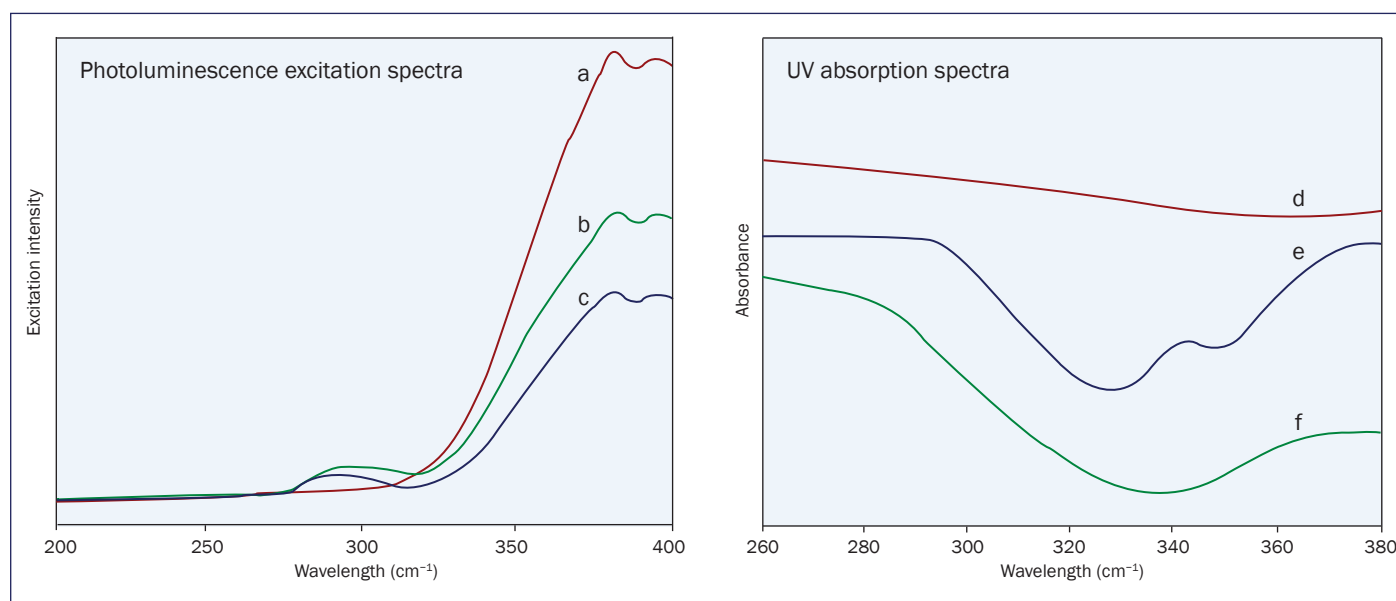Figure 5: Details of the photoluminescence excitation spectra of Cr in Al_2O_3 (left) and UV absorption spectra (right) of natural and synthetic corundum.
(a) Natural, sample No. 4; (b) hydrothermal synthetic, sample No. 35; (c) flux synthetic, sample No. 23; (d) natural, sample No. 14; (e) flux synthetic, sample No. 24; (f) hydrothermal synthetic, sample No. 35.

New data for distinguishing between hydrothermal synthetic, flux synthetic and natural corundum
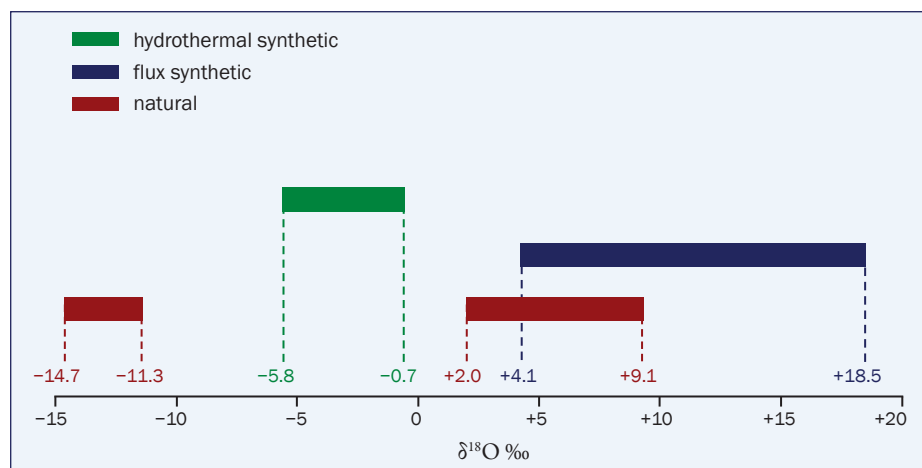

Figure 6: The oxygen isotopic composition ranges of corundums from different sources. The chart includes data for flux-grown corundum from Giuliani et al. *(2005).*

reason for this line is not known and further studies using a large collection of different flux corundums should be undertaken. Quantitative and non-destructive UV absorption spectrometry has also been described by Bosshart (1982).

The oxygen isotope compositions of corundum from igneous, skarn, hydrothermal and metamorphic deposits in Russia, and of some flux and hydrothermal synthetic corundums, are listed in *Table I*, see also *Figure 6*.

The $\delta^{18}O$ values for most natural samples lie in the range from +2.0 to +9.1‰, and taking into account published data (Giuliani *et al.,* 2005) this range increases up to +23.0‰; the one exception concerns corundums from the Khitostrovskoye deposit, Karelia, Russia, where this value lies in the range −14.7 and −11.3‰. Oxygen isotopic composition of flux corundum (+4.1 – +14.8‰) is similar to that for natural corundum.

The literature information about oxygen isotopic composition of hydrothermal synthetic corundum is limited. The work of Pomian-Srzednicki, 1997, for example, contains only one specimen of such material: hydrothermal synthetic corundum from Novosibirsk, Russia, with a $\delta^{18}O$ value of −11.5‰. Oxygen isotope compositions of six hydrothermal synthetic corundums of different colours in the present study indicate that their $\delta^{18}O$ values are distinctly

different from natural and flux corundum, ranging from −5.8 to −0.7‰.

The oxygen isotope compositions of these studied corundums reflect the source compositions of water involved in their crystallization. The unusual $\delta^{18}O$ value for natural corundum from Khitostrovskoye is negative, and we postulate that fluids involved in its generation could well have involved predominantly meteoric water, while for other natural corundums, meteoric water was negligible.

Conclusions

Spectroscopic and isotopic studies of natural corundum from different deposits, as well as synthetic corundum grown by flux and hydrothermal methods have revealed some distinctive features:

1. PL excitation spectroscopy may allow one to determine whether the studied stone is natural or synthetic. The 290 nm excitation band due to F^+ complexes was found only in synthetic corundum (both flux and hydrothermal).

2. For identifying flux-grown corundum, UV-absorption spectroscopy can be useful, as a narrow band with a maximum at 342 nm occurs only in their spectra.

3. New oxygen isotope compositions of hydrothermal synthetic corundums and of natural corundums from different deposits allows one to distinguish

between them very clearly. The differently coloured hydrothermal synthetic corundums have $\delta^{18}O$ values ranging from −5.8 to −0.7‰, which are distinct from those of nearly all natural and flux specimens which are more than +2.0‰. The corundums of the Khitostrovskoye deposit, Karelia, Russia, are unusual in having very low $\delta^{18}O$ values from −14.7 to −11.3‰; this allows us to distinguish the stones from this deposit. The main disadvantage of isotope analysis for gem testing is that it is a destructive technique, so studies are best carried out on rough corundum.

Acknowledgements

References

Allen, R.M., 1991. The Yogo sapphire deposit: New discoveries create more interest in America's finest gemstone. *Gem. Diary,* **3**(2), 9–16

Bosshart, G., 1982. Distinction of natural and synthetic rubies by ultraviolet spectrophotometry. *Jour. Gemm.,* **18**(2), 145–60

Hughes, R., 1997. *Ruby and Sapphire*. RWH Publishing. Boulder, Colorado. 512 pp

Faure, G., 1986. *Principles of isotope geology*. John Wiley and Sons Inc., New York. 589 pp

Giuliani, G., Fallick, A.E., Garnier, V., France-Lanord, C., Ohnensteter, D., and Schwarz, D., 2005. Oxygen isotope composition as a tracer for the origins of rubies and sapphires. *Geology,* **33**(4), 249–52

Hoefs, J., 1997. *Stable isotope geochemistry*. Springer-Verlag, Berlin, 201 pp

Polyakov, V.B., and Ustinov, V.I., 1997. Equilibrium isotopic constants ($\beta^{18}O$-factors) of corundum. *Geochemistry,* **10**, 1019–25 (in Russian)

New data for distinguishing between hydrothermal synthetic, flux synthetic and natural corundum

Pomian-Srzednicki, I., 1997. *Caractérisation des corindons par mesure du rapport isotopique de l'oxygéne $^{16}O/^{18}O$*. Université de Lausanne, Institut de Minéralogie et Pétrographie (unpublished dissertation)

Syurdo, A.I., Kortov, V.S., Pustovarov, V.A., Sharafutdinov, F.F., and Zinin, E.I., 1998. SR-excited luminescence of corundum with native defects. *Nuclear Instruments and Methods in Physics Research Section A: Accelerators, Spectrometers, Detectors and Associated Equipment,* **405**(2–3), 408–11

The Authors

Alexei S. Bidny, Olga S. Dolgova, Ivan A. Baksheev and Irina A. Ekimenkova

Division of Mineralogy, Department of Geology, Lomonosov Moscow State University, Moscow, Russia.

www.msu.ru

email: alexei.bidny@gmail.com

Raise your profile . . .
Raise customer confidence with

Gem-A
Corporate Membership

Gain advantages including:

- Use of Gem-A logo or Coat of Arms (illustrated right)
- Discounts on laboratory services
- Special prices on courses and workshops
- Discounts on books and instruments
- Network and information exchange meetings

Any UK-based company may apply to become a Corporate Member of Gem-A if their business is the sale, auction, manufacture or appraisal of gems or gem-set jewellery

If you employ a Fellow (FGA) or Diamond member (DGA) of Gem-A you may apply for Gold Corporate Membership, entitling you to display the Gold Corporate Coat of Arms stating that you employ a qualified gemmologist — the ultimate sign of gem excellence.

The annual membership fee for Corporate Members and Gold Corporate members for 2011 is £160.00.

However, it may cost you nothing extra for 2011 if you already employ and pay the subscriptions for two Fellow, Diamond or Associate members of Gem-A. This is because the Corporate Membership subscription includes two individual subscriptions.

For further details and to apply, go to www.gem-a.com/membership/corporate-membership.aspx or contact Carlos Witkowski on 020 7404 3334 or email carlos.witkowski@gem-a.com

A Gem-A initiative to support your business

**Gem-A Corporate
Membership Logo**

**Gem-A
Gold Corporate
Coat of Arms**

A cautionary tale about a little-known type of non-nacreous calcareous concretion produced by the *Magilus antiquus* marine snail

Thomas Hainschwang, Thomas Hochstrasser, Irka Hajdas and Wolfgang Keutschegger

Abstract: Four most unusual objects represented as gastropod-shaped non-nacreous pearls (calcareous concretions) were analysed at the GEMLAB laboratory by standard gemmological and laboratory techniques. They were consistent with natural non-nacreous pearls, but these methods did not provide unambiguous proof that the samples are or are not unusual fossilized gastropods or something else. Therefore the objects were subjected to scanning electron microscopy and finally to a method only rarely used in the gemmological field — ^{14}C age determination. Results were still inconclusive until consultation with malacologists and conchologists led to the conclusion that the specimens are natural and belong to the species *Magilus antiquus*. Their terminology is discussed

Keywords: aragonite, calcareous concretion, calcite, flame pattern, non-nacreous pearl

1. Introduction

Challenges are a daily routine in a gemmological laboratory, but there are times when you are confronted with something that neither you nor your colleagues have ever seen; this paper describes such an event and how it was finally resolved.

Although natural nacreous and non-nacreous pearls are found in a wide variety of different molluscs around the globe, in fresh- and salt-water, due to environmental circumstances natural pearls are becoming increasingly difficult to find from many sources (Strack, 2001). The Philippines is one of the few countries where natural nacreous and non-nacreous pearls are still being found in appreciable but still very limited quantities. In past years the authors have examined many different and exotic natural pearls from this and other locations, but the four gastropod-shaped objects described as pearls and submitted to the GEMLAB for identification were by far the most unusual to date.

It is known that objects or animals trapped within a mollusc may end up as blisters or even as blister pearls, since the mollusc reacts to the intrusion of an object/animal with the formation of nacre (Strack, 2001). Therefore worms, small bivalves and even fishes can be found within blister pearls. Such intruder-formed blisters are often at least partially hollow and the object/animal can always be found in the interior (Hainschwang *et al.,* 2009).

If the gastropod-shaped objects described in this paper are pearls that would indicate that the captured gastropods had not been covered by $CaCO_3$, but that the hollow shells of the animals had been completely filled by the pearl substance. The difficulty of explaining the formation of such pearls and their unusual shapes raised doubts about their identity and the final task was to investigate whether they were counterfeits, fossilized gastropods or some other type of material.

A a little-known type of non-nacreous calcareous concretion produced by the *Magilus antiquus* marine snail

2. Materials and Methods

Figure 1: The largest gastropod-shaped sample of 84.77 ct, represented as a natural non-nacreous white pearl. Photo by T. Hainschwang.

Four non-nacreous white gastropod-shaped specimens weighing 7.06, 14.99, 19.74 and 84.77 ct *(Figure 1)* were studied.

They were examined using light microscopy, fluorescence microscopy, scanning electron microscopy, ultraviolet visible near infrared (UV-Vis-NIR) spectroscopy, Fourier transform infrared (FTIR) spectroscopy, photoluminescence spectroscopy, energy dispersive X-ray fluorescence (EDXRF) and scanning electron microscope/energy dispersive X-ray (SEM-EDX), chemical analysis, radiography and finally ^{14}C age determination.

Microscope observations were made in reflected light and darkfield illumination using a Leica M165C binocular microscope equipped with a Schott LED light source and a Leica DFC420 CCD microscope camera with a resolution of 5 megapixels.

Luminescence of the samples was observed using a standard long wave and shortwave ultraviolet radiation lamp (365 and 254 nm respectively) and by the prototype of the GEMLAB fluorescence microscope using a selectively filtered 200 W xenon light source adjustable to a tuneable monochromatic excitation light source whenever necessary.

SEM imaging and semi-quantitative chemical analysis were carried out using a Zeiss Supra 40VP scanning electron microscope equipped with an EDAX Genesis 2000 EDX spectrometer at the research facilities of Ivoclar in Schaan/ Liechtenstein.

Specular reflectance infrared spectra of all specimens were recorded in the range of 4000–400 cm^{-1} at 4 cm^{-1} resolution with a Perkin Elmer Spectrum BXII FTIR spectrometer. The instrument was equipped with a DTGS detector and a KBr beam splitter. A Perkin Elmer fixed angle specular reflectance accessory was used for experiments.

Reflectance UV-visible-near infrared absorption spectra in the 240–1050 nm range were recorded for two samples with the prototype of the GEMLAB Xenon UV-Vis-NIR spectrometer system with a resolution of 0.6 nm; the samples were examined in a reflectance setup within a custom made integration sphere.

Photoluminescence (PL) spectra of two specimens were recorded using a custom-built system using 532 nm and 473 nm diode-pumped solid state lasers coupled to an Ocean Optics Maya

spectrometer with a resolution of 0.9 nm.

Quantitative EDXRF chemical analysis of all samples was carried out with a custom-built system equipped with a 40 kV X-ray tube and a thermoelectrically cooled Si detector; the analyses were done in air and for one sample under a helium atmosphere. Quantitative chemical analysis of one sample was carried out using the EDX system of the scanning electron microscope described above.

A ^{14}C isotope analysis of one specimen was carried out at the accelerator mass spectrometry (AMS) facilities of the Ion Beam Physics Department, ETH Zurich, for age determination. For this destructive method a small piece weighing 0.015 g was carefully removed from one of the objects and dissolved in concentrated phosphoric acid. The released CO_2 was then graphitized (Hajdas *et al.,* 2004) and pressed into cathodes for AMS measurements using a mini radiocarbon dating system (MICADAS) (Synal, 2007). In this method ions obtained from the graphite are accelerated to high kinetic energies to enable separation of the ^{14}C and ^{12}C isotopes.

For comparison, samples of aragonite (crystals, stalactitic aggregates ['eisenbluete']), calcite crystals and natural nacreous and non-nacreous pearls were analysed by FTIR, UV-Vis-NIR and photoluminescence spectroscopy as well as EDXRF chemical analysis.

3. Results and discussion

3.1. Visual observation, microscopy and luminescence

The four objects in this study apparently belong to the same species of gastropod; their form and shape are similar and there is variation in only minor details *(Figure 2)*. The samples were all non-nacreous white, semi-translucent, and their surfaces show great details of the original shell without any indications

whatsoever of polishing or any other form of working, except that the original aperture of the gastropods showed indications that they were polished/ worked.

All four specimens contain small holes such as that in the 7.06 ct specimen *(Figure 3a)*; such holes are present in most sea shells and can be caused by drill molluscs or parasitic worms. Microscopic observation showed a distinct concentric structure in the zone of the

original aperture of the shell, and in the 7.06 ct specimen there is a central grain surrounded by darker matter *(Figure 3b)*.

A faint flame pattern is present in all samples but only clearly visible when the surface of the pearls was viewed carefully under the microscope *(Figure 4)*. Such a flame pattern is characteristic for certain non-nacreous pearls, of which the pink to orange pearls from *Strombus gigas* and *Melo melo* gastropods are the best known (Hänni, 2009; Strack, 2001). Besides

A little-known type of non-nacreous calcareous concretion produced by the *Magilus antiquus* marine snail
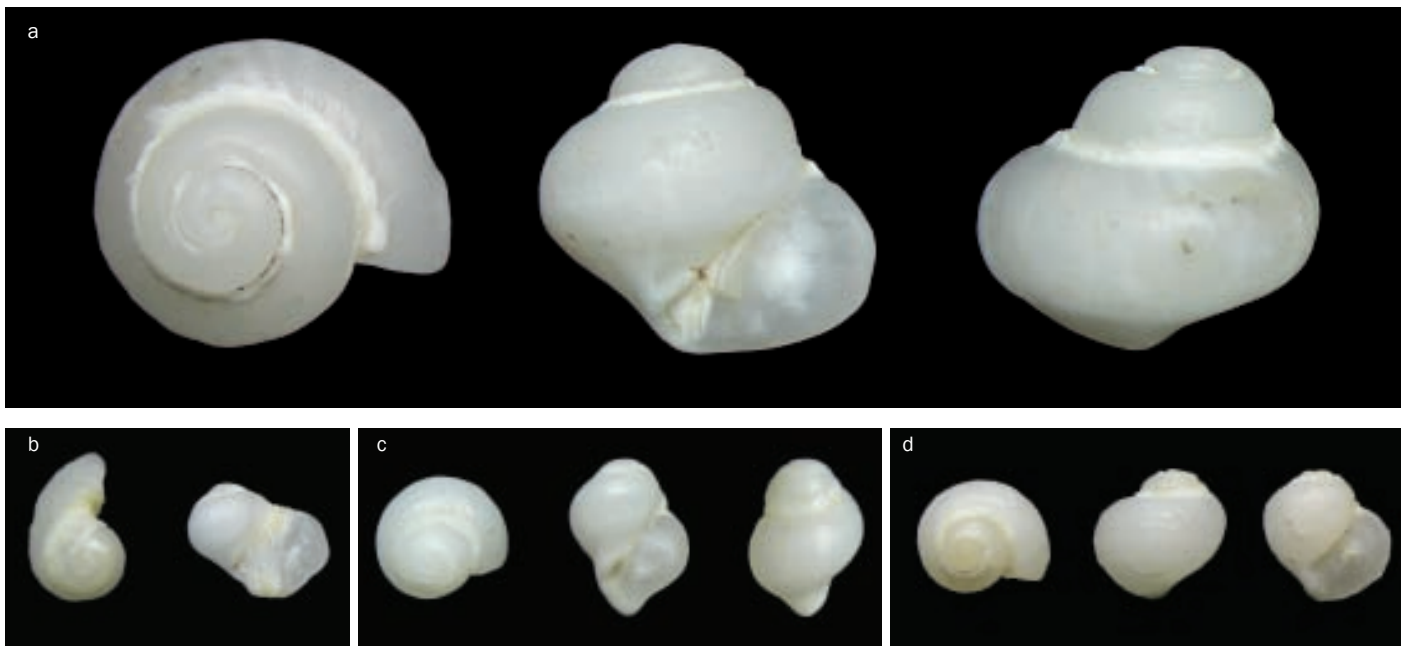

Figure 2: Different views of the four specimens examined in this study: (a) 84.77 ct, (b) 19.74 ct, (c) 14.99 ct and (d) 7.06 ct. The general shape of the specimens indicates that they belong to the same or a very similar species of gastropod. Photos by T. Hainschwang.

these pearls, this kind of flame pattern is also known from other non-nacreous gastropods and certain bivalve molluscs.

Under intense UV illumination, as used in the GEMLAB fluorescence microscope, all specimens exhibited a distinct blue fluorescence, reminiscent of the emission known for many pearls. In three specimens a lighter and yellower fluorescence was visible in the central portion of the gastropods' original aperture *(Figure 5)*. This emission followed the most evident concentric structures visible.
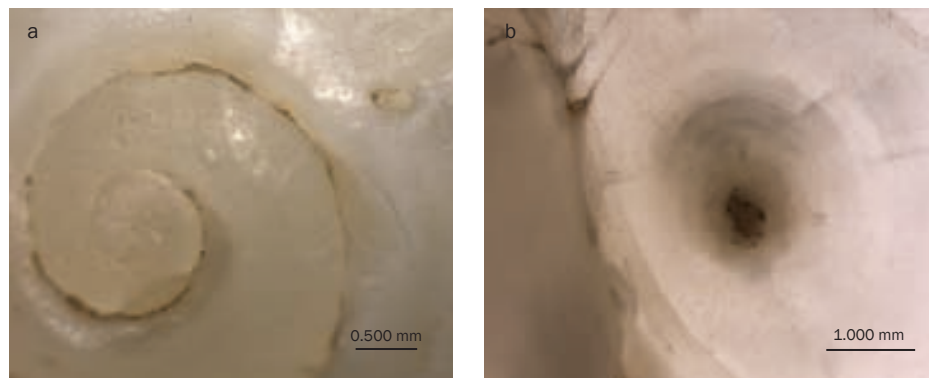
Figure 3: Close-up views of the 7.06 ct specimen: (a) view of the spiral and of a parasite-caused drill hole; (b) the concentric structure and central grain at the original aperture of the gastropod. Photos by T. Hainschwang.
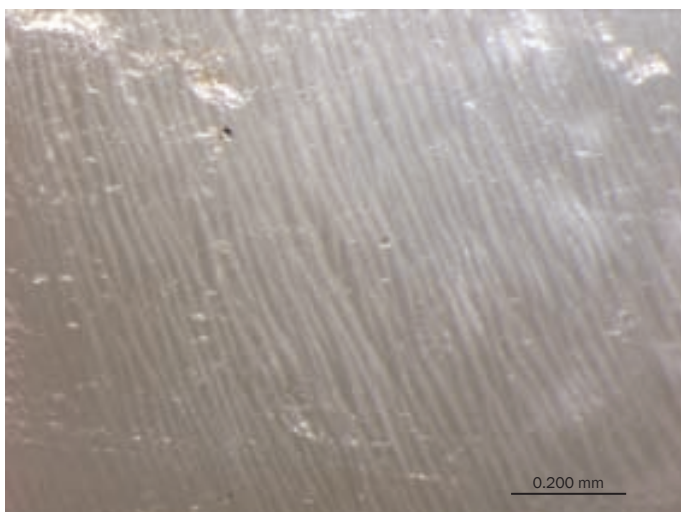
Figure 4: The fine flame pattern seen in the largest specimens, as seen in reflected light. Photo by T. Hainschwang.

Figure 5: The 7.06 ct gastropod-shaped specimen under strong UV excitation shows distinct zoning at the gastropod's original aperture. Photo by T. Hainschwang.

A little-known type of non-nacreous calcareous concretion produced by the *Magilus antiquus* marine snail
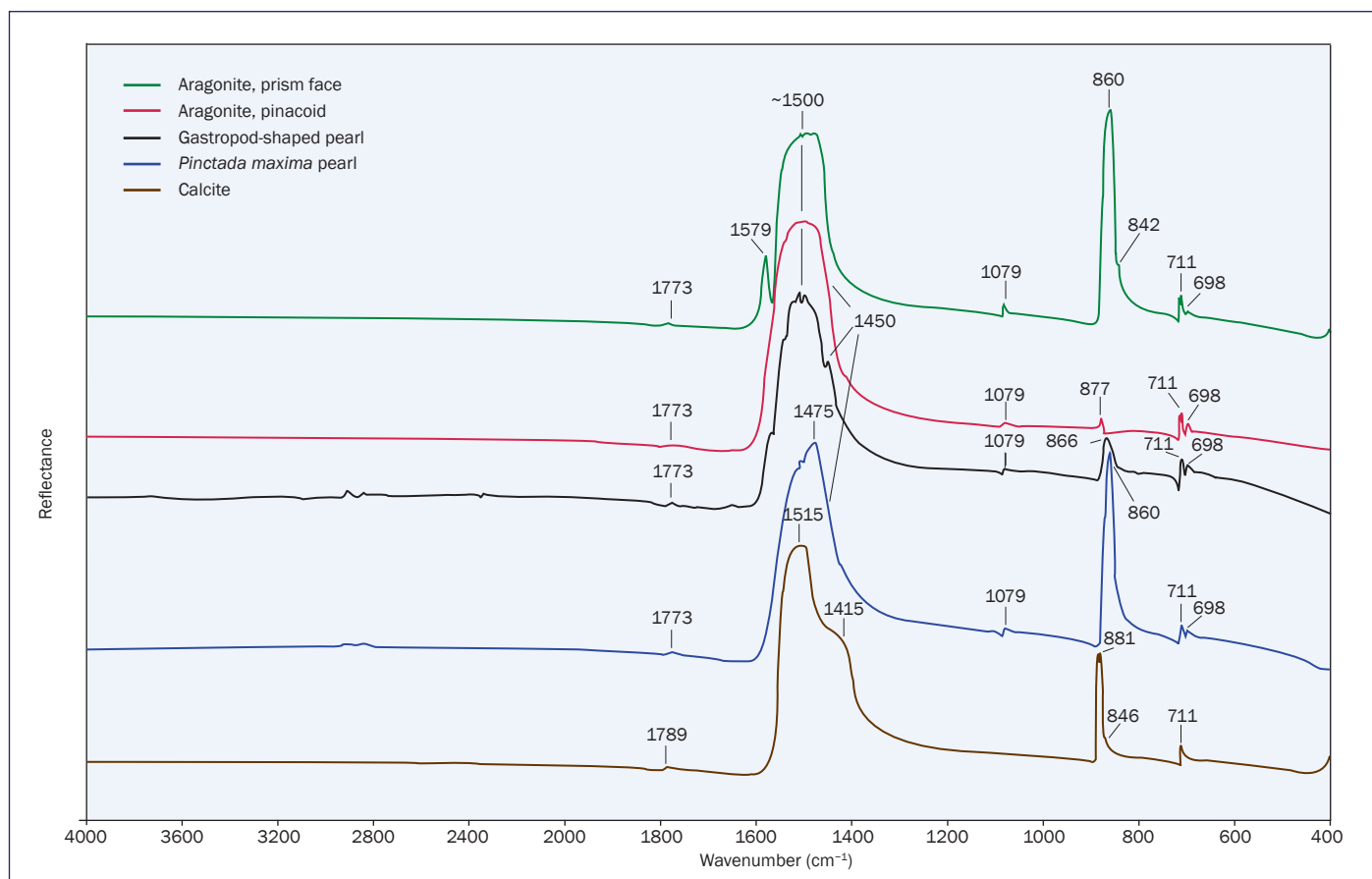
Figure 6: Specular reflectance infrared spectra of aragonite, calcite, a non-nacreous white pearl and a gastropod-shaped sample.

The initial results from these classical gemmological approaches seemed to indicate that the gastropod-shaped specimens were neither forgeries nor fossils; at the time of analysis in the laboratory it was believed that non-nacreous pearls and certain sea shells were the only materials exhibiting the characteristic flame structure visible in *Figure 4.* The lack of banded layers in strong transmitted light indicated that the objects could not be polished from shell, which is a common type of forgery to imitate non-–nacreous natural pearls. The specimens appeared to be most unusual pearls, but the fact of the existence of such gastropod-shaped pearls would contradict all classical explanations of pearl formation and so further examination to try and clarify how they were formed was desirable.

3.2. EDXRF chemical analysis

Using EDXRF analyses major calcium and minor but distinct strontium were detected, a perfect match with what would be expected when testing saltwater aragonitic materials. The near-absence of manganese is consistent with a saltwater origin (Hänni *et al.,* 2005). One sample (7.06 ct) was additionally analysed by SEM-EDX, with identical results. For comparison, EDXRF data were collected for aragonite (crystals, stalactitic aggregates ['eisenbluete']), calcite crystals and natural nacreous and non-nacreous pearls. The chemical compositions of the nacreous and non-nacreous pearls were practically identical, while the aragonite and calcite mineral samples all contained significantly lower strontium.

3.3. Specular reflectance FTIR spectroscopy

Specular reflectance FTIR spectra recorded from all specimens confirmed that their main constituent is aragonite. The commonest polymorphs of $CaCO_3$ — calcite and aragonite — can be easily distinguished using this method since their band positions vary slightly and aragonite also exhibits weak features around 1085 cm^{-1} and 697 cm^{-1} which are absent in the calcite spectra *(Figure 6)* (Hainschwang and Notari, 2008). Certain non-nacreous pearls are calcitic (e.g. Pinna pearls), but we have not yet had a white non-nacreous pearl that was dominantly calcitic in the GEMLAB laboratory; so far all have been dominantly of aragonitic composition.

3.4. Reflectance UV-Vis-NIR spectroscopy

The spectra of all four specimens are identical to the spectra of white nacreous and non-nacreous pearls, with a strong absorption band at 285 nm; this band is characteristic for all aragonitic materials, including aragonite itself and is thus of no diagnostic value to distinguish a white non-nacreous pearl from other aragonitic materials.

3.5. PL and Raman spectroscopy

The PL spectra recorded with 473 nm

A little-known type of non-nacreous calcareous concretion produced by the *Magilus antiquus* marine snail

Figure 7: The PL spectra excited with 532 and 473 nm lasers of a non-nacreous white pearl and a gastropod-shaped sample (left), compared to aragonite ('eisenbluete') and calcite (right). The sharp features present and indexed in the graphs are Raman scattering peaks.
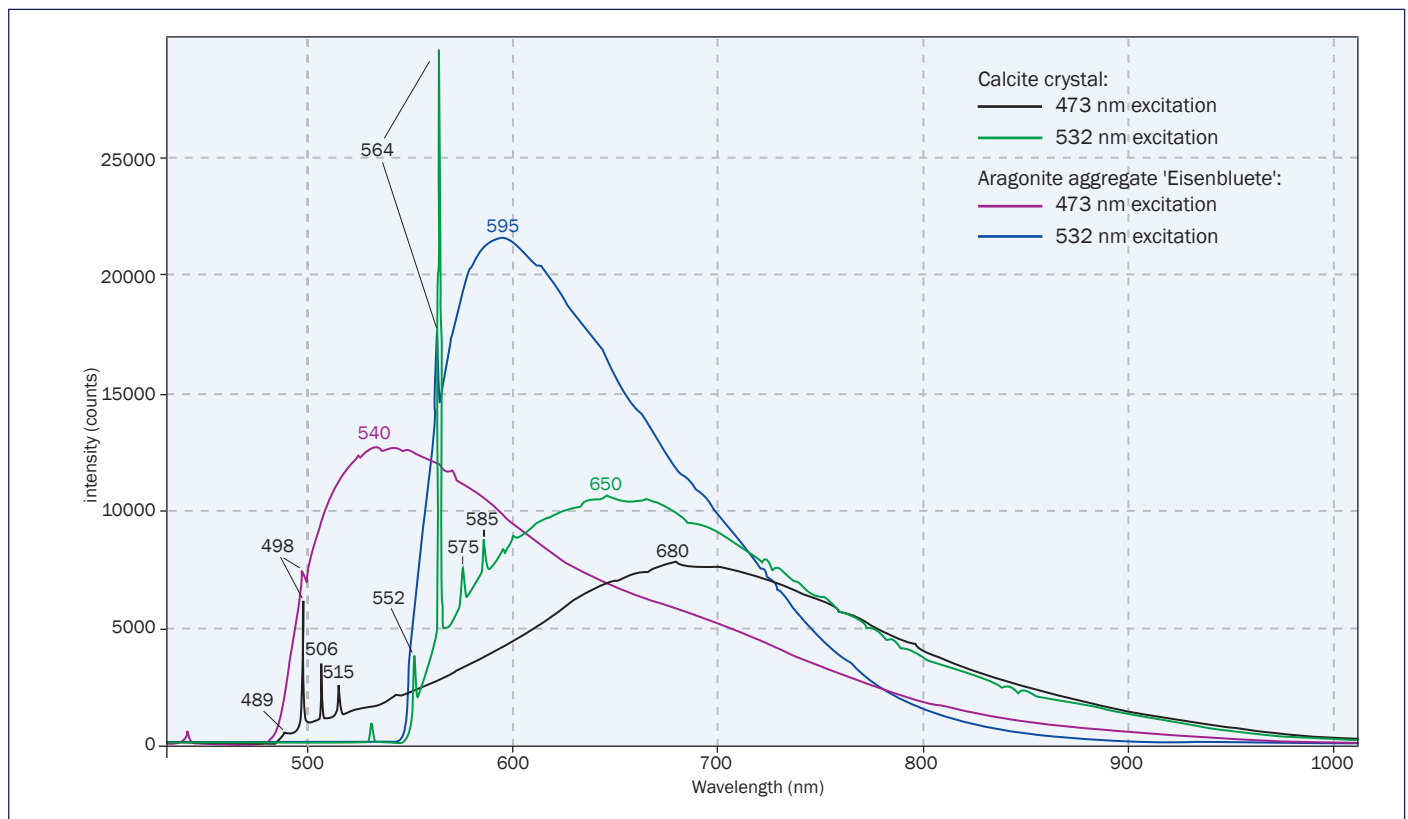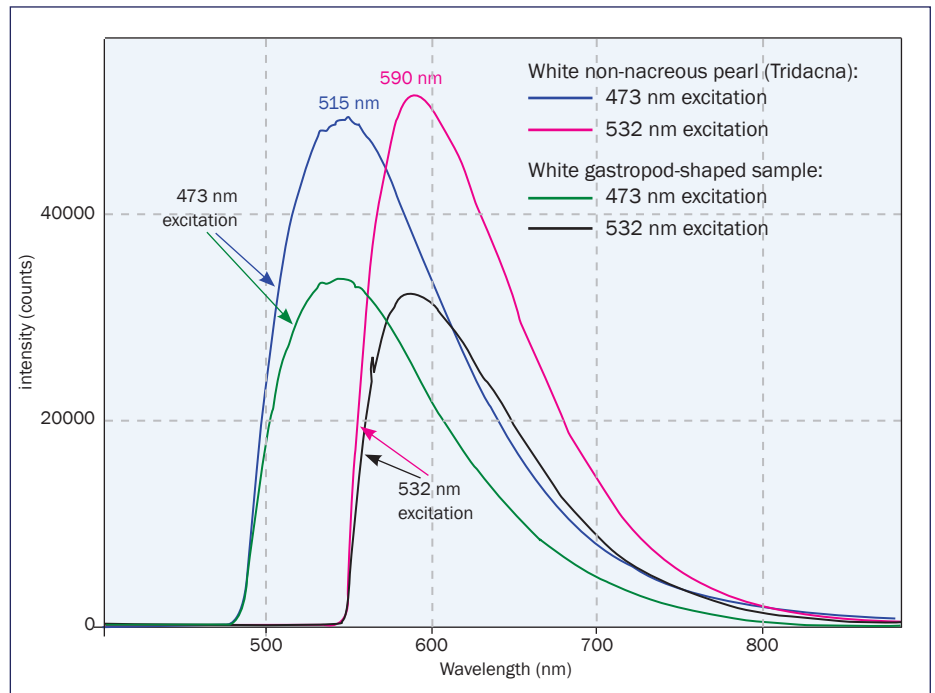
and 532 nm laser excitation are identical to the spectra obtained from non-nacreous white pearls. The spectra consist of a simple broad band emission centred at about 545 and 590 nm respectively with sharp peaks corresponding to the Raman lines of aragonite. The fibrous aragonite 'eisenbluete' samples that were used for comparison exhibit a very similar broad band PL while calcite shows a different broad band emission centred at 680 nm (473 nm excitation) and 650 nm (532 nm excitation) respectively *(Figure 7)*.

3.6. Radiography

Radiography of the samples revealed that the objects are all solid. Little structure is visible and no remnants of, for example, the original shell that could be trapped within the objects were found. The only significant features are the drill holes that can also be seen under the microscope *(Figure 8),* and some of these holes cross the whole specimen. The

A little-known type of non-nacreous calcareous concretion produced by the *Magilus antiquus* marine snail
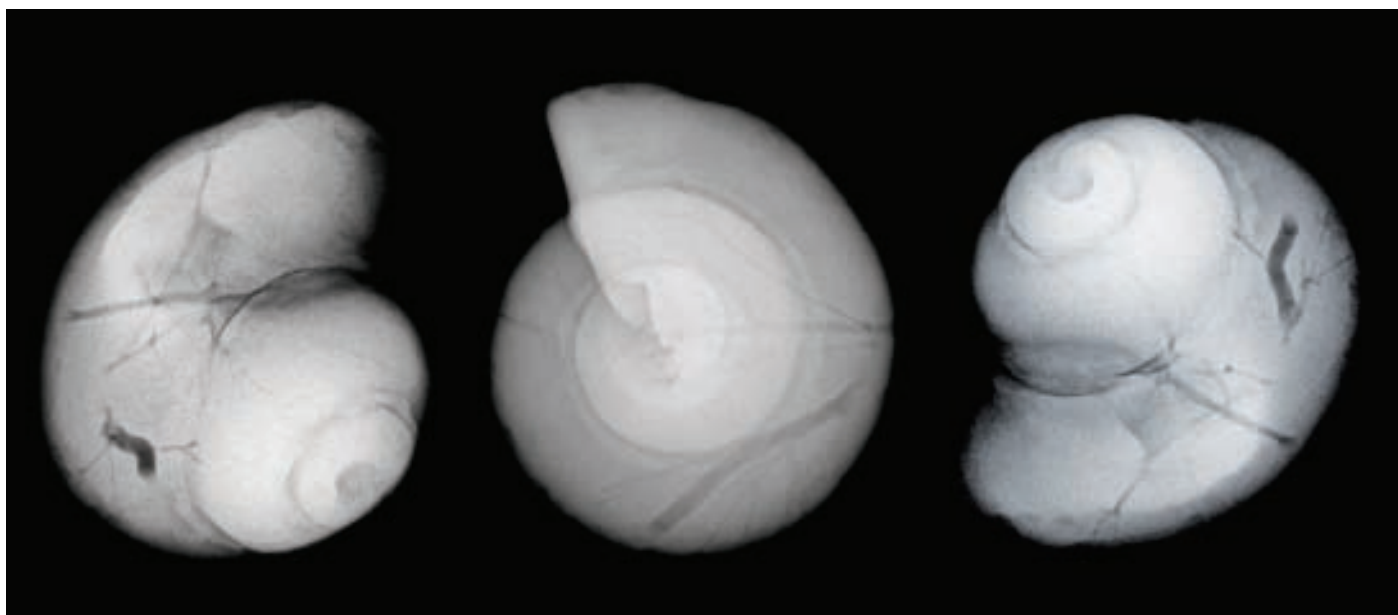

Figure 8: Radiographs in three different orientations of the largest gastropod-shaped sample. The grey linear features of variable width represent the hollow drill channels present in all the specimens.

extremely subtle structure of natural non-nacreous white pearls is — in the authors' experience — generally not visible in conventional radiography. When white non-nacreous pearls are sawn in half, there is normally no evidence of circular growth structure and only diffuse bands of slightly variable coloration can be seen.

The radiographs clearly pointed towards naturally grown solid pearl-like objects.

3.7. SEM

The 7.06 ct specimen was examined using the SEM in order to get a better picture of the structure of the material *(Figure 9)*.

The SEM images revealed platy and fibrous crystals of aragonite, which were in part arranged in a concentric structure. The fibres are not all near-parallel but are distributed in the form of 'bundles', some of which have a V-like appearance. The presence and distribution of these fibres is the reason for the flame pattern that is visible on the surfaces of the specimens (Hänni, 2009). These results are consistent with what would be expected from a natural non-nacreous pearl.

Although the presence of the concentric structure at the original aperture indicated that some of the original piece may be missing, there was

no evidence of polishing; a possibility would be that part of the sample was broken off the original piece.

3.8. ¹⁴C age determination

Radiocarbon dating was carried out to determine whether or not the specimens could be an uncommon type of fossilized sea mollusc.

The analysis of a small piece removed from one specimen indicates that the material was no more than 400 to 500 years old. That is, its age is well within the historical period and therefore it is not a fossil. Also, this is consistent with the fact that most aragonite transforms to calcite when aragonitic shells are fossilized. Aragonite in fossils is only known in the iridescent surface layers of so-called 'ammolite'.

4. Discussion

The data obtained using the above methods prove that the samples are not man-made forgeries, that they have not been polished from shell material and that they are not fossils. The composition of the specimens was identified as principally aragonite with distinct traces of strontium, radiography proved their solid nature and the presence of concentric growth structure combined with a very fine flame pattern due to fibrous aragonite

growth in all samples, clearly points to the specimens being natural non-nacreous pearls.

Because we had no plausible explanation for the formation of solid non-nacreous gastropod-shaped pearls, we sought an expert in molluscs and shells (a malacologist and conchologist) who could identify the species that was represented by these specimens. The information obtained from two conchologists was a revelation: the specimens were confirmed to be of natural origin, but they were not formed inside another marine mollusc, but by the gastropod itself (Massin, 1982). There are some most unusual gastropods that live on and in, and feed from corals ('coral dwellers') and that grow together with the coral. Our four specimens were identified as *Magilus antiquus* (Montfort, 1810), belonging to the family Muricidae (subfamily Coralliophilinae, a name meaning 'liking coral'). When the coral grows, the *Magilus* fills up its shell with aragonite and lives on some sort of pedestal close to the surface of the coral (Oliverio, 2009, Figures 11F, G). Complete specimens usually have a rather long tube-like uncoiled shell; this solid tube-like 'prolongation' of the juvenile coiled shell is used as a 'house' by the animal, which can live close to the surface of the

A little-known type of non-nacreous calcareous concretion produced by the *Magilus antiquus* marine snail
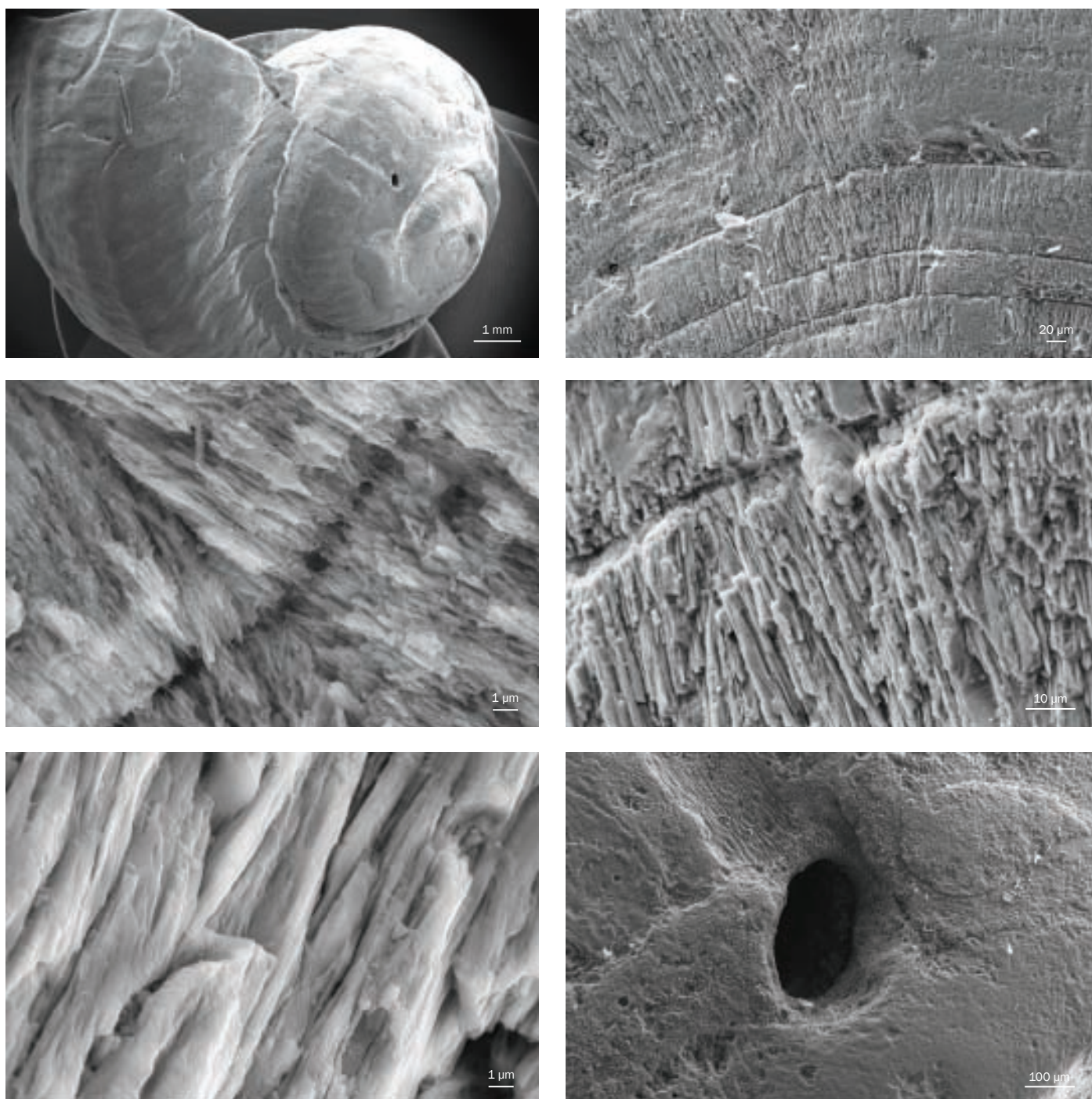
Figure 9: SEM images showing details of the gastropod-shaped specimen of 7.06 ct.

coral thanks to the pedestal. As the coral grows, the animal produces more and more aragonite to keep the pedestal at about the same distance from the coral surface. The shell of this gastropod is as white as the 'filled' pieces described in this study, but with time it becomes absorbed in the juvenile part. In the parts of the gastropod buried deeply in the coral, there is rarely any trace of the original shell remaining.

5. Conclusions

The four specimens described above constitute a clear demonstration that the utmost care must be taken before drawing conclusions about uncommon or new materials. The specimens of *Magilus antiquus* were sold as natural non-nacreous pearls and this is the basis on which they were examined. In this outstanding case the material showed exactly the same properties as the material

that it was meant to imitate (a natural non-nacreous pearl); only the fact that there was no explanation for the formation of these objects finally led to the discovery of the real nature of these 'pearls'.

Concerning the nomenclature of such calcareous concretions formed by coral-dwelling gastropods, it is unclear whether they should be declared as 'non-nacreous pearls' or simply as 'calcareous concretions'; probably the

A little-known type of non-nacreous calcareous concretion produced by the *Magilus antiquus* marine snail

material, which demonstrably represents the filled shell of a mollusc, should be called a calcareous concretion. Although it is formed by marine gastropods, the process and motivation of the formation is quite different from that of 'regular' non-nacreous pearls and the fact that the animal lives on this formed material makes the decision on what to call these 'magilus pearls' an ambiguous one.

Despite the doubts over their name, these unusual objects could make attractive and very individual pieces when mounted in jewellery.

Acknowledgements

References

Hainschwang, T., Hochstrasser, T., and Bürgin, T., 2009. A most unusual blister pearl. *Gems & Gemology,* **45**(4), 300–1

Hainschwang, T., and Notari, F., 2008. Specular reflectance infrared spectroscopy — A review and update of a little exploited method for gem identification. *Journal of Gemmology,* **21**(1–2), 23–9

Hajdas, I., Bonani, G., Thut, J., Leone, G., Pfenninger, R., and Maden, C., 2004. A report on sample preparation at the ETH/PSI AMS facility in Zurich. *Nuclear Instruments and Methods in Physics Research Section B: Beam Interactions with Materials and Atoms,* **223–224**, 267–71

Hänni, H.A., 2009. Zur Flammenstruktur bei einigen porzellanartigen Perlen. *Gemmologie. Z. Dt. Gemmol. Ges.,* **58**(1–2), 47–52

Hänni, H.A., Kiefert, L., and Giese, P., 2005. X-ray luminescence, a valuable test in pearl identification. *Journal of Gemmology,* **29**(5/6), 325–9

Massin, C., 1982. Contribution to the knowledge of two boring gastropods with an annotated list of the genera Magilus Montfort, 1810 and Leptoconchus Rüppell, 1835. *Bulletin de l'Institut royal des Sciences naturelles de Belgique, Biologie,* **53**, 1–28 + 1 pl.

Oliverio, M., 2009. Diversity of Coralliophilinae (Mollusca, Neogastropoda, Muricidae) at Austral Islands (South Pacific). *Zoosystema,* **31**(4), 759–89

Strack, E., 2001. *Perlen.* Rühle-Diebener-Verlag GmbH & Co. KG, Stuttgart, 696 pp.

Synal, H. A., Stocker, M., and Suter, M., 2007. MICADAS: A new compact radiocarbon AMS system. *Nuclear Instruments & Methods in Physics Research Section B-Beam Interactions with Materials and Atoms,* **259**, 7–13

The Authors

Thomas Hainschwang
Director and research gemmologist at the GEMLAB Laboratory in Balzers, Liechtenstein (thomas.hainschwang@gemlab.net)

Thomas Hochstrasser
Owner of Hochstrasser Natural Pearls in Dörflingen, Switzerland

Dr Irka Hajdas
Research Associate at the ETH/PSI Ion Beam Physics in Zurich, Switzerland

Wolfgang Keutschegger
Responsible for the SEM facility at Ivoclar in Schaan, Liechtenstein

Identification of CVD-grown synthetic melee pink diamond

Hiroshi Kitawaki, Ahmadjan Abduriyim, Jun Kawano and Makoto Okano

Abstract: Forty-eight faceted intense orangey-pink CVD-grown synthetic diamonds, most of which weighed less than 0.2 ct, have been examined in the GAAJ-ZENHOKYO laboratory. All proved to be coloured by the N-V centre that was formed by irradiation and annealing at low temperature after CVD synthesis and succeeding HPHT treatment. Using a combination of pinpoint inclusions and birefringence strain patterns, infrared absorption peaks in the range of 3150-2700 cm^{-1}, significant photoluminescence absorption lines at 575, 637 and 737 nm, and DiamondView™ and cathodo-luminescence images of layer growth patterns, CVD synthetic diamond can be distinguished from natural diamond. Annealing could change the colour of CVD diamond significantly from pink to purple but its colour was not stable and returned to its initial pink colour by UV radiation exposure in a short period. Features in the UV-Visible absorption spectra will be affected by annealing and UV radiation reaction.

Keywords: annealing, colour variation, crystal growth pattern, CVD-grown synthetic diamond, diamond treatment, melee
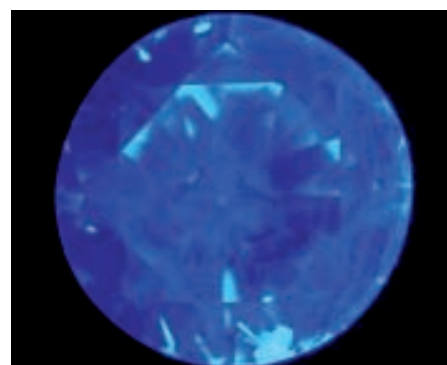
Introduction

Synthetic diamonds started to circulate in the gem market in the 1990s and became known to the gem industry. Most of such synthetics were grown by the high-pressure high-temperature (HPHT) method and the identification techniques revealed to date are all reliant on a knowledge of the growth environment or crystal forms essentially typical of HPHT synthesis. After Apollo Diamond Inc. announced their plan to sell them for jewellery use in August 2003 (Priddy, 2003), CVD-grown synthetic diamonds attracted attention first in the gem industry and then in the gemmological literature (Wang *et al.*, 2003, 2007; Deljanin *et al.*, 2003; Martineau *et al.*, 2004). Recently, fancy intense pink CVD type IIa diamonds in a size range of 0.28 to 0.67 ct and supplied by Apollo Diamond Inc. have been reported by Wang (2009).

The majority of natural pink diamonds are type I from the Argyle mine in Australia, and it is a concern for the gem trade that their price may increase due to the higher costs of moving from open-pit to underground mining. However, pink colours can also be produced in diamond containing isolated substitutional nitrogen atoms associated with vacancies (N-V centres: nitrogen vacancy pairs) by irradiation and annealing processes, and either natural or HPHT-grown synthetic diamonds with this property are used as raw material for such treatment.

Materials and methods

The samples used in this study consist of 48 loose pink diamonds, allegedly natural diamonds treated by a HPHT process, brought in to the GAAJ-ZENHOKYO Laboratory by a client for colour origin determination (*Figure 1*). All stones are round brilliant-cut, six lie in the range 0.20–0.27 ct, and 42 in the melee size range of which seven are 0.10–0.19 ct, and 35 are under 0.10 ct.

An Olympus gemmological microscope was used to examine external features and inclusions. UV fluorescence was observed in a perfectly dark room using long- (365 nm) and short-wave (253.6 nm) UV lamps manufactured by the Manaslu Co. A Shimadzu recording

Identification of CVD-grown synthetic melee pink diamond

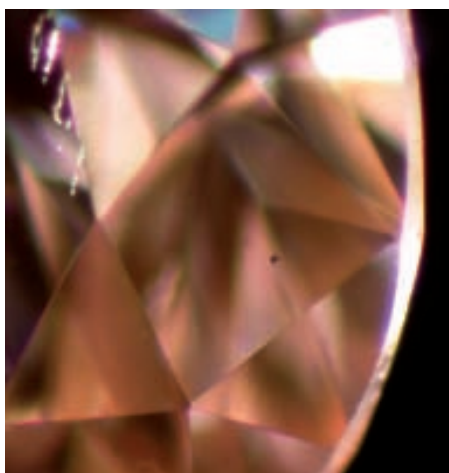*Figure 1: Forty-eight CVD-grown synthetic pink diamonds (0.01 ct – 0.27 ct). Photo by H. Kitawaki.*

Figure 2: Black pinpoints seen in almost all samples appear dark and are irregular in shape (field of view 1 mm); they are probably non-diamond structure carbon. Photo by A. Abduriyim.
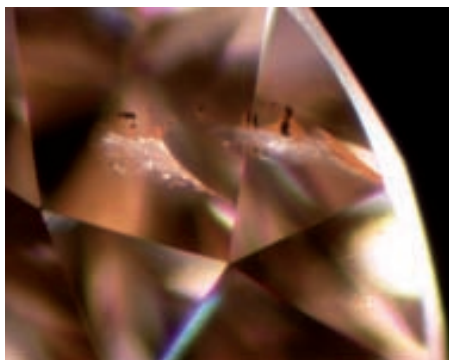
spectrophotometer UV 2400 was used at room temperature for UV-Visible spectral analysis within the range 220 to 860 nm in reflection mode. Infrared spectral analysis was carried out using a Shimadzu IR Prestige-21 instrument equipped with a KBr beam splitter and DLATGS detector. The analytical range was 4000–400 cm^{-1} with resolution of 1.0 cm^{-1} and 50 scans per spectrum were collected. Photoluminescence (PL) analysis was performed with all samples being immersed in liquid nitrogen using a Renishaw inVia Raman Microscope using two lasers: He-Ne 633 nm and He-Cd 325 nm, recording ranges of 650–850 and 330–800 nm respectively. A Renishaw Raman system-model 1000 with an Argon-
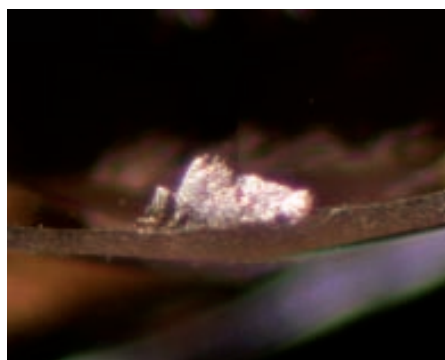
ion laser excitation at 514.5 nm was used to record the range 520–800 nm. UV luminescence images were observed using a DTC DiamondView™. A Premier American Technologies Corp. ELM-3R Cathodo-luminoscope was used for CL imaging. The colours and clarities of the diamonds were assessed by diamond graders using the JJA/AGL grading system, but one should note that in this system, regulations stipulate that synthetic diamonds are not graded.

Results and discussion

Gemmological observations

Among the 48 samples, colour grades ranged from fancy intense orange pink to fancy pinkish orange to light pinkish orange. The 13 stones over 0.1 ct were graded for clarity: three are VVS2, four are VS1, three are VS2, two are SI1 and one is SI2.

Most of the stones contain a few tiny pinpoints *(Figure 2)*; at high magnification they are dark with irregular shapes and are presumably non-diamond structure carbon. The pink colour is even in each stone and no patchiness in colour distribution was found. Several samples contain black graphite in their cleavages *(Figure 3)* and etched surface features resembling frosted glass *(Figure 4)*. These features are similar to those seen in HPHT-treated diamonds, so their presence strongly indicates that the samples have been HPHT treated after CVD synthesis. Many type Ia natural pink diamonds show traces of etching and almost all such stones display characteristic colour zoning described as 'pink graining'; this feature makes them clearly distinguishable from CVD-grown synthetic diamond. HPHT-grown synthetic pink diamonds which have been irradiated and annealed may be recognized by the presence of metal inclusions.

Most of the CVD-grown synthetic diamonds show double refraction in low-order interference colours in a characteristic streak pattern. The streaks run parallel with the growth direction of the crystal (when viewed through the pavilion side), parallel to {100} and were

Figure 3: Traces of dark graphitization in a cleavage of CVD-grown synthetic pink diamond (right, cleavage width 300 μm). It is probably evidence of HPHT treatment. Photo by A. Abduriyim.

Figure 4: Etched surface resembling frosted glass in a CVD-grown synthetic pink diamond (frosted surface width 200 μm). It is probably evidence of HPHT treatment. Photo by A. Abduriyim.

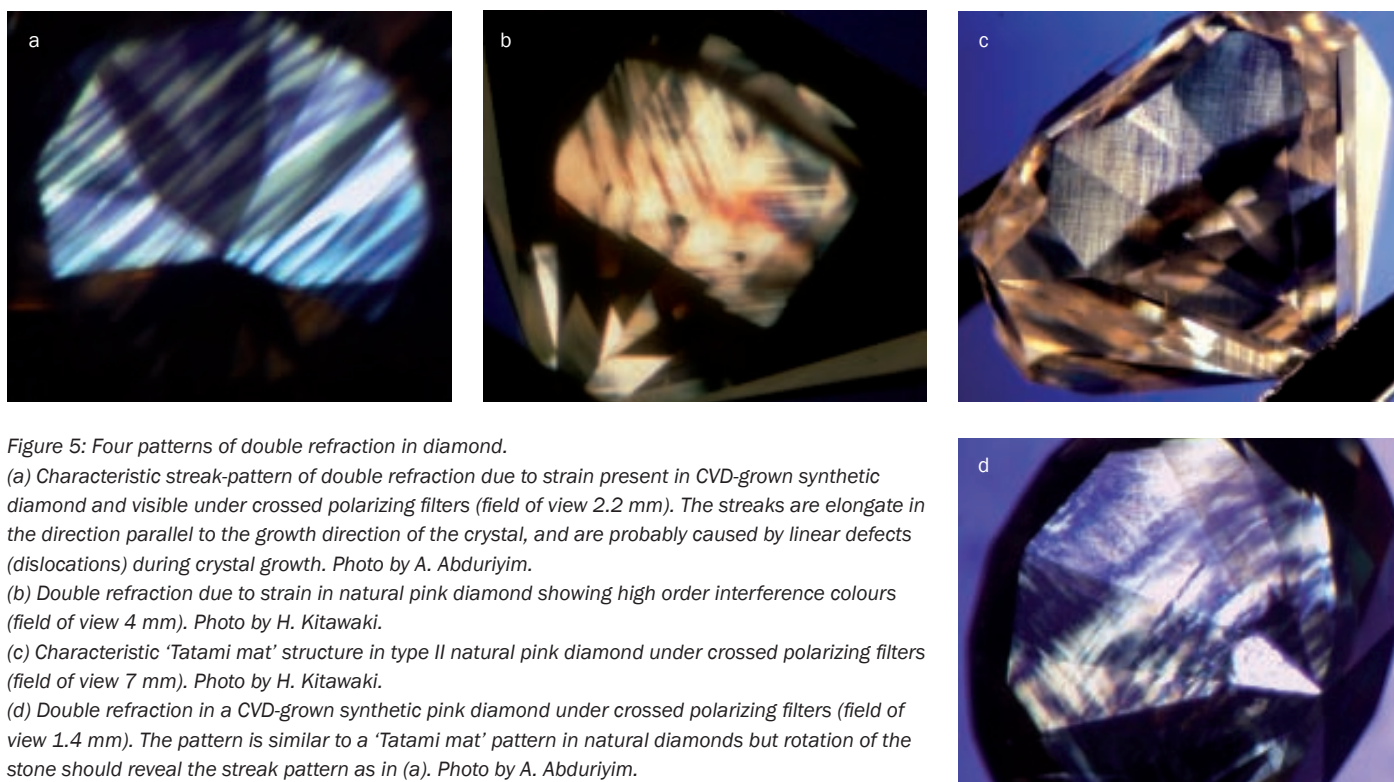## Identification of CVD-grown synthetic melee pink diamond

Figure 5: Four patterns of double refraction in diamond.

(a) Characteristic streak-pattern of double refraction due to strain present in CVD-grown synthetic diamond and visible under crossed polarizing filters (field of view 2.2 mm). The streaks are elongate in the direction parallel to the growth direction of the crystal, and are probably caused by linear defects (dislocations) during crystal growth. Photo by A. Abduriyim.

(b) Double refraction due to strain in natural pink diamond showing high order interference colours (field of view 4 mm). Photo by H. Kitawaki.

(c) Characteristic 'Tatami mat' structure in type II natural pink diamond under crossed polarizing filters (field of view 7 mm). Photo by H. Kitawaki.

(d) Double refraction in a CVD-grown synthetic pink diamond under crossed polarizing filters (field of view 1.4 mm). The pattern is similar to a 'Tatami mat' pattern in natural diamonds but rotation of the stone should reveal the streak pattern as in (a). Photo by A. Abduriyim.

supposedly produced by linear defects (dislocations) during crystal growth, causing internal strain *(Figure 5a)*. The kind of birefringence seen in natural pink diamond originates from plastic deformation and in most stones, strain accompanied by high order interference colours is associated with 'pink graining' *(Figure 5b)*. Rare type II natural diamonds also display strain but it appears under crossed polars as a pattern resembling a 'Tatami mat' *(Figure 5c)*. CVD-grown synthetic diamond is type IIa but some stones can show a 'Tatami mat'-like appearance if observed in directions other than the growth direction and care should be taken *(Figure 5d)*.

All the CVD-grown synthetic diamonds examined showed very strong orange fluorescence under UV, but no phosphorescence *(Figure 6)*. The fluorescence, generally stronger under LWUV than SWUV, originates from the N-V centre (associated with absorption at 575 nm), which was presumably formed as a result of the introduction of nitrogen gas to accelerate growth rate, and then by irradiation and annealing after the growth. Although some natural pink type IIa diamonds show orange fluorescence

the great majority fluoresce bluish white. Irradiated and annealed natural or HPHT-grown synthetic diamonds also show orange fluorescence that originates from N-V centres.

Spectral analysis
UV-Vis-NIR

The UV-Visible absorption spectrum measured at room temperature and shown in *Figure 7* is representative of 13 CVD

Figure 6: When exposed to long- and short-wave UV radiation, the CVD-grown synthetic diamonds display strong reddish orange fluorescence. Photo by A. Abduriyim.

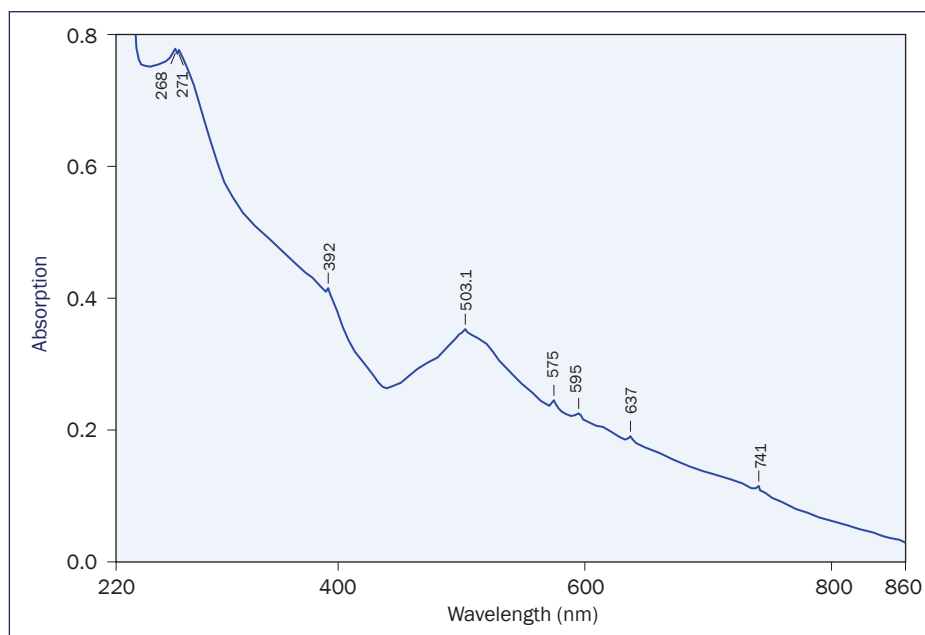## Identification of CVD-grown synthetic melee pink diamond

Figure 7: UV-Vis-NIR absorption spectrum of a representative CVD-grown synthetic diamond (from the stone weighing 0.19 ct) analysed at room temperature. Weak but sharp peaks at 637, 595, 575 and 503 nm were detected in 13 samples, but some samples showed very weak peaks at 741, 271 and 268 nm. There was no evidence of an absorption band at 737 nm, which is related to a silicon vacancy, in any of the samples.

synthetic diamonds weighing more than 0.1 ct. All displayed absorption at 637 nm due to the N-V⁻ centre and at 595 and 575 nm due to the N-V⁰ centre, but these samples exhibited much stronger absorption at 575 nm than at 637 nm. In addition, some of the stones showed very weak peaks at 741 (GR1), 503 nm (H3), 392 (ND1), and at 271 and 268 nm from isolated nitrogen centres. Among those, the GR1 and 595 nm peaks are related to irradiation and they indicate that these CVD-grown synthetic diamonds have been irradiated. Broad absorption centred at about 500–510 nm associated with the N-V⁰ centre is the cause of the pink colour, a result consistent with current work elsewhere (P.M. Martineau, pers. comm., 2010). Wang (2009) showed that a broad band which has a maximum intensity near 550 nm in a CVD-grown pink diamond is the vibronic band associated with the 637 nm line related to the N-V⁻ centre. In the present study, all the melee CVD synthetic diamond has a strong pink hue and their spectra have a broad band centred at 500–510 nm; the spectra were recorded before ultraviolet exposure to the UV-radiation lamp used in routine gem testing and the DiamondView™. To explore this difference between the broad band position in the spectra and determine whether this spectrum represented that from the as-produced material, we re-measured the absorption spectrum after an annealing experiment on two CVD synthetic diamonds weighing 0.25 and 0.08 ct using a Linkham LK-600 microscope hotstage to around 800 K in air in the dark. After annealing, a significant change was recorded from their original colour of Fancy Intense orangey-pink to Fancy Intense purple (*Figure 8a and b*). A strong broad band centred near 555 nm was recorded, and the relative intensities of absorption bands at 637 and 575 nm reversed after annealing (*Figure 9*). This broad band may be the vibronic band associated with the 637 nm line. The purple hue changed slightly with time when the samples were kept in the dark, but returned to the initial pink colour when the stones were placed under the diamond grading lamp or in daylight for less than half hour. Also the purple colour returned to pink immediately after exposure to strong UV radiation when examined in the DiamondView™ instrument.

Heating to 800 K could increase the 637 nm absorption (related to the N-V⁻ centre) intensity considerably, depending on the electron concentration in the vacancy defect, and result in an intense pinkish purple body colour. However, although the UV radiation exposure from daylight, a diamond grading lamp, gem testing UV lamp or a DiamondView™ instrument may produce a colour change in CVD-grown synthetic diamond from purple to orangey pink after the annealing process, this significant colour reaction may not be seen in natural pink diamond. Natural pink diamonds show a broad absorption band centred at 550 nm that is derived from plastic deformation and most of the stones show the N3 absorption at 415 nm. Natural or HPHT-grown synthetic pink diamonds which have been coloured
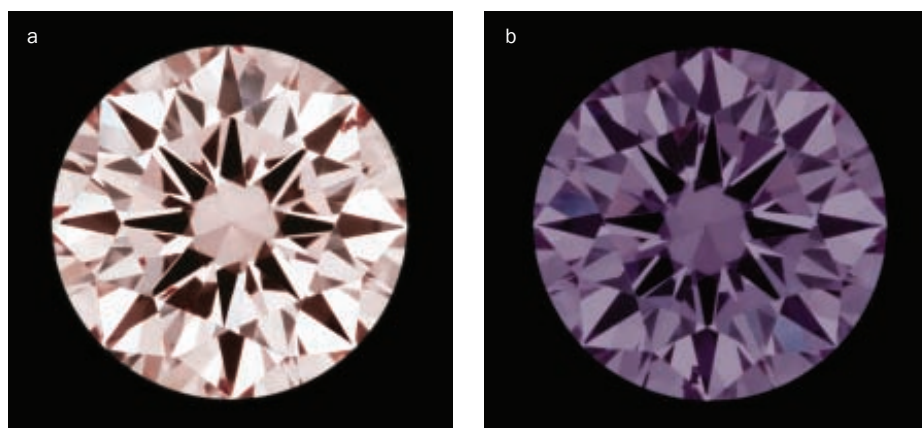

Figure 8: (a) The 0.08 ct CVD-grown synthetic diamond was graded as Fancy Intense orangey pink before the annealing experiment. (b) A significant colour change to Fancy Intense purple resulted when the samples were heated up to 800 K and then cooled over a period of one hour. Photo by K.Hirama.

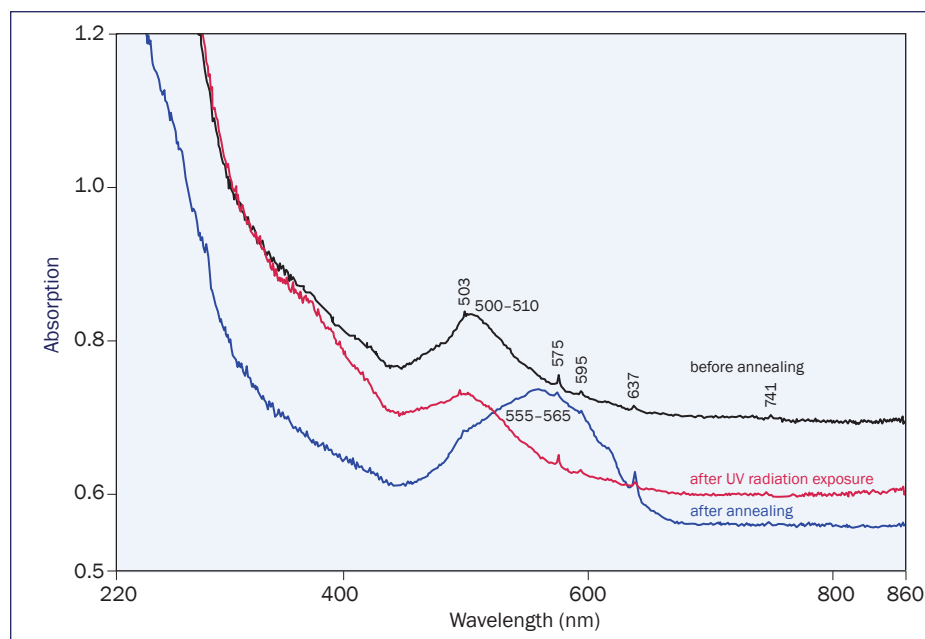## Identification of CVD-grown synthetic melee pink diamond

Figure 9: The UV-Vis-NIR spectra of this orangey-pink 0.08 ct CVD-grown synthetic diamond shows absorption characteristics before and after the stone was annealed at 800 K and after UV exposure under the standard daylight diamond grading lamp, respectively. The spectra show a decrease of absorption at 575 nm, an increase at about 637 nm, and a shift of broad band centre near 500 nm to near 555 nm after annealing at 800 K.
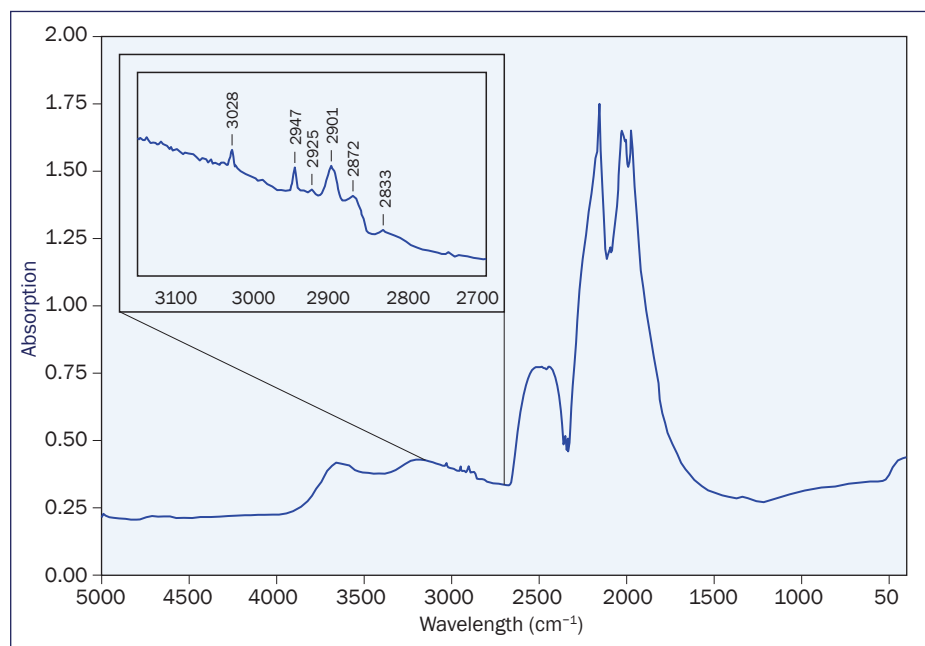

Figure 10: Infrared spectrum typical of our 48 CVD-grown synthetic diamonds which are all type IIa. The small absorption bands shown at 3028, 2947, 2925, 2901, 2872 and 2833 cm⁻¹ were detected in only some of the samples. Isolated nitrogen-related peaks were not detected in any of our CVD diamonds.

pink by irradiation and annealing also show 637 and 575 nm absorptions similar to those in CVD-grown synthetic pink diamonds and the former also show absorption at 415 nm due to the N3 centre.

In addition, any absorption at 737 nm related to the silicon vacancy was not detected in these room temperature spectra (Zaitsev, 2001; Wang, 2009).

FTIR

Infrared spectra were obtained from all 48 stones. As they were apparently free of nitrogen, they were classified as type IIa. Absorption at 1344 cm⁻¹ that originates from isolated single nitrogen atoms was not detected in any sample. However, it is well known that diamonds classified as type IIa using infrared spectroscopy can, nevertheless, contain small concentrations of nitrogen. Fisher and Spits (2000) for example, were also able to detect absorption in the 270 nm band (produced by isolated nitrogen centres) in some diamonds that showed no absorption at 1344 cm⁻¹. A hydrogen-related lattice defect absorption at 3123 cm⁻¹, which has been reported by Fuchs *et al.* (1995a, b) and also reported for stones produced by Element Six and Apollo Diamond Inc. as characteristic of CVD-grown synthetic diamond (Martineau *et al.*, 2004; Wang, 2009), was not detected in our samples. Wang *et al.* (2007) noted that this 3123 cm⁻¹ line and other absorption lines in the near infrared range 5500–8900 cm⁻¹ can be removed by HPHT treatment. In the range 3150–2700 cm⁻¹, we have found one or more weak absorptions of unknown origin at 3136, 3118, 3107, 3028, 2947, 2925, 2901, 2885, 2855, 2846, 2837, 2788, 2773, 2747 and 2724 cm⁻¹ in 29 samples (see *Figure 10* for an example showing some of these peaks). These absorptions presumably originated from stretching vibrations due to hydrogen impurities in CVD-grown synthetic diamond. A C-H absorption at 3107 cm⁻¹ which is common in natural diamond was not recognized as a distinct peak in some samples and was only vague in others.

Photoluminescence (PL)

PL spectra were obtained from all 48 stones stimulated by lasers of wavelengths 633 nm (red), 514.5 nm (green) and 325 nm (ultraviolet) as excitation sources. PL spectra stimulated by the He-Ne 633 nm laser in all 48 CVD diamonds contain a 737 nm peak, due to the presence of the silicon-vacancy defect, and the GR1 zero phonon line at 741 nm (which resolves to a doublet of 740.9 and 744.4 nm) *(Figure 11a)*. In one stone weighing 0.25 ct the

Identification of CVD-grown synthetic melee pink diamond
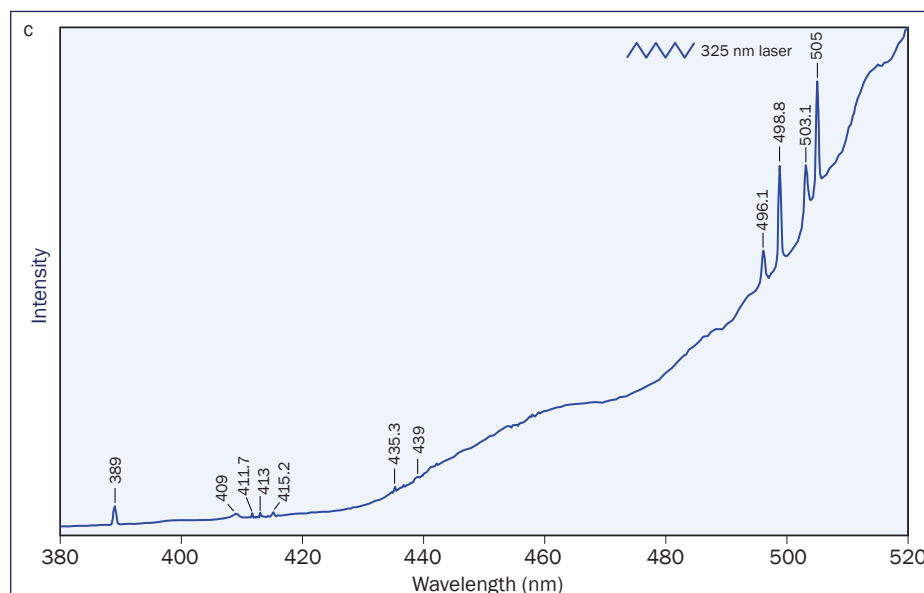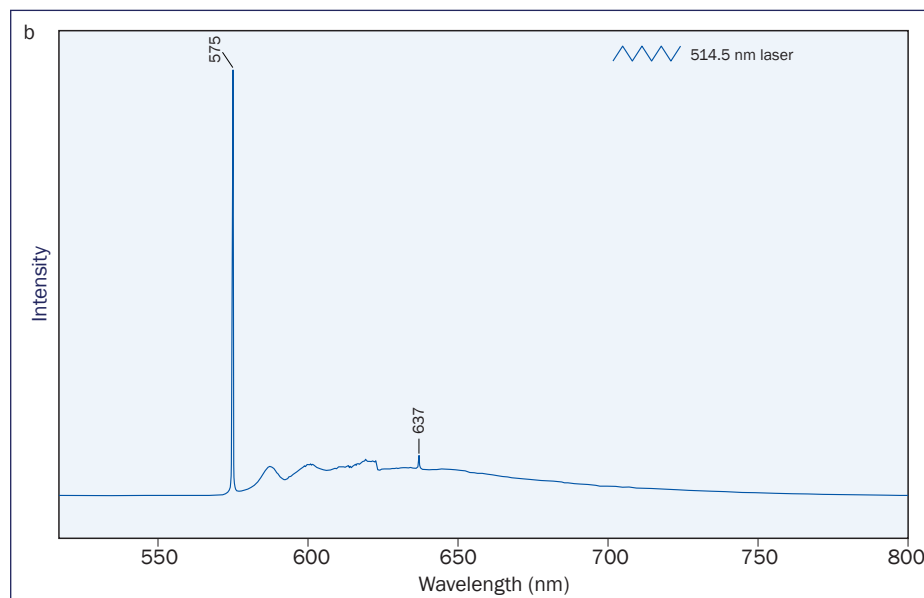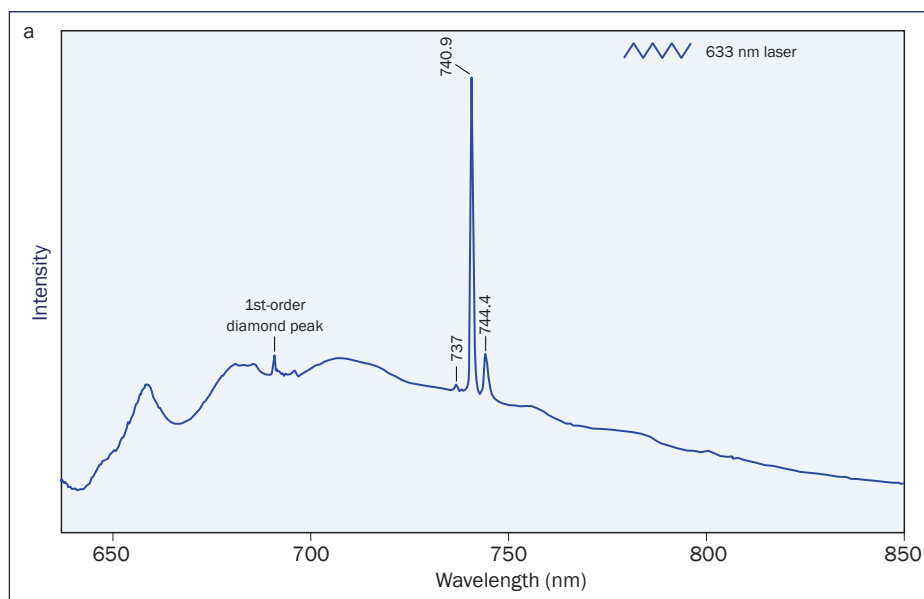
737 nm emission was detected in only one of five spots analysed on the table facet. *Figure 11b* shows a representative spectrum stimulated by the 514 nm laser with the typical presence of 575 and 637 nm peaks. A weak peak at 737 nm was found in only four stones and the peak at 741 nm in only one stone.

PL spectra from the 325 nm laser in all samples show a 503.1 nm (H3) peak along with peaks at 498.8 and 505 nm *(Figure 11c)*. In 31 stones, a 496.1 nm (H4) peak is also present.

In six samples, a very weak peak at 415.2 was detected; this emission line is produced by the N3 centre that is commonly observed in natural diamond (Collins *et al.*, 1990; Martineau *et al.*, 2004), but the spectrum of one stone also contained a weak peak at 435.3 nm which may be unique to CVD diamond (see, e.g., Zaitsev, 2001). In all 48 stones, peaks at 389, 409, 411.7, 413 and 439 nm were detected, and these are probably related to irradiation and annealing.

Luminescence imaging

UV luminescence images of all 48 samples were observed using DTC DiamondView™ equipment. This instrument employs short wavelength UV light (<230 nm) instead of an electron beam that is used in the cathodoluminescence (CL) method and it proves very flexible and effective for preliminary observation before CL analysis.

Of our 48 CVD diamonds, seven show parallel laminated growth structure when examined in the DiamondView™, which may indicate an even rate of deposition of diamond from vapour *(Figure 12a)*. CL images of 13 stones weighing more than

Figure 11: Representative photoluminescence spectra stimulated by three lasers of wavelengths 633, 514.5 and 325 nm.
(a) A 737 nm emission line is present in all spectra obtained using the 633 nm red laser, but was not displayed by most of the samples when stimulated by the other two lasers.
(b) Strong emissions at 575 and 637 nm, due to the N-V centre, are common in all stones.
(c) N3-centre-related luminescence at 415 nm was observed in six of the 48 stones.

Identification of CVD-grown synthetic melee pink diamond

0.1 ct and 13 weighing less than 0.1 ct were then obtained and a similar growth structure was observed in 15 of the 26 stones *(Figure 12b)*. In our experience, CL imaging has a lower penetration depth than UV but provides a highly sensitive image. All the samples showed vivid orange fluorescence due mainly to the N-V centre (in both UV and CL images).

Most natural pink diamonds show blue fluorescence and many display patterns indicating growth parallel to octahedral faces or growth of mixed-habit, in which domains of cubic and octahedral faces co-exist *(Figure 13a)*. Very rarely some natural diamonds may show orange luminescence (due to the N-V centre), but they also show a mosaic pattern that has not been seen in CVD-grown synthetic diamond *(Figure 13b)*. Irradiated pink diamonds similarly show orange fluorescence due to the N-V centre, but when the diamonds irradiated are natural,

Figure 13: Four CL images of natural and synthetic diamond.
(a) CL image of natural pink diamond showing mixed-habit growth, in which growth domains of cubic and octahedral faces co-exist (field of view 8 mm). Photo by H. Kitawaki.
(b) Orange luminescence in a CL image of type IIa natural diamond with a rarely seen mosaic pattern (field of view 4.2 mm). Photo by H. Kitawaki.
(c) Irradiated pink natural diamonds show orange fluorescence (due to the N-V centre) with an intersecting linear pattern (field of view 6 mm). Photo by H. Kitawaki.
(d) HPHT-grown synthetic diamond showing characteristic sector zoning which indicates a combination of {100} and {111} faces (field of view 3.5 mm). Photo by H. Kitawaki.

Figure 12: (a) All CVD-grown synthetic diamonds in this study display a strong orange fluorescence under UV radiation in the DiamondViewTM instrument. Parallel laminated growth layers were observed in seven samples, but no structural features were evident in the other 41 stones. Photo by J. Kawano.
(b) CL images of CVD-grown synthetic pink diamond showing a unique laminated growth structure. Photo by A. Abduriyim.

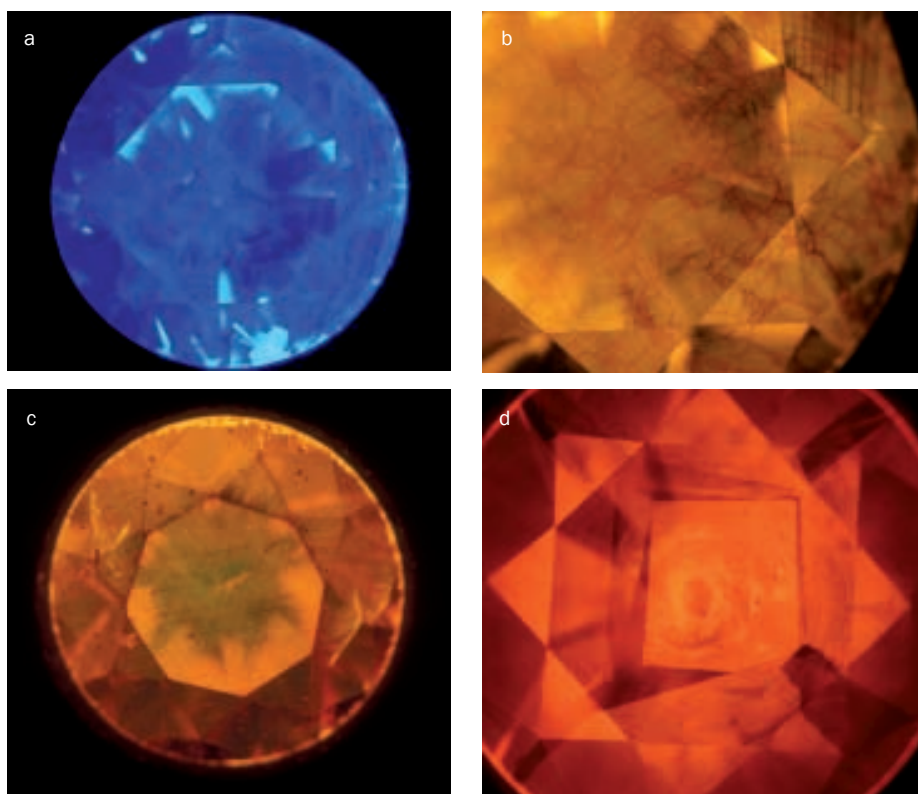they show an intersecting linear pattern *(Figure 13c),* and when they are HPHT-grown synthetic, they show characteristic sector zoning *(Figure 13d)*.

Conclusion

CVD-grown synthetic pink diamonds in melee size can be easily distinguished from most natural pink diamonds (such as those from the Argyle mine) by means of their vivid orange UV fluorescence derived from the 575 nm centre. Diamonds (either natural or HPHT-grown synthetic) coloured pink by irradiation and annealing processes similarly show orange UV fluorescence but they may be distinguished on the basis of their different CL images. In the diamonds studied in the present investigation, the 737 nm peak related to Si was detected in the PL spectra excited by a 633 nm laser; this can be an important indication of

CVD-grown synthetic diamond.

Use of CVD-grown synthetic diamonds in jewellery has just begun and production is limited so far, but the potential of the CVD-grown synthetic diamond for expanded technological application brings a sense of expectation for further technical development. The characteristic features described for the diamonds in this report are in stones being produced at the present time and gemmological laboratories should continue to make every effort to develop identification techniques for such new materials.

Acknowledgements

References

Collins, A.T., Kamo, M., and Sato, Y., 1990. A spectroscopic study of optical centers in diamond grown by microwave-assisted chemical vapor deposition. *Journal of Materials Research,* **5**(11), 2507–14

Deljanin, B., Hainschwang, T., and Fritsch, E., 2003. Update on study of CVD diamonds. *Jewellery News Asia,* No.231, November, 134–9

Fisher, D., and Spits, R.A., 2000. Spectroscopic evidence of GE POL HPHT-treated natural type IIa diamonds. *Gems & Gemology,* **36**(1), 42–9

Fuchs, F., Wild, C., Schwarz, K., Muller-Sebert, W., and Koidl, P., 1995a. Hydrogen induced vibrational and electronic transitions in chemical vapor deposited diamond, identified by isotopic substitution. *Appied Physics Letters,* **66**(2), 177–9

Fuchs, F., Wild, C., Schwarz, K., and Koidl, P., 1995b. Hydrogen-related IR absorption in chemical vapour deposited diamond. *Diamond and Related Materials,* **4**(5–6), 652–6

Martineau, P. M., Lawson, S.C, Taylor, A.J., Quinn, S.J., Evans, D.J.F., and Crowder, M.J., 2004. Identification of synthetic diamond grown using chemical vapor deposition (CVD). *Gems & Gemology,* **40**(1), 2–25

Priddy, S., 2003. See Web list

Wang, W., Moses, T., Linares, R., Shigley, J.E., Hall, M., and Butler, J.E., 2003. Gem-quality synthetic diamonds grown by a chemical vapor deposition (CVD) method. *Gems & Gemology,* **39**(4), 268–83

Wang, W., Hall, M.S., Moe, K.S., Tower, J., and Moses, T.M., 2007. Latest–generation CVD-grown synthetic diamonds from Apollo Diamond Inc. *Gems & Gemology,* **43**(4), 294–312

Wang, W., 2009. See Web list

Zaitsev, A.M., 2001. *Optical properties of diamond.* Springer-Verlag, Berlin, 502 pp

Web list

Priddy, S., 2003. Apollo Diamond to release CVD diamonds in Q4. Rapaport News, < Posted:08/11/03 > http://www.rapnet.com/News/NewsItem.aspx?ArticleID=8374

Wang, W., 2009. 'CVD-Grown Pink Diamond.' GIA News from Research http://www.gia.edu/research-resources/news-from-research/treated_pink_CVD_06.24.09.pdf

The Authors

Hiroshi Kitawaki
Director of laboratory, Gemmological Association of All Japan (GAAJ)-ZENHOKYO, 5-25-11 Ueno Taitoku, Tokyo, 110-0005, Japan
email: h-kitawaki@gaaj-zenhokyo.co.jp

Dr Ahmadjan Abduriyim
Chief research scientist, Research laboratory, GAAJ-ZENHOKYO
email: Ahmadjan@gaaj-zenhokyo.co.jp

Dr Jun Kawano
Research scientist, Research laboratory, GAAJ-ZENHOKYO

Makoto Okano
Senior Research Gemmologist, Research laboratory, GAAJ-ZENHOKYO

Appearance of new bead material in cultured pearls

Prof. Dr H.A. Hänni FGA, Dr M.S. Krzemnicki FGA and Laurent Cartier MSc FGA

Abstract: A range of different materials has already been used as cores in beaded cultured pearls, and now two new alternative options, baroque shaped shell beads and Chinese freshwater cultured pearls, are being used. Experiments with beads of the latter, approximately 6.5 mm across, have been carried out with marine *Pinctada maxima* and *Pinctada margaritifera* oysters. After 13 months, nearly 200 pearls of each kind were harvested. Cross sections and further observations of resulting pearls are described. X-radiographs and X-ray microtomography are found to generally deliver clear evidence for identification. These pearls have been found to be very suitable for subsequent drilling. Natural pearls also have been used as nuclei for producing cultured pearls. The material used is either non-nacreous, brown or of an unattractive appearance. This new kind of cultured pearl is difficult to identify, because the radiographic structures of the natural cores are masking these cultured pearls.

Keywords: baroque-shaped beads, bead nucleus, Chinese freshwater cultured pearls, cultured pearls, South Sea cultured pearls, Tahiti cultured pearls, X-ray microtomography
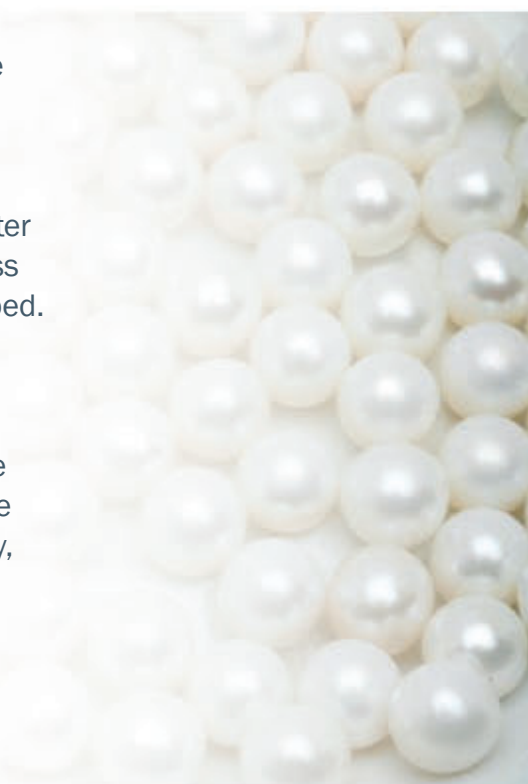
Introduction

Techniques concerning production of cultured pearls have been described in a number of recent books and papers (Müller, 1997; Hänni, 2002; Strack, 2006; Southgate and Lucas, 2009). A number of options for pearling can be selected and combined to produce cultured pearls successfully, and these are summarized in *Table I*.

Traditionally, most beads for cultured pearls have been manufactured from shell material from the Mississippi area, USA (pigtoe, washboard, butterfly, three ridge, dove shell) but since production is in decline and prices are rising, alternative materials are being tested. Recently, an excellent paper comparing different bead materials used in cultured pearls was published by Superchi *et al.* (2008) in which the following materials are mentioned: banded freshwater mother-of-pearl, banded saltwater mother-of-pearl, Tridacna shell and Bironite. The use of lauegrams to detect the structures of beads has been practised for more than

Table I: Possible combinations of parameters to produce cultured pearls — the two major ways are given in blue.

Host and medium	Pearl location in the body	Presence of bead	Examples and comments
Oyster saltwater	gonad-grown	yes	Akoya, Japan; Tahiti; South Sea
		no	'keshi', bead rejected
	mantle-grown	no	new type, baroque shape
		yes	not yet encountered
Mussel freshwater	mantle-grown	no	Biwa, Japan; China; USA
		yes	Chinese, 'coin bead', round
	gonad-grown	no	not yet encountered
		yes	not yet encountered

Appearance of new bead material in cultured pearls
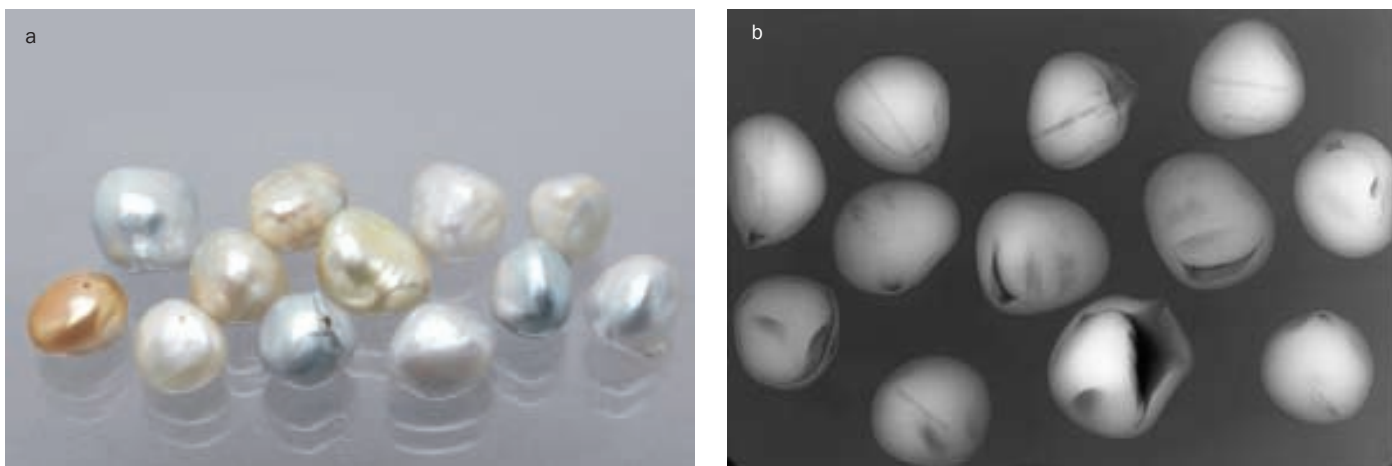
Figure 1: (a) Baroque-shaped South Sea cultured pearls containing irregularly-shaped shell beads. A number of such cultured pearls (largest dimension 17 mm) are seen in the left image. (b) A radiograph showing the irregular outlines of the bead material and some structures typical of growth near the hinge of the shell. Photo © H.A.Hänni and SSEF.

Figure 2: Gonad-grown cultured pearls of P. maxima (left) and P. margaritifera (right) containing a CFCP as a nucleus bead. Diameter of the final product is approx. 9 mm. Photo © H.A.Hänni and SSEF.

Figure 3: A sample of Chinese cultured pearls (mantle-grown, beadless CFCPs) as used for beading of South Sea oysters P. maxima and P. margaritifera. For a first beading of the oyster a diameter of approx. 6.5 mm is required. Photo © H.A. Hänni and SSEF.

50 years, and in this context the structure of Tridacna shell and other non-nacreous shell has been discussed recently by Hanni (2004, 2009a). Besides Bironite, which consists of altered dolomitic marble, pressed barium sulphate beads in different colours have also been reported as cores in engraved dark *P. margaritifera* pearls (Hänni, 2009b). The latest substance used for producing baroque-shaped cultured pearls is irregularly-shaped shell material, used in *P. maxima* (Figure 1).

Another new material, thus far unreported, is probably still being used on an experimental scale. This material is a freshwater cultured pearl and the aim of this article is to shed light on this alternative, as it is likely to be increasingly applied and encountered in future *(Figure 2)*.

From a consumer point of view, the composition of the core in the bead-cultured pearl may not seem to be important as this material is not visible. However, to give the feeling of a pearl, it should have the heft of a pearl (this means that light materials such as plastic are not appropriate). From a production point of view, a suitable material should be accepted by the oyster or mussel and possess properties suitable for drilling. For about 100 years shell beads have satisfied these requirements (Muller, 1997). Nacre has the perfect heft as it is of the same material as natural pearls. But its layered structure sometimes can be a source of difficulties: when the drilling hole is at a low angle to the layers, a tendency to split along the layers can divert the drill off course. When the drill is parallel to the layers, the bead often breaks along the layers. The use of bead material made from the Tridacna shell is now defunct mainly because this bivalve is a protected species, but also because it has a fibrous structure that is difficult to drill due to the criss-cross array of fibres (Hanni, 2009b).

Such constraints are not encountered when concentrically structured nacre, such as that in a beadless cultured pearl, is used as bead material. Considering that Chinese freshwater cultured pearls

Appearance of new bead material in cultured pearls

(CFCPs) of this kind are available in large quantities, close to round in shape, of white colour and at low prices, such material seems a perfect alternative to beads fashioned from shell. The only apparent disadvantage seems to be the lesser degree of roundness compared to the traditional manufactured beads. However, beadless CFCPs can easily be polished to spheres of standard sizes.

Figure 4: Cultured pearls containing the new CFCP beads from P. maxima oysters (white) and P. margaritifera oysters (black) harvested after 13 months. The pearls are between 7.5 and 9 mm across. Photo © H.A.Hänni and SSEF.

The experiment

Mantle-grown beadless CFCPs (Figure 3) were used to study the usability of the new bead material. A second objective was to examine the possibilities of identifying these alternatively beaded pearls in a gemmological laboratory. Because beadless CFCPs may exhibit concentric growth structures similar to those in natural pearls, it is important to find distinguishing features that one can use to differentiate these from natural pearls. Two hundred near-round to round and white to pale cream beadless CFCPs, unprocessed and with a diameter of

approx. 6.5 mm, were delivered to each farm, one working with *P. maxima* and one with *P. margaritifera*. They went through the same preparatory steps in the pearl farms as conventional nacre beads. For comparison, a significant group of oysters was grafted and beaded with standard beads. After 13 months the pearls were harvested and the yield of CFCP beaded pearls was compared with the average of the normal production. The rejection rate was slightly lower for the CFCPs than for the traditional beads. This was the case for both *P. maxima*

and *P. margaritifera*. The final cultured pearls from both farms had diameters between 7.5 and 9 mm. *Figure 4* shows a representative selection of the two lots produced from *P. maxima* and *P. margaritifera* oysters.

Twenty pearls from each production were randomly selected for tests. Some pearls were cut in half and polished so that the equatorial plane could be inspected under magnification (*Figure 5*). Other samples were analysed non-destructively by X-ray techniques.
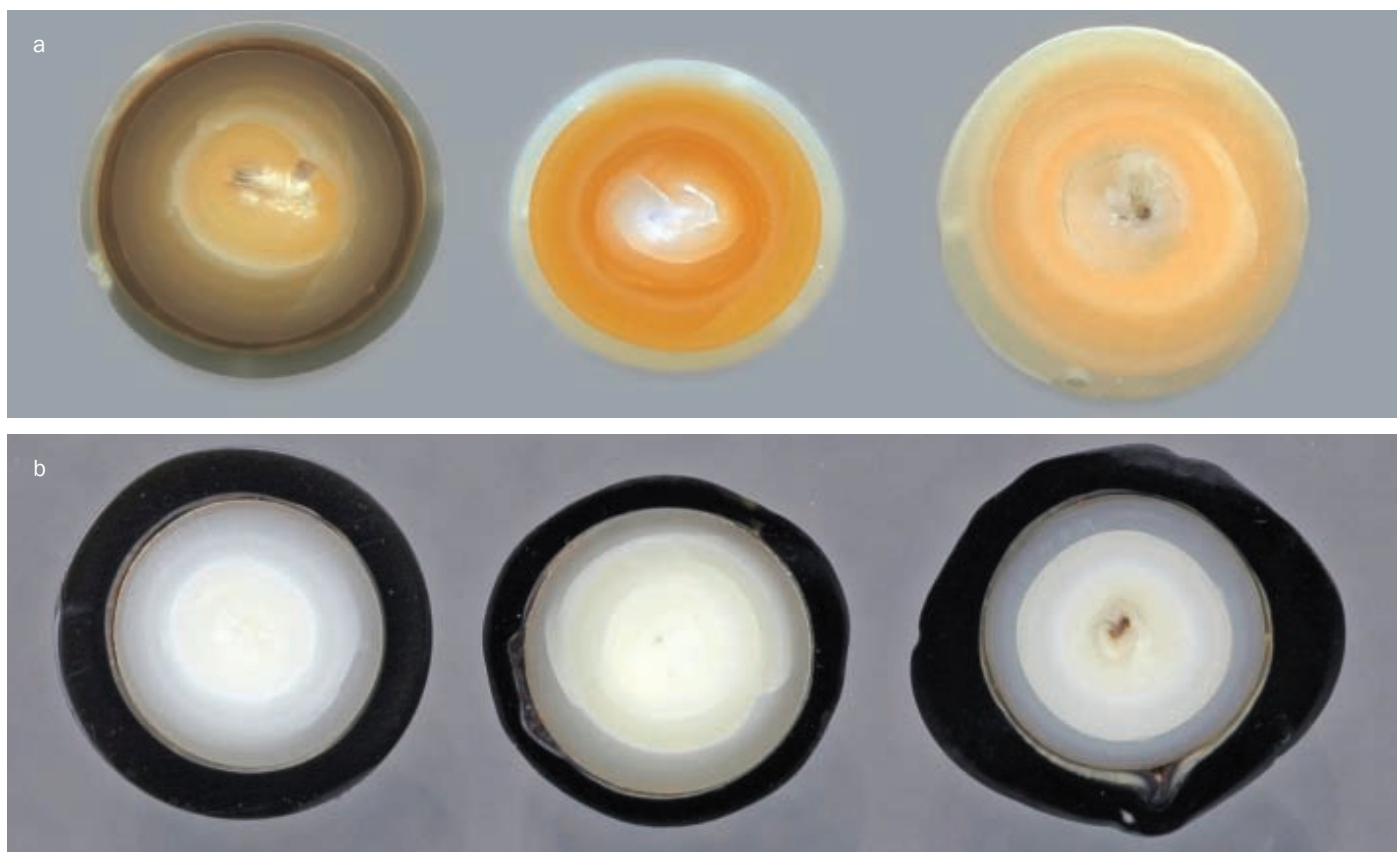

Figure 5: Cross sections through marine cultured pearls, containing a CFCP as a core. (a) Samples from the P. maxima oyster, and (b) those from the P. margaritifera oyster. Photo © H.A.Hänni and SSEF.
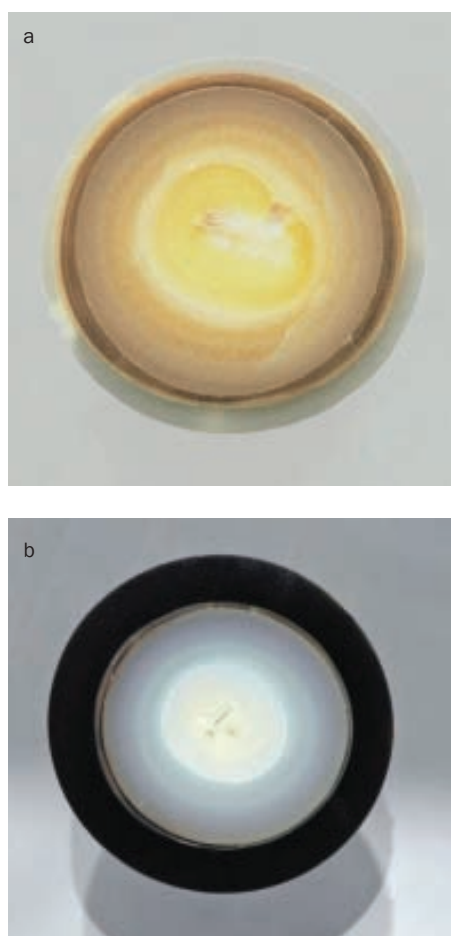
Appearance of new bead material in cultured pearls

Figure 6: Cross-sections through P. maxima and P. margaritifera cultured pearls, each containing a CFCP as a bead. The cavity, typically of complex shape, is visible in the centre and surrounded by a chalky area overgrown by nacre of the freshwater cultured pearl. These beads are coated by (a) white nacre in P. maxima and by (b) dark brown nacre in P. margaritifera oysters. Photo © H.A.Hänni and SSEF.

Identification

The core

The most significant structure visible in the centre of the freshwater pearls used as beads is the central cavity. This complex cavity is bordered by the first precipitation in the young nascent pearl sac, and may be further surrounded by undulating hairlines and fine fissures between subsequent growth layers. In natural pearls, such fissures are concentric and bow-shaped. Drying fissures in natural pearls are usually across the pearl and cut through the concentric growth structure. The area immediately around the central cavity commonly consists of non-nacreous, pale yellow material that may include vaterite (Soldati et al., 2008). This set of observations is typical for the CFCP bead material shown in Figures 5 and 6.

In comparison, natural pearls show an off-round central area consisting of a radiating array of pale brown columns, many of which have been identified as calcite (Lowenstam and Weiner, 1989; Baronnet et al., 2008) (see Figure 7). This inner region contains more organic material and thus absorbs less X-ray energy, consequently appearing darker on the radiograph. It corresponds to the first formation of $CaCO_3$ deposited by the juvenile cells of the pearl sac. With increasing age, the cells change to

producers of aragonite tablets and form a coat of nacre on the primary body. More on the formation of natural pearls is described by Hänni (2002) and Bari and Lam (2009).

The overgrowth

An average nacre thickness of 0.5 – 1.8 mm was measured on the beads. This overgrowth is less than usual because the growth time was only 13 months. Usually the overgrowth on the experimental beads sits very tightly on the CFCP. In some the innermost deposition on the bead is of columnar $CaCO_3$; this forms before the pearl sac begins to precipitate $CaCO_3$ as aragonite tablets, i.e. nacre; in others, aragonite is deposited directly on the bead. Most white South Sea pearls are close to round, but it is not uncommon for the black Tahiti pearls to have circle and drop shapes; this shape variation is not related to the material of the beads.

Identification by X-ray shadow pictures on film or digital image is usually a straightforward procedure for beaded pearls. The presence of a central cavity in the shape of a so-called 'moustache' structure, which is typical of beadless cultured pearls including CFCPs, would be a clear indicator of a bead's character (see Figure 8). In situations where such structures are not clearly shown at the first attempt, a rotation of the pearl can result in better exposure of the cavity. Any flat
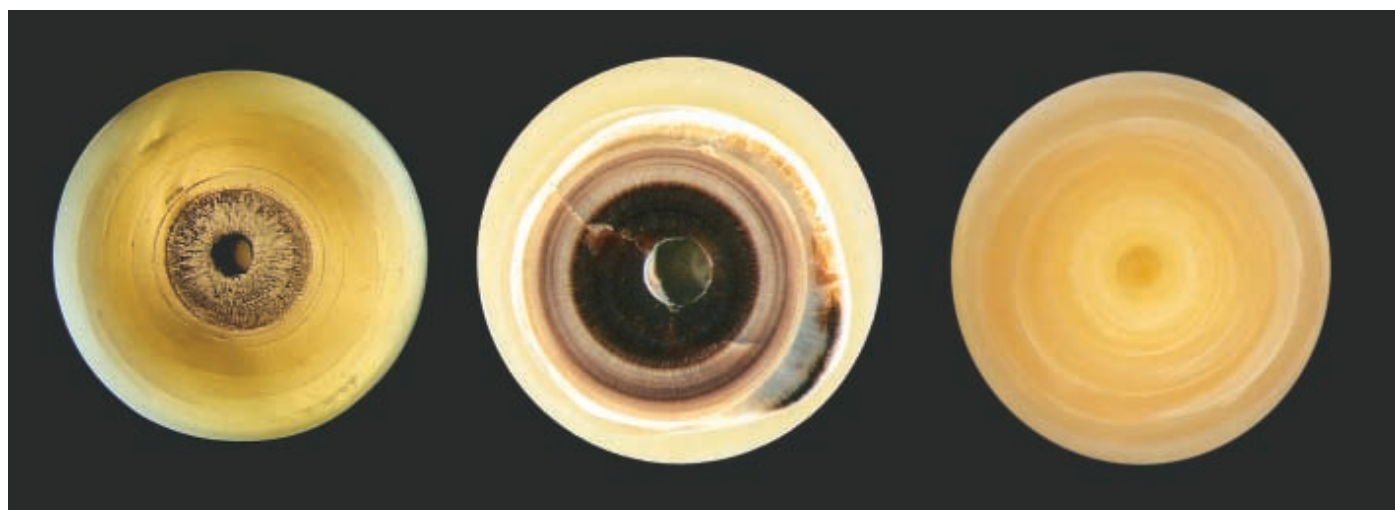
Figure 7: Sections through three natural pearls. The centres show radiating prismatic $CaCO_3$, containing brown organic material. This core is overgrown with nacre. Some natural pearls, such as the sample on the right, may lack the columnar brown part. Photo © H.A.Hänni and SSEF.

Appearance of new bead material in cultured pearls
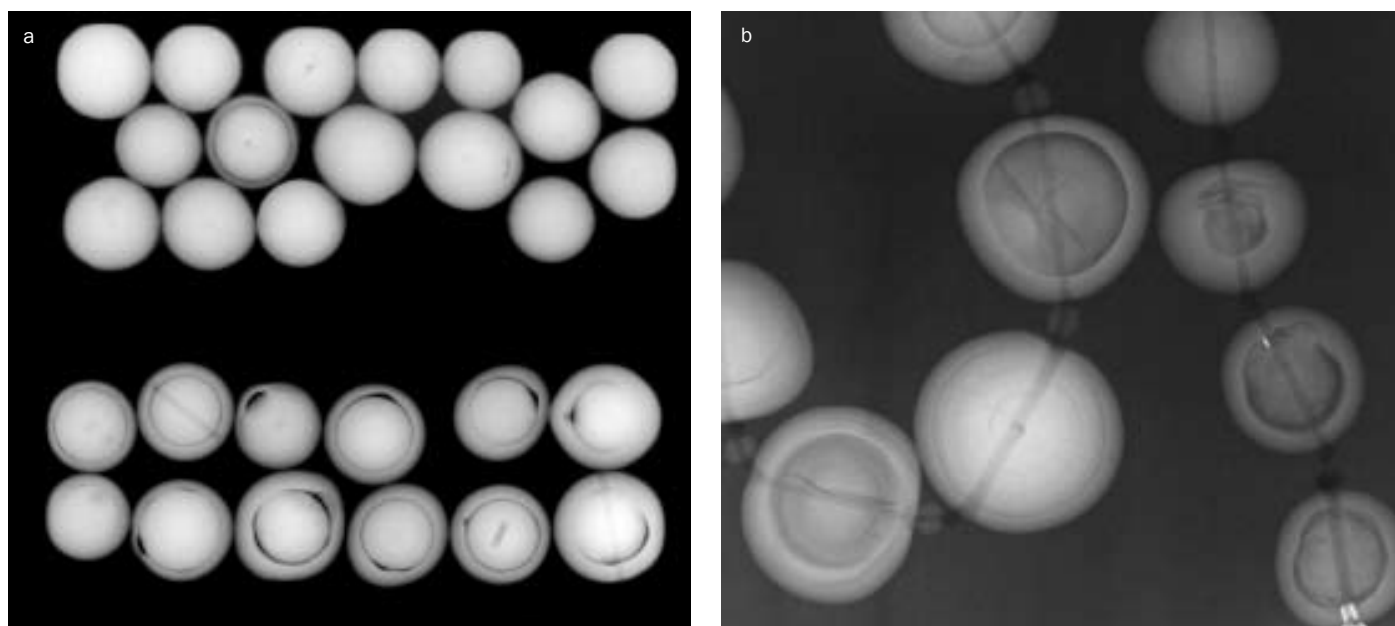
Figure 8: (a) Traditional X-radiographs, the central parts of which are examined under magnification, to look for the 'moustache' structure. The upper group are white South Sea beaded cultured pearls and the lower group consist of black South Sea cultured pearls. The straight line shadows indicate drill holes in three pearls of the lower group, and most pearls in this group show a clear gap between bead and nacre overgrowth.
(b) Radiographs of natural pearls with off-round outlines, most showing a conchiolin-rich central area and irregular wavy lines indicating fissures caused by drying. Only one pearl lacks a conchiolin-rich centre and that is the white one in the lower centre of the picture. Photo © H.A.Hänni and SSEF.

structure appears much more clearly when it is parallel to the incoming rays, thereby producing a sharp line. When the cavity is rather thin and flat and perpendicular to the incoming rays, it may be difficult to detect. It thus becomes clear that dynamic investigation such as real time radiography (Sturman, 2009) with the opportunity to rotate specimens is preferable for obtaining reliable results more quickly. In addition to the comments made above, it is worth noting that since freshwater pearls contain manganese, they are more absorbent of X-rays and thus appear brighter on the radiograph.

The latest development in pearl investigation by X-ray technology is X-ray microtomography (Strack, 2006, 2007; Wehrmeister *et al.*; 2008, Anon, 2009; Krzemnicki *et al.*, 2009). By three dimensionally recording the radio density of a pearl in very small increments, a complete representation of the interior of a pearl is obtained. Sections in all directions can be looked at and ultra-fine structures in pearls can be visualized. With a set of mapped tomography data it is possible to view a scan through a pearl, and find the features necessary for identification. As this instrument remains
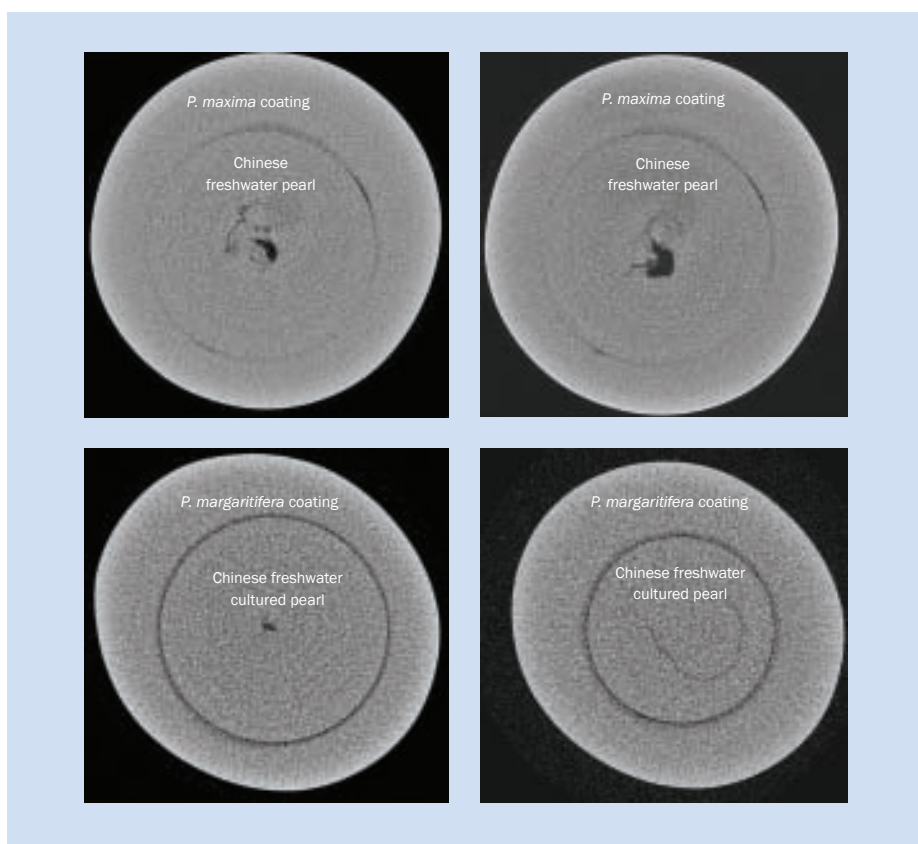
Figure 9: X-ray microtomographic sections of beaded cultured pearls. The beads consist of beadless CFCPs, showing central cavities and some irregular hairline fissures. The upper images are virtual cross-sections of a pearl from a white South Sea oyster P. maxima *taken at different levels and showing close contact of the bead and the nacre overgrowth. The lower images are virtual cross-sections of a pearl from a dark South Sea oyster* P. margaritifera. *This one has a prominent gap between core and overgrowth. Image © S. Friess, Gloor Instruments.*

Appearance of new bead material in cultured pearls

expensive, it is currently used in rather exceptional situations where conventional radiography is not conclusive. To obtain tomographic data for the new type of beaded cultured pearls, two samples were recorded at Gloor Instruments (Uster) using a SkyScan microtomograph. Two cultured pearls with CFCP beads are shown in *Figure 9*. The CFCPs show central cavities and some irregular hairline fissures and again the boundary between the bead and the nacre coating is much more pronounced in the *P. margaritifera* oyster (lower) than in the *P. maxima* oyster. However, these are preliminary results and subject to change when more examples are available.

Larger CFCPs (from 9 mm upwards) can serve as second beads, after the first cultured pearl has been harvested, when the pearl sac is recharged.

Discussion

The purpose of creating a beaded cultured pearl is to produce an object of given shape and size coated with nacre to appear like a natural pearl. In the classical Japanese akoya cultured pearls the excellent nacre of the *Pinctada maxima* oyster can cover the nucleus with less than a millimetre of deposition, but this is only a thin paintwork to hide the nature of the core. Cultured pearls of better qualities usually display more than a millimetre of overgrowth. With this the body grows in size and optical attractiveness.

Seeing that the use of beadless freshwater cultured pearls in saltwater oysters causes no apparent problems, the next step seems logical. Unattractive natural pearls could be provided with a more beautiful surface if they stayed for a while in a farm-oyster. In order to recognize and understand the features of possible future varieties of cultured pearls, one author (HAH) has been experimenting with natural pearls as bead material. This turns out to be very relevant as recently cultured pearls with natural pearls as beads have reached the pearl trade, see reports on the internet (Gemlab, 2010; SSEF, 2010). This situation has similarities with that of

blue sapphire in the 1980s. At that time, greyish unattractive rough corundum (geuda) could be transformed into a transparent blue gemstone rivalling natural sapphire. Although the pearl and sapphire technologies are different, the general aim is the same — that of transforming unattractive natural objects into good-looking and desirable jewels.

Conclusions

Market pressure for large, fancy-shaped cultured pearls has stimulated the use of baroque shaped pieces of shell to use as nuclei for South Sea cultured pearls. Using radiographs, these pearls are easily identified as cultured. Now a new bead material, which can be used for the first beading where a pearl sac has to be formed from a tissue graft around a spherical hard nucleus, has been found for cultured pearls: CFCPs are a viable replacement for beads cut from shell material. Experiments have shown that the new bead material gives good results in white South Sea oysters *P. maxima*, and dark South Sea oysters *P. margaritifera*. In a gemmological laboratory the CFCP beads can be identified using conventional radiography or X-ray microtomography. In each method the typical characteristics, a central complex cavity 'moustache' and undulating dark lines, can be detected. The comparative costs of these CFCP beads and conventional shell beads will probably determine whether this new bead material will be preferred in the trade. Since the structure of a CFCP bead is concentric, it is suitable for most drilling purposes as any variation in hardness due to growth factors will tend to be perpendicular to the drill direction.

Use of natural pearls of low quality (nacreous or non-nacreous) as beads is pushing the gemmological laboratories to develop new testing methods, and adapt terminology. Indeed, in some instances the authenticity of a pearl cannot conclusively be decided; structures such as those shown in *Figure 6* are no longer proof of authenticity. Some non-nacreous pebbles of columnar calcite have been called 'unripe pearls' by one author (HAH). Such 'pearls' have been

harvested before deposition of a nacreous layer by the pearl sac, the latter still being at a juvenile stage before developing the capacity to form aragonite (Hänni, 2002). It seems that the lack of a nacreous layer on a pearl can now be remedied by a visit to a domestic oyster, but then of course, the status of the pearl changes from natural to cultured.

References

Anon, 2009. SSEF offers X-ray microtomography as a client service for pearl testing. *Jewellery News Asia*, 304, 47

Bari, H., and Lam, D., 2009. *Pearls*. Skira, Milan. ISBN 978-99921-61-15-9

Baronnet, A., Cuif, J.P., Dauphin, Y., Farre, B., and Nouet, J., 2008. Crystallization of biogenic Ca-carbonate within organo-mineral micro-domains. Structure of the calcite prisms of the Pelecypod *Pinctada margaritifera* (Mollusca) at the submicron to nanometre ranges. *Min. Mag.,* **72**(2), 617–26

Hänni, H.A., 2002 (see web list)

Hänni, H.A., 2004. Gem News: 'Shell pearls' with Tridacna shell clam beads. *Gems & Gemology*, **40**(2), 178

Hänni, H.A., 2008. *The different kinds of cultured pearls.* Proceedings of the 2nd International Gem and Jewellery conference, Bangkok, ISBN 978-974-519-218-8, 231-233

Hänni, H.A., 2009a (see web list)

Hänni, H.A., 2009b. Zur Flammenstruktur bei einigen porzellanartigen Perlen (Explaining the flame structure of some non-nacreous pearls). *Gemmologie. Z. Dt. Gemmol. Ges.,* **58**(1/2), 47–52

Appearance of new bead material in cultured pearls

Krzemnicki, M.S., 2010 (see web list)

Krzemnicki, M.S., Friess, S., Chalus, P., Hajdas, I., and Hänni, H.A., 2009. New developments in pearl analysis: X-ray microtomography and radiocarbon age dating. *Journal of the Gemmological Association Hong Kong* (in press)

Lowenstam, H.A., and Weiner, S., 1989. *On Biomineralization.* Oxford University Press, Oxford

Müller, A., 1997. *Zuchtperlen , die ersten hundert Jahr*e. Andy Müller and Golay Buchel Holding S.A., Lausanne, Switzerland. ISBN 4-9900624-1-8

Soldati, A.L., Jacob, D.E., Wehrmeister, U., Häger, T., and Hofmeister, W., 2008. Micro Raman spectroscopy of pigments contained in different calcium carbonate polymorphs from freshwater cultured pearls. *Journal of Raman Spectroscopy*, **39**, 525–36

Southgate, P.C., and Lucas, J.S., 2008. *The Pearl Oyster.* Elsevier, Oxford

Strack, E., 2006. *Pearls.* Rühle-Diebener-Verlag, Stuttgart

Strack, E., 2007. Computer tomography – a new testing method for pearls. *Gems & Jewellery*, **16**(5), 10

Sturman, N., 2009 (see web list)

Superchi, M., Castaman, E., Donini, A., Gambini, E., and Marzola, A., 2008. Nucleated Cultured Pearls: What is there inside? *Gemmologie. Z.Dt. Gemmol.Ges.,* **57**(1/2), 33–40

Wehrmeister, U., Jacob, D.E., Soldati, A.L., and Hofmeister, W., 2008. *Computerised x-ray microtomography: A non destructive insight into the internal structures of pearls.* Extended abstract, Proceedings of the 2nd International Gem and Jewellery conference, Bangkok, ISBN 978-974-519-218-8, 214-217

Web list

Gemlab, 2010. Important Pearl Laboratory Alert. Gemnotes 1(2), May 2010. http://www.gemlab.net/website/gemlab/fileadmin/user_upload/GEMNOTES/Gemnotes-16-05-10.pdf

Hänni, H.A., 2002. SSEF Tutorial 'Pearls' (CD-ROM), www.ssef.ch

Hänni, H.A., 2009a. Engraved cultured pearls with an unexpected bead. *SSEF Facette,* 16, p.11, http://www.ssef.ch/en/news/facette_pdf/facette16_small.pdf

Krzemnicki, M., 2010a. SSEF Newsletter (12 May 2010). Trade Alert: 'Keshi' cultured pearls are entering the natural pearl trade. http://www.ssef.ch/en/news/news_pdf/newsletter_pearl_2010May.pdf

Krzemnicki, M., 2010b. SSEF Newsletter (20 May 2010). Addendum: And what happens with the beaded cultured pearls? http://www.ssef.ch/en/news/news_pdf/newsletter_pearl_2010May_add.pdf

Sturman, N., 2009. The microradiographic structures of non-bead cultured pearls. August 20 2009. *Lab Notes*, http://www.giathai.net/lab.php

The Authors

Prof. Dr H.A. Hänni (corresponding author)
Research Associate, SSEF Swiss Gemmological Institute, Basel, Switzerland
email: info@gemexpert.ch

Dr Michael Krzemnicki
SSEF Swiss Gemmological Institute, Basel, Switzerland
email: gemlab@ssef.ch

Laurent E. Cartier
Department of Environmental Sciences, University of Basel, Bernoullistrasse 30, CH-4056 Basel, Switzerland

The over-grading of blue-fluorescent diamonds: the problem, the proof and the solutions

Michael D. Cowing

Abstract: Decades after the establishment in the mid-twentieth-century of ultraviolet-free illumination for colour grading a diamond, an examination of diamond trade and laboratory grading practices finds nearly everyone employing some type of fluorescent tube lighting containing significant ultraviolet. This paper demonstrates and quantifies the over-grading of blue-fluorescent diamonds that often can result. Simple methods are proposed that, by themselves or in combination, provide inexpensive and workable solutions to resolve this problem.

Keywords: colour grading, diamond, fluorescence

Introduction

For over a hundred years, it has been recognized that the light yellowish tints in a type 1a diamond combine with the various amounts of blue fluorescence, stimulated by daylight and other illumination containing ultraviolet (UV) energy, to give blue-fluorescent diamonds a whiter perceived colour than the colour seen in lighting where fluorescence is not stimulated to a noticeable degree.

The problem is how to colour grade blue-fluorescing diamonds, which can appear a whiter colour grade in daylight than their colour as seen indoors under typical artificial lighting.

Not long after Robert Shipley founded the Gemological Institute of America (GIA) in 1931, he recruited academic members to a GIA advisory board to help advance the gemmology movement in America. An important contributor among these members, especially in the field of diamond science, evaluation and valuation, was Frank Wade. Wade was a

pioneer in America of "the first series of scientific articles (from 1915 to 1948) on diamonds and gems written especially for the jeweler" (Gilbertson, 2007). Given his own studies and input from diamond experts and educators like Wade, it is no surprise to find Shipley concerned about fluorescence in the colour grading of diamonds. He addressed this fluorescent diamond grading problem in *Gems & Gemology,* 1941. There he says: "One of the most important causes of the anomalies that so often trouble a diamond grader is the change of colour shown by many fluorescent stones when viewed under different light conditions. Often a fluorescent diamond which appears slightly yellowish under artificial light, appears distinctly bluish in daylight" (Shipley and Liddicoat, 1941).

This simple term 'daylight' disguises the large variation in UV content depending on time of day, geographic location, and whether or not the day was sunny or cloudy. With the perceived

colour of fluorescent diamonds varying with the illumination, what lighting should be used in laboratory colour grading? Historically, the standard lighting for colour grading was 'northern daylight', such as that through north-facing windows, for example in the Israel Diamond Exchange *(Figure 1)*.

In 1941, the GIA produced their first diamond colour grading instrument called the Diamolite (later renamed the DiamondLite), using an incandescent filament type of light source and a 'daylight filter' which produced "the equivalent of north light without the UV radiation" (GIA, 1969). At the same time the GIA stated that "a reasonably good substitute for the DiamondLite can be made by adapting a simple desk lamp fixture containing cool white fluorescent tubes". However, they caution: "The disadvantage of this kind of illumination is that fluorescent tubes emit a significant percentage of UV radiation. Although this does not affect the grading of non-

Figure 1: Trading floor of the Israel Diamond Exchange. (Inset) A closer look at the lights in use.
Courtesy of the Israel Diamond Exchange.

fluorescent stones, it causes fluorescent diamonds to be graded higher than is actually warranted due to the neutralizing, or masking effect, of the fluorescent colour on the true body colour" (GIA, 1969). Yet, by the 1970s we find that gemmologists and the diamond trade worldwide are universally using some form of UV-emitting fluorescent light to colour grade diamonds. An important example is the later version of the GIA DiamondLite that substituted unfiltered fluorescent tubes for the daylight-corrected incandescent light source in the early model.

In 1997, Moses *et al.* indicated that digital radiometer readings of UV content revealed similar intensities of long-wave UV content in four sources of fluorescent lighting including the Verilux tubes in the DiamondLite. They also found "indirect daylight through our windows has about as much UV radiation as the fluorescent light sources". With the GIA's finding that "fluorescent lighting" and "daylight through a window" have a similar amount of UV radiation, it would be expected that blue-fluorescing diamonds would be perceived to be whiter in daylight through a window and in the DiamondLite than they would when viewed on social occasions in indoor artificial lighting.

In 2008, King *et al.* described the evolution of colour grading lights and how the original UV-free source had changed to one with characteristics of daylight including its fluorescence-stimulating UV component. They concluded: "We believe that a standard light source for diamond colour grading should have key characteristics of daylight, including a UV component." (King *et al.*, 2008, p.320.)

GIA's study findings and conclusions are best summed up in the words of Moses (2001) who stated the GIA belief "that the best man-made light sources reproduce all the characteristics of traditional north daylight, including the 'good deal' of UV ... Not only do members of the trade typically buy and sell diamonds under lighting conditions that have a UV component, but they also colour grade them with a lamp that has

The over-grading of blue-fluorescent diamonds: the problem, the proof and the solutions

Figure 2: Six diamonds graded I colour in a DiamondLite showing a range of fluorescence. Picture reproduced courtesy of GIA; these three photographs were used in the assembly of Figure 3, I colour set pictured in the paper by Moses et al., 1997, p. 249

some UV content. Grading in a UV-free environment is contrary to this accepted practice and will cause confusion." (Moses, 2001).

However, not addressed in the 1997 and 2008 articles was consideration of the intensity of the UV and visible-violet (VV) energy present at typical light-to-diamond distances in normal viewing circumstances compared to the energy intensity present at the much closer distances to the lighting in grading instruments.

The key point is that most diamonds are seen in most forms of artificial illumination at night or indoors out of daylight, and in these viewing environments the UV and visible violet are too weak to stimulate grade-whitening fluorescence. In contrast, the relatively strong UV and visible violet at typical distances of 1 to 7 in. from the fluorescent tubes of grading instruments can stimulate a good deal of fluorescence which whitens the appearance of a diamond. The use of such unfiltered fluorescent lighting has today become almost universal and is an abandonment of the diamond grading standards originally established by GIA in accordance with diamond-trade practice at that time.

A closer look at the Israel Diamond Exchange in *Figure 1 (inset)* reveals the

kind of fluorescent desk lamps being used in diamond grading. There is nearly universal use of fluorescent lighting in spite of it being the very same source of grading illumination that was originally considered by many to result in the over-grading of fluorescent diamonds. Corrective solutions are needed to this almost universal use of some form of fluorescent light to colour-grade diamonds at major grading laboratories and within the trade.

Where is the proof of the over-grading of many blue-fluorescing diamonds? To quote Tashey (2009): "I was shocked when I made the initial discovery, by placing a clear, UV filter, plastic film between the Verilux lamps in the GIA DiamondLite and the diamonds to be graded, that stones with very strong blue fluorescence could change to a lower colour by three or four letter grades." He spoke of a 0.89 ct marquise brilliant with 'Very Strong Blue' fluorescence: "In the DiamondLite [Verilux lamps, without UV filter] this stone was graded table down as a high 'D'. ... When viewed table down, with the UV filter between the lamps and the diamond, the colour grade of the diamond shifted to that of a low 'H'." Tashey (2000) had earlier found that diamonds with 'medium' to 'strong' blue

fluorescence generally shifted one to two colour grades when the filter was used.

This example in a 'Very-Strong-Blue' fluorescing marquise diamond of close to a five grade colour improvement to high D in the DiamondLite from the UV-free colour grade of low H may be met with disbelief by professionals in the trade, all of whom grade in some form of UV-containing fluorescent illumination, and so have not witnessed this large a shift in colour. However, the data base in the current investigation contains a 0.63 ct marquise diamond with a similar close to five grade improvement in the DiamondLite over its unimproved colour as determined in UV-free artificial lighting.

Evidence of the over grading of blue-fluorescent diamonds was also contained in a photograph in the paper by Moses *et al.* (1997). Their *Figure 2* includes a set of six diamonds graded I colour in the DiamondLite and these show clear colour differences. The photograph was taken in incandescent illumination (Erica Van Pelt, pers. comm.,) which (by its nature and distance from the subject) was UV-free compared to the DiamondLite. This picture is reproduced here courtesy of GIA *(Figure 2)* and affords an opportunity to relate the colour differences, particularly in the face-up images, to the strengths of fluorescence. The fluorescent strengths, from left to right, are: 1 Medium, 2 Very Strong, 3 Faint, 4 Strong, 5 None and 6 Strong

Stones 2, 4 and 6 appear to have substantially more colour than the other three in spite of having been graded as I colour. It is no coincidence that these are the three with the strongest blue fluorescence. Revealed in this relatively UV-free lighting of the photographer is the darker colour unenhanced by blue fluorescence of the strongly fluorescing members of this I colour set.

While the difference is apparent, the magnitude of over-grading relative to the colour unenhanced by fluorescence cannot be quantified from this photograph. That quantification was accomplished by analysis of grading of the 25 diamond data base central to this study.

The over-grading of blue-fluorescent diamonds: the problem, the proof and the solutions

Figure 3: The 25-diamond data base in lighting showing diamond brilliance and fire.
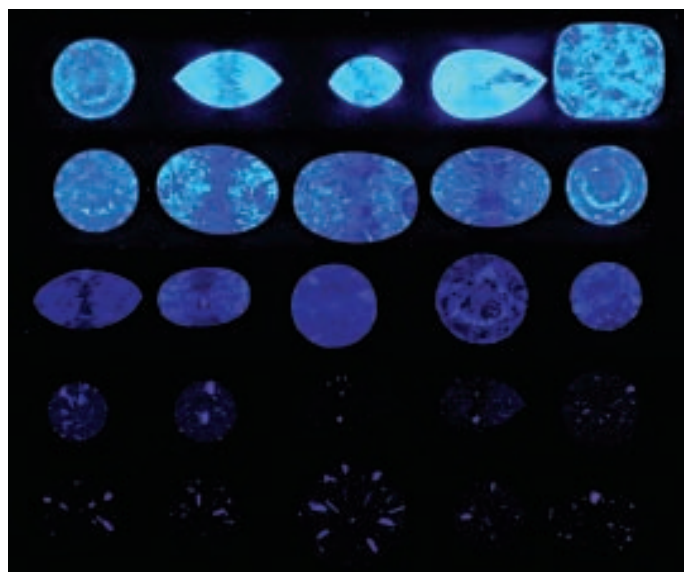

Figure 4: The 25-diamond data base in long wave UV 'black lighting'. Not to be mistaken for fluorescence are the flashes of visible violet reflected from the diamonds with negligible fluorescence in rows four and five.

Investigation

To explore and quantify the extent of the over-grading of blue fluorescent diamonds, and find possible solutions to this problem, a set of 25 diamonds with fluorescent strengths from 'none' to 'very strong' was assembled . The analysis contains not only the author's grading of the diamonds in several lighting environments, including the DiamondLite and the DiamondDock, but also the grading of GIA's Gem Testing Laboratory (GIA GTL) and the American Gem Society's Laboratory (AGSL). GIA's current grading environment and light grading standard consists of grading at a 7 in. distance from the twin 17 in. Verilux fluorescent tubes in their DiamondDock. It is the standard in use at GTL since 2000 (R. Geurtz, pers. comm.). The GIA grading reports on the diamonds in this study are all dated post-millennium. AGSL's grading of these diamonds was likewise accomplished in a DiamondDock.

One goal was to determine the range of perceived colour improvement or change in each fluorescent strength category caused by grading in these various lighting circumstances. A second goal was to investigate techniques to create illumination in which fluorescence is not noticeably stimulated. This was pursued both by using new, UV-free LED lighting and by modifications to currently used fluorescent tube lighting.

Observations on the five fluorescence strengths in the 25-diamond data base.

Investigation and photography of the fluorescence properties of the data base's 25 diamonds utilized a Raytech UV Lamp (black light), Model LS-88, with an LW-8, 8 in., 6W, mercury vapour, LWUV tube. This delivers an intensity of UV radiation centred near 360 nm of 180 µW/cm² at a distance of six inches.

The 25 diamonds are set out in *Figure 3* in five rows of five diamonds of each fluorescent strength. They are numbered from 1 to 25 from left to right and top to bottom. Strengths of blue fluorescence are indicated in grading reports by the major laboratories with the descriptions of Very Strong Blue, Strong Blue, Medium Blue, Faint or None. These five groups of fluorescent strength are visually apparent in *Figure 4*.

There can be variation in these descriptions from lab to lab especially for borderline stones. Nevertheless, for the purposes of this study it is desirable to assess fluorescence as accurately as possible.

Observations of blue fluorescence in particular data-base diamonds

Looking at *Figure 4*, the 'Very Strong Blue' fluorescing diamonds, 2, 3 and 4

appear the strongest fluorescing in this category. Diamond 5 is borderline with GIA calling it 'Strong Blue' and AGS 'Very Strong Blue'. Diamonds 1 and 6 appear identical in strength with both called 'Very Strong Blue' by AGS and a third lab, International Gemological Institute (IGI) calling 6 only 'Strong Blue'. The laboratories' descriptions were in agreement in the rest of the row of 'Strong Blue' diamonds: 7, 8, 9 and 10. The 'Medium Blue' row of diamonds 11–15 were so graded by everyone with the exception of 15 which only GIA called 'Strong Blue'.

So, this analysis and the photograph in *Figure 4* show reasonable consistency in describing fluorescent strength with an occasional miscategorization or equivocal borderline case.

Note the wide range of intensity in the 'Very Strong Blue' category. The ten diamonds in the 'Faint' and 'None' categories (which AGSL calls Negligible) are important to this investigation as a control group to provide data concerning variation in colour grading when there is no variability due to fluorescence.

### Measurements of UV content in natural and artificial lighting

The degree of any perceived colour improvement due to fluorescence is proportional to both the diamond's

The over-grading of blue-fluorescent diamonds: the problem, the proof and the solutions

Box A: Analysis of fluorescence of diamond No. 5 in this investigation

Thomas Hainschwang has kindly provided the following details: fluorescence measurements of the 3.02 ct diamond 5 were obtained by exciting the diamond with near-monochromatic light in steps of 5 nm from 340 to 415 nm, produced from a Xenon light source via a monochromator; by this technique it is possible to excite fluorescence with any desired wavelength of the lightsource. The fluorescence was recorded for each excitation wavelength with a high sensitivity CCD spectrometer and the results normalized. Each recorded curve (in black) in *Figure A* represents fluorescence spectrum excited by the the near-monochromatic light tuned to distinct wavelengths. To give an example, the first emission curve in *Figure A* represents the intensity of the fluorescence of the diamond when excited by near-monochromatic light with a central wavelength of 340 nm. The 3D graph in *Figure A* thus shows the fluorescence intensity profile when the diamond is excited with such near-monochromatic light of various wavelengths.

These curves show what early diamond industry experts did not know, not just UV light, but also visible light up to 415 nm excites the blue fluorescence caused by the N3 centre (three nitrogen atoms surrounding a vacancy) in any diamond containing appreciable concentrations of A and B aggregates, and consequently N3 centres. Consequently wavelengths up to 415 nm can be important
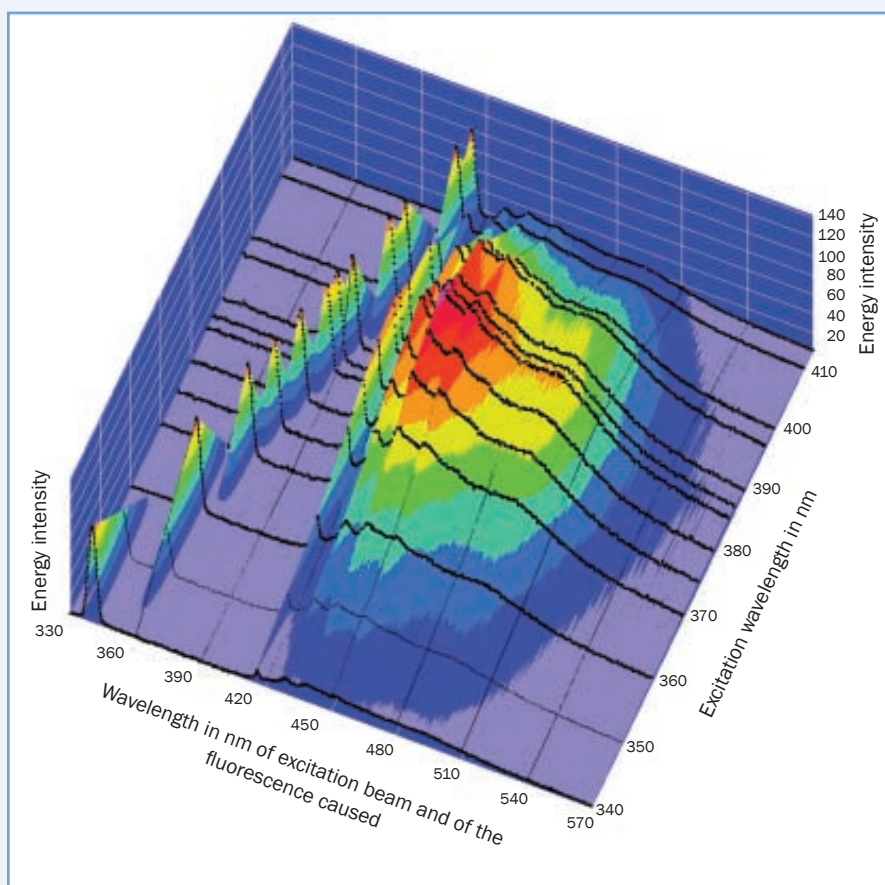
Figure A. Blue fluorescence intensity stimulated by UV and visible-violet radiation in diamond no. 5. The peaks of the near-monochromatic exciters are shown in the line of peaks on the left, and the fluorescence generated in the diamond is the colour-contoured profile centre-right. Energy intensity is shown in arbitrary units and colour-coded with red being the most intense. Courtesy of Thomas Hainschwang, Gemlab.

contributors to blue fluorescence in Cape Series diamonds. At normal viewing distances from artificial illumination the violet light intensity, just like the UV, is too weak to excite noticeable fluorescence. But observation too close to either fluorescent or incandescent lighting, where the intensity exceeds about 400 fc or 4000 lux, was found to excite blue

fluorescence (fc and lux are the units used in photometry as measures of visible light intensity, as perceived by the human eye. They are analogous to the radiometric unit $\mu W/cm^2$, but with the intensity at each wavelength weighted according to the luminosity function, a standardized model of human visual brightness perception.)

fluorescent strength and the strength of the UV energy from the light source used in grading. A Dazor Model 5.7 (UVA + B) total UV instrument was employed to measure the amount of UV present in each lighting environment. This meter was calibrated to NIST standards, and measures the UV band from 280–400 nm over a range of 0 to 1999 $\mu W/cm^2$.

Typical measurements of UV in blue sky, northern daylight in Maryland, at 11:00 a.m. 7 December 2008, were 500–600 $\mu W/cm^2$. The UV rapidly increased as the detector was rotated south and the vicinity of the sun was approached. Near but not including direct sun, the reading quickly exceeded the meter range of 1999 $\mu W/cm^2$. Hazy overcast and cloudy skies absorb UV

and were observed to reduce these figures by more than a factor of two. On 8 March 2009 at noon on an overcast day readings in north light of 800–1100 $\mu W/cm^2$ were obtained. This large and highly variable amount of UV in natural daylight makes it clear why this illumination is unsuitable for consistent grading of fluorescent diamonds.

The over-grading of blue-fluorescent diamonds: the problem, the proof and the solutions

Discussions of lighting standards for colour grading are often concerned with the variability of daylight's colour temperature, which ranges from the reddish light of early morning and evening to the bluish mid-day light from a cloudless north sky. The historical north-daylight standard for colour grading was derived from the traditional lighting from large north-facing window areas in diamond bourses in the Northern Hemisphere *(Figure 1)*, and the restriction of grading times to between late morning and early afternoon. A colour temperature of 6500K is widely accepted. The more problematic, often unknown and neglected consideration for accurate and consistent colour grading is the variable stimulation of blue fluorescence by the highly variable amounts of UV and visible violet present in daylight from open sky, or from north-facing windows, and the fluorescent lighting used in diamond colour grading.

Away from open daylight and indoors, the UV intensities dropped by factors of 100 to 1000, and in typical artificial light to less than 1µW/cm². The greatest indoor sources of UV at noon were large glass windows and doors which faced daylight. These large glass areas filter out short wave UV, but pass a proportion of long wave UV. At the window surface the reading at the December 2008 date and time was 150 µW/cm² dropping to 65 µW/cm² at 3 ft and 35 µW/cm² at 6 ft.

In all other areas illuminated by artificial fluorescent and incandescent ceiling illumination the readings at typical 3–4 ft viewing distances from ceiling lights were an essentially UV-free, 0–1 µW/cm². These readings are consistent with results from extensive surveys conducted by the author and others and provide support for the observation that at distances of more than 3 ft from artificial illumination, including ceiling mounted fluorescent lighting, indoor light is essentially UV free. In addition, because the light intensity is below 400 fc, usually under 100 fc and often less than 50 fc, there is no noticeable stimulation of fluorescence from the visible violet.

The light sources used in this
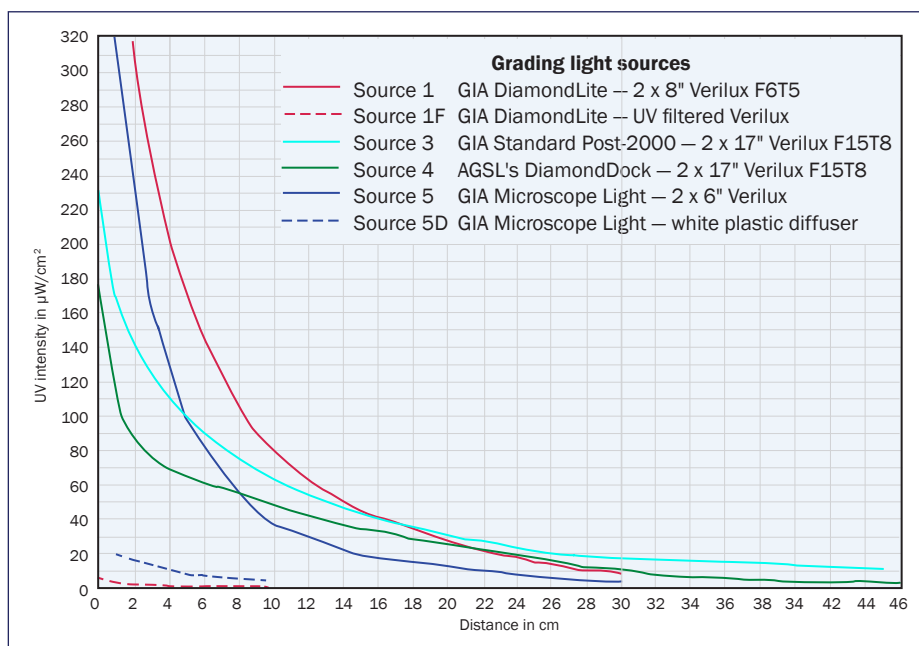
Figure 5: Reduction in intensity of UV with distance from study light sources.
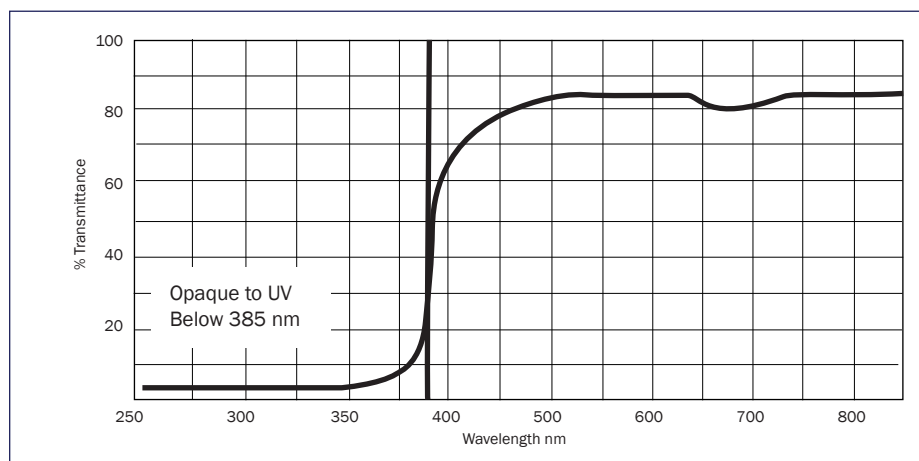
Figure 6: Graph of transmittance of polycarbonate UV filter. Courtesy of Dazor Lighting Manufacturing.

investigation were measured for UV energy intensity, which was plotted as a function of distance from the source. The graph in *Figure 5* shows those curves of UV fall off with distance from Source 1 and 1F (UV filtered), the DiamondLite; Source 3, a two tube desk lamp with the post 2000 GIA Lighting Standard of the twin Verilux tubes used in the DiamondDock; Source 4, AGSL's DiamondDock and Source 5 and 5D (diffused), the GIA Microscope Light. These plots document the high amount of UV present at close grading distances from all of the unfiltered fluorescent light tubes, and also show the rapid fall off with distance from them. Sources 3 and 4 (the cyan and green curves), both

employing the post 2000 GIA standard grading illumination of twin 17" Verilux tubes are important examples showing the variability of this standard's UV component.

Lexan and Makrolon polycarbonate filters were used when experimenting with the removal of UV from the various lights used in grading. Polycarbonate plastic is particularly suited to removing UV without significant or noticeable effect on the visible light spectrum. Note that the dashed Source 1F red curve in *Figure 5* shows that the UV has been reduced to less than 1 µW/cm² within 3 in. of the DiamondLite filtered with Lexan polycarbonate plastic. It is opaque to UV below 385 nm and is transparent

The over-grading of blue-fluorescent diamonds: the problem, the proof and the solutions
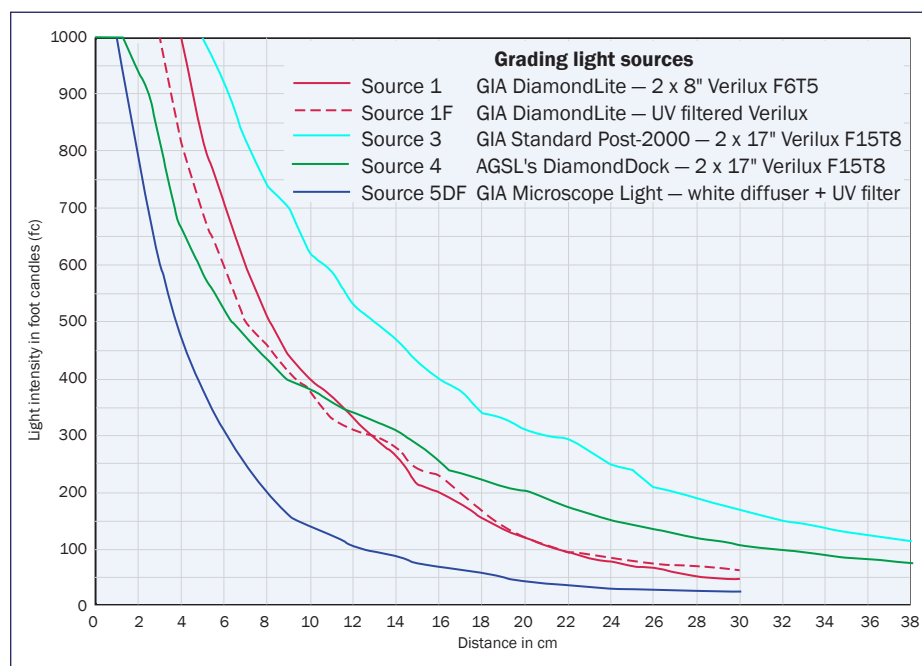
Figure 7: Reduction of light intensity with distance from study light sources.

to the visible spectrum. The range of wavelengths visible to the human eye is often listed as 400 to 700 nm, but "for the human eye, the visible radiations range from violet light, in which the shortest rays are about 380 nm, to red light, in which the longest rays are about 750 nm." (Curtis and Barnes, 1994). It should be stressed however that the eyes of any one individual may not possess this wide range. So for some fortunate individuals there could be 20 nm overlap between UV and visible violet from 380 to 400 nm. This region is at the transmission edge of the polycarbonate filter (see *Figure 6*).

Because the visible wavelengths at and below the 415.2 nm, N3-centre in diamond also excite blue fluorescence (see Box A), it was additionally important to measure the light intensity as a function of the distance from each of the grading lights to explore the visible light component's influence on grading of fluorescent diamonds. Measurements in foot candles of visible light intensity at different grading distances were obtained using a GE Light meter, Type 217. The curves in *Figure 7* show light intensity reduction with distance from four of the grading light sources. The shapes of these curves are broadly similar to the unfiltered UV curves, because the rate of reduction

with distance is a function of the lighting geometry and essentially the same for visible and UV wavelengths.

Colour grading instruments and their light-source properties

Seven sources of light were investigated to study their influence on the colour grading of each of the five levels of diamond fluorescent strength present in the 25 diamonds. Each light source was used unfiltered or with the UV component filtered out.

1. The DiamondLite

The DiamondLite, shown in *Figure 8*, contains two Verilux F6T5 fluorescent tubes. In the 1960s it replaced the original Diamolite, renamed DiamondLite, which Shipley had designed to be largely UV free. It incorporated Verilux fluorescent tubes also believed to have a "minimum of UV." In the 1990s it came to be realized that their output contained a significant component of UV.

Because of the rapid increase in both UV and visible light intensity on coming close to the Diamondlite's fluorescent tubes, a colour grade given to a blue-fluorescent diamond could be significantly

influenced by how close to these tubes it was graded. Conversations with former and current GIA GTL diamond graders indicate that grading was done between 1 and 4 in. from the fluorescent tubes to the diamonds in the DiamondLight tray or on a white plastic sheet on the instrument base. Grading practice varied somewhat at different times and with different graders. K. Hurwit (pers. comm., 2009), grader of diamond masters, relates that she adhered to Liddicoat's instruction to grade in the tray on the base, but would sometimes elevate the tray for a better view. Senior diamond grader, P. Yantzer, related a standard lab practice used by him and other lab graders since 1972; they placed the diamond table-down, with master stones, toward the rear on a flat sheet of plastic on the base and tilted or elevated this sheet towards the light when comparing to the masters (Yantzer, pers. comm., 2009).

In the 1 to 4 in. range available for grading in the DiamondLite, there are significant amounts and large ranges of UV and visible-violet energy. This variation makes for inconsistent colour grading of blue-fluorescent diamonds. The grading of the data-base diamonds was done between 2 and 3 in. beneath the tubes. At this typical grading distance a spot reading found the UV energy to be about 150 μW/cm², and the light intensity about 600 fc. As the radial distance from the diamonds to the nearest of the twin Verilux tubes increases from 1 to 4 in. the UV decreases from the vicinity of 300 μW/cm² to 80 μW/cm², as shown in *Figure 5*. These are the greatest amounts of UV found among the seven lighting environments investigated, and provide the reason that the unfiltered DiamondLite was found to cause the greatest whitening and, consequently, the greatest over-grading of blue-fluorescent diamonds.

2. GIA DiamondDock

At the turn of the twenty-first century the GIA discontinued the manufacture and use of the DiamondLite and replaced it with the DiamondDock, which employs two 17 in. F15T8VLX Verilux full spectrum fluorescent tubes. Diamonds

The over-grading of blue-fluorescent diamonds: the problem, the proof and the solutions

Figure 8: GIA DiamondLite containing two Verilux F6T5 fluorescent tubes.

Figure 9: Grading in the DiamondDock at the AGS Laboratory with (inset) a 10-diamond master set. Courtesy of AGSL.

are graded on a white tray placed on the DiamondDock shelf, which means that there is a 7 in. grading distance from the light tubes (see discussion below). The basic technical specifications of the DiamondDock lighting were given by King *et al*. (2008), and include:

- Stable, fluorescent lamps 17 in. (43 cm) or longer
- An intensity of light in the range of 2000–4500 lux at the surface of the grading tray
- An 8–10 in. distance between the lamps and the grading tray
- A colour spectrum close to CIE D55-D65
- A colour temperature between 5500 K and 6500 K
- A colour rendering index of 90 or above
- No noticeable output in the short- or medium-wave UV range (or a filter available to eliminate UV in this range)
- An emission for long-wave UV (between 315 and 400 nm, close to the reference spectrum of D55-D65)

It should be stated that although a grading distance of 8 to10 in. is specified, the maximum distance in the box that the diamonds can be positioned from the lamps is 7 in. Looking in *Figure 5* at the green graph of reduction in intensity of UV with distance in the AGSL's DiamondDock, the UV intensity at 7 in, is 28 µW/cm² falling to 17 µW/cm² at 10

in. The UV intensity is 65% higher at 7 in. compared to that at 10 in. The exact distance is important to establish what is, in essence, the chosen standard amount of UV and visible violet. GIA researcher R. Geurtz (pers. comm.) confirmed that the distance between the light source and the diamond will be close to 7 in.. He explains: "With the distance between shelf and the centre of the bulb at 8 to 10 in., the distance between the diamond and the surface of the bulb is around 7 in." But he notes another important point: the allowed range of light intensity of 2000–4500 lux at the surface of the grading tray means that the amount of UV and visible violet also can vary over the same 2.25 times range. Such an allowed range of UV and visible violet could lead, in different instruments, to different colour grades for a blue fluorescent diamond.

3. Floating arm desk lamp

For the multitude of owners of a standard floating-arm desk lamp, throughout the global diamond trade, this may be the most economical solution for those desiring compatibility with the GIA's DiamondDock. Two 17 in. F15T8VLX Verilux 'full spectrum' fluorescent tubes (the GIA standard lighting used in the DiamondDock) provide the light. Grading was done, without UV filtering at the 7 in. distance, as in the DiamondDock.

Figure 10: Microscope light fitted with white diffuser and Lexan UV filter.

4. AGSL DiamondDock

The DiamondDock in use at the AGS Laboratory is shown in *Figure 9;* the inset shows their ten-diamond E–N master set.

5. GIA microscope fluorescent light

GIA microscopes have provided a less expensive alternative to grading in a standard lightbox. These are fitted with a swing arm light attached to the front of the microscope stage, containing twin Verilux, 6 in. fluorescent tubes, whose light is filtered and diffused with a white plastic cover. This was a daylight-balanced grading light recommended to GIA students and is used to this day by many gemmologists and appraisers (the author included) as lighting for both diamond colour grading and final judgements of clarity grade. The author's

The over-grading of blue-fluorescent diamonds: the problem, the proof and the solutions

Table I: Colour grades of 25 diamonds with a range of fluorescence strengths.

No.	Cut	Weight (ct)	Fluorescence	Source 1 GIA DiamondLite 2–3 in. No filter 600 fc 150 µW/cm² MDC	Source 1 UV filter 600 fc 1 µW/cm² MDC	Source 2 GIA DiamondDock 7 in. No filter GIA GTL	Source 3 Two Verilux 7 in. No filter 350 fc 33 µW/cm² MDC	Source 4 AGSL's DiamondDock 7 in. No filter 230 fc 31 µW/cm² AGSL	Source 5 GIA Microscope Lamp 1 in. Diffuser (D) 600 fc 9 µW/cm² MDC	Source 5 D+UV filter 600 fc 1 µW/cm² MDC	Source 6 Dazor – Lumileds 3–5 in. Diffuser 600 fc 0 µW/cm² MDC	Source 6 Diffuser 200 fc 0 µW/cm² MDC	Source 7 Philips 4 × 32 W 36 in. Diffuser 200 fc 0 µW/cm² MDC
Diamonds with GIA report													
1	R	0.92	VST Blue	E	G	E	G	F		G		H	H
2	M	0.63	VST Blue	E	H	F	G	G	G	H	I		J
4	P	1.13	VST Blue	F	H	H	H	H		H		J	J
5	C	3.02	ST Blue (VST)[2]	D	D	D	D	D		D	E		E
7	O	2.01	ST Blue	E	E	E	E	F		E	F		G
8	O	2.02	ST Blue	E	E	E	E	F		E	F		G
9	O	1.56	ST Blue	E	F	F	E	F		F	G		G
10	R	1.00	ST Blue	E	E	E	E	G		F		G	G
12	O	0.68	MED Blue	F	F	F	F	G		F	F		G
13	R	1.09	MED Blue	G	G	G	G	G		G	G		G
15	R	0.59	ST Blue (MED)	E	E	E	E	F		E		E	E
20	R	1.01	None	J	J	J	J	J		J	J		J
21	R	0.77	None	G	G	G	G	H		G	G		G
22	R	0.73	None	G	G	G	G	G		G	G		G
23	R	2.28	None	H	H	I	H	H	H	H	H		H
Diamonds without GIA report							**Non-GIA grading**						
3	M	0.50	VST Blue	E	G		G	G		H	H		I
6	R	1.05	ST Blue	I	J	I(IGI)	I	I	I	J	J		K
11	M	0.84	MED Blue	G	G		G	H		G	H		H
14	R	1.50	MED Blue	G	H		G	H		G	H		H
16	R	0.50	Faint	D	D	D(EGL)	D	D		D	D		D
17	R	0.42	Faint	D	D		D	E		D	D		D
18	P	0.70	Faint	G	G		G	G		G	G		G
19	P	0.62	Faint	D	D		D	D		D	D		D
24	R	0.71	None	H	H		H	H		H	H		H
25	M	0.71	None	D	D		D	D		D	D		D

NB 1. Grader abbreviations: MDC = M.D. Cowing; GIA GTL = Gemological Institute of America Gem Testing Laboratory; AGSL = American Gem Society Laboratory; IGI = International Gemological Institute; EGL = European Gemmological Laboratories.

2. Brackets in this column indicate an AGSL opinion where it differs from that of GIA.

The over-grading of blue-fluorescent diamonds: the problem, the proof and the solutions

microscope light with the addition of a Lexan polycarbonate UV filter is shown in *Figure 10*. Unfiltered, at a distance of about an inch, this light has a strong UV component of 200 µW/cm² and a strong visible light intensity of 1000 fc. The standard white plastic diffuser reduces the UV to 10 µW/cm² and the light intensity to 800 fc. With the addition of a Lexan filter, the UV drops to a small 1 µW/cm² and the light intensity to 740 fc.

In the Verilux tubes in the DiamondLite and all commercial mercury vapour fluorescent lighting, at typical close grading distances the visible-violet wavelengths add to the stimulation of blue fluorescence formerly attributed only to UV. Even after filtering out UV, the visible violet present in light intensities at or above about 600 fc was found to whiten some 'Strong' and 'Very Strong Blue' fluorescent diamonds. To prevent the energy in the visible violet from noticeably affecting fluorescent diamond colour, provisional tests indicate that the maximum fluorescent-tube light intensity should not exceed 400 fc. This compares with the lighting intensity range of 2000–4500 lux listed by King *et al*. (2008), this being the equivalent of 186–418 fc.

6. LED desk lamp

In order to investigate the potential of LED technology for use in diamond colour grading, especially as a solution to the over-grading of blue-fluorescing diamonds, a white LED light, which emits no UV, was tested. It contains six high-power 'lumiled' LEDs with a high quality, thermally-managed, consistent 6000 K colour. An additional feature of this lamp, of interest because of visible-violet stimulation of blue fluorescence, is the ability to dim the light while maintaining its colour temperature. Initial grading of the 25 diamonds in the data base indicated that at a brightness of 600 fc the grades recorded were slightly whiter than those recorded in light of 200 fc (i.e. within the range recommended above); in the absence of UV this was attributed to fluorescence stimulation by the visible violet.
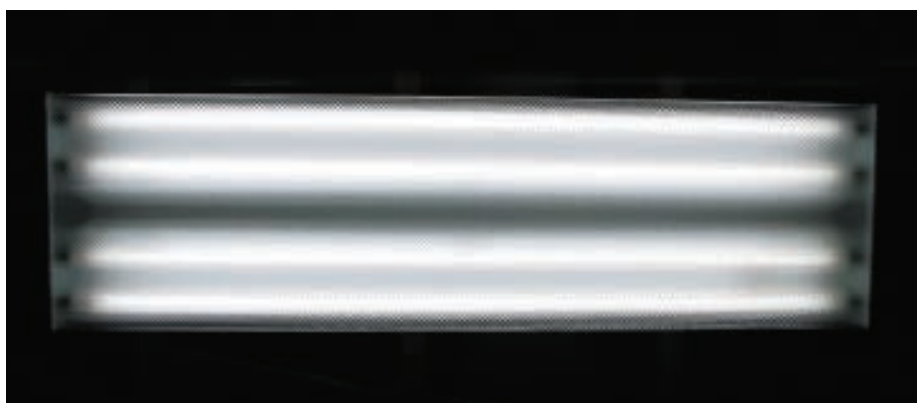

Figure 11: Overhead north-daylight balanced, (D65) fluorescent lighting.

7. Northern daylight balanced ceiling-mounted fluorescent light

The colour of a diamond can be seen and graded against master diamonds at distances from daylight fluorescent overhead illumination of 3 to 4 ft. Such distances are typical of those at which diamonds are viewed in a variety of social occasions. At this distance there is negligible UV and the amount of visible violet is not strong enough to whiten the colour grade. The example of this lighting chosen was the overhead daylight fluorescent light *(Figure 11)* containing four, 32 W Philips F32T8/DX tubes behind a clear plastic diffuser. Almost any artificial ceiling lighting could have been used, since at normal diamond viewing distances such illumination is essentially UV-free and has a visible light intensity which does not stimulate noticeable fluorescence. This lighting has a colour temperature of 6500 K, and at a distance of 3 ft, an intensity of 200 fc with no measureable UV.

Evaluation of the grading of the 25 diamonds

In *Table I* are the colour grades of the 25 diamonds in the data base obtained in each of the light environments.

To get a better visual understanding of the changes in grading which relate to different fluorescent strengths and light sources, the letter grades were changed to integers, 0 for D, 1 for E and so on. The integer number of grades improvement over the colour determined in the absence

of fluorescence stimulation was then recorded in the 3-D scatter plot in *Figure 12* for each light source arranged in UV-strength order from the back: Row 1, Source 1, the unfiltered DiamondLite having the most UV to Row 6, Source 6, LED lighting front-left having no UV. In order of decreasing UV, Row 2, Source 2 is GIA's grading in the DD, Row 3, Source 3 is the author's grading in GIA standard DD type lighting, Row 4, Source 4 is AGSL grading in their DD, and Row 5, Source 5 is the author's grading in the UV-filtered and white-plastic-diffused microscope lighting.

Examination of the chart and scatter plot supports the observations of whitening from blue fluorescence made by Tashey (2009). The improvement due to blue fluorescence from both the UV and visible violet in 'Very Strong' blue-fluorescing diamonds was found to be up to four and one-half grades. By filtering out the UV it was calculated that between one and two grades of this four and a half was due to stimulation by the remaining energy post filtering, chiefly the visible-violet. In 'Strong Blue' fluorescent diamonds, the colour-change due to fluorescence was typically two grades. In 'Medium Blue' fluorescent diamonds the change was generally between zero and one grade. As expected, no differences in grade from UV stimulation were found in the 'Faint' and 'None' categories of diamond.

An issue arising in the course of this investigation was the observation by the author and many other gemmologists

The over-grading of blue-fluorescent diamonds: the problem, the proof and the solutions
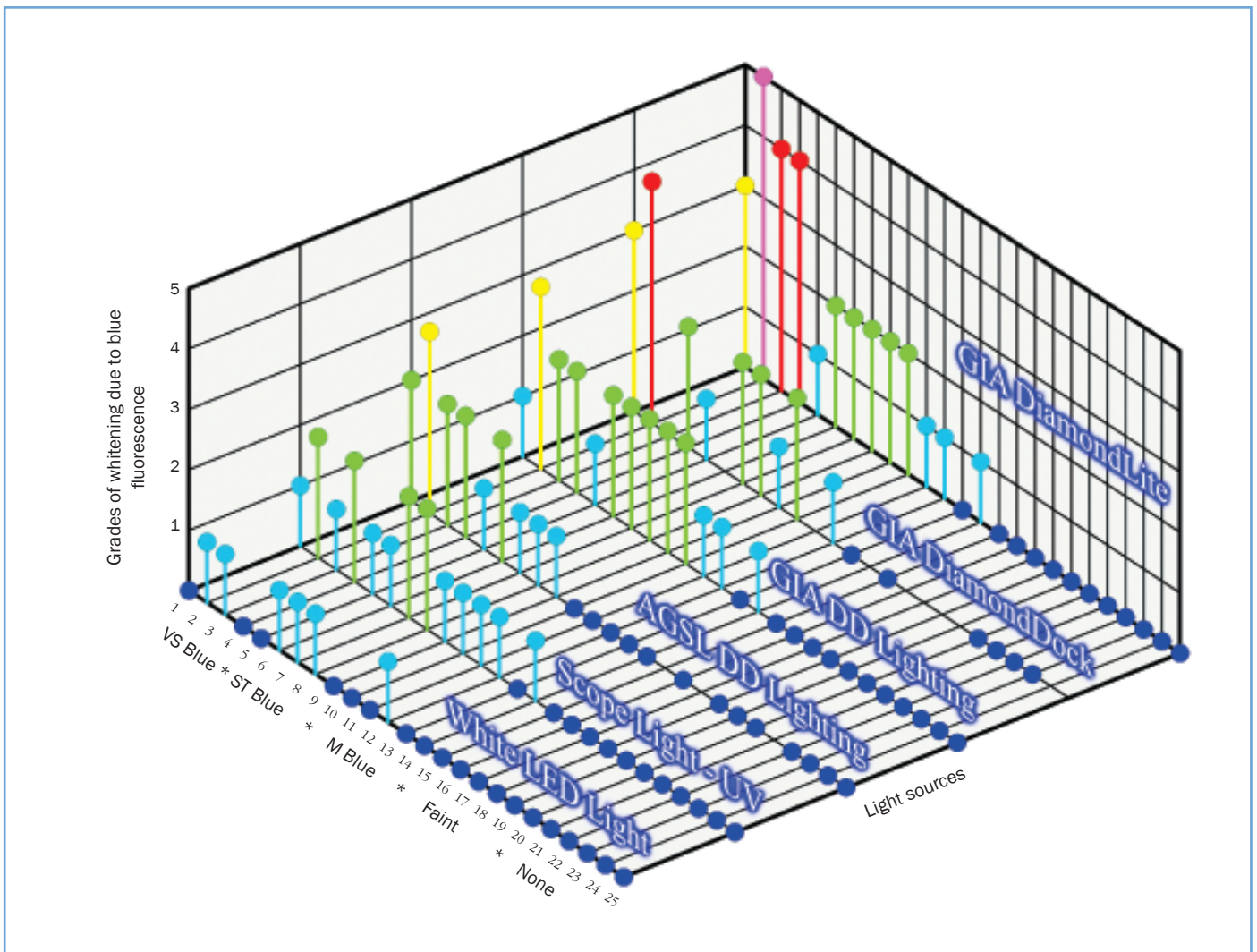

Figure 12: Scatter plot of grade changes of 25 diamonds under different light sources. The diamond numbers and their fluorescence characteristics are on the lower left; the light source numbers from the right are in sequence 1 (DiamondLite) to 6 (white LED light) — see text and Table I.

of a whitish, foggy fluorescence in 'Strong Blue' fluorescent diamonds seen in the high intensity incandescent light of the dark field illumination in gemmological microscopes. This study found that fluorescence stimulation from the relatively intense incandescent illumination that exists at short distances in gemmological microscopes and in other high intensity incandescent lighting was capable of causing colour improvement in some 'Strong' and 'Very Strong' blue-fluorescent diamonds. Even after filtering out UV from the high intensity incandescent microscope lighting, the excitation from the remaining narrow band of visible violet up to 415.2 nm was observed to stimulate this fluorescence. These observations of fluorescence

stimulation from the UV and visible violet at short distances in high intensity incandescent lighting point to why not only fluorescent grading light but also incandescent light must be UV filtered and of intensity below 400 fc to grade fluorescent diamond colour consistently and unenhanced by blue fluorescence.

What was learned from the grading of 25 diamonds in different light environments

Degree of over-grading of 'Very Strong Blue' fluorescent diamonds

First and foremost is the documentation in 'Very Strong Blue' diamonds 2, 3 and 4 of a four

grade improvement in the unfiltered DiamondLite (DL) compared with the colour grade in UV-free light. Diamond 2 changed from J to F in DiamondDock (DD) (GIA) to borderline E in the DiamondLite (DL), and to G in AGSL's DD. Diamond 3 with a grade of I was a low E in the DL; and diamond 4 with a grade of J changed to F in the unfiltered DL.

Stone 4 is particularly important to note, because its grading in the DL compared to its grading in the current DD standard illustrates the consequences of the change in GIA lighting standards brought about by the switch from grading at a distance of 2 to 4 in. in the DL, to 7 in. in the DD. Contrast the grade of F obtained in the unfiltered DL with the H

The over-grading of blue-fluorescent diamonds: the problem, the proof and the solutions

obtained by GIA, AGS and the author in the DD lighting. H is two grades lower and closer to the grade of J obtained in UV-free light. This is due to the much lower UV content and light intensity at the working distance of 7 in. in the DD. In changing from grading in the DL to the DD, the UV content in the lighting decreases from the vicinity of 150 µW/cm² to around 31 µW/cm², and the light intensity from 820 fc to 225 fc. The colour grade of J is obtained in both the Source 6, LED lighting with zero UV and the ceiling-mounted Source 7, fluorescent lighting.

So the changes from DiamondLite to DiamondDock and in procedure from grading at 2 to 4 in. to grading at 7 in. result in a lowering of both the UV and visible violet, and a consequent change in this instance of two letter grades closer to the unimproved colour for a 'Very Strong Blue' fluorescent diamond.

Degree of over grading of strong and medium blue fluorescent diamonds

Looking at the scatter plot of the 'Strong Blue' diamonds 6 to 10 a quite consistent two grade whitening is evident in the unfiltered DiamondLite as well as in the DiamondDock standard Verilux lighting used in the GIA and the author's grading, compared with the grades obtained in UV-free light. AGSL's grading of these 'Strong Blue' diamonds differed, obtaining on average only one grade of whitening in their DiamondDock lighting. Judging from this limited sample size, the change in lighting from the DiamondLite to the DiamondDock, while clearly reducing the likely amount of over-grading in 'Very Strong Blue' diamonds, appears to result in a less consistent reduction in the 'Strong Blue' fluorescent diamonds. The same can be said for the less consistent reduction seen in the half to one grade whitening typically seen in the 'Medium Blue' diamonds in the unfiltered DiamondLite. This lack of consistency is related to the stated range in strength of UV and visible light in the unfiltered Diamond Dock lighting.

Overall though, the scatter plot of this limited number of the five strengths of

fluorescence shows a direct correlation between UV content in the grading light and diamond fluorescent strength, and the likely number of grades of whitening compared with their colour in UV-free light. Counting from the back in *Figure 11,* GIA's Source 2, DD grading, the author's grading in Source 3, DiamondDock fluorescent light, and AGSL's grading in their Source 4 DiamondDock, all use the new Verilux lighting in the DiamondDock. Although well within the allowed variation in strength in the current DiamondDock standard lighting, the grading of the data base diamonds by GTL and AGSL in this lighting varied by as much as two grades and was as much as four grades whiter than grades obtained in UV-free light.

<div style="border:1px solid">

Box B: Effect of fluorescence on diamond values in the gem trade

Example of inadequate discounting of fluorescent diamonds

Stone 4 is a textbook example of a 'false colour' diamond warned about by Wade in 1916. Based upon the possible over-grading of this type of fluorescent diamond, it would be reasonable to conclude that typical trade discounting of substantially sized 'Very Strong Blues' like 4 may be insufficient. For example, a 3 ct pear-shaped F VS2 'Very Strong Blue', might be discounted between 10 and 20% from its asking price of $54,000 to around $45,900. At its grade of J in UV-free light its corresponding price would be $33,600, well below the trade's typical discounted price of $45,900. (Note: the significance of these high wholesale asking prices from Rapaport (2009) lies more in their comparative values than in the absolute amounts.)

Example of over discounting of the rarer diamonds historically described as 'blue white'

Consider how unreasonable the current practice is of applying similar discounts to all 'Very Strong Blue' fluorescent diamonds in a particular colour and clarity range without knowledge of their colour in UV-free light. Where diamond 4 is likely not to be discounted enough, it appears unfair to similarly discount diamond 5, a 3.02 ct cushion shaped D VS1 'Very Strong Blue' that holds its colour within a grade in UV-free light. Diamond 5 is one of the rarer fluorescent diamonds whose price today would be discounted the same percentage from $73,000 to $62,000. Its price at its grade of E in UV-free light would be $69,000, $7000 above its discounted price. This rare D with its blue-white appearance in daylight, should command the premium it once did over the more common diamonds that are graded D because of their fluorescence.

This data base clearly indicates that these rare diamonds in the blue fluorescence strengths of 'Very Strong', 'Strong' and 'Medium' that hold their colour in the absence of UV can be unfairly discounted.

</div>

Solutions to the over-grading of blue-fluorescent diamonds

The curves in *Figure 5* illustrate that the UV energy in fluorescent and other indoor artificial illumination falls off rapidly with distance from the source. The reduction in UV with distance could provide a partial solution to the over-grading of blue-fluorescent diamonds: this is to grade the diamond at a sufficient distance from UV-containing grading lights that any fluorescence in the diamond being graded is not stimulated beyond faint. This study found no colour difference due to fluorescence in the strengths of 'Faint' and 'None'. However, because lab grading is done from about

The over-grading of blue-fluorescent diamonds: the problem, the proof and the solutions

2 to 10 in. from fluorescent tubes with significant fluorescence-stimulating UV and visible violet, increases in grading distance within that range can help, but do not solve the problem of over-grading diamonds with fluorescent strengths of 'Medium Blue', 'Strong Blue' and 'Very Strong Blue'.

The change in the lighting characteristics from the DL lighting environment containing upwards of 150 $\mu W/cm^2$ to DD lighting having in the vicinity of 30 $\mu W/cm^2$ was seen to reduce the typical amount of overgrading in Very Strong Blues from as much as four grades to two grades. With this change in the standard grading light the potential for over grading has been reduced but not eliminated.

A more practical way to eliminate UV in grading illumination, and at the same time not noticeably affect the visible spectrum is filtration by polycarbonate plastic, such as Lexan or Makrolon. As shown in *Figure 6,* polycarbonate is an effective and inexpensive filter to remove UV below 385 nm. At the same time there is negligible change to the visible spectrum that could affect grading the D-Z tints of yellow in diamond.

To reduce fluorescence stimulated by visible violet, an equally practical and inexpensive solution is the use of flat-white plastic diffusers which attenuate violet and all visible wavelengths equally. Below 400 fc or about 4000 lux, the reduced amount of visible violet does not excite noticeable fluorescence, and the diamond's colour is unaffected. Such white diffusers have the additional feature of reducing spectral reflections and glare. They were employed on GIA microscope lights *(Figure 10)* for this purpose and to filter UV.

Another solution with potential is the use of white LED technology. In this investigation, a Dazor LED desk lamp not only provided inherently UV-free grading light, but was dimmable without change in colour temperature down to 2000–4000 lux, so as not to stimulate fluorescence from the visible violet. Possible concerns about differences between LEDs and fluorescent lights in their colour rendering indexes (CRIs) should be resolved with further comparative studies in both diamond grading environments.

Conclusions

The term 'blue-white' had been synonymous with top diamond colour for centuries. But after the explosion in supply of Cape-series diamonds from South Africa in the late nineteenth century, the term was so misused that it became as synonymous with deception as with fine quality. In the early twentieth century, Wade (1916) warned diamond dealers to be "on their guard" against blue-fluorescent, 'false colour' diamonds that failed to hold their colour (colourlessness) in all lighting conditions. Those that didn't were penalized in value to the extent to which their body colour was revealed to be yellowish (Cape) when seen in artificial lighting. The more yellow the unimproved colour, the less the stone's value.

In social situations, diamonds are most commonly seen at viewing distances of a few feet in many kinds of artificial illumination at night or indoors away from daylight. In these viewing environments the UV and visible violet are too weak to stimulate grade-whitening fluorescence. This is in contrast to most colour grading environments where the diamond is typically 2 to 7 in. from fluorescent lighting with significant UV and visible-violet components.

Only by grading in lighting that does not stimulate grade whitening fluorescence can grading consistency be achieved. Yet, today gemmologists are advised to use unfiltered UV-containing fluorescent lighting that approximates northern daylight as the standard for colour grading. This requirement for UV in the lighting is an abandonment of Shipley's colour grading philosophy. In addition, the variability in UV in fluorescent lighting is a cause of inconsistent grading of fluorescent diamonds.

It is time to solve the problem of over-grading blue-fluorescent diamonds. The desired grade for a blue-fluorescent diamond should be re-established as that colour seen in typical artificial lighting where fluorescence is not noticeably stimulated.

Since lab grading is done close to fluorescent tubes, the use is recommended of a polycarbonate plastic (Lexan or Makrolon are examples) as an effective and inexpensive filter to remove UV below 385 nm. This polycarbonate filter is designed to screen out UV only, avoiding noticeable alteration of the visible spectrum.

Wavelengths in the visible-violet must also be reduced so they too do not stimulate noticeable fluorescence. This can be accomplished without altering the diamond's colour by keeping the visible light intensity below 400 fc by means of a white plastic diffuser. In addition to lowering the light intensity, such white diffusers were recommended to reduce UV and also reduce spectral reflections and glare from the diamonds being graded.

A different but equally effective solution is to use white LEDs such as this investigation's Dazor LED desk lamp. It not only provides inherently UV-free grading light, but is dimmable without change in colour temperature down to 200–400 fc (about 2000–4000 lux).

Either solution would be consistent with the aim that diamonds should be examined for their unenhanced body colour in lighting free of UV which is diffused to the extent that neither UV nor visible-violet excite any significant fluorescence.

A return to this procedure would benefit the diamond industry in a variety of ways. First it would remove the distrust and stigma attached to fluorescent diamonds. Second, the rarer blue-fluorescent diamonds that hold their high-white colour in the absence of fluorescence would be recognized for their superior beauty and rarity. Thirdly, blue-fluorescent diamonds could be shown to whiten, and sometimes appear blue-white in natural daylight. Promoting this advantage in comparison with non-fluorescent diamonds of similar grade would be of substantial benefit in the marketing of blue fluorescent diamonds.

Acknowledgements

References

Curtis, H., and Barnes, N.S., 1994. *Invitation to Biology.* 5th edn. Worth Publishers, New York. 163

Gemological Institute of America, 1969. The GIA Diamond Course, Assignment #35, 3-6

Gilbertson, A.M., 2007. *American Cut: The First 100 Years.* Gemological Institute of America, Carlsbad, CA. 214 pp

King, J.M., Geurts, R.H., Gilbertson, A., and Shigley, J.E., 2008. Color grading "D-to-Z" diamonds at the GIA Laboratory. *Gems & Gemology,* **44**(4), 296–321

Moses, T., Reinitz, I.M., Johnson, M.L., King, J.M., and Shigley, J.E, 1997. The effect of blue fluorescence on the appearance of diamonds. *Gems & Gemology,* **33**(4), 244–59

Moses, T., 2001. Response to The Professional Gemologist article regarding fluorescence in diamonds. *The Professional Gemologist,* **3**(2), 1–2

Rapaport, M., 2009. (see web list)

Shipley, R.M., and Liddicoat, R.T. Jr., 1941. A solution to diamond color grading problems. *Gems & Gemology,* **3**(11), 162–80

Tashey, T., 2000. The effect of fluorescence on the color grading and appearance of white and off-white diamonds. *The Professional Gemologist,* **3**(1), 5–7

Tashey, T., 2009. Letters. More on D-Z diamond color grading. *Gems & Gemology,* **45**(2) 51–2

Wade, F.B., 1916. *Diamonds.* G.P. Putnam's Sons, New York and London, 150 pp

Web list

Rapaport, M., 2009. Rapaport Price Lists July on line at http://www.diamonds.net

The Author

Michael D. Cowing FGA
AGA Certified Gem Laboratory
email: michaelgem@gmail.com

High pressure high temperature treatment of diamonds — a review of the patent literature from five decades (1960–2009)

Dr Karl Schmetzer

Abstract: The relevant patent literature describing high pressure high temperature treatment processes of natural and synthetic diamonds is reviewed. A general overview about high pressure high temperature treatment for various technical applications is presented and colour changes for jewellery-quality diamonds are described in detail. Three major groups of patent documents exist that deal with the treatment of intense yellow type Ib synthetic diamonds, the colour alteration of brown natural diamonds and colour improvement of chemical vapour deposition grown synthetic diamonds, respectively. The reaction mechanisms involved in various processes of colour alteration are briefly discussed. In an extended version on the worldwide web, the different types of patent documents are explained, and the most relevant technical descriptions of a range of equipment used to perform HPHT treatment of diamonds are summarized in appendices.

Keywords: cause of colour, CVD, colour alteration, colour centres, defects, HPHT, natural diamond, synthetic diamond, treated diamond

Introduction

Within the last two decades, the major challenge for gemmological laboratories has moved from problems of distinguishing natural gemstones from their synthetic counterparts more towards the recognition and proper disclosure of various treatment processes. Detailed knowledge of possible treatment processes is essential for the recognition of treated gemstones in the laboratory. Since the late 1990s, in addition to the diffusion treatment of rubies and sapphires, a 'new' treatment process

for diamonds, mainly a decoloration of natural brown stones, caused major irritation in the trade when the first faceted stones that had undergone this enhancement for colour alteration in the laboratories or production plants of General Electric were brought to the market in 1999 (Moses *et al.,* 1999).

According to a comparison with patents issued by General Electric and De Beers in the late 1970s to early 1980s, which dealt with colour alteration of type Ib natural and synthetic intense yellow diamonds, first speculations

pointed towards a possible application of a high pressure high temperature (HPHT) treatment for the 'new' process (Schmetzer, 1999a), which was later confirmed by General Electric (Anthony and Casey, 1999). Patent documents by General Electric, which had been filed and issued in the 1990s, were discussed

Above: This type Ia diamond of 0.07 ct was originally brown and treated in a three-step process by a) HPHT, b) electron irradiation and c) annealing. Photograph by courtesy of T. Hainschwang, Gemlab, Gemological Laboratory, Balzers, Liechtenstein.

Figure 1: This type IIa diamond of 1.20 ct was originally brown and treated in a HPHT process.
Figures 2 and 3: These type Ia diamonds of 1.00 ct and 1.60 ct respectively, were originally brown and treated in a HPHT process.
Photographs courtesy of E. Erel, Carat Gem Lab, Gemological Laboratory, Montigny-les-Metz, France.

by Schmetzer (1999b, 2000). These documents are considered to describe a precursor of the new treatment, mainly the enhancement of synthetic diamonds grown by chemical vapour deposition (CVD). The reduction of defects and strain and the improvement of optical properties are caused in CVD-grown synthetic diamonds by the HPHT treatment process. The application of HPHT treatment to natural type IIa brown diamonds also causes the reduction of defects and strain and results, at least partly, in a decoloration (Smith et al., 2000) or in a transformation into light yellow, pink (Figure 1) or blue diamonds. In contrast, the application of HPHT treatment to type Ia brown diamonds causes a colour alteration to yellowish green, greenish yellow or yellow (Figures 2 and 3; Reinitz et al., 2000; Hainschwang et al., 2005).

Although the patent documents from the late 1970s to the mid 1990s mentioned in the papers by Schmetzer (1999 a,b, 2000) were briefly reviewed recently by Overton and Shigley (2008), only some of the documents (which describe treatments of mostly brown or brownish natural stones), published mainly within the last decade, were mentioned in this article. Other, older, processes dating back to the 1960s as well as some additional technical developments and applications of HPHT treatment processes described since then for natural and synthetic diamonds are largely unknown to gemmologists. Thus, the author presents an overview of five decades of HPHT treatment of diamonds as disclosed in issued patent documents and patent application publications.

More details about patent documents can be found in an expanded version of this paper on the worldwide web where

a short summary about patents and types of patent documents is given in Appendix A. Because technical details of the processes applied are largely unknown to gemmologists and only briefly discussed in gemmological papers, Appendix B is dedicated to the technical aspects of HPHT treatment processes.

General overview and chronology of HPHT treatment processes

The patent documents dealing with HPHT treatment of diamonds are listed in Table I; numbers in the right-hand column relate to superscript numbers in this text, and n, s and c relate to natural, synthetic (HPHT) and CVD-grown diamonds. The oldest documents known to the author date to the 1960s and describe diffusion treatment with aluminium and boron and the formation of diamond with semiconductor properties for electrical devices. In these two patents by General Electric[1] first hints towards a possible colour change are also given.

In later decades, numerous patents were filed by the two global players in diamond crystal growth on the world market, General Electric and De Beers (including their subsidiaries), by other companies involved in diamond synthesis (Sumitomo in Japan and Iljin in Korea), by research institutes (e.g. Carnegie Institution of Washington) and by companies involved in the application of diamond for electronic devices (e.g. Nippon Telegraph and Telephone Corporation or Akhan Technologies).

A group of patent documents from the late 1970s/early 1980s[2,3] described the treatment of natural and synthetic

diamonds to alter and improve colour. In 1975, a first patent was filed by General Electric which described the improvement of mechanical properties of diamonds by annealing the samples in the field of plastic deformation.[4] A similar process was described by The Australian National University in 1990.[5] From 1988 to 1990, patent applications by Sumitomo again described the formation and alteration of specific defects (colour centres) and the improvement of colour in synthetic diamonds.[6,7,8,9] Since 1995, patent applications have been filed by General Electric which described the improvement of toughness and strength in diamonds. Parts of these applications dealt with synthetic diamonds grown by the HPHT techique,[10,11] but other documents described the treatment of synthetic diamonds grown by the CVD method.[12,13] In general, how defects in the diamond lattice are relieved and voids and stresses are removed by HPHT treatment were described. As mentioned above, the documents of this series are considered as precursors of the processes developed for decoloration and colour change of natural brown diamonds, the results of which were released to the market in Spring 1999.

A first document by Umeda[14] described the improvement of brightness and colour tone of jewellery-quality diamond. Shortly thereafter, the treatment of brown natural diamonds was described in a series of worldwide applications by General Electric[15,16,17,18] and De Beers.[19,20,21] The treatment of different types of diamond was described for decoloration of brown diamonds, and for changing this colour into yellow, orange, greenish yellow and yellowish green (Figure 4) and into pink and blue in such stones. All

Figure 4: These type Ia diamonds of 1.20 ct (left) and 1.10 ct were originally brown and treated in a HPHT process. Photograph courtesy of E. Erel, Carat Gem Lab, Gemological Laboratory, Montigny-les-Metz, France.

HPHT treatment of diamonds — a review of the patent literature from five decades (1960–2009)

Table I: Chronology of HPHT patent applications and granted patents for the HPHT treatment of diamonds.

Author(s), applicant priority publication/date and/or WO publication/date	Related patents (patent family)/date	Temperature (°C)	Pressure (kilobars)	Time	Results	No. *
Cannon, General Electric US 3,134,739 (1964)	DE 1168396B (1964) FR 1341561A1 (1963)	700–1500	10–60	20 min	Diffusion of aluminium to modify electrical characteristics and colour	1 n,s
Wentorf , General Electric US 3,141,855 (1964)	GB 1014226A (1965)	1300–2000	8.5 or 63	12 or 15 min	Diffusion of boron to modify electrical characteristics and colour	n,s
Strong et al., General Electric US 4,124,690 (1978)	DE 2732793A1 (1978) GB 1578987A (1980)	1500–2200	48–80	1 min–50 hr	Partial or total conversion of Ib to Ia nitrogen, lighter yellow colour	2 n
Strong et al., General Electric US 4,174,380 (1979)	FR 2359071A1 (1978)	1500–2200	48–80	1 min–50 hr	Partial or total conversion of Ib to Ia nitrogen, lighter yellow colour	s
Evans and Allen, De Beers EP 0014528A1 (1980)	EP 0014528B1 (1983) US 4,399,364 (1983)	1600–2200	80	20 min–6 hr	Reduction of yellow colour in irradiated type Ib synthetic diamond	3 s, (n)
De Vries et al., General Electric US 4,181,505 (1980)	DE 2519116A1 (1975) GB 1500817A (1978) FR 2275405A1 (1976)	Below 1500	Below 55	1–30 min	Improving mechanical properties of crystals by annealing in the field of plastic deformation	4 n,s
Ringwood, The Australian National University WO 86/01433A1 (1986)	US 4,874,398 (1989) US 4,948,388 (1990) US 4,985,051 (1991) EP 0191067B1 (1992)	1100–1600	10–40	3–60 min	Improving mechanical properties (hardness, strength) by annealing in the field of plastic deformation	5
Tsuji and Sato, Sumitomo Electric JP 63–291896A (vvvv JP 01–183409A JP 63–291896 (1988)		1500–2200	10–30		Conversion of Ib to Ia nitrogen in irradiated type Ib synthetic diamond	6 s
Tsuji and Sato, Sumitomo Electric JP 01–020689A (1989) JP 02–000385A (1989)	EP 0275063A2 (1988) US 4,880,613 (1989)	1700–2500	> 30	> 20 hr	Conversion of Ib nitrogen in irradiated type Ib diamond, irradiation and heat treatment after HPHT treatment	7 s
Satoh and Tsuji, Sumitomo Electric JP 01–183409A (1989)	EP 0324179A1 (1989) EP 0324179B1 (1992) US 4,959,201 (1990)	> 1600	> 30	5–30 hr	Treatment of an irradiated Ib diamond to produce a green colour	8 s
Nakajima et al., Sumitomo Electric JP 02–018980A (1990)		> 2000	> 30	> 5 hr	Formation of N3 centres in a type Ib synthetic diamond for use as diamond laser element	9 s
Jackson and Park, General Electric US 5,523,071 (1996)	JP 07–165494A (1995) EP0638670A1 (1995) EP 0638670B1 (2001)	800–1600	Up to 45	5 min–10 hr	Annealing in reducing atmosphere to improve the toughness and strength of diamond grains	10 s
Banholzer et al., General Electric	EP 0668377A1 (1995) JP 08–002997A (1996)	900–2000	10–70	5 min–10 hr	Annealing in non-oxidizing atmosphere to improve the toughness and strength of diamond grains	11 s

HPHT treatment of diamonds — a review of the patent literature from five decades (1960–2009)

Ref	Purpose	Time			Patent numbers	Authors
12 c, (n,s)	Remove voids and stress to improve toughness in colourless CVD synthetic diamond	minutes–several days	10–200	1000–2000	EP 0671482A1 (1995) JP 07–331441A (1995)	Anthony et al., General Electric
13 c, (n,s)	Annealing in a non-oxidizing medium to improve the toughness of CVD synthetic diamond thin films by removing stress and voids	2–60 min	above 3	1100–2300		Anthony et al., General Electric US 5,672,395 (1997)
14	Improve the quality and colour tone of jewellery-quality diamond					Umeda & Miyamoto, Umeda JP 09–164329A (1997)
15 n	Production of yellowish-green, greenish–yellow and neon greenish-yellow stones from discoloured natural diamonds	30 sec–96 hr	10–100	1500–3500	EP1210171B1 (2006) EP 1645328A1 (2006) CA 2382785A1 (2001) DE 6002744IT2 (2006)	Anthony & Vagarali, General Electric WO 01/14050A1 (2001)
16 n	Production of colourless stones from discoloured natural diamonds	30 sec– 96 hr	10–100	1500–3500	US 2002/0081260A1 (2002) US 2003/0143150A1 (2003) US 2004/0146451A1 (2004) US 2005/0249655A1(2005) US 6,692,714B2 (2004) US 7,323,156B2 (2008)	Vagarali et al., General Electric US 2001/0031237A1 (2001)
17 n	Production of colourless, yellow, greenish yellow, pink, red, and blue stones from discoloured (mostly brown) natural diamonds	30 sec–500 hr	50–200	1500–2700		Vagarali et al., General Electric, US 2002/0172638A1 (2002)
18 n	Production of colourless and fancy coloured stones from discoloured natural diamonds	30sec–96 hr	10–100	1500–3500	EP 1315558B1 (2006) EP 1637218A2 (2006) US 2005/0260935A1 (2005) US 7,241,434B2 (2007)	Anthony et al., General Electric WO 02/139558A2 (2002)
19 n	Production of pink stones from discoloured natural brown diamonds	10 min–10 hr	69–85	1900–2300	EP 1272264B1 (2006) CA 2405362 (2001) DE 6012359IT2 (2007)	Burns and Fisher, De Beers WO 01/72404A1 (2001)
20	Production of blue stones from discoloured natural brownish grey or grey diamonds	10 min–20 hr	67–90	1800–2600	EP 1272266B1 (2006) CA 2405409A1 (2001) DE 60123593T2	Burns et al., De Beers WO 01/72405A1 (2001)
21 n	Production of colourless stones from brown diamonds	90 min –5 hr	76–90	2200–2600	EP 1272265B1 (2006) CA 2405420A1 (2001) DE 60123592T2 (2007)	Burns et al., De Beers WO 01/72406A1 (2001)
22 c	Improving optical, electrical, thermal and mechanical properties of synthetic CVD diamonds	1–30 min	at least 40	1500–2900	US 6811610B2 (2004)	Frushour and Li, Diamond Innovations US 2003/0230232A1 (2003)
23 c	Improving optical, electrical, thermal and mechanical properties of synthetic CVD diamonds	1–30 min	at least 40	1500–2900		Frushour and Li, Diamond Innovations WO 2005/031033A1 (2005)

HPHT treatment of diamonds — a review of the patent literature from five decades (1960–2009)

Table 1: Chronology of HPHT patent applications and granted patents for the HPHT treatment of diamonds (continued)

Author(s), applicant priority publication/date and/or WO publication/date	Related patents (patent family)/date	Temperature (°C)	Pressure (kilobars)	Time	Results	No. *
Vins, Vins RU 2237113C1 (2004) WO 2004/113597A1 (2004)	EP 1645664A1 (2006) US 2007/0053823A1 (2007)	> 2150	60–70	10 min	Production of fancy red diamonds, irradiation and heat treatment after HPHT treatment	24 n
Baek et al., Iljin Diamond KR 20040042576 (2004)					Colour change of diamond from brown to yellow, greenish yellow, yellowish green or colourless	25 n
D'Evelyn et al., General Electric US 2004/0000266A1 (2004)	US 2006/0096521A1 (2006) US 7,175,704B2 (2007) EP 1378591A1 (2004) EP1715086A1 (2006) JP 2004–161604A (2004) JP 2007–015918A (2007)	1000–2000	55	30 min	Reduction of defect concentrations and strain in various non-diamond crystals, e.g. SiC, GaN, GaAs	26
Gill et al., Element Six WO 2004/074557A1	US 2007/0054124A1 (2007)				Annealing CVD synthetic diamonds to enhance the wear rate	27 c
Godfried et al., Element Six WO 2004/046427A1 (2004)	US 2004/0229464A1 (2004) GB 2432592A (2007) GB 2433737A (2007) GB 2433738A (2007)				Annealing CVD synthetic diamonds to enhance optical properties and to reduce strain	28 c
Twitchen et al., Element Six WO 2004/022821A1 (2004)	CA 2495840A1 (2004) US 2004/0175499A1 (2004) US 2007/0079752A1 (2007) US 2009/0291287A1 (2009) US 7,172,655B2 (2007) GB 2430194A (2007)	1200–2500	65–80	3 sec–835 hr	Production of a desired colour in CVD– grown synthetic diamond, e.g. colourless or pink or green	29 c
Hemley et al., Carnegie Institution of Washington US 2005/0025886A1 (2005) US 2006/0144322A9 (2006)	WO 2005/007936A2 (2005) WO 2005/007937A2 (2005) US 2006/0185583A1 (2006) US 2007/0290408A1 (2007) US 2008/0241049A1 (2008) US 7115241B2 (2006) US 7309477B2 (2007)	1800–2900	50–70	1–60 min	Enhancement of diamonds grown by microwave plasma chemical vapour deposition, lightening brown or yellow coloration, improvement of mechanical properties, e.g. hardness	30 c
Hemley et al., Carnegie Institution of Washington US 2006/0065187A1 (2006)	WO 2007/018555A2 (2007) US 7594968B2 (2009)	2000–2700	50–70	10 min	Enhancement of diamonds grown by microwave plasma chemical vapour deposition, removal of brown coloration, increase of hardness	31 c

HPHT treatment of diamonds — a review of the patent literature from five decades (1960–2009)

No.	Authors / Applicant	Related patents			Time	Title
32 s	Namba et al., Sumitomo Electric Industries WO 2005/041279A1 (2005)	EP 1713116A1 (2006) US 2006/0177962A1 (2006)	800–1800	30–80	10 hr	Producing n-type semiconductor diamond by annealing Li- and N-bearing ion-implanted crystals
33 n	Tkachenko and Timofeev RU 2281350 C2 (2006)		1700–2300	60–90	8–30 min per step, 1–3 hr in total	Decoloration of diamond in several annealing steps at different temperatures
34 s	Summerton et al., Element Six WO 2006/061707A2 (2006)	US 2009/0258229A1 (2009)	2100–2500	60–80	0.1–48 hr	Improving the quality of type IIa HPHT- grown synthetic diamond
35 c	Williams et al., Element Six WO 2006/136929A2 (2006)	GB 2428690A (2007) US 2010/0015438A1 (2010)	1200–3000			Improvement of CVD-grown synthetic diamond
36 c	Kasu et al., Nippon Telegraph and Telephone Corporation WO 2006/137401A1 (2006)	EP 1895579A1 (2008) US 2008/0134959A1 (2008) US 2008/0134960A1 (2008) US2008/0217626A1 (2008) US 2009/0261347A1 (2009)	1200	60		Improving the properties of ion-implanted diamond semiconductor elements
37 s	Twitchen et al., Element Six WO 2007/066215A2 (2007)	US 2009/0127506A1 (2009)	1600–2500	60–80	0.1–48 hr	Improving the quality of HPHT-grown synthetic diamond which is used as seed for CVD growth
38 c	Khan, Akhan Technologies WO 2008/019404A2 (2008)	US 2008/0073646A1 (2008) DE 112007001892T5 (2009)	1200	60	1 hr	Improvement of properties of boron–doped diamond field effect transistor

* n: natural diamonds;
s: synthetic HPHT-grown diamonds;
c: synthetic diamonds grown by chemical vapor deposition (CVD)

- ■ HPHT treatment predominantly for colour improvement
- ■ HPHT treatment in combination with diffusion of aluminium or boron into the diamond
- ■ HPHT treatment in combination with irradiation
- ■ HPHT treatment predominantly for the improvement of mechanical properties
- ■ HPHT treatment predominantly for the improvement of parts for electrical devices

Notes:

1. Patents related to the design of the equipment to create the temperature and pressure conditions for diamond synthesis are not included in this table.

2. Related patents (patent family members) are patents with the same title and/or by the same inventors and/or by the same applicant; only a selection of patent family members are given, others in different languages, e.g. Japanese, Chinese, Russian, may also have been published.

3. The patent country codes are as follows: CA – Canada, DE – Germany, EP – Europe, FR – France, GB – Great Britain, JP – Japan, KR – Korea, RU – Russia, US – United States, WO –World Intellectual Property Organization.

HPHT treatment of diamonds — a review of the patent literature from five decades (1960–2009)

Table II: Colour change of diamonds by HPHT treatment

Starting material*	Original colour	Treatment	Colour after treatment	Mechanism	No.
n,s		HPHT + diffusion of boron	Patches of dark blue colour or dark blue surface regions	Diffusion of boron into the diamond structure	1
n,s		HPHT + diffusion of aluminium	Clearer and more colourless	Diffusion of aluminium along fractures	1
s Ib / n Ib or Ib-Ia	Greenish yellow or intense golden yellow or yellow	HPHT / HPHT	Towards yellow, paler yellow or almost colourless	Aggregation of single nitrogen atoms	1,2,30 / 2
s Ib		1) Irradiation 2) HPHT	Reduction of colour	1) Displacement of atoms 2) aggregation of single nitrogen atoms	3,6
s Ib	Bright yellow	1) Irradiation + 2) HPHT	Green	Formation of N-V-N centres	7
n Ia, IIa / n IIa / n IIb	Brown / Brown / Brown, brownish grey or grey	HPHT / HPHT / HPHT	Colourless or almost colourless / Pink / Blue	Removal of brown colour centres	16,17,18,21,25 / 16,17,18,19 / 16,17,18,20
n IaB and Ia A/B	Brown	HPHT	Yellowish green to greenish yellow or intense to light yellow	Removal of brown colour centres combined with the mobilization of vacancies, dissociation and association of A and/or B nitrogen defects, formation of N-V-N and other nitrogen-vacancy defects (colour centres)	15,16,17,18,25
n Ia	Near colourless to brown	1) HPHT + 2) irradiation + 3) annealing	Intense pink to red	1) Dissociation of A centres, 2) formation of vacancies 3) mobilization of vacancies and formation of N-V colour centres	24 (compare Ref. 7 for similar treatment of type Ib synthetic diamonds)
n	Brown, yellow and yellowish green	HPHT with annealing in different subsequent steps at various temperatures	Decoloration		33
c with variable nitrogen contents	Brown or orange brown or pinkish brown	HPHT	Near-colourless, pale brown or green or pink brown	Removal of an absorption band at 350 nm, at higher temperatures additional removal of a 510 nm band and a NIR absorption	29
c	Brown or yellow	HPHT	Colourless or near-colourless, reduces or eliminates yellow or brown colours	Removal of defects	30,31

* n: natural diamonds;.   s: synthetic HPHT–grown diamonds.   c: synthetic diamonds grown by CVD.

HPHT treatment predominantly for colour improvement

HPHT treatment in combination with diffusion of Al or B into the diamond

HPHT treatment in combination with irradiation

HPHT treatment of diamonds — a review of the patent literature from five decades (1960–2009)

Figure 5: This type Ia diamond of 1.51 ct was originally brown and treated in a three-step process by a) HPHT, b) electron irradiation and c) annealing. Photograph by courtesy of V. Vins, Institute of Single Crystals, Novosibirsk, Russia.

these documents contain the most detailed descriptions of colour alteration in natural brown diamonds. A similar application was also filed by Iljin in Korea.[25] A special process for the production of red and pink diamonds was described by Vins using a combination of HPHT treatment, with subsequent electron irradiation and annealing *(Figure 5)*.[24] An application by Tkachenka and Timofeev also described the decoloration of natural diamond.[33] With the exception of the Umeda[14] and the first General Electric[17] patents, the various applications mentioned in this paragraph for colour improvement of natural, mostly brown or pale brown diamonds, have been published within the last decade.

After the year 2000, although there were some applications dealing with the improvement of mechanical properties of synthetic diamonds grown by the HPHT technique,[34] most were for diamonds grown by CVD [22,23,27,28,35] and for related superhard materials.[26] One document contains a description of how to improve the properties of HPHT-grown synthetic diamond crystals which are used as seeds for the growth of larger CVD synthetic diamonds.[37] The interest for possible improvement of CVD-grown synthetic diamonds is based on technical progress in CVD-related processes resulting in the growth of synthetic diamond layers or crystals with larger thickness; such products could be cut as faceted stones for jewellery purposes. Consequently, HPHT treatment is also applied to change

or improve the colour of CVD-grown synthetic diamonds,[29,30,31] mainly to alter yellow and pale brown tones. The improvement of properties of specifically doped CVD synthetic diamonds for semiconductor application has also been described recently.[32,36,38]

Colour alteration of diamonds by HPHT treatment

In natural or synthetic diamonds destined for jewellery, the alteration and improvement of colour is the main purpose for application of HPHT treatment processes, although colourless type IIa synthetic diamonds have also been processed to improve quality and optical features.[34] The patents dealing with colour alteration clearly reflect the natural and synthetic material available and the desired colour changes to attain marketable material.

Diffusion treatment with boron and aluminium

Diffusion treatment with boron or aluminium is the oldest patent[1] dealing with the HPHT process applied for colour alteration of natural or synthetic diamonds which is known to the author. This described HPHT annealing in the presence of boron-bearing compounds which resulted in a blue coloration, at least of parts of the surfaces of the samples. Diffusion treatment with aluminium, on the other hand, was described to whiten the treated diamonds. It is not known to the author whether either process has been carried out commercially and samples released to the market, or whether any practical tests are available to detect this type of diffusion treatment and distinguish them from natural pale-blue to fancy-blue diamonds.

On request, the author received the following information from Victor Vins, Novosibirsk, Russia, which is helpful in assessing the potential of these two processes:

"In the mid 1980s we conducted experiments of thermal diffusion of boron and aluminium from the surface of natural

diamonds. The experiments were carried out at high P and T conditions, boron and aluminium were in the graphite mixture. We did observe the colour change and we at first thought that we had managed to introduce these elements into the diamond lattice. Then we examined these samples more closely and found out that the colour change was due to thin layers on the surface of natural diamonds. We gradually etched the diamond surface and soon the conductivity decreased from metallic to zero conductivity."

Boron diffusion into type I and type II natural diamond up to a depth of about 2 µm at low pressure and high temperature has been described by Popovici *et al.* (1995 a,b), Sung *et al.* (1996) and Krutko *et al.* (2000).

Thus, two explanations are possible to explain the results mentioned above:
(a) Thin layers of synthetic HPHT-grown boron-containing diamond were formed on the surface of the natural diamond crystals. These layers were removed by subsequent etching.
(b) Boron was diffused into an extremely thin surface layer of the diamond, a layer that could be removed by subsequent etching.

In summary, a possible diffusion treatment of boron would produce a blue coloration only in thin surface layers, but would definitely influence the colour of faceted diamond. However, it is questionable if the thin blue layer produced by this technique would survive any re-cutting and re-polishing.

Transformation of colour centres

The patent applications available as public documents which are relevant to colour alteration of diamond are numbered in *Table II* and can be considered in three groups dealing with
• Colour improvement and alteration of intense yellow type Ib natural and synthetic diamond;
• Colour improvement and alteration of brown type I and natural brown type II diamond;
• Colour improvement and alteration of yellow to brown synthetic diamond grown by CVD.

HPHT treatment of diamonds — a review of the patent literature from five decades (1960–2009)

Some applications also mention the lightening or decoloration of type Ia natural pale yellow diamonds.

In some patent documents, the 'prior art' (patent documents or scientific papers known to the applicant at the time of writing the text of the application or documents identified as relevant by an officer researching a patent application), including the mechanism of colour change and colour improvement is discussed, but in other documents only the desired process of colour alteration is stated, with no mention of the exact mechanism of colour change. From scientific research and review papers published within the last decade (e.g. Collins *et al.*, 2000; De Weerdt and Van Royen, 2000; Vins, 2001; Collins, 2001 a,b; De Weerdt and Collins, 2003; Avalos and Dannefaer, 2003; Katrusha *et al.*, 2003; Vins and Yelisseyev, 2008; Erel, 2009; Fisher, 2009; Fisher *et al.*, 2009) and patent documents the following general reaction mechanisms can be summarized as follows.

According to the type of nitrogen defects present in the diamond crystal and as a function of the annealing temperature(s) and the stabilizing pressure(s), nitrogen-related centres may associate and dissociate. In synthetic and natural type Ib diamonds containing isolated nitrogen atoms on carbon lattice sites (C centres), for example, nitrogen can migrate within the diamond structure and can form A centres (consisting of adjacent substitutional pairs of nitrogen). In natural type Ia diamond, A centres can transform into B centres (consisting of a vacancy trapped by four surrounding nitrogen atoms). A centres, on the other hand, can dissociate into isolated nitrogen atoms.

If vacancies (V) are produced, e.g. by electron or neutron irradiation, these vacancies can combine with existing nitrogen defects to form the following centres:

- C centre + V → N-V centre (a substitutional nitrogen atom adjacent to a vacancy);
- A centre + V → H3 centre (N-V-N centre, a vacancy trapped by a pair of substitutional nitrogen atoms); if an

electron is trapped at the H3 centre (with C centres as electron donors), the H2 centre is formed;
- B centre + V → H4 centre (4N-2V centre, consisting of two vacancies and four nitrogen atoms).

H4 centres, on the other hand can become unstable upon HPHT treatment and dissociate into two H3 centres.

Furthermore, in brown diamonds, brown colour centres can be removed by HPHT treatment. In this process, vacancies are also formed or released, which combine with existing nitrogen defects according to the possible reaction processes given above. Some of the new colour centres may become unstable and dissociate.

In the following paragraphs, only short explanations will be given about the various processes; it is beyond the scope of the present paper to discuss all possible processes at different temperatures and the interpretation of spectroscopic measurements in detail. For these discussions, the reader is referred to the numerous scientific papers available. Furthermore, the mechanisms described in various patent documents are not always consistent with each other, but it would be extremely confusing to discuss these differences and discrepancies. Consequently, for these details the interested reader should refer to the original documents (*Table I* and Appendix C).

Colour improvement and alteration of intense yellow type Ib natural and synthetic diamond

Several patents deal with colour improvement and colour alteration of type Ib diamonds containing predominantly isolated nitrogen atoms (C centres). Most synthetic diamonds grown by the HPHT process are of this type and reveal a greenish yellow or intense golden yellow to yellow or even orange coloration. This coloration, which is sometimes too brown or dark for jewellery purposes, can be changed to a brighter yellow (*Figure 6*) or towards a somewhat paler yellow or even approaching colourless, if desired.[1,2,30] The A centres formed by this treatment do

Figure 6: This type Ib synthetic diamond of 0.33ct was originally intense yellow and treated in a HPHT process. Photograph by courtesy of T. Hainschwang, Gemlab, Gemological Laboratory, Balzers, Liechtenstein.

not absorb light in the visible range and this explains the lightening of the yellow coloration. Although the same process is also described for natural diamonds,[2] type Ib natural 'fancy yellow' diamonds are very rare and sought after, and therefore the practical application of this treatment to such stones is assumed to be limited.

The same process can be carried out in a shorter overall time by first irradiating the diamond in a separate step before the HPHT treatment is performed.[3,6] Another patent application by Sumitomo Electric described electron irradiation to type Ib synthetic diamonds before HPHT treatment.[8] In this process, vacancies are formed which associate with two nitrogen atoms and form N-V-N centres (H3 and H2 centres). The colour of the processed diamond is green. This type of treatment was performed by Sumitomo for samples marketed by Chatham (for a gemmological description see Shigley *et al.*, 2004).

Colour improvement and alteration of type I and type II natural brown diamond

Details of the causes of colour in natural brown diamonds are still in debate (Hainschwang, 2003; Hainschwang *et al.*, 2005). Until recently, it was generally assumed that the coloration of most natural brown diamonds was associated with plastic deformation, which the diamonds had undergone between their formation and subsequent transport to the Earth's surface. Now, however, results of experimental research and theoretical considerations point towards a model in

HPHT treatment of diamonds — a review of the patent literature from five decades (1960–2009)

Table III: Colour alteration in diamond by HPHT treatment*

Diamond type	Colour before annealing	Medium	Pressure (in kbar)	Temperature (in °C)	Time (in min)	Colour after annealing
IIa	Steely grey brown	Graphite	80	2300	18	Colourless
Ia	Light brown	Graphite	80	2300	20	Pale green
Ia	Light brown	Graphite	80	2300	18	Yellow
Ia	Light brown	Graphite	77	1900	18	Light brown
Ia	Light brown	NaCl	80	2400	12	Yellow
Ia	Medium brown	NaCl	77	1900	18	Medium brown
Ia	Medium brown	NaCl	79	2050	18	Light yellow
Ia	Light yellow	NaCl + KNO_3	79	2200	18	Greenish golden yellow
Ia	Dark brown	Graphite	80	2300	17	Yellow
Ia	Light brown	NaCl	80	2200	18	Light greenish yellow
Ia	Dark brown	NaCl + KNO_3	80	2200	18	Greenish golden yellow
Ia	Light brown	NaCl	80	2300	18	Light yellow
Ia	Light brown	NaCl	80	2300	18	Light yellow
Ia	Light yellow	NaCl	80	2400	18	Brownish yellow
Ia	Very light brown	NaCl	80	2200	18	Light yellow
Ia	Light yellow	NaCl	80	2400	18	Orange
Ia	Light brown	NaCl	80	2400	18	Orange
IIa	Light brown	NaCl	80	2300	18	Colourless
IaA/B	Light brown	Graphite	79	2300	18	Deep yellow
IaA/B	Dark brown	Graphite	79	2300	18	Very light yellow
IaA/B	Dark brown	Graphite	79	2300	18	Colourless
IaA/B	Light brown	Graphite	79	2000	18	Colourless
IaB	Brown	Graphite	79	2000	18	Brown
IaB	Brown	Graphite	79	2000	18	Brown
IIb	Light steely brown	Graphite	79	2300	18	Light blue
IIa	Medium brown	Graphite	80	2300	18	Light pink

* From US 2002/0172638 A1,[17]

Inventors: S.S. Vagarali, S.W. Webb, W.E. Jackson, W.F. Banholzer, T.R. Anthony; applicant: General Electric Company, Schenectady, NY, USA

which vacancy clusters are assumed to be responsible for the brown coloration of natural diamonds. A recent review by Fisher (2009) summarizes these aspects. Because these vacancy clusters are altered and become partly unstable by HPHT treatment, this process is applied to large quantities of natural brown diamonds to transform their colour into one that is more desirable for jewellery purposes.

This more recent interpretation that the brown is due to vacancy clusters, however, is not referred to in the various patent documents which are reviewed and summarized in the present paper. If the cause of colour change is discussed in a patent, the older interpretation based on the removal of colour centres associated with plastic deformation is normally quoted.

Table III shows examples of HPHT treatment of pale to dark brown diamonds, based on a patent application by General Electric which had been filed in October 1997 but only published in 2002.[17] It shows how different the colours can be after treatment and the major types of change are shown in a diagrammatic overview in *Figure 7*.

In nitrogen-free type II and almost nitrogen-free type I natural diamonds, the removal of brown colour centres results in colourless *(Figure 8)* or almost

HPHT treatment of diamonds — a review of the patent literature from five decades (1960–2009)

HPHT colour enhancement of natural diamonds

Original colour (brown) → Final colour

Type IIa —HPHT→ Type IIa — Colourless (D–J)

Type IIa or Type IIb —HPHT→ Type IIa, Type IIa, Type IIb — Pink or blue

Type Ia —HPHT→ Type Ia, Type Ia / Type Ia, Type Ia, Type Ia — Yellow or greenish yellow to yellowish green

Type Ib —HPHT→ Type Ib — Yellow

Figure 7: Systematic overview of possible colour alteration by HPHT treatment of natural brown type I and II diamonds. This diagram is based on a somewhat smaller schema by V. Vins, Institute of Single Crystals, Novosibirsk, Russia, which has been extended by the present author.

Figure 8: This type IIa diamond of 0.70 ct was originally brown and treated in a HPHT process. Photograph by courtesy of J.-P. Chalain, SSEF Swiss Gemmological Institute, Basel, Switzerland.

Figure 9: This type IIa diamond of 0.50 ct was originally brown and treated in a HPHT process. Photograph by courtesy of E. Erel, Carat Gem Lab, Gemological Laboratory, Montigny-les-Metz, France.

colourless diamonds.[16,17,18,21,25] If pink colour centres or their precursors, whose exact nature is still in debate, are present in the untreated material but hidden by the brown coloration, after HPHT treatment and removal of the brown colour centres and possible alteration of precursor centres, the diamonds become pink (Figure 9), a colour which is highly sought after.[16,17,18,19] A similar mechanism applies to brown, brownish grey, grey or olive green samples with boron contents (type IIb diamonds, Figure 10). The HPHT treatment causes removal of brown colour centres and a possible change of blue precursor centres and can result in stones with the highly appreciated and extremely rare blue to pale blue coloration of natural

diamonds.[16,17,18,20] Details of the reaction mechanism involved in the formation and/or alteration of the blue and pink coloration of natural diamonds by HPHT treatment were recently summarized by Fisher et al. (2009).

Brown nitrogen-bearing natural diamonds can contain a range of brown colour centres, nitrogen related A and B centres and, rarely, C centres (type Ib natural brown diamond); they may also contain nitrogen trapped as N3 centres (3N-V centre, consisting of one vacancy and three nitrogen atoms) as well as N2 centres (another nitrogen-related defect). If only N3 and N2 colour centres were present, a more or less pale to intense yellow coloration would result from

treatment (Figure 11). The colours of these types of natural brown diamonds resulting from treatment (Figure 11) show some variability between yellowish green, greenish yellow, a more or less intense yellow, orange and greenish orange.[15,16,17,18,25] The different colours (Figures 12, 13 and 14) are a function of the different ratios of N3 and N2 centres versus H4, H3 and H2 centres present in the treated samples. The intensity of the yellow component is related to the relative concentration of N3, N2, H3 and H4 centres and the intensity of the greenish yellow to green component is related to the concentration of H2 centres. Many HPHT-treated brown nitrogen-bearing natural diamonds also exhibit green H3 luminescence which increases the amount of green perceived.

The complex reaction mechanism is summarized as follows: brown colour centres are removed or modified, a process which is associated with the mobilization of vacancies. The vacancies are trapped at various nitrogen defects

HPHT treatment of diamonds — a review of the patent literature from five decades (1960–2009)

present, e.g. at A and B centres forming N-V-N (H3) and other colour centres. The H4 centres formed in this process may become partly unstable and dissociate into H3 centres. The concentration of N3 centres may also be changed within these complex processes, especially when the samples are treated in a sequence of several steps at various temperatures.

Formation of intense pink to red diamonds by a three-step treatment process

The process discussed in this section is applied to natural type Ia colourless to brown diamonds.[24] HPHT treatment is performed for dissociation of A centres into N atoms that are isolated in the diamond structure (C centres). Subsequent electron irradiation forms a high concentration of vacancies, which combine with the isolated nitrogen atoms in a subsequent annealing step and form the desired N-V colour centres, which are responsible for the intense pink to red coloration of the diamonds (*Figure 15*). Due to the formation of other nitrogen-vacancy defects, the colour of a diamond after this three-step treatment process can vary between violet, purple red, red, orange red and orange (for a gemmological description and spectroscopic characterization of such kinds of stones see Wang *et al.*, 2005). A similar process but in four steps is applied to synthetic type Ib diamonds:[7]

1. irradiation,
2. HPHT treatment,
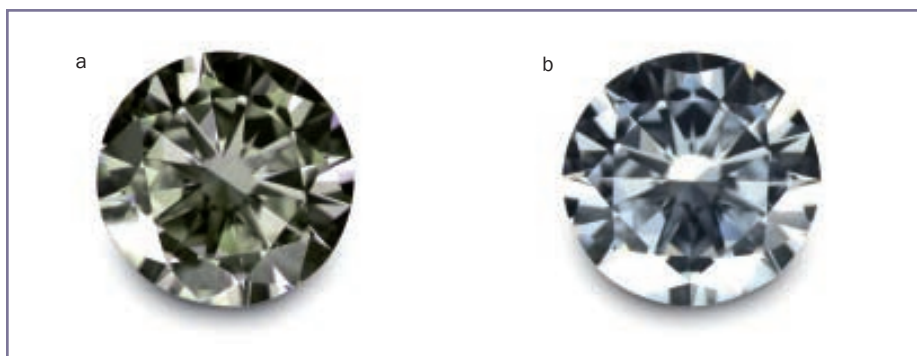3. second irradiation, and
4. annealing.

Figure 10 a,b: This type IIa diamond of 0.50ct (a) was originally olive green and treated in a HPHT process and became pale blue (b). Photograph by courtesy of T. Hainschwang, Gemlab, Gemological Laboratory, Balzers, Liechtenstein.
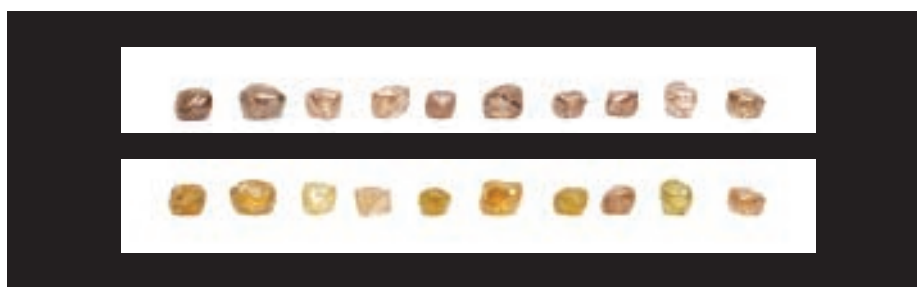

Figure 11: Suite of originally brown to yellowish brown diamonds before (above) and after HPHT treatment; weights range from 0.75 to 0.95 ct. Photograph by courtesy of J.-P. Chalain, SSEF Swiss Gemmological Institute, Basel, Switzerland.
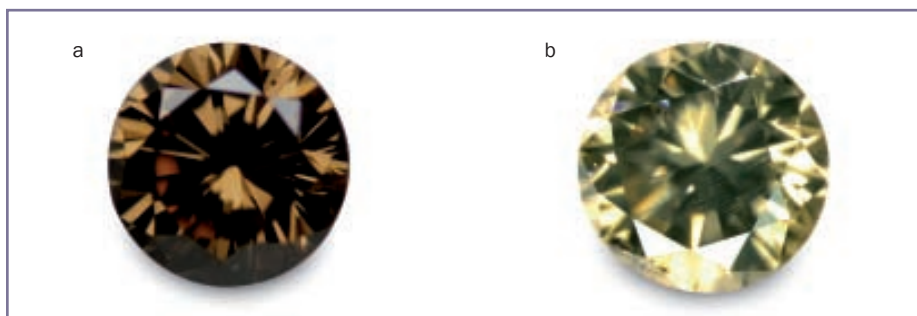

Figure 12 a,b: This originally brown type Ib diamond of 0.13 ct (a) was treated in a HPHT process and became pale yellow (b). Photograph by courtesy of T. Hainschwang, Gemlab, Gemological Laboratory, Balzers, Liechtenstein.

Figure 13: This type Ia diamond of 1.30 ct was originally brown and treated in a HPHT process. Photograph by courtesy of E. Erel, Carat Gem Lab, Gemological Laboratory, Montigny-les-Metz, France.

Figure 14 a,b: This type Ia diamond of 2.10 ct (a) was originally brown and treated in a HPHT process and became yellowish green (b). Photograph by courtesy of T. Hainschwang, Gemlab, Gemological Laboratory, Balzers, Liechtenstein.

HPHT treatment of diamonds — a review of the patent literature from five decades (1960–2009)

Figure 15: This type Ia diamond of 1.25 ct was originally brown and treated in a three-step process by a) HPHT, b) electron irradiation and c) annealing. Photograph by courtesy of V. Vins, Institute of Single Crystals, Novosibirsk, Russia.

In steps 1 and 2, some of the isolated nitrogen atoms (C centres) are transformed into aggregated nitrogen (A centres). In step 3, vacancies are formed which combine with C and A centres in step 4 to form N-V and H3 centres. Although the patent application primarily describes the production of synthetic diamond for laser applications, it is obvious that with the actual parameters within this four-step process, e.g. nitrogen contents of the sample and variable treatment conditions (irradiation doses, annealing temperatures) a great variety of colours may be produced.

Colour improvement and alteration of yellow to brown synthetic diamond grown by CVD

The progress in crystal growth within the last decade in application of the CVD technique leads to synthetic diamonds grown on diamond seeds or other diamond layers with sufficient thickness and quality to be cut as gems. The as-grown material may be brown, orange brown, pinkish brown or yellow. HPHT treatment is applied to remove defects in CVD-grown synthetic diamonds, which — at least partly — are different from the major defects found in natural and synthetic HPHT-grown diamonds. The resulting colour of the samples is closely related to the treatment temperature and the concentration of different defects in the as-grown diamond crystals or diamond layers.[29,30,31] It is reported that the resulting coloration after HPHT treatment is colourless or near colourless (Figure 16), but pale brown, green or pinkish brown colours may also result.

Conclusion

HPHT treatment of natural brown diamonds has become an important technical process of colour alteration in order to transform such diamonds into marketable qualities. With the progress of diamond synthesis by CVD, the importance of treatment of yellow to brown jewellery-quality CVD-grown synthetic diamonds is also increasing. The application of HPHT treatment in combination with electron irradiation is performed to acquire some specific rare colours, e.g. to transform the colour of natural diamonds into red or pink or to alter the colour of yellow synthetic diamonds to green or other colours.

References

Anthony, T., and Casey, J., 1999. Research on diamonds at the General Electric Company. *Gems & Gemology,* **35**(3), 15

Avalos, V., and Dannefaer, S., 2003. Vacancy-type defects in brown diamonds investigated by positron annihilation. *Physica,* **B 340-342,** 76–9

Barnard, A.S., 2000. NovaDiamond®. Colour enhanced yellow and yellow-green diamonds. *Australian Gemmologist*, **20**(12), 517–22

Collins, A.T., 2001a. High-temperature annealing of colour centres in diamond. In: Tzeng, Y. *et al.* (Eds). *Proceedings of the Sixth Applied Diamond Conference/Second Frontier Carbon Technology Joint Conference,* 223–31

Collins, A.T., 2001b. The colour of diamond and how it may be changed. *Journal of Gemmology,* **27**(6), 341–59

Collins, A.T., Kanda, H., and Kitawaki, H., 2000. Colour changes produced in natural brown diamonds by high pressure, high-temperature treatment. *Diamond and Related Materials,* **9**, 113–22

De Weerdt, F., and Collins, A.T., 2003. The influence of pressure on high-pressure, high temperature annealing of type Ia diamond. *Diamond and Related Materials,* **12**, 507–10

De Weerdt, F., and Van Royen, J., 2000. Investigation of seven diamonds, HPHT treated by NovaDiamond. *Journal of Gemmology,* **27**(4), 201–8

Erel, E., 2009. Diamants de couleur traits à haute température et à haute pression. *Revue de Gemmologie AFG*, **167**, 10–17
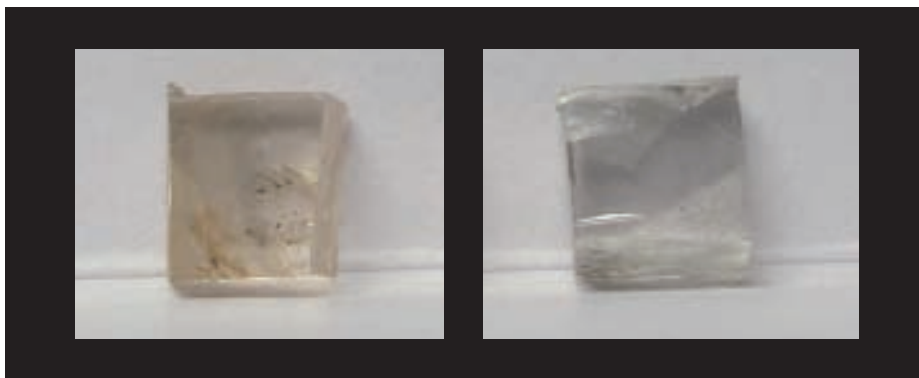
Figure 16: This pale brown CVD-grown synthetic diamond of about 0.25 ct (left) was treated in a HPHT process and became almost colourless (right). Photograph by courtesy of J.-P. Chalain, SSEF Swiss Gemmological Institute, Basel, Switzerland.

HPHT treatment of diamonds — a review of the patent literature from five decades (1960–2009)

Fisher, D., 2009. Brown diamonds and high pressure high temperature treatment. *Lithos,* **112S**, 619-24

Fisher, D., Sibley, S.J., and Kelly, C.J., 2009. Brown colour in natural diamond and interaction between the brown related and other colour-inducing defects. *Journal of Physics: Condensed Matter,* **21**(36), 10 pp

Hainschwang, T., 2003. *Classification and color origin of brown diamonds.* Diplôme d'Université de Gemmologie de Nantes, 91 pp

Hainschwang, T., Katrusha, A., and Vollstaedt, H., 2005. HPHT treatment of different classes of type I brown diamonds. *Journal of Gemmology,* **29**(5/6), 261–73

Katrusha, A.N., Zanevskyy, O.A., Ivakhnenko, S.A., and Vollstaedt, H., 2003. High pressure high temperature treatments (HPHT) for color changes of natural gem diamonds. *Jewellery Business, Kiev,* **2**(4), 42–7

Krutko, O.B., Kosel, P.B., Wu, R.L., Fries-Carr, S.J., Heidger, S., and Weimer, J., 2000. P-type polycrystalline diamond layers by rapid thermal diffusion of boron. *Applied Physics Letters,* **76**(7), 849–51

Moses, T.M., Shigley, J.E., McClure, S.F., Koivula, J.I., and Van Daele, M., 1999. Observations on GE-processed diamonds: a photographic record. *Gems & Gemology,* **35**(3), 14–22

Overton, T.W., and Shigley, J.E., 2008. A history of diamond treatments. *Gems & Gemology,* **44**(1), 32–55

Popovici, G., Wilson, R.G., Sung, T., Prelas, M.A., and Khasawinah, S., 1995a. Diffusion of boron, lithium, oxygen, hydrogen, and nitrogen in type IIa natural diamond. *Journal of Applied Physics,* **77**(10), 5103–6

Popovici, G., Sung, T., Prelas, M.A., Wilson, R.G., and Khasawinah, S., 1995b. Diffusion of boron, hydrogen, oxygen, and lithium in single crystalline and polycrystalline diamond. A novel method for the determination of the state of an impurity: forced diffusion of boron in Ia type natural diamond. In: Prelas, M.A., *et al.* (Eds). *Wide Band Gap Electronic Materials.* Kluwer Academic Publishers, Dordrecht, The Netherlands. pp 15–29

Reinitz, I.M., Buerki, P.R., Shigley, J.E., McClure, S.F., and Moses, T.M., 2000. Identification of HPHT-treated yellow to green diamonds. *Gems & Gemology,* **36**(2), 128–37

Schmetzer, K., 1999a. Behandlung natürlicher Diamanten zur Reduzierung der Gelb- oder Braunsättigung. *Goldschmiede Zeitung,* **97**(5) 47–8

Schmetzer, K., 1999b. Clues to the process used by General Electric to enhance GE POL diamonds. *Gems & Gemology,* **35**(4), 186–90

Schmetzer, K., 2000. Zum Behandlungsverfahren der GE POL-Diamanten. *Goldschmiede Zeitung,* **98**(6) 85–8

Shigley, J.E., McClure, S.F., Breeding, C.M., Shen, A.H., and Muhlmeister, S.M., 2004. Lab-grown colored diamonds from Chatham Created Gems. *Gems & Gemology,* **40**(2), 128–45

Smith, C.P., Bosshart, G., Ponahlo, J., Hammer, V.M.F., Klapper, H., and Schmetzer, K., 2000. GE POL diamonds: before and after. *Gems & Gemology,* **36**(3), 192–215

Sung, T., Popovici, G., Prelas, M.A., and Wilson, R.G., 1996. Boron diffusion coefficient in diamond. In: Dreifus, D.L. *et al.* (Eds). Diamond for electronic Applications. *Materials Research Society Symposium Proceedings,* 416, 467–70

Sundance Diamonds, 2006. See web list

Vins, V.G., 2001. Changing diamond colour. *Gemological Bulletin,* **3**, 19–30

Vins, V.G., and Yelisseyev, A.P., 2008. Physical fundamentals behind modern techniques of natural diamond enhancement. *Australian Gemmologist,* **24**(5), 219–21

Wang, W., Smith, C.P., Hall, M.S., Breeding, C.M., and Moses, T.M., 2005. Treated-color pink-to-red diamonds from Lucent Diamonds Inc. *Gems & Gemology,* **41**(1), 6–19

Web List

Sundance Diamonds, 2006. Understanding the basics of HPHT processing. http://www.sundancediamonds.com/files/The-Sundance-Process.pdf

More bibliographic data on patent documents cited in this review are given in Appendix C in the expanded version of the paper at http://tinyurl.com/gem-a-jog-32-schmetzer.

The Author

Dr Karl Schmetzer
D-85238 Petershausen, Germany
email: SchmetzerKarl@hotmail.com

The Gem-A TravelGem Microscope

A compact microscope designed for gemmologists — ideal for students, valuers and gem dealers.

Price: £325.00

plus VAT, postage and packing

A 10% discount is given on all instruments ordered by Gem-A members and Gem-A registered students.

- Fitted aluminium travel case
- 10x, 20x, 30x and 60x magnification
- Stone holder and dark field assembly can be removed to examine jewellery
- Runs on 110 and 220 volts (built in transformer)
- Bright field, dark field and top lighting

To order your TravelGem Microscope from the Gem-A shop go to www.gem-a.com/shop.aspx or contact Alan Clark on +44 (0)20 7404 3334, email shop@gem-a.com.

Gem-A
THE GEMMOLOGICAL ASSOCIATION OF GREAT BRITAIN

The gemmological properties and infrared spectra of brucite, an imitation of nephrite and Shoushan stone

Li Jianjun, Yu Xiaoyan, Cai Jia, Liu Xiaowei, Fan Chengxing and Cheng Youfa

Abstract: Nephrite and Shoushan stones have a long history of use as ornamental gem material for jewellery and carving in China. However, the reserves of the stones have dramatically decreased recently and a growing number of their imitations, such as brucite, have entered the Chinese market. Microscope examination, testing with dilute hydrochloric acid, Fourier Transform Infrared (FTIR) spectra and energy-dispersive X-ray fluorescence (EDXRF) spectra have proved to be useful techniques to distinguish nephrite or Shoushan stones from brucite.

Keywords: brucite, gemmological properties, infrared spectra, nephrite, Shoushan stone,

Introduction

In China over the past 5000 years, high quality nephrite has been carved as royal seals, the emblem of power of emperors (Yang *et al.*, 1986; Chen et al., 2004; Tang *et al.*, 2002). Shoushan stone has also been carved as seals, and is named from its source in Shoushan in the northern suburbs of Fuzhou, Fujian province, P.R. China (Wu and Cui, 1999). Shoushan stone comprises around one hundred varieties, among which 'Tianhuang stone' is the most precious and enjoys a reputation as 'the emperor of stones'. Ever since Tianhuang stone became the favourite of Qianlong, an emperor of the Qing Dynasty, its price has been high. It is said that one Liang (a unit of mass equivalent to 50 g used in ancient China) of Tianhuang stone is worth ten Liang of gold.

However, because of scarce reserves,

the trade price of Tianhuang stone has been up to a hundred times that of gold. In turn, this helps raise the price of other varieties of Shoushan stone.

In recent years the most sought-after gem materials mentioned above have become more available and have sold for very high prices. This in turn has led to a wider range of material being considered as gemstones. Hitherto, most Shoushan stone has consisted of the kaolin group minerals dickite and nacrite, or of pyrophyllite, rarely of illite (see Box A). This paper aims to characterize a recent imitation of nephrite and Shoushan stone which consists of brucite.

Materials and methods

The Laboratory of the National Gold and Diamond Testing Center (NGDTC) of P.R. China recently received a sample

(numbered B1) that was described as Shoushan stone from the Shanbowei deposit by the retailer. Its diaphaneity, lustre and colour (greyish green and reddish brown) *(Figure 1)* are indeed similar to some varieties of Shoushan stone. In addition, two strands of beads (B2 and B3) *(Figure 2)* were submitted by a client who stated that they were sold to him as nephrite. However, both strands showed an unusually dim lustre compared to nephrite. B1, B2 and B3 are actually all the same material, brucite, although they show considerable differences in appearance. For the purposes of this investigation, a glass imitation of nephrite (B4) and a strand of nephrite beads with relatively strong lustre numbered B5, are characterized for comparison.

The samples were tested by routine gemmological methods. Mohs'

The gemmological properties and infrared spectra of brucite, an imitation of nephrite and Shoushan stone

Table I: Gemmological properties of samples B1 to B5, and Shoushan stone of the dickite and/or nacrite type and Shoushan stone of the pyrophyllite type.

| Property | Carving | Strands of beads | | | | Shoushan stone of the dickite and/or nacrite type† | Shoushan stone of the pyrophyllite type† |
	B1	B2	B3	B4	B5		
Size (mm)	130×100×85	8	12	8	8		
Colour	greyish-green and reddish brown	white	white	white	white	greyish white, greyish yellow, brownish red	white, yellowish green, dark purple, yellow, brownish red, grey
diaphaneity	translucent to semitranslucent	translucent	translucent	translucent	semitransparent to translucent	semitranslucent to opaque	semitranslucent to opaque
Lustre	greasy	waxy	waxy	vitreous	vitreous	subvitreous to waxy	waxy
SG	2.39	*	*	*	*	2.57~2.68‡	2.65~2.90‡
Mohs' hardness	2.5	2.5~3	2.5~3	6	3~6.5	2.5~3	2~3
RI distant vision	1.55	1.56	1.56	1.52	1.57~1.62	1.56~1.57	1.56~1.57
UV fluorescence							
short-wave	inert	inert	very weak	weak to faint white	very weak	inert-strong white	inert-strong white
long-wave	inert	inert	parts faint white	strong bluish white	parts faint white	inert-strong white	inert-strong white
Internal features	resemble veins in radishes	wispy inclusions resembling cotton	fine-grained wispy inclusions	radial microcracks	fine-grained texture resembling 'glutinous rice'	fine pyrite inclusions, red spots, resemble veins in radishes	most common were red or yellow spots, red healed fractures
Reaction to hydrochloric acid (HCl)	no gas bubbles, but etch pits were observed	none to few gas bubbles with etch pits	none to few gas bubbles with etch pits	inert	abundant gas bubbles to no gas bubbles	inert	inert

* SGs of beads not measured

† Data from Sun *et al.* (2003) and Feng *et al.* (2008)

‡ SG data is a very important feature in distinguishing the two types of Shoushan stone, while advanced instruments should be applied to identify them with accuracy

The gemmological properties and infrared spectra of brucite, an imitation of nephrite and Shoushan stone

hardnesses were obtained using standard minerals and the 2.5 values in *Table I* refer to comparisons with fingernails. Refractive indices (RIs) using the distant vision method were measured with a gemmological refractometer; specific gravity (SG) values were obtained using an electronic balance with deionized water as a measuring medium. Fluorescence was tested using standard long-wave (365 nm) and short-wave (254 nm) UV lamps. Internal features were examined with a binocular gemmological microscope using darkfield and brightfield illumination at 10× to 70× magnification.

In addition, dilute hydrochloric acid was used to test inconspicuous areas on the five samples to see if there was any effervescence.

A Thermo Nicolet NexusTM 470 Fourier Transform Infrared (FTIR) spectrometer equipped with a specular reflection accessory and a CentaurµsTM Infrared (IR) Microscope was used to obtain IR spectra. The range between 6000–400 cm^{-1} at a standard resolution of 4 cm^{-1} with 16 scans (per spectrum), was recorded for each sample using two methods. Powdered samples were compressed into KBr pellets for measurement in transmission mode; and the specular reflection method was used on the solid sample. The IR spectra of five samples were obtained before the backgrounds were scanned at room

Figure 1: Carving of a Chinese traditional pattern in brucite (sample B1); it is 130 mm tall and 100 mm wide. This imitates high quality Shoushan stone. Photo by Li Jianjun.

temperature. The IR spectra of B1 were recorded using the specular reflection accessory because its size exceeds the sample stage of the IR microscope. Other samples were examined by using the IR microscope.

X-ray fluorescence spectra of B2 and B3 were recorded using a Thermo Noran QuanX EC EDXRF spectrometer at 20 kV with a Rh target and no filter. The data acquisition time was 100 seconds for each sample spectrum at vacuum.

Results and discussion
Gemmological properties

Samples B1–B5 were subject to routine gemmological examination and the results are presented in *Table I*; the properties of Shoushan stone of the dickite and/or nacrite type as well as Shoushan stone of the pyrophyllite type are also given for comparative purposes.

No obvious absorption spectra were observed in samples B1–B5 when viewed with a hand-held spectroscope examined at NGDTC. The gemmological properties of B4 (*Table I*) indicate that the beads are glass and those of B5 suggest that the beads are nephrite, but the SG, hardness and RIs of B1, B2 and B3 are not diagnostic for identification.

FTIR spectroscopy

Two beads from B2 and three beads from B3 were selected at random and IR spectra obtained using the FTIR microscope. Also, spectra from B1 were obtained using the specular reflection accessory. Infrared spectra typical of the different kinds of Shoushan stone are given in *Box A*

In the range 1200–400 cm^{-1}, the IR reflectance spectra of B1, B2 and B3 showed strong and broad reflection bands below 800 cm^{-1} (*Figure 3*) indicating the presence of a metal oxide or hydroxide; this is consistent with the results of the IR transmission spectra of B3 (see *Figure 5*).

In the range 2000–800 cm^{-1}, B1, two beads from B2 (see *Figure 4,* B2a and B2b) and one bead from B3 (see *Figure 4,* B3a) exhibited broad reflection bands positioned at ~1550–1400 cm^{-1}. These are due to the stretching vibrations of the CO_3^{2-} group. Bands centred at 890 cm^{-1} detected in B1 (see *Figure 4,* B1) and B2 (B2a and B2b) can be assigned to the bending vibrations caused by the CO_3^{2-} group which are consistent with magnesite (MgCO$_3$) (Santillan *et al.*, 2005). Therefore both B1 and B2 contain a metal oxide or hydroxide as the main component and a small amount of magnesite.

Transmission IR spectra from a mineral mixed with KBr commonly give results

Figure 2: Sections of four strands of beads (of diameters between 8 and 12 mm) sample numbers B2, B3, B4 and B5. They are all pale grey and have a vitreous to waxy lustre that could easily be confused with white nephrite or some varieties of Shoushan stone. These strands of beads are identified as brucite (B2 and B3), glass (B4) and nephrite (B5). Photo by Li Jianjun.

The gemmological properties and infrared spectra of brucite, an imitation of nephrite and Shoushan stone
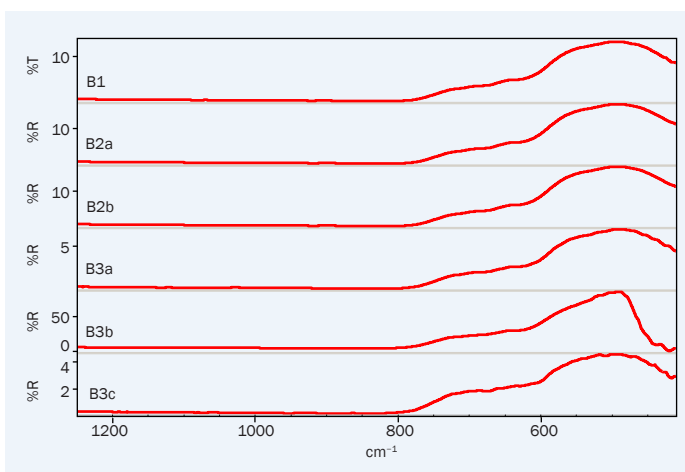

Figure 3: Reflectance IR spectra of sample B1 and five beads randomly selected from samples B2 and B3 show similar broad reflection peaks, centred below 800 cm⁻¹, indicating that all three materials are the same.
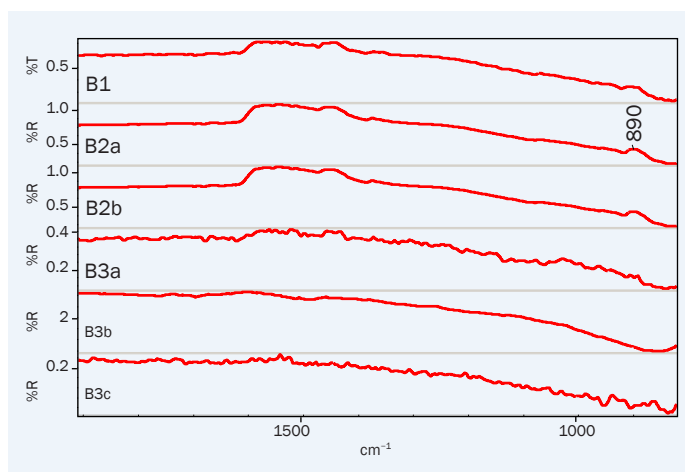

Figure 4: Reflectance spectra of the samples in Figure 3 in a different IR range, showing similar reflection bands between ~1550 and 1400 cm⁻¹ due to the stretching vibration of the CO_3^{2-} group. B1, B2a and B2b show reflection bands centred at 890 cm⁻¹ caused by bending vibrations of the CO_3^{2-} group, indicating that magnesite ($MgCO_3$) is present.

which are more accurate than spectra from the reflection mode. Therefore one bead of B3 was selected and powder scraped from an inconspicuous area. *Figure 5* shows the transmission spectrum of B3. In the 4000–3000 cm⁻¹ region, a sharp band centred at 3698 cm⁻¹ along with a broad band at 3420 cm⁻¹ correspond to vibrations and stretching of OH bonds (Braterman and Cygan, 2006). Comparing the IR spectra of B1, B2 and B3 with those published by Peng and Liu (1982), the carving and beads

can be identified as brucite ($Mg(OH)_2$).

The reflection IR spectra recorded from each bead of B4 were almost the same; the broad peak between 1200 and 800 cm⁻¹ is assigned to Si-O vibrations in the $[SiO_4]$ group. No split peaks caused by silicate minerals were observed, indicating that the beads are amorphous (see *Figure 6*).

However, the reflection IR spectra of beads of B5 showed obvious variation *(Figure 6)*. The main mineral component of B5 is tremolite and in some beads there

are small amounts of ferroan dolomite (ankerite) which is indicated by reflection peaks in the 1600–1400 cm⁻¹ region; these are due to stretching vibrations of the CO_3^{2-} group; also a peak at 877 cm⁻¹ is assigned to a CO_3^{2-} group bending vibration. The presence of ferroan dolomite in B5 (nephrite) is in agreement with the fact that the nephrites occur in dolomitic marbles associated with metasomatic alteration (Wang *et al.*, 1990; Yui and Kwon, 2002).
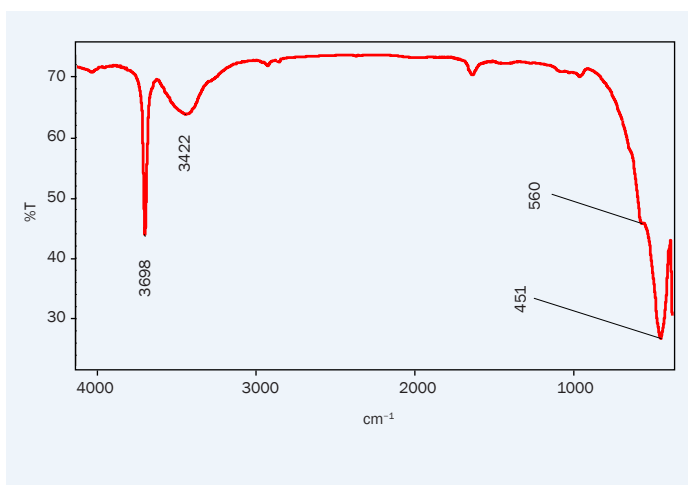

Figure 5: Transmittance IR spectrum obtained from powder from the drill hole of a B3 bead mixed with KBr and pelletized. The bands positioned at 3698 and 3422 cm⁻¹ can be assigned to OH stretching vibrations (Braterman and Cygan, 2006). The bands at 451 and 560 cm⁻¹ are consistent with brucite ($Mg(OH)_2$) (Peng and Liu, 1982).
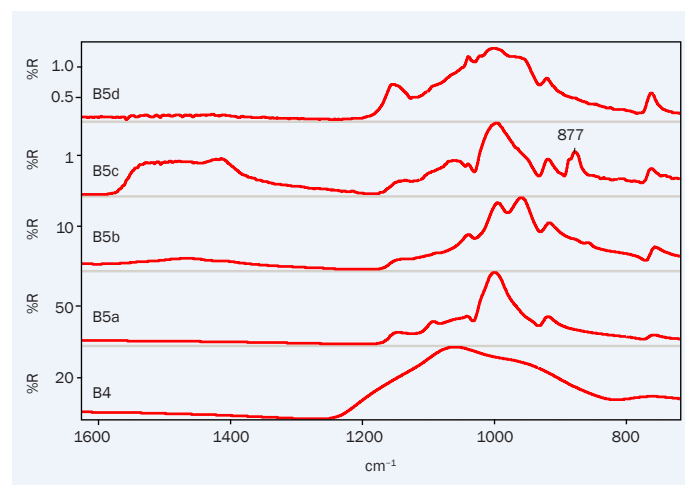

Figure 6: The reflectance IR spectrum of B4 shows only one broad band positioned at 1100–800 cm⁻¹ due to Si-O vibrations, suggesting that it is amorphous. The reflectance spectra of the nephrite beads B5 show obvious variation. Note particularly that in the 1600–1400 cm⁻¹ range, there are peaks in B5c which can be assigned to stretching vibrations of the CO_3^{2-} group, and a peak at 877 cm⁻¹ due to bending vibrations in the CO_3^{2-} group, both indicating the presence in the nephrite of a carbonate mineral.

The gemmological properties and infrared spectra of brucite, an imitation of nephrite and Shoushan stone

Box A

Almost all Shoushan stone is composed either of dickite and/or nacrite, or of pyrophyllite; rare specimens consist of illite and sericite.
Typical IR spectra of the main Shoushan stone constituents are given below with comments.
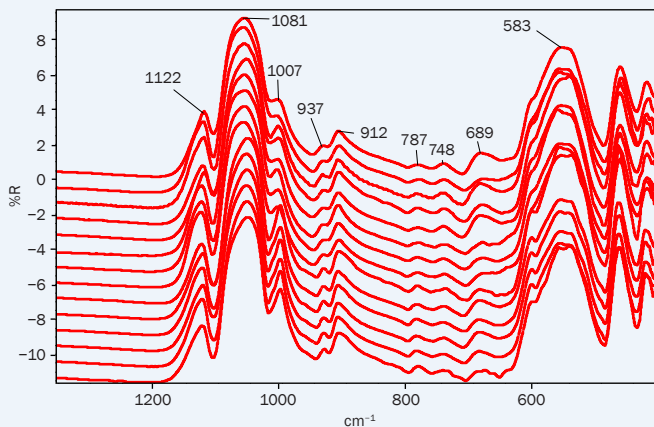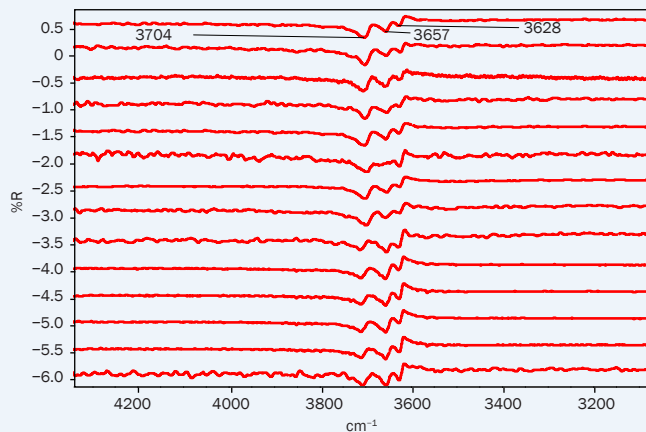
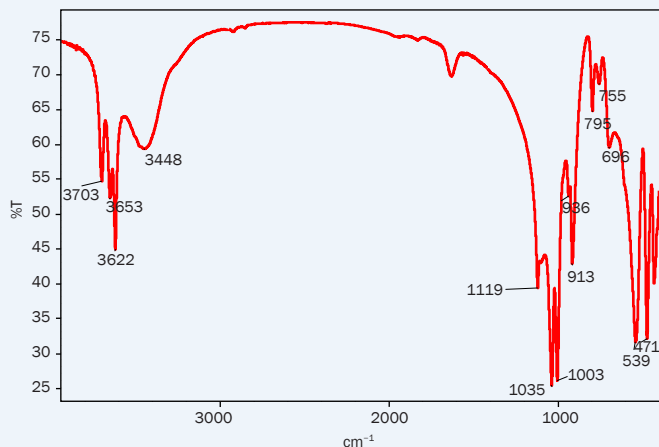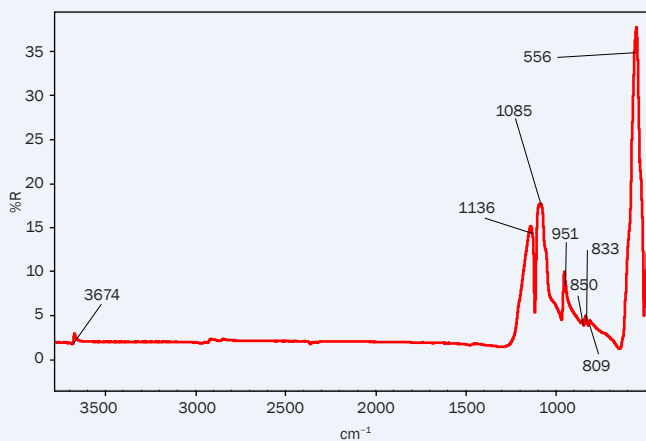*Figure A1*

Figure A2

Figure A3

Figure A4

Figure A5
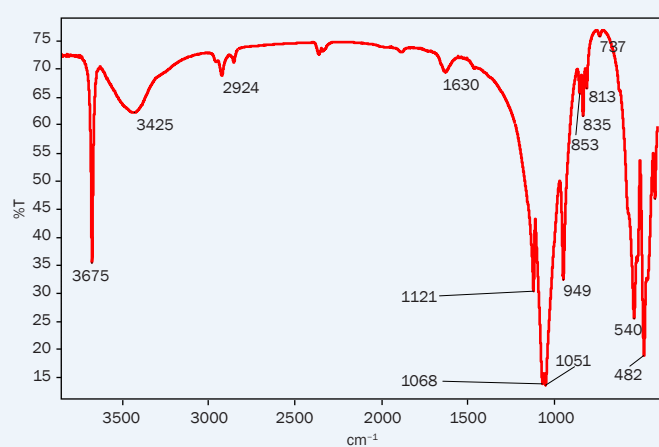
Figure A1: Reflectance spectra of Shoushan stone of the dickite and/or nacrite type showing peaks in the 1200–1000 cm^{-1} range arising from stretching vibrations of Si-O bonds (Shoval et al., 2002), 912 and 1007 cm^{-1} caused by bending vibrations of OH bonds (Fang et al., 2005).

Figure A2: Reflectance spectra of Shoushan stone of the dickite and/or nacrite type showing bands centred at 3704, 3657 and 3628 cm^{-1}, which are assigned to O-H stretching bonds (Franco et al., 2006).

Figure A3: Transmission IR spectrum of dickite showing peaks at 3703, 3653 and 3622 cm^{-1} corresponding to OH stretching bonds (Balan et al., 2002).

Figure A4: The IR reflection spectrum of Shoushan stone of the pyrophyllite type showing a weak band at 3674 cm^{-1} which arises from the u(OH) vibration (Wang et al., 2002); the peaks at 850 and 809 cm^{-1} show the presence of quartz and kaolinite (Amritphale et al., 1992).

Figure A5: Transmission spectrum of Shoushan stone of the pyrophyllite type showing a sharp band at 3675 cm^{-1} due to the u(OH) vibration (Ignacio Sainz-Diaz et al., 2004).

The gemmological properties and infrared spectra of brucite, an imitation of nephrite and Shoushan stone

EDXRF

Samples B2 and B3 were quantitatively analysed using an EDXRF spectrometer and the results indicate major Mg along with Si, Ca and Fe as trace elements in both samples (Li *et al*., 2008).

Conclusions

Brucite, a layered magnesium hydroxide, is extracted on an industrial scale along with dolomite, dolomite marble and serpentinite and refined to produce magnesium. Most is white but some is multicoloured when traces of iron or manganese are present. Some of the more attractive material is now being used as an imitation of nephrite jade and Shoushan stone, both of which are highly valued by the Chinese people.

As the price of high-quality nephrite increased by virtue of its rarity, lower quality nephrite came onto the market to meet the demand for 'jade'. This lower quality nephrite can contain impurities of calcite and dolomite — which lower the RI, SG and hardness of the stone and, at the same time, provide the opportunity for materials of similar properties to come onto the market. Brucite is a good example.

It is not easy to identify brucite by using standard gemmological techniques although its unusually dim lustre would suggest that the material being examined is an imitation. EDXRF may provide clues to determine the material by analysing the major and minor elements it contains, but further work is necessary to confirm the applicability of this testing procedure. When examining samples like brucite which have gemmological properties such as a Mohs' hardness of 2–4 and are translucent to opaque, routine gemmological examinations are not sufficient to determine their identity. However, FTIR spectroscopy using both KBr pellets in transmission mode and the solid sample in reflection mode can provide conclusive evidence that the imitation is actually brucite.

Acknowledgement

References

Amritphale, S.S., Navin, C., and Rajendra, K., 1992. Sintering behaviour of pyrophyllite mineral: effect of some alkali and alkaline-earth metal carbonates. *Journal of Materials Science,* **27**, 4797–804

Balan, E., Allard, T., Morin, G., and Calas, G., 2002. Incorporation of Cr^{3+} in dickite: a spectroscopic study. *Physics and Chemistry of Minerals,* **29**, 273–9

Braterman, P.S., and Cygan, R.T., 2006. Vibrational spectroscopy of brucite: a molecular simulation investigation. *American Mineralogist,* **91**, 1188–96

Chen T.H., Calligaro, T., Pages-Camagna, S., and Menu, M., 2004. Investigation of Chinese archaic jade by PIXE and μRaman spectrometry. *Applied Physics A,* **79**, 177–80

Fang Z.D., Wang D.J., and Zhang C.Y., 2005. Thermal decomposition and non-isothermal kinetics of dickite. *Chinese Journal of Chemical Physics,* **18**(4), 619–24

Feng Y., Di J.R., Yao C.M., and Zheng J., 2008. Study on composition characteristics of reddish brown series of larderite. *Journal of Gems and Gemmology,* **10**(4), 13–17

Franco, F., and Ruiz Cruz, M.D., 2006. A comparative study of the dehydroxylation process in untreated and hydrazine-deintercalated dickite. *Journal of Thermal Analysis and Calorimetry,* **85**, 369–75

Ignacio Sainz-Diaz, C., Escamilla-Roa, E., and Hernandez-Laguna, A., 2004. Pyrophyllite dehydroxylation process by first principles calculations. *American Mineralogist,* **89**, 1092–100

Li Jianjun, Cheng Youfa and Liu Huafeng, 2008. Identification of brucite. *Journal of Gems & Gemmology,* **10**(2), 30–33

Parise, J.B., Leinenweber, K., Weidner, D.J., Tan, K., and Von Dreele, R.B., 1994. Pressure-induced H bonding: neutron diffraction study of brucite, $Mg(OD)_2$, to 9.3 GPa. *American Mineralogist,* **79**, 193–6

Peng Wenshi and Liu Gaokui, 1982. *Data pool of the spectra of minerals.* Publishing House of Science, Beijing, China. 129 pp

Santillan, J., Catalli, K., and Williams, Q., 2005. An infrared study of carbon-oxygen bonding in magnesite to 60 GPa. *American Mineralogist,* **90**, 1669–73

Shoval, S., Michaelian, K.H., Boudeulle, M., Panczer, G., Lapides, I., and Yariv, S., 2002. Study of thermally treated dickite by Infrared and micro-Raman spectroscopy using curve-fitting technique. *Journal of Thermal Analysis and Calorimetry,* **69**, 205–25

Sun N., Cui W.Y., and Xu X., 2003. Mineralogical characteristics and genesis of Shoushan Stone in Jialiangshan, Fujian Province. *Acta Petrologica et Mineralogica,* **22**(3), 273–8

Tang D.P., and Zheng Z.T., 1999. Mineralogy and gemmology of Shoushan Stone. *Journal of Gems and Gemmology,* **1**(4), 28–36

Tang Y.L., Liu D.Q., and Zhou R.H., 2002. Study on name, culture, quality and mineral deposit of Hetian jade. *Acta Petrologica et Mineralogica,* **21**, Supp., 13–21

Wang C.Y., Zhang H.F., and Ren G.H., 1990. Sub-microscopic textures and retrogressive metamorphic origin of Longxi nephrite. *Chinese Journal of Geochemistry,* **9**(2), 182–6

Wang L., Zhang M, Redfern, S.A.T., and Zhang Z., 2002. Dehydroxylation and transformation of the 2:1 phyllosilicate pyrophyllite at elevated temperatures: an infrared spectroscopic study. *Clays and Clay Minerals,* **50**, 272–83

Wu X.F., and Cui W.Y., 1999. A mineralogical and petrographical study of Shoushan stone (Agalmatolite). *Acta Petrologica et Mineralogica,* **18**(2), 186–92

Yang H.C., Yi X.R., Yi S.T., Song J.Z., and Min Y.M., 1986. *Xinjiang's gems and jades.* Xinjiang People's Publishing House, Urumqi, Xinjiang, China.

The gemmological properties and infrared spectra of brucite, an imitation of nephrite and Shoushan stone

73–110

Yui T.F., and Kwon S.T., 2002. Origin of a dolomite-related jade deposit at Chuncheon, Korea. *Economic Geology,* **97**, 593–601

The Authors

Li Jianjun (geoli@vip.sina.com) and **Cheng Youfa**
National Gold & Diamond Testing Center of China (NGDTC), Jinan, Shandong Province, P.R. China

Dr Yu Xiaoyan
The professor in Gemological College at the China University of Geosciences, Beijing, P.R. China

Cai Jia
China University of Geosciences, Beijing, P.R. China

Liu Xiaowei
Shandong Institute of Metrology (SDIM), Jinan, P.R. China

Fan Chengxing
Shenzhen laboratory of the National Jewellery Quality Supervision and Inspection Center of China (NJQSIC)

A new approach to the teaching and use of the refractometer

Darko B. Sturman

Abstract: Sets of simple and reliable procedures for determining gemstone RIs on the refractometer have been assembled. They have been tested with 70 calculated patterns of movements of shadow edges during the rotation of a gemstone on the refractometer. Some procedures described in literature are shown to have been based on limited understanding of observations; this may lead to incorrect identifications which can cause confusion, loss of confidence, and ultimately may lead to a waste of teaching time. All observations on isotropic, anisotropic uniaxial and biaxial gemstones in every possible orientation of the optical elements and facets can be represented by seven patterns described in graphical form in *Chart 1.* The chart shows how to identify a pattern and what can be determined from each one. Interpretation of observed data and identification of a gemstone is made on a birefringence/RI_{max} chart *(Chart 2)*. Most known faceted gemstones with RIs < 1.8 are shown on a single two-page chart.

Keywords: gem identification, optical properties, refractive index, refractometer

Introduction

Modern testing of gemstones relies more and more on the use of complex and expensive instruments. The role of the refractometer is diminished but it is still an instrument which is easily available to many gemmologists and gives very reliable and accurate data. Its proper use and proper interpretation of data may increase the confidence of observers and may give a feeling of great satisfaction to gemmologists.

Modern refractometers have better optics and larger scales than earlier models and monochromatic light is available in very small, inexpensive, easily portable and battery-operated units. Unfortunately, present practice and interpretation of data have not kept pace with improvements to the instruments; if anything, today's instructions are worse than they were a hundred years ago. Identifications of gemstones on the refractometer are still an important part of many gemmology courses but the better instruments and the greatly improved presentation possibilities have not resulted in the reduction of time needed to learn its proper use.

The reason for this is the existence of many confusing, incomplete and, even, incorrect procedures that can be found in many important textbooks or in the teaching manuals prepared by diploma-granting institutions. For a hundred years any statement or a procedure on the use of the refractometer could not be tested and, even if they were suspect, they were repeated from one edition of a textbook or a teaching manual to another.

Today, however, we have two methods available to calculate and predict the observations on any gemstone regardless of the orientation of its optical elements (optic axes or principal vibration directions X, Y and Z) and a facet. Xinhua Song *et al.* (2005) used the computer-assisted algebraic calculations to predict RI readings and the movement of the shadow edges during the rotation of a gemstone on the refractometer. Two years later in the same journal, Sturman (2007a, p.442) described a method based on the use of the stereographic projection to predict refractive index (RI) readings, movements of the shadow edges and, in addition, to determine the orientation of

the vibration directions of the shadow edges at any point during the rotation of a gemstone.

Therefore, it is now possible to test any procedure or any statement on this topic in the published literature. In preparing this paper about 70 calculated patterns were studied, changing the orientation in small or large steps and comparing patterns observed in special orientations and in 'not so perfect' special orientations. As a result, some procedures and statements in the literature were found to be incomplete, confusing or incorrect — with the potential to lead to incorrect identifications.

Two solutions to the problem offered themselves immediately: examine and test every procedure published anywhere in the literature and prepare and keep an up-to-date a list of incorrect procedures, or prepare a set of simple but accurate and safe procedures to use in teaching and, later, in practice.

I believe that the second solution is simpler and easier. For this reason, and to provide an opportunity for instructors to change their teaching approach, Part I of this article contains simple procedures that are reliable in all circumstances and Part II shows how to use observed data in identification in an equally simple and reliable way. In Appendix 3 several suggestions for faster and easier instructions are listed.

Examples of incorrect procedures can be found in many important textbooks and teaching manuals. In this introduction a brief review of some examples is presented with explanations and references offered in Appendix 1.

Description of procedures in the selected examples can range from the very simple to very complex. One simple but incorrect statement has been repeated from one edition to the next in the *Handbook of Gem Identification* by R.T. Liddicoat. Where β cannot be determined directly, it is suggested that β is calculated as the average of the two possible readings of β on biaxial gemstones. We know that one of these possible β readings is true but the other is false. Using the average between these two

numbers ensures that the result is always wrong. In some cases, the resulting error may be large enough to cause an incorrect identification. *Figures 1* and *2* in Appendix 1 show how a sinhalite may be identified as peridot if this procedure is followed.

Some textbooks and teaching manuals present incomplete and, therefore, potentially misleading information on observations on biaxial gemstones. For example, in *Gemmology* by P.G. Read referring to determination of the optic sign in biaxial gemstones, the statement that both variable shadow edges move to the same β reading is confusing for both student and graduate gemmologist because there is no indication in the text or drawings that this is observed on only a small number of gemstones — it can be seen only on facets where both optic axes are parallel, or almost parallel, to the facet (see *Pattern Va* and *b* in *Chart 1*). A gemmologist would very seldom, if ever, observe this on a gemstone. The unfortunate effects of a statement like this are that gemmologists will question their abilities as observers and, when they learn that the statement is incomplete, they may lose confidence in other statements in the book.

Similarly, a simple but incorrect statement can be found in *Gems* by R. Webster in editions up to 1994. It is stated that a gemstone with a small optic axial angle rotated on a refractometer shows one shadow edge that 'moves very little'. Studies by the author have shown that all biaxial gemstones with small, medium or large optic axial angles can have one shadow edge that 'moves very little'. Therefore, observing that one of the shadow edges of a biaxial gemstone has very little movement does not prove that it is a gemstone with a small optic axial angle. *Figure 3* in Appendix 1 shows that peridot, a gemstone with a large optic axial angle, in some orientations of the facet and the optical elements can have one shadow edge that 'moves very little'.

Another more complex procedure is found in Anderson's book (1990). Again, a diagram is used to show how, in some cases, a peridot gemstone can

be incorrectly identified as sinhalite if this procedure is followed and only "the amount of movement" on the gamma shadow edge is observed (see *Figure 3* in Appendix 1).

Teaching manuals prepared by institutions granting diplomas in gemmology (for example GIA and Gem-A) are not discussed here. They are rewritten and improved every few years but may still have incomplete or confusing statements about the use of the refractometer.

The damage caused by the presence of confusing and incorrect information in the literature is twofold: it greatly increases the time needed for teaching the use of the refractometer, which is a subject of many gemmology courses, and it negatively affects a student's confidence.

However, the examples described here from textbooks should not detract from their overall value and important role in the education of many gemmologists; my comments should be seen in the context of improving the teaching of use of the refractometer.

The key aspect of the new approach described in this article in Part I is a set of simple but safe rules to recognize a favourably oriented gemstone where several optical properties can be easily recorded (optic character, optic sign and principal RIs). Equally important is the ability to recognize the unfavourably oriented gemstones where it is possible to determine only the maximum and minimum RI values, and where determination of other optical properties requires use of the polarizing filter or more complex procedures.

The straightforward interpretation of observed data described in this article in Part II is based on a graphical presentation of the range of refractive indices and birefringence that can be observed in some gemstones. This, in turn, allows easy and fast identification of overlaps in RIs between two or more gemstones.

It is hoped that description of the procedures and identification process presented in this article will provoke discussion, bring suggestions and

A new approach to the teaching and use of the refractometer

Seven Possible Patterns

Chart 1

Patterns I to *VII* represent all possible observations on isotropic or anisotropic gemstones regardless of the orientation of the optical elements and the gem table.

Identification of a pattern is based on observations during the rotation of a gemstone on the refractometer and include:
- The number of shadow edges observed (one or two).
- If a shadow edge is variable (shows various RIs during the rotation) or constant (shows a constant RI).
- If shadow edges remain apart during the rotation or join (where a single shadow edge is observed in certain rotation positions).

In order to make identification of a pattern easier, rotations should start in the positions outlined below:
- *Patterns I and II:* start rotation from any position — the shadow edges stay the same during rotation.
- *Patterns III and IV:* start rotation where the shadow edges are at maximum separation.
- *Patterns V, VI and VII:* start rotation where the maximum RI is observed.

	Green dots show rotation positions at which principal RIs are determined.
PATTERN I A single shadow edge	**MUST BE ISOTROPIC** Make sure that the RI reading stays constant during the rotation of a gemstone on the refractometer and that the shadow edge is not polarized (see Appendix 2).
PATTERN II Two constant and parallel shadow edges	**MUST BE UNIAXIAL** Only RI_{min} and RI_{max} can be determined. Use a polarizing filter to determine the OPTIC SIGN.
PATTERN III One constant and one variable shadow edge touching	**MUST BE UNIAXIAL** Use the red box at the end of the Chart to determine the OPTIC SIGN from ω and ε. Make sure that shadow edges join at one point where only a single shadow edge is seen.

A new approach to the teaching and use of the refractometer

● Green dots show rotation positions at which principal RIs are determined.

PATTERN IV

One constant and one variable shadow edge not touching

CAN BE UNIAXIAL OR BIAXIAL — each possibility should be tested. The polarizing filter must be used in interpretation.

(a) Uniaxial, positive ($\omega < \varepsilon$)

(b) Biaxial, negative (β closer to γ)

(a) If the example is considered as uniaxial, it means that the gemstone would be positive, so it cannot be tourmaline, which is uniaxial negative.

(b) If the example is considered as biaxial, it could be actinolite, which is biaxial negative.

PATTERN V

One constant and one variable shadow edge intersecting

MUST BE BIAXIAL — record α, β and γ. Use the box below to determine the OPTIC SIGN.

(a)

(b)

The more commonly seen pattern is shown in (b) where shadow edges do not intersect but both move to similar readings of β. Test both possible β readings during interpretation.

PATTERN VI

Two variable shadow edges not touching

MUST BE BIAXIAL — only RI_{min} (α) and RI_{max} (γ) can be determined. Use a polarizing filter to determine the OPTIC SIGN.

PATTERN VII

Two variable shadow edges touching

MUST BE BIAXIAL — β is determined in the rotation position where a single shadow edge is seen. Use the red box below to determine the OPTIC SIGN from α, β and γ.

OPTIC SIGN	
Uniaxial: $\omega > \varepsilon$ – negative $\omega < \varepsilon$ – positive	**Biaxial:** β closer to γ – negative β closer to α – positive

A new approach to the teaching and use of the refractometer

improvements or completely new ideas that will lead to the development of the new approach to teaching and, in this way, greatly shorten the learning process.

Part I: Observations on the refractometer

A. General statements

Rotation of a gemstone through at least 180° is an essential part of every determination on the refractometer. The observation repeats itself on further rotation.

Monochromatic light (sodium light or a source near 589 nm) should always be used.

Use of the polarizing filter may increase the accuracy of determinations. The first observations should be made without the polarizing filter. It is then inserted and rotated until one shadow edge disappears — then the other may be seen with more contrast. Any further rotation of a gemstone must be followed by an adjustment (rotation) of a polarizing filter.

Maximum and minimum RIs (RI_{max} and RI_{min}) of any anisotropic gemstone can be determined on any facet, regardless of the orientation of the optical elements (principal vibration directions X, Y and Z or the optic axis) in it.

Some anisotropic gemstones have constant RIs and determination of the RI_{max} and RI_{min} is all that is required for reliable identification. However, other gemstones may belong to groups with variable chemical composition, which is reflected in variation of their RIs. This may lead to an overlap of RIs of two or more gemstones, with the result that exactly the same RI_{max} and RI_{min} and, of course, the same birefringence, can be observed on several different gemstones. In such cases, identification is based on determination of other optical properties such as the optic sign and optic character.

In observations on favourably oriented gemstones, it is possible to determine the optic sign and optic character at the same time as RI_{max} and RI_{min}. Observations on other gemstones require additional tests,

for example, the use of the polarizing filter for determination of the optic character or the optic sign.

A method is now available to predict observations on any gemstone (isotropic, uniaxial or biaxial) in any orientation of the optical elements and the facet (see Sturman, 2007a, p.442). All of these possible observations can be described in seven simple patterns *(Chart 1)* of the movement of shadow edges during the rotation of a gemstone on the refractometer.

B. Use of Chart 1

- *Patterns I* to *VII* are described in diagrams on *Chart 1*. The angle of rotation of the stone on the refractometer is plotted on the horizontal axis of the diagrams and the corresponding RI on the vertical axis.
- There is no need to keep a record of the rotation angles and the corresponding RIs or to construct a diagram for every observation. Identification of a pattern is based on facts 1 to 3 described below and also shown in the top panel of *Chart 1*.
  1. Determination of the number of shadow edges seen during the rotation of a gemstone on the refractometer.
  2. Determination of the shadow edges as
     - Constant (always giving the same RI reading during the rotation of a gemstone on the refractometer) or as
     - Variable (giving different RI readings — it seems that a shadow edge moves up and down during the rotation of a gemstone on the refractometer).
  3. Determine whether the shadow edges remain apart or join during rotation — a single shadow edge is seen at some rotation point.
- Identification of a pattern is further simplified by starting the rotation in preselected positions based on observation on the refractometer and not on the shape or marks on a gemstone.

1. For *Patterns I* and *II,* one can start from any position – the shadow edges stay the same during the rotation.
2. For *Patterns III* and *IV* rotation is started where the shadow edges are at the maximum separation.
3. For *Patterns V, VI* and *VII* rotation is started where the largest RI is observed.

- Once the pattern has been identified, diagrams on *Chart 1* show rotation positions where the RI_{max} and RI_{min} are determined and or — if possible — where the principal RIs are determined (γ, β and α, or ω and ε). *Chart 1* also shows what other optical properties (optic sign and optic character) can be determined from a particular pattern and how to do it.
- In many textbooks, observations on the refractometer are described in the same order as optical properties of gemstones — from isotropic to uniaxial and biaxial. This requires that all of these observations are perfectly memorized for the proper interpretation of data. All this information is available on *Chart 1*. Nothing has to be memorized.
- Additional comments on patterns in *Chart 1* are shown in Appendix 2. They do not have to be memorized but should be easily available when a particular pattern is identified.
- The report of the study on a gemstone must first describe the observed facts and then the interpretation on which the identification is based. Some examples which could be useful for students are shown in Appendix 3. Included are, also, several suggested simple examples to start the teaching, which should progress to the unknown or more complex examples when the students are familiar with the use of *Chart 1*.

Part II: Interpretation of data

A. General comments

Lists and tables of gemstone data are often large in size and are sometimes

A new approach to the teaching and use of the refractometer

difficult to use. In order to simplify interpretation of the data obtained from the refractometer (i.e. between the RI limits of 1.43 and 1.80), some changes to the traditional identification table are proposed.

1. There is no need to use all three constants (RI_{max}, RI_{min} and birefringence) in identification. They are related and exactly the same results can be obtained from the use of only two constants. The list (*Table I*) and *Charts* (*2A* and *2B*) are based on only two constants: RI_{max} and birefringence.
2. The use of only two constants allows easy graphical presentations. *Charts 2A* and *2B* clearly show the variations and possible overlaps in the RIs of several gemstone species.
3. In order to simplify use of the charts, gemstones are divided into two groups; common gemstones are shown on *Chart 2A* and both common and rare are shown on *Chart 2B*. This grouping should enable easier and faster identification.
4. *Table I* and *Chart 2* include only gemstones that are generally faceted from single crystals; for example, opal, amber and similar gems are not shown. Well-researched data have been used and the list includes all gemstones described in O'Donoghue (2006) which have RIs between 1.43 and 1.80.
5. Mineral names have been used for the groups in *Chart 2*. The chart and accompanying table are intended as a help in identification of an unknown gemstone from data observed on the refractometer. Each of the groups such as corundum, beryl and garnet are represented by a single shape; it is left to the observer to use other properties to identify a gemstone as ruby, sapphire, emerald, almandine, etc.
6. We hope to receive comments on how to improve *Chart 2* (enlarge or modify shapes, include additional gemstones, improve the use of colours or fonts etc.). These comments will be considered for the next edition of the chart.

B. The use of Chart 2A — common gemstones

To commence identification of a gemstone, its RI_{max} and RI_{min} are determined first and recorded. Birefringence is calculated as $RI_{max} - RI_{min}$. Only the RI_{max} and birefringence are used in the further search.

RI_{max} is plotted first on the horizontal axis of the chart and birefringence on the vertical axis. The point obtained in this way may be within a single shape or in an area where several shapes overlap. In the latter case, several gemstones must be considered in the identification process. Eventually, determination may be based on additional optical properties, such as optic character or optic sign. For this reason the information is shown on the chart as different colours or different fonts as described in the Legend.

(In the teaching process, it is suggested that one should introduce the use of the chart as a black-and-white copy of *Chart 2A* so that students can concentrate only on finding the shape, the names of the gemstones and possible overlaps. The coloured copy is used later when students are familiar with the concept.)

- Names of uniaxial gemstones are written in capital letters (for example TOURMALINE)
- Names of biaxial gemstones are written in lower case letters (for example, actinolite).
- Names of isotropic gemstones are written in grey italics and are plotted on the horizontal axis of the chart where birefringence is zero (for example, fluorite, garnet, spinel).
- The gemstones with a positive optic sign are indicated by red area boundaries and text (for example, QUARTZ).
- Blue is used in a similar way to indicate a negative optic sign (for example, SCAPOLITE).
- Grey is used for gemstones that have a variable optic sign usually accompanied by variation in their RIs (for example, feldspars).

Data for *Table I* and *Chart 2* are

drawn from gem and mineral textbooks. Shapes representing variations in RI_{max} and birefringence are interpretations of data in the literature. They indicate approximate limits for a particular gemstone. In some gemstones where only two elements are variable (for example, iron and magnesium in peridot) the shape is very simple. Ideally, it should be a line but narrow ovals were used to indicate that data in different publications are not always in perfect agreement.

Many gemstone species show a correlation between RI and birefringence. A quick look at *Chart 2A* shows that the great majority of the elongated shapes are inclined. In some gemstones a small increase in RI_{max} is accompanied by a large change (usually increase) in birefringence (for example, scapolite, epidote, iolite). In others the variation in RI_{max} is accompanied by only a small change in birefringence (for example, peridot).

Gemstones that have more than two variable elements may have more complex relations between RI_{max} and birefringence. Wide ovals or squares are used to represent these gemstones (for example tourmaline and feldspars). Where there is variation in properties, the shapes on the chart are drawn to include the maximum range known from measured gemstones.

This means that, for example, although peridot is part of the olivine group, the composition range in this group that provides the gemstones is relatively small and this is what is represented on the chart. Similar considerations apply to tourmaline.

The gemstones that do not show any variation in RIs, for example quartz, should ideally be represented by a small dot. However, in order to make them more visible on the chart, they are shown as small circles.

C. The use of Chart 2B (common and rare gemstones)

Chart 2B contains all the gemstones shown in *Chart 2A* and 80 rarer gemstones which, for reasons of clarity, are represented by numbers in circles and elongate ovals. The names of these rare

A new approach to the teaching and use of the refractometer

Table I: The maximum RIs up to 1.8 and birefringences of faceted gemstones cut from single crystals.

Common faceted gemstones – shown by name on the charts.
Rare faceted gemstones shown by number on the charts.
Isotropic gemstones (*I*) names and numbers in italics on charts and the table.
Uniaxial (U) and biaxial (B) gemstones and the optic sign (+ or -) in normal text in the table.

No. (see Chart 2B)	Name	RI$_{max}$	Optic character and sign	Birefringence	No. (see Chart 2B)	Name	RI$_{max}$	Optic character and sign	Birefringence
	Fluorite	*1.432-1.434*	*I*		23	Shortite	1.570	B-	0.039
1	Kogarkoite	1.442	B+	0.003	24	Kammererite	1.576-1.597	B+/-	0.003
	Sodalite	*1.483-1.487*	*I*		25	Brucite	1.580	U+	0.020
	Natrolite	1.485-1.496	B+	0.012			-1.600		0.010
2	Creedite	1.485	B-	0.024	26	Zektzerite	1.584	B-	0.002
	Analcime	*1.487*	*I*			Augelite	1.588	B+	0.014
3	Ettringite	1.491	U-	0.021	27	Eudialyte	1.588-1.638	U+/-	0.004
4	Thaumasite	1.498-1.507	U-	0.036		Herderite	1.589-1.620	B-	0.029-0.030
5	Tugtupite	1.499-1.502	U+	0.006-0.008	*28*	*Zunyite*	*1.592-1.600*	*I*	
6	*Hauyne*	*1.502*	*I*		29	Leucophanite	1.593-1.598	B-	0.028
7	Yugawaralite	1.502-1.504	B+/-	0.009	30	Wardite	1.595-1.604	U+	0.009
8	Mesolite	1.505	B+	0.001		Amblygonite	1.598	B+/-	0.018
9	Leucite	1.509	U+	0.001		(incl. Montebrasite)	-1.633		0.027
10	Cancrinite	1.515-1.524	U-	0.022	31	Hurlbutite	1.604	B-	0.009
11	Kurnakovite	1.515-1.525	B-	0.030	32	Howlite	1.605	B-	0.022
	Petalite	1.516-1.523	B+	0.013	33	Sogdianite	1.608	U-	0.002
12	Scolecite	1.517-1.521	B-	0.007	34	Pezzottaite	1.612-1.620	U-	0.009-0.011
	Pollucite	*1.518-1.525*	*I*		35	Meliphanite	1.613	U+	0.019
13	Thomsonite	1.518-1.544	B+	0.021		Colemanite	1.614	B+	0.028
14	Leifite	1.519	U+	0.004	36	Sarcolite	1.615	U+	0.011
15	Carletonite	1.521	U-	0.004	37	Phosphophyllite	1.616-1.620	B-	0.021-0.033
	Feldspars	1.522		0.006		Topaz	1.618	B+	0.010
		-1.588	B+/-	0.010			-1.638		0.008
		-1.599		0.011	38	Friedelite	1.620-1.625	U-	0.030
16	Nepheline	1.526-1.542	U-	0.004		Brazilianite	1.621-1.623	B+	0.019-0.021
17	Shomiokite	1.531	B+	0.009	39	Chondrodite	1.621	B+	0.028
18	Poudrettite	1.532	U+	0.021			-1.636		0.034
19	*Langbeinite*	*1.532*	*I*			Grandidierite	1.623-1.639	B-	0.039
	Apophyllite	1.532-1.538	U/B+	0.000-0.002	40	Vlasovite	1.625	B-	0.019
20	Milarite	1.532-1.551	U/B-	0.003		Apatite	1.625-1.645	U-	0.002-0.004
	Cordierite (Iolite)	1.537	B+/-	0.005	41	Richterite	1.627-1.641	B-	0.017
		-1.578		0.018		Hambergite	1.628-1.631	B+	0.072
21	Canasite	1.543	B-	0.009	42	Catapleiite	1.629	B+	0.039
22	Ussingite	1.543-1.545	B+	0.039		Actinolite	1.630	B-	0.026
	Quartz	1.553	U+	0.009		(incl. Tremolite)	-1.644		0.023
	Scapolite	1.546	U-	0.005		Tourmaline	1.630-1.650	U-	0.018
		-1.600		0.035			1.640-1.660		0.024
	Beryllonite	1.561	B-	0.009	43	Celestine	1.631	B+	0.012
	Beryl	1.564	U-	0.006	44	Wollastonite	1.631-1.653	B-	0.015
		-1.600		0.009	45	Burbankite	1.632	U-	0.012

A new approach to the teaching and use of the refractometer

No. (see Chart 2B)	Name	RI$_{max}$	Optic character and sign	Birefringence
46	Prehnite	1.632 -1.665	B+	0.021 0.033
47	Pectolite (incl. Serandite)	1.632 -1.703	B+	0.036 0.028
	Danburite	1.633-1.639	B+/-	0.006-0.008
48	Hemimorphite	1.636	B+	0.021
	Lazulite (incl. Scorzalite)	1.637 -1.680	B-	0.031 0.040
49	Narsarsukite	1.644-1.647	U+	0.033
	Andalusite	1.644 -1.648	B-	0.007 0.011
50	Jeremejevite	1.644 -1.652	U-	0.007 0.013
51	Durangite	1.647-1.685	B-	0.050
	Barite	1.648	B+	0.012
52	Weloganite	1.648	B-	0.090
53	Whewellite	1.649-1.650	B+	0.159-1.163
54	Rinkite	1.651-1.681	B+	0.009
55	Clinohumite	1.651 -1.728	B+	0.024 0.036
	Enstatite (incl. Bronzite)	1.657 -1.693	B+/-	0.010 0.014
	Calcite	1.658	U-	0.172
56	Hureaulite	1.660-1.667	B-	0.012
57	Eosphorite	1.660-1.680	B-	0.035
58	Dickinsonite	1.662-1.671	B+	0.013
	Spodumene	1.662 -1.679	B+	0.014 0.027
59	Vayrynenite	1.664-1.667	B-	0.026
60	Strontianite	1.666	B-	0.150
	Datolite	1.666-1.670	B-	0.044-0.047
	Phenakite	1.667-1.670	U+	0.016
	Axinite	1.668-1.701	B-	0.010-0.012
	Boracite	1.668-1.673	B+	0.011
	Euclase	1.669-1.675	B+	0.020
	Peridot	1.670 -1.705	B+/-	0.035 0.038
61	Sillimanite	1.672 -1.683	B+	0.020 0.022
	Kornerupine	1.674 -1.684	B-	0.013 0.017
62	Lithiophilite incl. Triphylite	1.674 -1.702	B+/-	0.008 0.005
	Aragonite	1.676-1.679	B-	0.150
63	Dolomite	1.681	U-	0.179
64	Lawsonite	1.682-1.686	B+	0.019
65	Ludlamite	1.688-1.697	B+	0.038-0.044
	Rhodizite	*1.694*	*I*	
	Diopside	1.694 -1.710	B+	0.026 0.030
	Dioptase	1.697-1.709	U+	0.053
	Tanzanite	1.700	B+	0.009
	Zoisite	1.695 -1.710	B+	0.005 0.015
66	Bustamite	1.701	B-	0.018
	Vesuvianite (Idocrase)	1.703-1.752	U+	0.001-0.004
	Sinhalite	1.705-1.712	B-	0.035-0.037
67	Sapphirine	1.705-1.734	B+/-	0.006
68	Serendibite	1.706-1.743	B-	0.005
	Clinozoisite	1.709 -1.734	B+	0.005 0.015
	Magnesite	1.710	U-	0.202
	Garnet	*1.714-1.8*	*I*	
	Taaffeite	1.717-1.727	U-	0.004-0.009
	Spinel	*1.718-1.794*	*I*	
	Willemite	1.719-1.725	U+	0.028
69	Dumortierite	1.723	B-	0.037
70	Johachidolite	1.724	B+	0.007
	Rhodonite	1.724-1.748	B+	0.013
	Kyanite	1.724-1.734	B-	0.017
71	Nambulite	1.730	B+	0.023
72	Holtite	1.730-1.761	B-	0.015
	Diaspore	1.732-1.750	B+	0.048
73	Neptunite	1.734	B+	0.029-0.045
	Epidote	1.734 -1.797	B-	0.015 0.049
	Periclase	*1.735-1.745*	*I*	
	Legrandite	1.740	B+	0.060
74	Chambersite	1.744	B+	0.012
75	Hodgkinsonite	1.746	B-	0.026
76	Staurolite	1.746 -1.761	B+	0.011 0.015
77	Pyroxmangite	1.746-1.758	B+	0.016-0.020
	Chrysoberyl	1.750-1.760	B+	0.008-0.010
78	Parisite	1.757-1.771	U+	0.081
79	Adamite	1.758-1.773	B+/-	0.041-0.050
	Corundum	1.767-1.772	U-	0.007-0.009
80	Scorodite	1.768-1.8	B+	0.027-0.030
	Zircon	1.780 -1.8	U+	0.001 0.007

A new approach to the teaching and use of the refractometer

Chart 2A: Common faceted gemstones

LEGEND

Optic character:
Biaxial
UNIAXIAL
Isotropic

Optic sign:
negative (–)
positive (+)
can be either +/–

birefringence

0.200
0.100
0.090
0.080
0.070
0.060
0.050
0.040
0.030
0.025
0.020
0.015
0.010
0.005

1.43 1.45 1.50 1.55 1.60 1.65 1.70 1.75 1.80

RI$_{max}$

MAGNESITE, CALCITE, Aragonite, Legrandite, Diaspore, DIOPTASE, Sinhalite, Hambergite, Peridot, Lazulite, Datolite, WILLEMITE, Diopside, Grandidierite, Herderite, Colemanite, Amblygonite, Brazilianite, Euclase, Spodumene, PHENAKITE, TOURMALINE, Actinolite, Kor   upine, Kyanite, Epidote, Rhodonite, Clinozoisite, Zoisite, Axinite, Enstatite, Boracite, Tanzanite, Barite, Andalusite, SCAPOLITE, Augelite, Feldspars, Topaz, Danburite, BERYL, QUARTZ, Beryllonite, Cordierite, Petalite, Natrolite, APATITE, APOPHYLLITE, Pollucite, Sodalite, Alalcime, Chrysoberyl, TAAFFEITE, CORUNDUM, ZIRCON, VESUVIANITE, Periclase, Garnet, Rhodizite, Spinel, Fluorite

Page 82

A new approach to the teaching and use of the refractometer

Chart 2B: Common and rare faceted gemstones

LEGEND

		Optic sign:
common	rare	negative (−)
(names)	(numbers)	positive (−)
Optic character:		can be either +/−
biaxial	12	
UNIAXIAL	20	
isotropic	28	

RI$_{max}$

birefringence

(Chart labels: MAGNESITE, Legrandite, Diaspore, Sinhalite, WILLEMITE, Diopside, Kyanite, Kornerupine, Zoisite, Tanzanite, Clinozoisite, TAAFFEITE, CORUNDUM, ZIRCON, Chrysoberyl, Periclase, Garnet, Spinel, Rhodizite, VESUVIANITE, DIOPTASE, Aragonite, CALCITE, Peridot, Datolite, Spodumene, Euclase, PHENAKITE, Axinite, Enstatite, Andalusite, Grandidierite, Hambergite, Lazulite, Actinolite, TOURMALINE, Barite, Boracite, Topaz, Danburite, APATITE, Herderite, Colemanite, Amblygonite, Brazilianite, Augelite, SCAPOLITE, Feldspars, BERYL, Cordierite, QUARTZ, Beryllonite, APOPHYLLITE, Pollucite, Natrolite, Petalite, Sodalite, Analcime, Fluorite, Rhodonite, Epidote)

Axis values — RI$_{max}$: 1.43, 1.45, 1.50, 1.55, 1.60, 1.65, 1.70, 1.75, 1.80

Axis values — birefringence: 0.200, 0.100, 0.090, 0.080, 0.070, 0.060, 0.050, 0.040, 0.030, 0.025, 0.020, 0.015, 0.010, 0.005

A new approach to the teaching and use of the refractometer

gemstones are in the list in *Table I*.

As in *Chart 2A*, the colours of numbers and outlines are used to identify the optic sign:

- red for positive
- blue for negative and
- grey for gemstones that may have positive or negative optic sign.

Some numbers are underlined or are written in italics to show the optic character of the gemstone:

- italics for isotropic (shapes and numbers are black),
- normal numbers for uniaxial gemstones
- underlined numbers for biaxial gemstones

The decision on whether to use *Chart 2A* or *Chart 2B* for identification depends on other observed data. *Chart 2A* can be used if a gemstone is already identified as one of the common gemstones by other tests and determination on the refractometer is used just for confirmation. *Chart 2B* should be used when an unknown gemstone is studied and all possibilities should be kept in mind.

Conclusions

This new approach introduces several new aspects in interpretation and procedures for identifying gemstones using the refractometer.

1. Nothing has to be memorized. *Chart 1* contains information on
   - how to identify a pattern,
   - what can be observed about a particular pattern and
   - further procedures and limitations.
   Many textbooks and teaching manuals describe observations on the refractometer in the same order as that in which the optical properties of gemstones are described — from isotropic to uniaxial and, finally, to biaxial gemstones. The gemmologist is expected to commit this information to memory and to accurately remember the range of possible observations on uniaxial and biaxial gemstones and their proper interpretation. Use of *Chart 1* simplifies this process and makes it more efficient in obtaining reliable results.

2. Many textbooks rely on three parameters RI_{max}, RI_{min} and birefringence in identifications. This practice makes tables or lists larger and, especially, increases the difficulty in identification of overlaps of RIs of gemstones. The range in RIs of many gemstones is best defined using only the two parameters RI_{max} and birefringence, which makes graphical presentations very simple. RI_{min} is used to calculate the birefringence but is not shown in the chart.
   Use of RI_{max} and birefringence in *Charts 2A* and *2B* allows presentation of information for a large number of gemstones on a single graph. This information includes variation in RIs, variation in birefringence, in addition to optic sign and optic character.

3. RI_{max} and birefringence should be shown to three decimal places. The figures for quartz for example are RI_{max} 1.553 and birefringence 0.009. In many textbooks and teaching manuals RIs are given only to two decimal places, and for quartz RI_{max} is given as 1.55 and RI_{min} as 1.54 or even as 1.56 to 1.54. However, birefringence may also be given as 0.009 (three decimal places). This means that quartz must be considered as a possible solution in any interpretation of data where there is a birefringence of 0.009 and RI_{max} and RI_{min} are between 1.535 and 1.565. This extended range includes many feldspars and scapolite.

Acknowledgements

References

Liddicoat, R., 1981. *Handbook of gem identification*. Gemological Institute of America, Santa Monica, CA

O'Donoghue, M. (Ed.), 2006. *Gems. 6th edn*. Butterworth-Heinemann, Oxford

Read, P.G., 1999. *Gemmology. 2nd edn*. Butterworth-Heinemann, Oxford

Sturman, B.D., 2005. Use of the polarizing filter on the refractometer. *J. Gemm.,* **29**(5/6), 341–8

Sturman, B.D., 2007a. Clarification of measurements of the RIs of biaxial gemstones on the refractometer. *J. Gemm.,* **30**(7/8), 434–42

Sturman, B.D., 2007b. Determination of the optic axial angle in biaxial gemstones and its use in gemmology. *J. Gemm.,* **30**(7/8), 443–52

Webster, R., 1994. *Gems, their sources, descriptions and identification. 5th edn*. Ed. P.G. Read. Butterworth, London

Xinhua Song, Ruihua Wu and Weizheng Wu, 2005. The variation of RI with rotation of a doubly refractive gemstone on the refractometer hemicylinder. *J. Gemm.,* 29(5/6), 331–40

A new approach to the teaching and use of the refractometer

Appendix 1: Examples from the literature of confusing or incorrect procedures for use of the refractometer

Several examples from the literature are presented here in order to justify the need for a new approach to the teaching and use of the refractometer. The procedures described in these examples may work in many situations but they are not 100% reliable. They may lead to incorrect identifications of a gem when it is cut with the optical elements in some orientations with respect to the facet and these situations are presented with drawings in *Figures 1* to *4*. The descriptions of procedures are taken from excellent textbooks that have played a very important role in the training of many gemmologists and are still often used in practice. The authors were excellent gemmologists who successfully transferred their great experience to the books. However, in the attempts to simplify refractometer procedures, some descriptions have been made too brief and, for some gemstones, have become unreliable.

Calculated patterns of peridot and sinhalite gemstones in *Figures 1* to *4* and diagrams of *Pattern V* in *Chart 1* are used to show how procedures described by Liddicoat, Read, Webster and Anderson can be confusing and may lead to incorrect identifications. Instead of saving time, they may greatly increase the learning time needed to master the use of the refractometer.

Handbook of Gem Identification

Liddicoat (1981, p.61) describes in detail the interpretation of a relatively seldom observed situation when the optic axis is exactly parallel to a facet. In other orientations, the two shadow edges do not join at a point and Liddicoat suggests the following procedure:

"In this event approximate the position of the intermediate index by taking a figure midway between … the minimum position of the high reading and the maximum of the low."

In biaxial gemstones one shadow edge gives true β and the other gives a false β (see *Figure 1*). Taking the average between the incorrect (false) value of β and the true one will always give an incorrect result. It is another question whether the error introduced by this procedure is large enough to lead to an incorrect identification but there is no doubt that this procedure is not reliable.

Figure 1 shows a pattern of movement of shadow edges when a sinhalite gemstone is rotated on the refractometer. The diagram shows the readings of principal refractive indices α and γ as well as of true β and false β.

Peridot and sinhalite may have very similar α and γ but the value of β is very different and can be used to differentiate between the two:

- in peridot β is close to the halfway point between α and γ, whereas
- in sinhalite β is close to γ.

Figure 2 shows the calculation of

Figure 1: A pattern of movement of shadow edges observed on a sinhalite during rotation on the refractometer. Principal RIs, α, β and γ, are shown on the diagram.

Figure 2: A pattern observed on a sinhalite. Two possible β readings (β_1 and β_2) were measured but a polarizing filter was not used to determine which was true. Instead the procedure described by Liddicoat was followed and average β (β_av) was calculated. β_av is in excellent agreement with β expected in peridot; the calculated β (1.688) is the same as the halfway point (HWP) between γ and α (1.688). Thus, an incorrectly determined β leads to an incorrect identification of a sinhalite as a peridot.

A new approach to the teaching and use of the refractometer

Liddicoat's average β which is identical to a half-way point (HWP) between α and γ. This procedure leads to the incorrect identification of this sinhalite gemstone as peridot.

Gemmology

An example of incomplete instruction occurs in Read (1999, p.91) who suggests that two variable shadow edges observed on biaxial gemstones move to the same reading.

"This minimum RI reading of the γ ray is designated β. Note: On further rotation of the biaxial stone, the α ray shadow edge also moves from its lowest RI reading to a higher RI one, which is the same value as β for the γ ray."

There is no indication in the further text or in figures that this pattern is observed only from facets with special orientation — as shown in *Pattern V* in *Chart 1*. It is very seldom seen in practice; the great majority of observations on biaxial gemstones concern two variable shadow edges that do not move to the same value.

This observation of the movement of shadow edges is simplified even more in *Figure 9.13* (op. cit. p.92). In the caption of the Figure:

"If the higher RI γ′ shadow edge moves more than halfway toward the lowest RI position of the α′ shadow edge, the optic sign is positive (left). If the γ′ shadow edge moves less than halfway, the 20 optic sign is negative (right)."

These statements and procedures are misleading for two reasons:

1. It is implied or suggested that whenever two variable shadow edges are observed during a 180° rotation, they will reach the same RI reading at some positions. However, a student would see this happen on only very few gemstones — the great majority of biaxial gemstones tested will have two variable shadow edges that do not reach the same value.

2. It is also suggested in Figure 9.13 that one should observe only the γ′ shadow edge to determine the optic sign. This

works only if the principal refractive β is in the γ′ shadow edge. If β is in the α′ shadow edge, this procedure cannot be used. For biaxial gemstones with large to medium optic axial angles, it is estimated that β is found in the α′ shadow edge in about half of the observations and in the other half β is found in the γ′ shadow edge. Using this procedure therefore could lead to incorrect identifications in about half of all observations.

Gems

This very important textbook initially by Webster has had several editions and, latterly, several editors. The latest edition (O'Donoghue, 2006) has left out the section on identification of gemstones, but previous editions kept an unchanged description of a procedure for use of the refractometer that may lead to incorrect identifications:

"When the angle between the optic axes is small, either the shadow edge with the higher index or that with the lower index will move very little; then
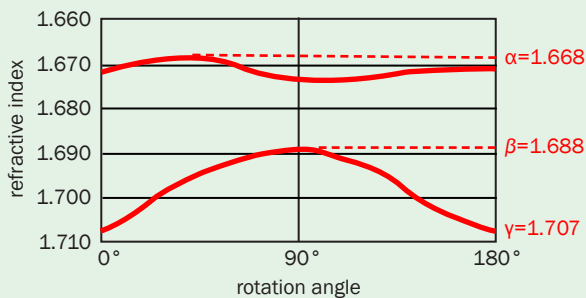
Figure 3: This pattern was observed on a peridot — a gemstone with a large angle between the optic axes (2V is about 90°). Note that there is only small variation in the α value; according to Webster (see text), this could indicate a stone with a small optic axial angle, which here is not the case.
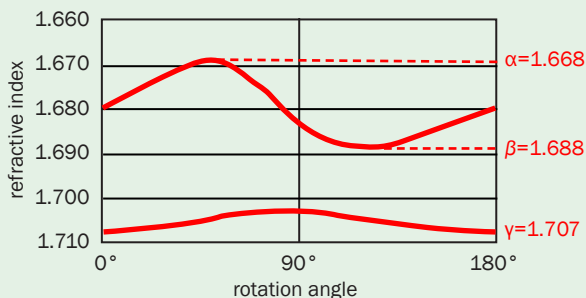
Figure 4: A pattern of movement of shadow edges observed on peridot. Note that the small movement on the γ shadow edge does not indicate that the stone could be sinhalite (see text concerning Anderson's comments).

A new approach to the teaching and use of the refractometer

it will be easy to see whether the sign is positive (β nearer to α) or negative." (Webster, 1994, p.713.)

This is misleading because any biaxial gemstone may be cut to produce a pattern with one of the shadow edges that moves a little. A pattern that may be observed on peridot — a gemstone with a large optic axial angle (about 90°) shown in *Figure 3* — has one shadow edge that moves a little and on the basis of the above quotation could indicate incorrectly a gemstone with a small optic axial angle. So it is important to establish that a pattern with one shadow edge that moves a little does not prove that a gemstone has a small optic axial angle or that its optic sign can be determined in this way.

Gem Testing

Anderson (1990, p.276) describes the following procedure to distinguish between sinhalite and peridot:

"In such a case, separation by means of refractive index readings depends upon the amount of movement seen in the shadow-edge representing the higher refractive index: in sinhalite the value for the intermediate 'beta'

index is much nearer the maximum or 'gamma' edge than the lowest or alpha edge, whereas in peridot the value for the 'beta' index is nearly half-way between the greatest and the least index."

Therefore, Anderson correctly concludes that in all sinhalite gemstones a small movement on the γ' shadow edge is observed – from γ to β (if β is in the γ' shadow edge) or even less (if β is in the α' shadow edge).

This example best shows the problem that gemmologists faced before calculated patterns were available. Today on calculated patterns, it can be easily seen that peridot gemstones may also show small amount of movement of the γ' shadow edge in certain orientations — as in *Figures 3* and *4*. In fact, peridot and sinhalite may show identical movement on the γ' shadow edge and this test alone should not be used in identifications.

Descriptions not included in some textbooks and teaching manuals

Equally damaging to the learning process are descriptions of observations on the refractometer that are left out. An

interested student looking through the literature may learn about the possibility of seeing a pattern where one optic axis is parallel to a facet (*Pattern VII* in *Chart 1*). They can then learn about a pattern where both optic axes are parallel to a facet (*Pattern V* in *Chart 1*), but I am not aware of both patterns described in the same textbook or teaching manual. It is left to the student to conclude that both patterns are possible.

Furthermore, making it even more difficult for a student is the fact that little or nothing is said about the most common patterns shown by biaxial gemstones where none of the optic axes are parallel to a facet (*Pattern VI* in *Chart 1*).

Some textbooks and teaching manuals describe in detail the determination of the optic sign of uniaxial gemstones from a constant and variable shadow edges but some do not even mention the fact that exactly the same pattern can be observed on biaxial gemstones (see *Pattern IV* in *Chart 1*), and neither do they mention that in this situation all three principal refractive indices (α, β and γ) can be easily determined.

Appendix 2: Additional comments on the patterns in *Chart 1*

Pattern I

A single shadow edge is shown by isotropic gemstones (cubic and amorphous, for example garnets and glass). This has a constant RI value during the rotation of a gemstone on the refractometer and is produced by light rays that are not polarized. A polarizing filter may be used to confirm this — the intensity of the shadow edge does not essentially change as the polarizing filter is rotated.

A single shadow edge can also be shown by anisotropic gemstones because:
- the other shadow edge is so far away that it may be overlooked, or
- the RI of the other shadow edge is higher than 1.8 and is outside the range of the refractometer, for example in gems such as benitoite and rhodochrosite.

Such a shadow edge can be easily recognized because it is polarized and its intensity will change from strong to zero when a polarizing filter is rotated on the eyepiece. The shadow edge is seen with maximum intensity when its vibration direction is parallel with the vibration direction of the polarizing filter and is invisible when its vibration direction is perpendicular to the polarizing filter.

Pattern II

This pattern is observed only on uniaxial gemstones. Light rays that produce two parallel and constant shadow edges are polarized and the polarizing filter must be used to identify which shadow edge is the ordinary ray and which the extraordinary ray (see Sturman, 2005). When ω and ε are determined then identification of the optic sign is shown in

the red box at the end of *Chart 1*.

Pattern III

This pattern is observed only in uniaxial gemstones. If there is any doubt that the shadow edges come together, then the interpretation should follow the procedure discussed in *Pattern IV*. Identification of the optic sign is shown in the red box at the end of *Chart 1*.

Pattern IV

This is the only pattern that may be shown by uniaxial and biaxial gemstones. The polarizing filter must be used to identify the optic character (uniaxial or biaxial) and principal RIs ω and ε or α, β and γ. This in turn allows determination of the optic sign.

Sometimes, simply interpreting the observed data as uniaxial and then

A new approach to the teaching and use of the refractometer

as biaxial, may lead to elimination of a particular gemstone from further consideration. This process may take an additional 30 seconds but can lead to reliable identification as is shown by an example on the chart.

In the example on *Chart 1*, a constant shadow edge was observed at RI_{min} = 1.621 and the variable shadow edge gave RI_{max} = 1.643, a birefringence of 0.022. When these figures are plotted on *Chart 2A* the point falls in the middle of the tourmaline field. The point is also very close to the edge of the actinolite field and both of these gemstones must be considered in the identification process. Tourmaline is uniaxial and actinolite is biaxial, and the polarizing filter may be used to identify the optic character (uniaxial or biaxial). However, in this case, consideration of the optic sign can be used to eliminate one of the two possible gemstones.

First, the observed data are used to
- determine ω and ε — as if the gemstone is uniaxial and then
- determine α, β and γ — as if the gemstone is biaxial.

Interpretation of the observed data as uniaxial is shown on *diagram IVa;* ω = 1.621 and ε = 1.643. This gemstone — if it is uniaxial — must have a positive optic sign (ω < ε), so it cannot be tourmaline, which has a negative optic sign (ω > ε).

The pattern is then interpreted as biaxial *(diagram IVb)*. The constant shadow edge gives α = 1.621 and the variable shadow edge gives β = 1.633

and γ = 1.643. This gemstone — if it is biaxial — must have a negative optic sign (β closer to γ) which is in good agreement with actinolite, which is biaxial, negative.

Therefore, the gemstone in the example in *Pattern IV* on *Chart 1* is identified as actinolite.

This is a good place to make a general comment on identifications based on observation on the refractometer or some other instrument. The identification is based on comparison of the observed data with the expected observation on all of the known gemstones. At present, we do not know of any uniaxial positive gemstone with RI_{max}=1.643 and birefringence of 0.022 and, in this case, a gemstone in the example in *Pattern IV* in *Chart 1*, can be safely identified as actinolite. Our identifications are only as good as our knowledge of properties of gemstones.

Pattern V

This pattern is easy to recognize because first the one and then the other shadow edge come to similar readings and stay stationary during much of the rotation; one of these readings will be β. However, the other shadow edge then can change rapidly on rotation and care should be taken to record the proper values of α and γ.

The pattern on the left is very seldom observed. It is seen only where both optic axes are exactly parallel to the facet. Much more common is the pattern on the right where one or even both optic axes are

not perfectly parallel with the facet.

Determination of α and γ is the same in both patterns. The RI value at the intersection indicates β in *diagram Va*, but in *diagram Vb* each shadow edge may give slightly different values of β (the highest reading on α′ shadow edge and the lowest reading on γ′ shadow edge). In this case, both values of β must be used in interpretation (see Sturman, 2007). For example, both values of β may give the same optic sign — this is then reliable information that may be used in identification. However, if each β value leads to different optic signs, the polarizing filter must be used to identify true β and calculate the optic sign.

Pattern VI

This is the most common pattern observed in biaxial gemstones. Only α and γ can be determined without use of the polarizing filter. It is important to remember that α and γ are usually determined at different rotation positions and that each shadow edge must be observed separately.

Pattern VII

This is another pattern seen on biaxial gemstones that is the result of a particular orientation of the optical elements and a facet. It is observed when one of the optic axes is exactly parallel with the facet. Determination of all three principal RIs (α, β and γ) and, from them, determination of the optic sign is straightforward.

Appendix 3: Selection of examples for students and keeping a record

Examples and tests

Teaching should start with good examples of seven possible patterns *(Chart 1)*. Then low birefringence examples or more complex examples can be introduced when students become familiar with the chart. Monochromatic light must be used.

1. Students should first learn to recognize patterns with a single shadow edge *(Pattern I)*, and then move on to two

shadow edges *(Patterns II to VII)*. Good examples can be garnet, peridot and tourmaline.
2. Students should next learn to identify the shadow edges as constant or variable. Good examples can be tourmalines *(Patterns II and IV)* and peridots *(Pattern VI)*.
3. Finally, students should learn to identify patterns where shadow edges touch at one or two positions during

rotation for 180° of the gemstone. Good examples are tourmalines *(Pattern III)* and peridots *(Patterns V and VII)*.
Note: *Patterns III, V* and *VII* do not have to be perfectly oriented. It is important that students can see what is expected in perfectly oriented patterns — how two shadow edges come closer and closer and may eventually touch (a single shadow edge is seen).

A new approach to the teaching and use of the refractometer

4. Finding the starting point and identification of a pattern is based on instructions in *Chart 1*. There is no need to construct diagrams for each observation. Good examples of each of the seven patterns are necessary.
5. Observe and record data for each pattern following the instructions on *Chart 1*.

Keeping a record

The observations on the seven examples in *Chart 1* should be recorded as:

Pattern I: isotropic, RI = 1.716

Pattern II: anisotropic, uniaxial, RI_{max} = 1.553, B = 0.009, optic sign ?

Pattern III: (a) anisotropic, uniaxial, ω = 1.544, ε = 1.553, optic sign positive ($\omega < \varepsilon$): search on *Chart 2* for uniaxial (+), RI_{max} = 1.553, B = 0.009 or on the lower diagram

(b) *Pattern III,* anisotropic, uniaxial, ω = 1.555, ε = 1.544, optic sign negative ($\omega > \varepsilon$): search on *Chart 2* for uniaxial (-), RI_{max} = 1.555, B = 0.011

Pattern IV:

(a) anisotropic, uniaxial or biaxial, RI_{max} = 1.643, B 0.022

Interpretation:

If uniaxial, then ω = 1.621, ε = 1.643, optic sign (+) , ($\omega < \varepsilon$)

(b) If biaxial, then α = 1.621, β = 1.633, γ = 1.643, optic sign (-), (β closer to γ) search on *Chart 2* for uniaxial (+), RI_{max} = 1.643, B = 0.022 or search on *Chart 2* for biaxial (-), RI_{max} = 1.643, B = 0.022

Pattern V:

(a): anisotropic, biaxial, α = 1.668, β = 1.688, γ = 1.707, optic sign (-), (β closer to γ)

(b): anisotropic, biaxial, α = 1.668, β = 1.690, γ = 1.707, optic sign (-), (β closer to γ) or anisotropic, biaxial, α=1.668, β=1.688, γ=1.707, optic sign (-), (β closer to γ).

Pattern VI: anisotropic, biaxial, α = 1.668, γ = 1.707, optic sign ?

Pattern VII: anisotropic, biaxial, α = 1.668, β = 1.698, γ = 1.707, optic sign (-), (β closer to γ).

The Author

Darko B. Sturman

Curator Emeritus, Royal Ontario Museum, Toronto, Ontario, Canada

Use of the polarizing filter on the refractometer in determinations of the optic sign or optic character of a gemstone

Darko B. Sturman and Duncan Parker FGA FCGmA

Abstract: Calculated patterns of movement of shadow edges during observations on the refractometer were used to modify procedures for the use of the polarizing filter in determination of the optic sign and the optic character. New procedures are presented in graphic form in three charts. Eight calculated patterns to suggest these procedures are presented in the Appendix.

Keywords: gem testing, optic character, optic sign, refractometer, RI
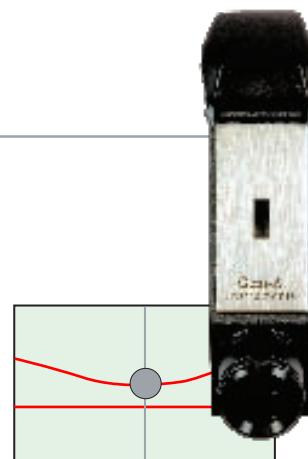
Introduction

The great majority of identifications of gemstones on the refractometer are based on determination of the maximum and the minimum refractive index (RI). The measurements can be made on any gemstone regardless of the orientation of the gem table and optical elements (optic axes or the principal vibration directions X, Y and Z).

In our descriptions we often refer to measurements taken from the gem table when set on the refractometer prism but any plane facet can be suitable.

The use of sodium or monochromatic light near 589 nm greatly increases the potential accuracy of determination. Easily portable monochromatic sources powered by batteries are now available.

Some gemstones have constant RIs and determination of the RI_{max} and RI_{min} is all that is required for reliable identification. Other gemstones have variable chemical compositions and this may be reflected in variation of their RIs. Where there is overlap of RIs of two or more gemstones, identification is based on determination of other optical properties

such as the optic character or the optic sign. In some cases, determination of these optical properties is easy if the optical elements are favourably oriented with respect to the gem table. On other gemstones determination of the optic sign or the optic character r equires the use of a polarizing filter.

The movement of shadow edges on all gemstones during rotation on the refractometer and consequent variation in the RI readings can be summarized in seven patterns. Sturman (2010a) presented all patterns on a chart with information on how to identify them, described what can be observed on each pattern and gave instructions on how to do it. On four of these seven patterns the optic sign and the optic character can be easily identified without use of the polarizing filter. On the remaining three patterns determination of the optic sign or the optic character requires use of the polarizing filter with known vibration direction.

Hurlbut (1984) published the first article in the modern literature that described the use of the polarizing filter for determination on the refractometer

of the optic character or the optic sign of gemstones. Since then several other descriptions have been published but they all followed his general concept and reasoning. This article does not compare or evaluate these subsequent methods or procedures but is intended to discuss a new aspect discovered during a study of calculated patterns.

Below, we describe first the problem, then the method used in this study and, finally, present the solution. At the end, we present modified procedures based on this new understanding summarized in three charts.

- *Chart A* refers to determination of the optic sign on uniaxial gemstones (Pattern II, Sturman, 2010a) where the optic axis is perpendicular, or near perpendicular, to the gem table. This pattern is easily recognized and is characterized by two constant shadow edges which stay at the same RI readings during the rotation of a gemstone on the refractometer.

- *Chart B* refers to determination of the optic sign on biaxial gemstones in their most commonly encountered

orientation (Pattern VI, Sturman, 2010a) where none of the principal vibration directions is perpendicular to the gem table. This pattern is characterized by two variable shadow edges that stay separated during rotation of a gemstone on the refractometer.

- *Chart C* refers to determination of the optic character (uniaxial or biaxial) on patterns, which consist of one constant and one variable shadow edge (Pattern IV, Sturman, 2010a); during rotation of a gemstone these shadow edges stay separated — two shadow edges are seen at all times. This pattern may be observed on uniaxial or on biaxial gemstones and the polarizing filter is used to differentiate between the two.

The problem

The use of the polarizing filter in all previously published methods is described using examples of gemstones where the optical elements — principal vibration directions (X, Y, Z) or the optic axis — are exactly perpendicular or parallel to a facet or the gem table.

In these procedures, based on what may be called perfectly oriented examples:

1. a gemstone is identified as the one that requires the use of the polarizing filter for determination of the optic sign or the optic character;
2. (if needed) a gemstone is rotated to a particular position;
3. the polarizing filter is inserted with its vibration direction set in a certain position — usually in the E–W or N–S direction on the eye-piece;
4. the insertion of the polarizing filter leads to a disappearance of one of the two shadow edges and this allows identification of the optic sign or of the optic character of a gemstone.

Extending these procedures, we examined patterns from gemstones where the optical elements were not in such perfect orientations with the gem table. The study showed that, during rotation on the refractometer, many gemstones with not-so-perfect orientation produce very similar patterns to those with the exact

orientation. In fact, the observations are not identical but the differences are too small to be seen on the refractometer scale. There was, however, one very important visible difference: when a not-so-perfectly oriented gemstone is observed and previously described points 1 to 3 exactly followed (including the placing of the polarizing filter on the eyepiece), then one shadow edge may not disappear as is described in the instructions (see point 4).

The study

The first assumption was that variation of about 0.001 in the RI readings during rotation of a gemstone was not detectable on a standard refractometer. Then patterns were produced where variation in RI readings on one shadow edge was 0.001 or less during extended rotation; this led to the discovery that orientations of vibration directions of shadow edges may substantially change during rotation while RI readings stay nearly the same. In consequence, at some rotation positions, the vibration direction of the shadow edge may be exactly perpendicular to the polarizing filter but at other positions the vibration direction of the shadow edge and the polarizing filter are *not* perpendicular to each other and some light may get through the filter – resulting in the shadow edge staying visible.

It is important to remember that the polarizing filter does not work as some kind of venetian blind letting through only the polarized rays that vibrate exactly parallel to the mobile strips see Sturman (2010b). In most cases, some light will be transmitted — the amount (intensity) depending on the angle between the vibration directions of the incoming ray and the polarizing filter (see *Figure 1* of the Appendix). Only if the vibration direction of the incoming ray is exactly perpendicular to the vibration direction of the polarizing filter will no light be transmitted.

Predicting orientations of vibration directions of the shadow edges for any gemstone during rotation on the refractometer is easy and very accurate

(see Sturman, 2007). For example, in this study, calculated patterns for uniaxial gemstones were prepared using apatite and tourmaline showing variation of 0.001 in the extraordinary shadow edge. It was, then, easy to compare changes in the vibration directions of shadow edges of the two patterns (see *Figures 3* and *4* of the Appendix).

However, predicting the effect of the change in vibration direction of the shadow edge on its visibility through the polarizing filter is a much more complex problem. Whether a shadow edge is visible when its vibration direction is 10° or 20° or 30° away from perpendicular to the polarizing filter, depends on many factors such as the quality of polish of gemstone, and the construction and quality of the refractometer. However, the crucial point for a gemmologist to keep in mind is the possibility that a shadow edge may not disappear as expected.
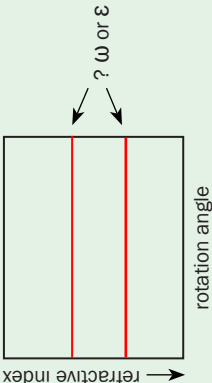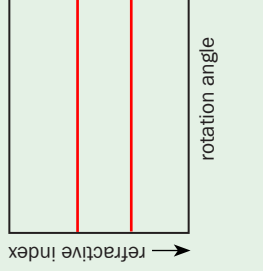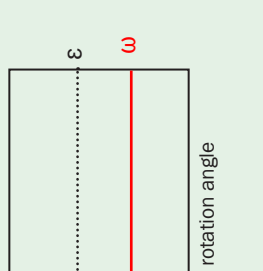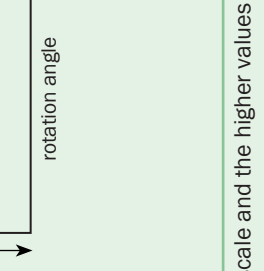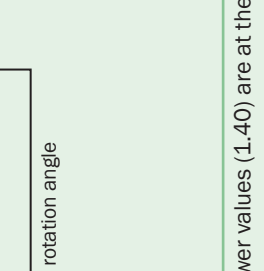
The solution

Several examples in the Appendix describe various reasons why a shadow edge does not disappear as might be expected when a polarizing filter is inserted. However, in routine work a gemmologist does not have to remember or to refer to these examples or reasons. All that is required is to accept the fact that in some gemstones both shadow edges may stay visible when the polarizing filter is inserted and then to follow procedures presented in *Charts A, B* and *C*.

The new procedures are slightly modified from Hurlbut (1984) and other authors. In some cases the procedures described in our charts may require more time but gemmologists may be assured that these procedures are reliable in all gemstones whatever their orientation. When the time needed to prepare a gemstone for determination and the time needed for the cleaning afterwards is taken into account, then any added time needed for additional rotation of a gemstone is very small in comparison.
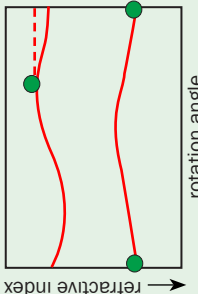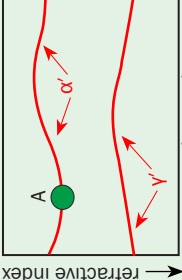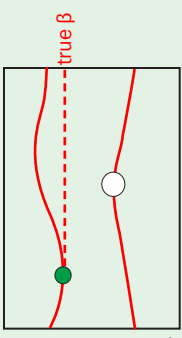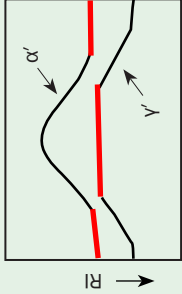
All our examples show that the simple gradual rotation of a gemstone on the

Use of the polarizing filter on the refractometer in determinations of the optic sign or optic character of a gemstone
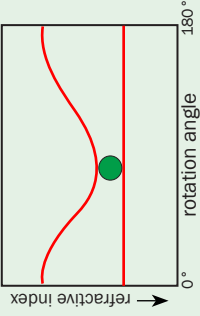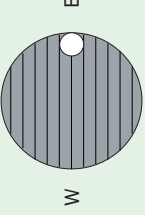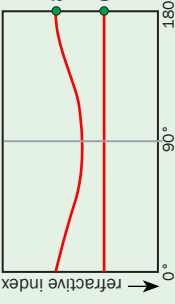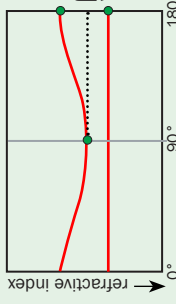
Chart A: Determination of the optic sign in uniaxial gemstones.
The pattern consists of two constant and parallel shadow edges

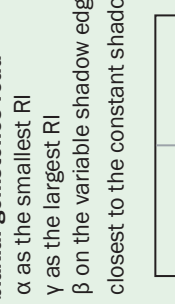

STEP 1

refractive index →

rotation angle

? ω or ε

Observe each shadow edge separately to make sure that they stay constant during the rotation of a gemstone.

STEP 2

Insert the polarizing filter with vibration direction in the E-W position.
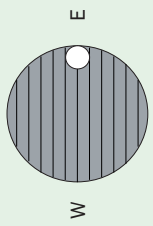
Test with the polarizing filter can be made at any point during the rotation of a gemstone.

If needed, rotate a gemstone until one shadow edge disappears.

STEP 3

ε shadow edge disappears.

Determine ω

refractive index →

rotation angle

ε / ω

refractive index →

rotation angle

ω / ε

STEP 4

REMOVE FILTER

STEP 5

Determine ε

refractive index →

rotation angle

ε / ω

refractive index →

rotation angle

ω / ε

STEP 6

Determine the optic sign.

ω < ε positive

ε < ω negative

Note: The RI scale on these diagrams copies the scale on the refractometer, i.e. the lower values (1.40) are at the top of the scale and the higher values (1.80) are at the bottom.

Use of the polarizing filter on the refractometer in determinations of the optic sign or optic character of a gemstone

Chart B: Determination of true β in biaxial gemstones.
The pattern consists of two variable shadow edges not touching.

STEP 1
Determine α (the smallest RI observed) and γ (the largest RI observed).

Each pattern has two positions where β can be determined — true β and 'false' β. They are marked A on the α' shadow edge and G on the γ' shadow edge.

Each shadow edge must be observed separately.

STEP 2 (A)
Rotate a gemstone to the position marked A — the highest reading on the α' shadow edge.

STEP 3 (A)
Insert the polarizing filter in the E–W position.
If needed, gradually rotate a gemstone left or right to make the α' shadow edge disappear.
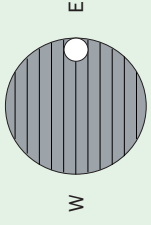
STEP 4 (A)
If the α' shadow edge disappears in this rotation position or close to it, this is 'false' β.
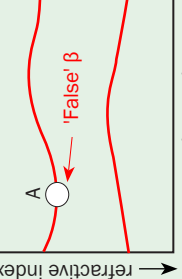
STEP 5 (A)
Remove filter.
Determine true β on the other shadow edge — the lowest reading on the γ' shadow edge.

STEP 6
Determine the optic sign.

β closer to α
Positive

β closer to γ
Negative

If the α' shadow edge does not disappear in the rotation position 'A' (or close to it), try γ' shadow edge in the position 'G' (or close to it).

STEP 2 (G)
Rotate a gemstone to the position marked G — the highest reading on the γ' shadow edge.
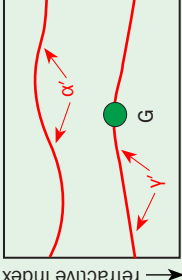
STEP 3 (G)
Insert the polarizing filter in the E–W position.
If needed, gradually rotate a gemstone left or right to make the γ' shadow edge disappear.
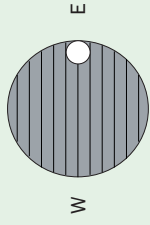
STEP 4 (G)
If the γ' shadow edge disappears in this rotation position or close to it, this is 'false' β.
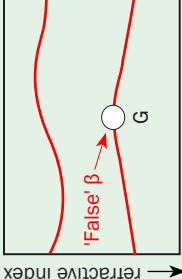
STEP 5 (G)
Remove filter.
Determine true β on the other shadow edge — the highest reading on the α' shadow edge.

Note: In some orientations (Y almost perpendicular to the gem table) both shadow edges disappear in the rotation positions A and G, when the polarizing filter is inserted with the vibration direction set in the E–W position. It is impossible to distinguish between 'false' and 'true' β.

In this event:
- both shadow edges give the same, or almost the same, readings for possible β
- both shadow edges are relatively constant for much of the rotation.

These rotation positions are shown by the heavy red lines on the example to the right.

Use of the polarizing filter on the refractometer in determinations of the optic sign or optic character of a gemstone

Chart C: Determination of the optic character in uniaxial or biaxial gemstones.
The pattern consists of one variable and one constant shadow edge, not touching.

STEP 1

Rotate the gemstone to the position where the shadow edges are closest (shown by a green dot).

STEP 2

Insert the polarizing filter with vibration direction in the E-W position.

STEP 3

Determine the optic character.

Observe which shadow edge disappears.

If needed, rotate a gemstone left or right in small movements until one shadow edge disappears.

If the variable shadow edge disappears the stone is uniaxial.

If the constant shadow edge disappears this stone is biaxial.

STEP 4

REMOVE FILTER

STEP 5

Determine principal RIs (ω/ε or α/β/γ)

In uniaxial gemstones read
- ω on the constant shadow edge
- ε on the variable shadow edge where they are separated the most
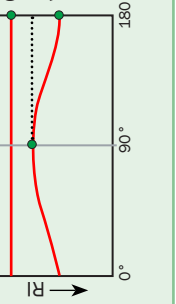
In biaxial gemstones read
- α as the smallest RI
- γ as the largest RI
- β on the variable shadow edge closest to the constant shadow edge

STEP 6

Determine the optic sign.

ω > ε = negative

In uniaxial gemstones

ω < ε = positive

β closer to α = positive

In biaxial gemstones

β closer to γ = negative

Use of the polarizing filter on the refractometer in determinations of the optic sign or optic character of a gemstone

refractometer from the originally required rotation position would bring about the desired effect — a disappearance of one shadow edge.

Use of charts

Diagrams on the charts are calculated patterns of movements of the shadow edges during the rotation of a gemstone on the refractometer. Rotation angles are plotted on the horizontal axis of diagrams and RI readings of the shadow edges are plotted on the vertical axis. Six steps are used in all charts to describe the required procedures. The reasoning and the examples used in preparation of the charts are described in the Appendix.

Chart A describes procedure for determination of the optic sign on patterns composed of two shadow edges that stay parallel to each other and give the same RI readings during the rotation of a gemstone on the refractometer. This pattern can be observed only on uniaxial gemstones where the optic axis is perpendicular, or near perpendicular, to the gem table or facet being measured. The vibration direction of the extraordinary ray (see detailed explanation in the Appendix) is then perpendicular, or near perpendicular, to the vibration direction of the polarizing filter, which is set in the E–W orientation.

In perfectly oriented gemstones, the extraordinary ray shadow edge disappears when the polarizing filter is inserted during the rotation of a gemstone.

In not-so-perfectly oriented gemstones, the extraordinary shadow edge disappears in some rotation position but may be visible in other rotation positions.

If both shadow edge are still visible, when the polarizing filter is inserted, then the gemstone is rotated gradually left or right until one shadow edge disappears; this is always the extraordinary ray. Then the reading is made of ω on the shadow edge, which stays visible. Then the polarizing filter is removed (Step 4) and the reading of ε is made on the now visible shadow edge of the extraordinary ray (Step 5). Finally, ω and ε are compared

and the optic sign is determined as shown in Step 6.

Chart B describes the procedure for determination of the intermediate RI β in biaxial gemstones; the position of β and whether it is closer to α or γ is then used to determine the optic sign. The pattern composed of two variable shadow edges can be observed only on biaxial gemstones; principal RIs α (RI_{min}) and γ (RI_{max}) are determined as the smallest and the largest RI observed during rotation of a gemstone on the refractometer. Determination of the principal RI β requires the use of the polarizing filter. Each shadow edge must be observed separately and must be rotated to different positions marked A and G on the chart. One of them is true β and the other is 'false' β. When the polarizing filter is inserted in an E–W orientation one shadow edge disappears and the true β is then determined on the other (visible) shadow edge.

Two problems may be encountered when this procedure is followed:
1. It may be difficult to locate the rotation positions A or G precisely if a shadow edge moves only slightly up or down when the gemstone is rotated near these positions.
2. Tests with the polarizing filter at positions A and G may give similar results; namely, the α' shadow edge disappears in rotation position A and the γ' shadow edge disappears in the rotation position G, i.e. both shadow edges behave as having a 'false' β.

To deal with the first problem, a gemstone is set in the approximate position A, then the polarizing filter is inserted and the α' shadow edge is observed as shown in Step 3(A). If it disappears right away, or if it disappears after further gradual rotation of a gemstone to the left or right, then it is the 'false' β. The same procedure is repeated on the other shadow edge (γ') when the gemstone is rotated to the position G as shown in Step 3(G).

It is important to observe each shadow edge separately — one shadow edge always disappears during gradual rotation left or right (either from position

A or from position G) - as its vibration direction becomes perpendicular to the polarizing filter. This is the 'false' β. The true β is determined on the other shadow edge. Then follow instructions on the chart to determine α and γ, and calculate the optic sign.

The second problem arises in some biaxial gemstones where the principal vibration direction Y is perpendicular, or nearly perpendicular, to the gem table. In this situation the true β shadow edge may also disappear when the polarizing filter is inserted. Fortunately the pattern caused by this orientation can be easily recognized as is described in the note on *Chart B*. The readings of 'false' β and true β should be very close and, in most cases, may lead to the same optic sign.

It is important to keep in mind in any further interpretation that only one of these readings is true β — but that it is impossible to identify it.

On *Chart C,* when a gemstone is rotated to a position where the shadow edges are the closest, there are two possible reasons why neither of the shadow edges disappears when the polarizing filter is inserted.
1. Because the variable shadow edge moves very little up and down during rotation, it is difficult to locate the precise position where the shadow edges are at their closest.
2. The constant shadow edge may only appear to be constant, because the variation in readings may be 0.001 and not detectable for certain. However, the vibration direction of this shadow edge is not perpendicular to the gem table in every rotation position and in some positions it can be as far as 45° away from perpendicular. In this case, this shadow edge may not disappear as expected when the polarizing filter is inserted.

The solution to both problems is the same: a gemstone is rotated to the position where the two shadow edges appear to be at their closest. There is no need to waste time trying to make it perfect. Then the polarizing filter is inserted and the gemstone is gradually rotated left or right until one shadow

Use of the polarizing filter on the refractometer in determinations of the optic sign or optic character of a gemstone

edge disappears (Step 2). Then follow the procedure in *Chart C*.

Conclusions

The gemmological refractometer was one of the first instruments designed for the study of gemstones. It is still a very important tool for many gemmologists and a large part of any gemmological training includes practical use of the instrument. Modern refractometers have better optics, a larger scale for better readings of the RIs, and monochromatic light is available in small battery-operated and easily transported units.

It is unfortunate that these technical improvements to the instrument have not resulted in improved and more confident use. One reason for this is the limited time allocated to the teaching of the refractometer because of the ever increasing number of other subjects that most be covered in gemmology courses. Several attempts have been made to

simplify concepts and procedures but they have resulted in many incomplete, confusing, or, even, incorrect descriptions and statements. The fact that there was no way to properly test these new proposed procedures made the situation even worse.

Today we finally have a method for predicting the observations on the refractometer that includes the changes in vibration directions of the shadow edges during rotation of a gemstone on the refractometer (Sturman, 2007). The great advantage of this method is the possibility to gradually change the orientation of the optical elements in a gemstone and observe the corresponding changes in the vibration directions of shadow edges and, eventually, to predict observations with the polarizing filter.

The new procedures, based on better understanding of observations on the refractometer are presented in *Charts A, B and C*. There is no need for gemmologists

to memorize these procedures; all that is required is to follow the instructions on the charts presented in six simple steps.

Figures 2 to *9* in the Appendix present some of the examples used in preparation of the charts.

References

Hurlbut, C.S., 1984. The jeweller's refractometer as a mineralogical tool. *American Mineralogist,* **69**, 391–8

Sturman, B.D., 2007. Clarification of measurements of the RIs of biaxial gemstones on the refractometer. *The Journal of Gemmology,* **30**(7/8), 434–41

Sturman, B.D., 2010a. A new approach to the teaching and use of the refractometer. *The Journal of Gemmology*, **32**(1–4), 94–110

Sturman, B.D., and Parker, D., 2010b. Use of the polarizing filter to improve observation of the shadow edges on the refractometer. *The Journal of Gemmology,* **32**(1–4), 121–5

Appendix

Observations on the refractometer during rotation of a gemstone *(Figures 2* to *9)* are presented on diagrams in which the horizontal axis of a diagram shows the rotation angle and the vertical axis shows the observed RI. The scale on the vertical axis of the diagrams reflects the scale on the refractometer, with the lower RIs at the top and the higher RIs at the bottom. In some figures the vibration directions of the shadow edges at some rotation positions are shown by two-way arrows. The numbers next to the arrows indicate their directions, for example, 0° is vertical, 10° is 10° away from vertical, 30° is 30° away from vertical and 90° is horizontal.

In the procedures shown in *Charts A, B* and *C,* the polarizing filter is inserted in an E–W orientation. The shadow edge with a vertical vibration direction disappears when the polarizing filter is inserted because vibration direction of a shadow edge (vertical) is exactly perpendicular to the vibration direction of the polarizing filter (horizontal). However,

as was mentioned before, the orientation of vibration direction of a shadow edge may vary during rotation of a gemstone on the refractometer. In this case, a shadow edge with vibration direction which is 20° or 30° away from vertical may still be visible.

Figure 1: The amount of transmitted light depends on the angle between the vibration direction of the incoming ray (shadow edge) and the polarizing filter. In this drawing the arrows (red for the transmitted light and black for the incoming light) are proportional to the intensity of light. The amount of the transmitted light increases proportionally with the increase in the angle between the vibration directions of the incoming light and perpendicular to the polarizing filter.

Figures 2, 3 and *4* were used to prepare *Chart A*. The shadow edge of the extraordinary ray in the apatite gemstone, which has an optic axis exactly perpendicular to the gem table, gives a constant reading during rotation

on the refractometer — ε = 1.640 (see *Figure 2*) and its vibration direction remains perpendicular to the gem table. This shadow edge disappears when the polarizing filter is inserted in an E–W orientation.

A not-so-perfectly oriented gemstone (apatite) is shown in *Figure 3*. In apatite the birefringence is only 0.004 and in order to produce small variation of 0.001 in readings on the extraordinary shadow edge the optic axis must be inclined for 30° away from vertical. This in turn makes orientation of the vibration direction of the extraordinary ray as far away as 30° from vertical. In some rotation positions the extraordinary shadow edge may be visible when the polarizing filter is inserted in the E–W (horizontal) orientation.

Another not-so-perfectly oriented gemstone (tourmaline) is shown in *Figure 4*. In tourmaline the birefringence is five times stronger than in apatite and in order to produce a variation of 0.001 in

Use of the polarizing filter on the refractometer in determinations of the optic sign or optic character of a gemstone
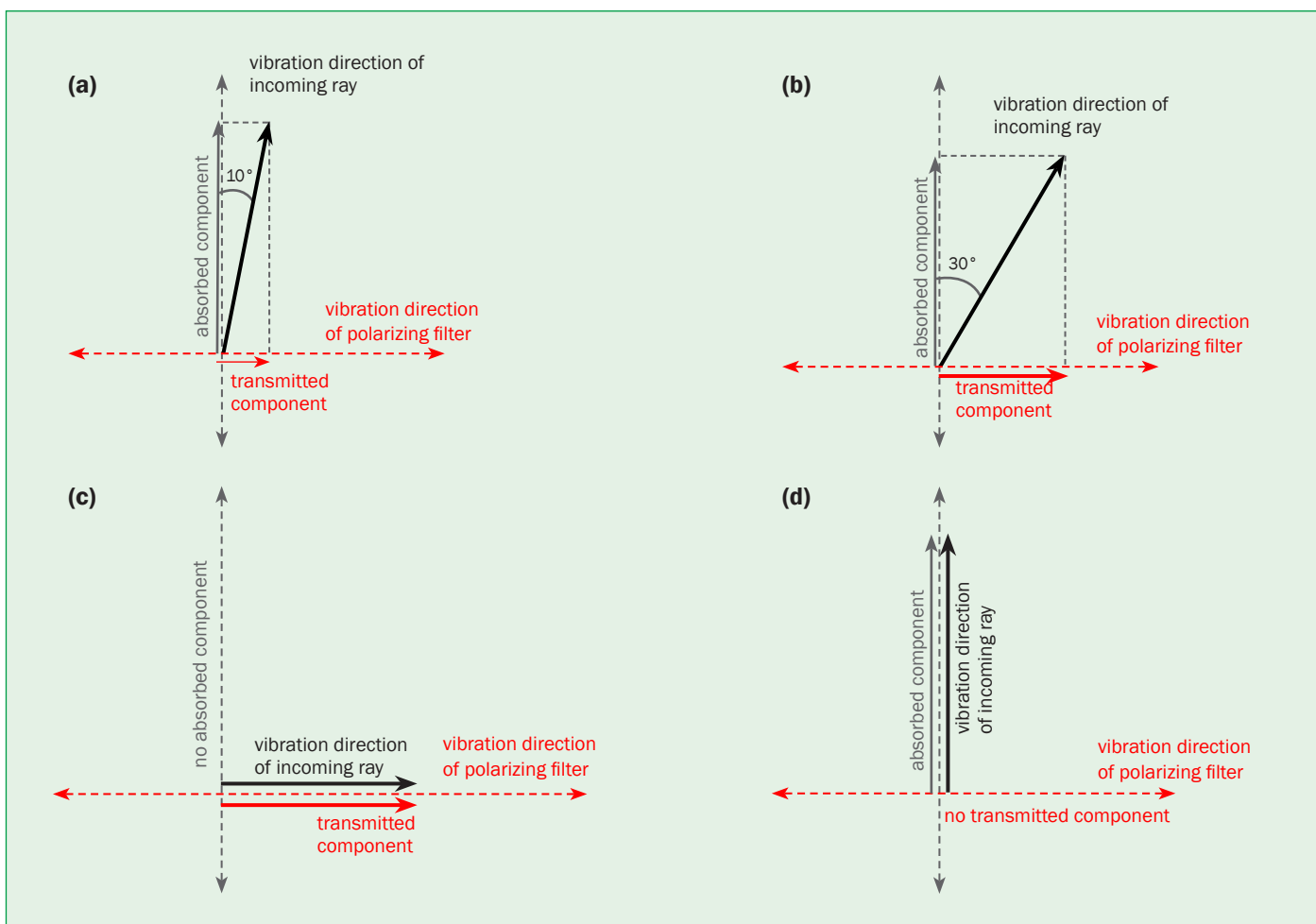

Figure 1: The amount of light transmitted through the polarizing filter depends on the angle between the vibration directions of the incoming ray (solid black arrows) and the polarizing filter (dashed red line).
(a) and (b): The amount of transmitted light (proportional to the red arrows) increases as the angle between the vibration direction of the incoming ray changes from perpendicular to 10° or 30° away from perpendicular.
(c): The maximum amount of light is transmitted when these vibration directions are parallel.
(d): No light is transmitted when these vibration directions are perpendicular to each other.

readings on the extraordinary ray shadow edge the optic axis must be inclined at only 13° away from vertical. This in turn makes orientation of the vibration direction of the extraordinary ray only 13° away from vertical. When the polarizing filter is inserted in the E–W (horizontal) orientation, the vibration direction of the extraordinary shadow edge is vertical, or near-vertical, during rotation of the gemstone. The extraordinary ray shadow edge totally disappears in some rotation positions and is very close to disappearance in others. The overall effect is that the extraordinary ray shadow edge is faint or invisible in every rotation position.

In this particular procedure *(Chart A)* not-so-perfectly oriented gemstones and

perfectly oriented gemstones may produce identical patterns. However, on gemstones with a birefringence or 0.010 or less the extraordinary ray shadow edge may still be visible in some rotation positions.
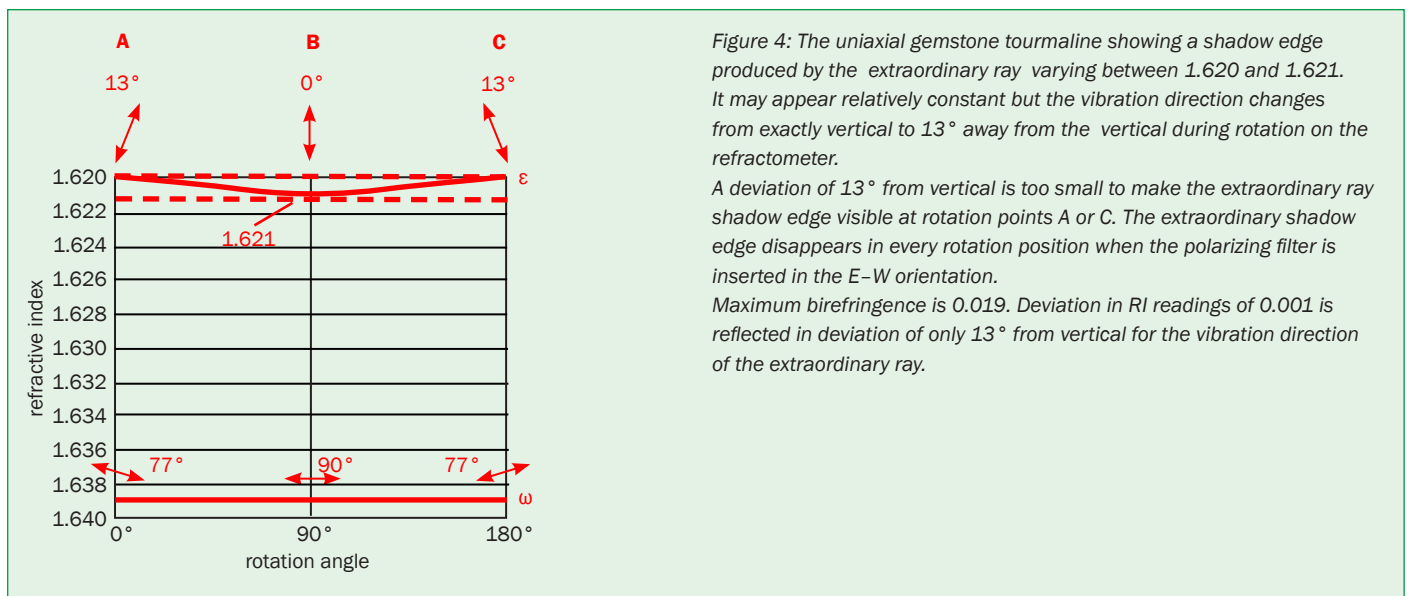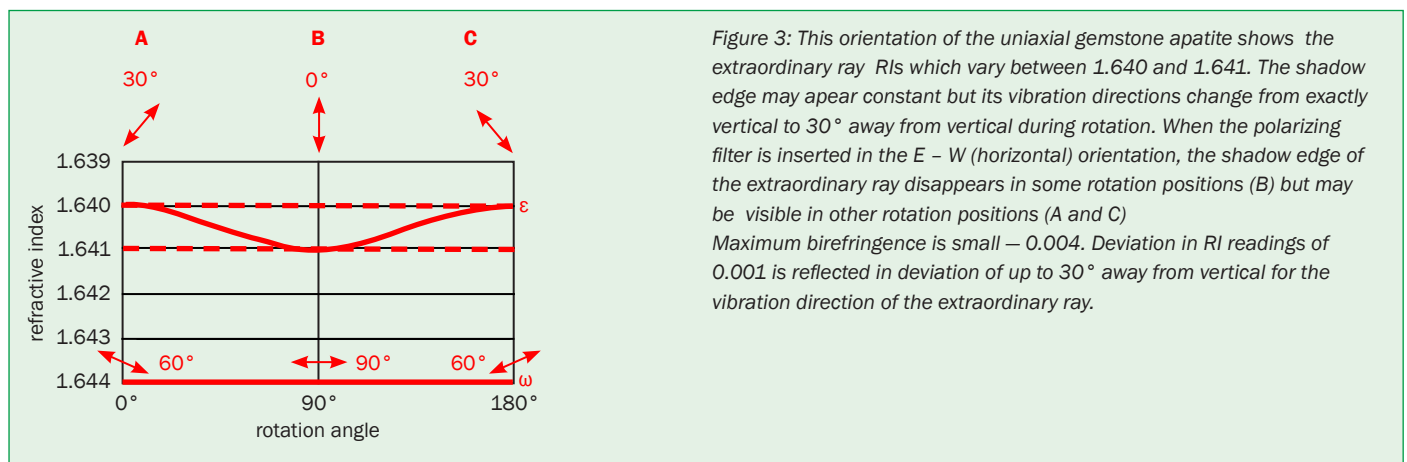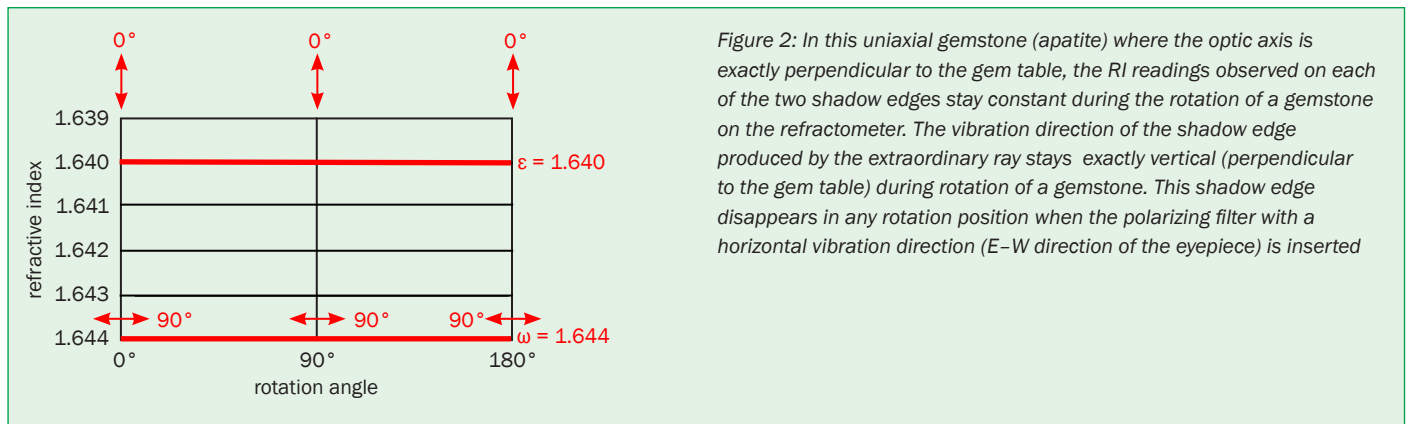
Figures 5 and *6* were used to prepare *Chart B*. A biaxial gemstone (peridot) in general orientation is shown in *Figure 5*. None of the principal vibration directions X, Y and Z are perpendicular to the gem table. Sometimes it may be difficult to find the exact position of A or G if the shadow edges move only slightly on rotation. However, simple gradual rotation left or right from the estimated position A or G should result in one shadow edge ('false' β) disappearing

Figure 6 shows a pattern which can be observed on a biaxial gemstone

(sinhalite) where the principal vibration direction Y is nearly vertical (perpendicular to the gem table). In this example it is 20° away from vertical but the shadow edge may disappear when the polarizing filter is inserted in the E–W (horizontal) orientation. It may be difficult to distinguish between true and 'false' β (see comments in the section on use of the charts).

Figures 7, 8 and *9* were used to prepare *Chart C. Figure 7* shows the importance of rotating a uniaxial gemstone to the required position B — the rotation position where the constant and the variable shadow edge are at their closest. In this rotation position the vibration direction of the variable shadow edge in uniaxial gemstones is exactly

Use of the polarizing filter on the refractometer in determinations of the optic sign or optic character of a gemstone

Figure 2: In this uniaxial gemstone (apatite) where the optic axis is exactly perpendicular to the gem table, the RI readings observed on each of the two shadow edges stay constant during the rotation of a gemstone on the refractometer. The vibration direction of the shadow edge produced by the extraordinary ray stays exactly vertical (perpendicular to the gem table) during rotation of a gemstone. This shadow edge disappears in any rotation position when the polarizing filter with a horizontal vibration direction (E–W direction of the eyepiece) is inserted

Figure 3: This orientation of the uniaxial gemstone apatite shows the extraordinary ray RIs which vary between 1.640 and 1.641. The shadow edge may apear constant but its vibration directions change from exactly vertical to 30° away from vertical during rotation. When the polarizing filter is inserted in the E – W (horizontal) orientation, the shadow edge of the extraordinary ray disappears in some rotation positions (B) but may be visible in other rotation positions (A and C)
Maximum birefringence is small — 0.004. Deviation in RI readings of 0.001 is reflected in deviation of up to 30° away from vertical for the vibration direction of the extraordinary ray.

Figure 4: The uniaxial gemstone tourmaline showing a shadow edge produced by the extraordinary ray varying between 1.620 and 1.621. It may appear relatively constant but the vibration direction changes from exactly vertical to 13° away from the vertical during rotation on the refractometer.
A deviation of 13° from vertical is too small to make the extraordinary ray shadow edge visible at rotation points A or C. The extraordinary shadow edge disappears in every rotation position when the polarizing filter is inserted in the E–W orientation.
Maximum birefringence is 0.019. Deviation in RI readings of 0.001 is reflected in deviation of only 13° from vertical for the vibration direction of the extraordinary ray.

vertical and this shadow edge disappears when the polarizing filter is inserted in the E–W (horizontal) orientation. This position may be difficult to find precisely in gemstones with small birefringence because the variable shadow edge may move little up or down during rotation between A and C. However, gradual and small rotation of a gemstone left or right from the initially estimated position B, should result in the disappearance of the variable shadow edge.

Figure 8 shows a biaxial gemstone (topaz) with the principal vibration direction X exactly perpendicular to the gem table. The vibration direction of the constant shadow edge is also exactly perpendicular to the vibration direction of the polarizing filter set in the E–W orientation. The constant shadow edge disappears in every rotation position of the gemstone when the polarizing filter is inserted.

Figure 9 shows the same biaxial gemstone (topaz) as in *Figure 8* but the principal vibration direction X now makes an angle of 45° with the gem table.

Use of the polarizing filter on the refractometer in determinations of the optic sign or optic character of a gemstone
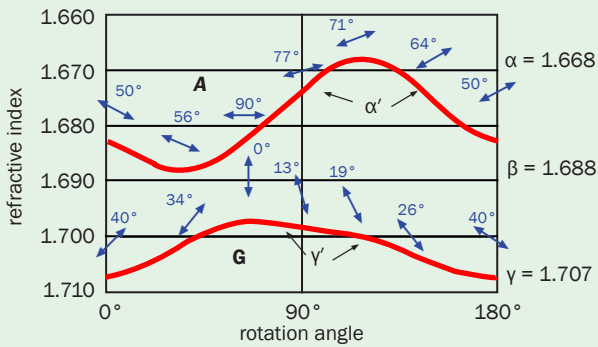

Figure 5: A biaxial gemstone (peridot) with two variable shadow edges α' and γ'. Each shadow edge must be examined separately. First, the α' shadow edge is rotated to position A and the polarizing filter inserted with E–W orientation. If the α' shadow edge does not disappear — as is the case in this example — then this is true β.

In order to confirm this, the γ' shadow edge is rotated to position G and the polarizing filter is inserted with E–W orientation. In the example shown in this diagram, the γ' shadow edge disappears proving that it is a 'false' β.

Note: A is the highest reading on the α' shadow edge and G is the lowest reading on the γ' shadow edge. Sometimes it is difficult to find the exact positions of A or G if the shadow edge moves very little up and down during the rotation. In this case, rotation of a gemstone left or right from the estimated positions A or G should result in the disappearance of one shadow edge.
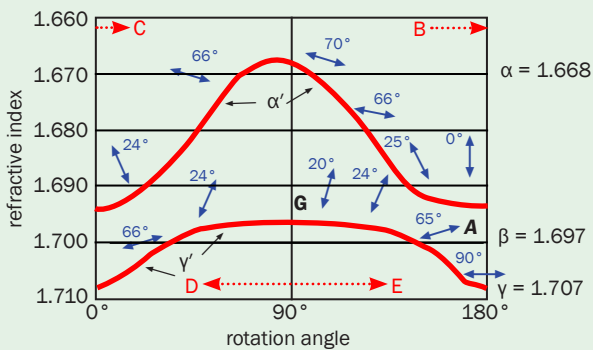
Figure 6: In this biaxial gemstone (sinhalite) both shadow edges have vertical, or near-vertical, vibration directions at rotation positions A and G and both my disappear when the polarizing filter is inserted in the E–W (horizontal) orientation. It may be very difficult, or even impossible, to distinguish 'false' β from true β. Fortunately, these patterns can be easily recognized because both shadow edges give almost the same readings for possible β and stay at these readings for much of the rotation (α' shadow edge from B to C and γ' shadow edge from D to E). However, since both shadow edges give similar readings for β, this is often sufficient for reliable identification.
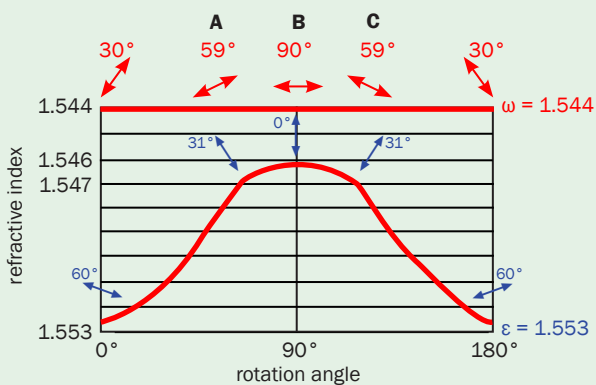

Figure 7: A pattern composed of one variable and one constant shadow edge can be observed on uniaxial and on biaxial gemstones. The pattern in this figure is of a uniaxial gemstone (quartz) – compare it to the pattern of a biaxial gemstone (topaz) in Figure 8. A gemstone must be rotated to the position B (where shadow edges are the closest); in uniaxial gemstones the variable shadow edge disappears when the polarizing filter is inserted in the E–W (horizontal) orientation. It may be difficult to find the exact position B if the readings on the variable shadow edge stay nearly the same (between 1.546 and 1.547) during the rotation of about 50° from A to C.

Both shadow edges may stay visible in positions A or C when the polarizing filter is inserted in the E–W orientation, but further rotation of the gemstone left or right will make the variable shadow edge disappear — proving that this is a uniaxial gemstone.

Use of the polarizing filter on the refractometer in determinations of the optic sign or optic character of a gemstone
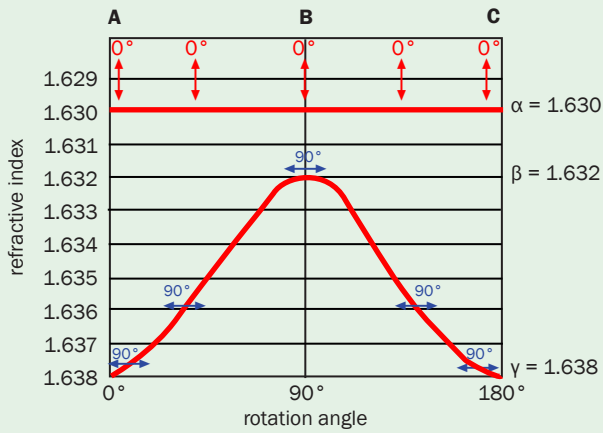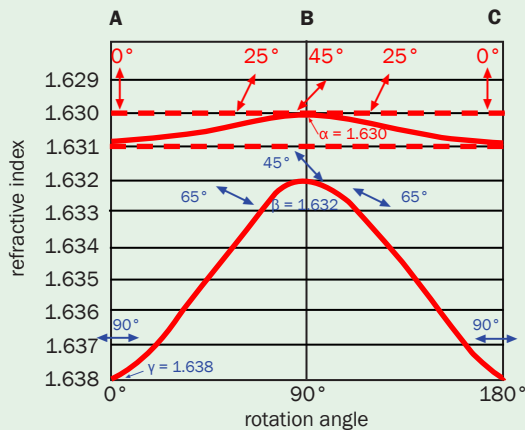

Figure 8: This is a pattern from a biaxial gemstone (topaz) where the principal vibration direction X is exactly perpendicular to the gem table. The vibration direction of the constant shadow edge remains vertical during 180° rotation of the gemstone. In biaxial gemstones, the constant shadow edge disappears when the polarizing filter is inserted in the E–W (horizontal) orientation.

Figure 9: A biaxial gemstone where the principal vibration direction X is not vertical (perpendicular to the gem table) but makes an angle of 45° to the gem table. The variation in the RI readings of the near-constant shadow edge is very small — from 1.630 to 1.631. Both shadow edges are visible (with the polarizing filter inserted in the E-W orientation) when a gemstone is in position B — the rotation position where the shadow edges are the closest — but further rotation to positions A or C will result in the disappearance of this shadow edge.

Although the variation of the constant shadow edge from 1.630 to 1.631 may not be noticed, this small variation in the RI is accompanied by a very large variation in the orientation of the vibration directions. *Figure 9* shows that both shadow edges are visible when a gemstone is rotated to the B position and the polarizing filter inserted, but on further rotation the near-constant shadow edge will disappear at positions A or C, proving that this is a biaxial gemstone.

The Authors

Darko B. Sturman
Curator Emeritus, Royal Ontario Museum, Toronto, Ontario, Canada

Duncan Parker FGA FCGmA
Harold Weinstein Ltd, Gemmological Laboratory, Toronto, Ontario, Canada

Use of the polarizing filter to improve observations of the shadow edges on the refractometer

Darko B. Sturman and Duncan Parker FGA FCGmA

Abstract: Proper use of the polarizing filter may greatly improve observation on the refractometer. Transmission of polarized light through a polarizing filter is described in detail and a simple construction is used to show how the strength of an image (for example, a shadow edge) depends on an angle between the vibration directions of the polarizing filter and the incoming polarized rays. Two examples are used to describe the incorrect use of the polarizing filter that may lead to wrong identifications.

Keywords: polarizing filter, proper measurement procedure, refractive index

Introduction

The polarizing filter is a very useful and a simple accessory of modern refractometers. It is easy to use and gives reliable results if proper procedures are followed.

In order to better follow instructions for the safe and reliable use of the polarizing filter, gemmologists should first have a full understanding of the way the polarizing filter works. This is described in the first section of this article. The correct procedure to increase the sensitivity of observation (to better see the shadow edges) is discussed in the second section. In the third section, two examples are used to show how incorrect use of the polarizing filter may lead to incorrect conclusions and, eventually, to incorrect identifications.

A. How does the polarizing filter work?

The polarizing filter does *not* work as some kind of vertical blind, for example, transmitting only rays with the vertical vibration direction when the vibration direction of the filter is set vertically.

The polarizing filter *transforms* the energy of an incoming polarized ray into two rays as the light moves through the filter; one ray is absorbed and the other is transmitted. The vibration direction of the transmitted ray is often marked on the filter and is referred to as the vibration direction of the polarizing filter. The intensity of an image, for example, the strength of the image of a shadow edge, depends on the angle between vibration direction of the polarizing filter and the vibration direction of light rays forming the shadow edge.

In *Figures 1, 2* and *3* a construction is used to indicate how the intensity of the transmitted ray, the strength of an image of a shadow edge, depends on the angle between the vibration directions of the incoming ray and the polarizing filter. In order to simplify this concept, we relate the word 'intensity' in these drawings to the lengths of the arrows. In fact, the lengths of the arrows represent the amplitudes of light waves, which are proportional to their intensities. The intensity of a light wave is the square of its amplitude. Therefore, if absolute values of intensities are calculated from these constructions, then the relation between the amplitudes and intensities must be taken into account.

Figures 1 and *2* show how a polarized ray is divided into two components by the polarizing filter. The intensity of a transmitted component — the strength of the image of a shadow edge — increases as the vibration directions of the polarizing filter and the incoming ray get closer.

In general, a part of the incoming ray is always transmitted through the polarizing filter but its vibration direction and the intensity are changed; however, there are exceptions to this general rule:

1. When vibration directions of the polarizing filter and the incoming ray are exactly parallel to each other then the intensity of the transmitted ray is identical with the incoming ray, and
2. When vibration directions of the polarizing filter and the incoming

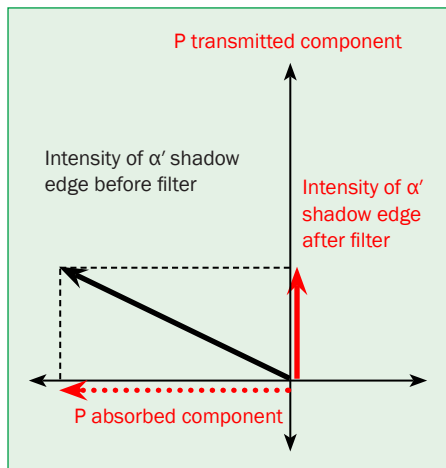## Use of the polarizing filter to improve observations of the shadow edges on the refractometer

Figure 1: Polarized light producing a shadow edge α′ is transformed into two components on entering the polarizing filter. Vibration directions of the incoming ray and the two components (transmitted and absorbed) in the polarizing filter are shown by arrows and their intensities are related to the lengths of the arrows.
Note: The lengths of the arrows show the amplitudes of the light rays, which are proportional to their intensities — the intensity is the square of the amplitude.
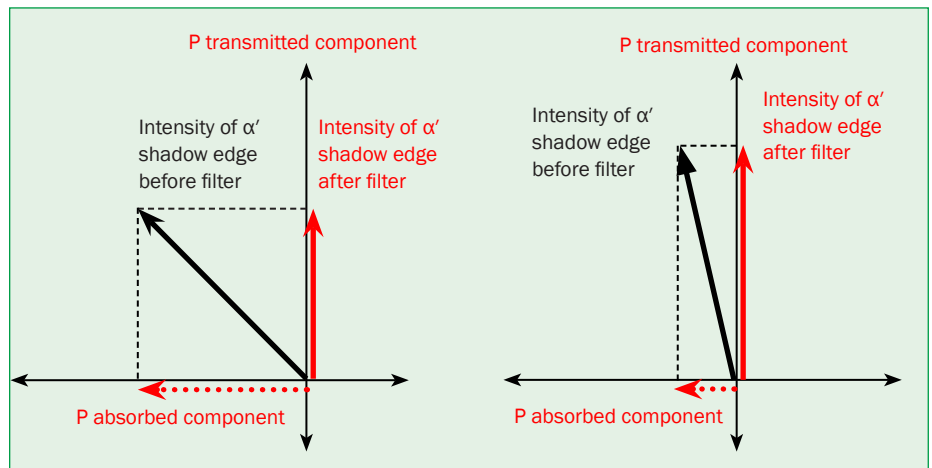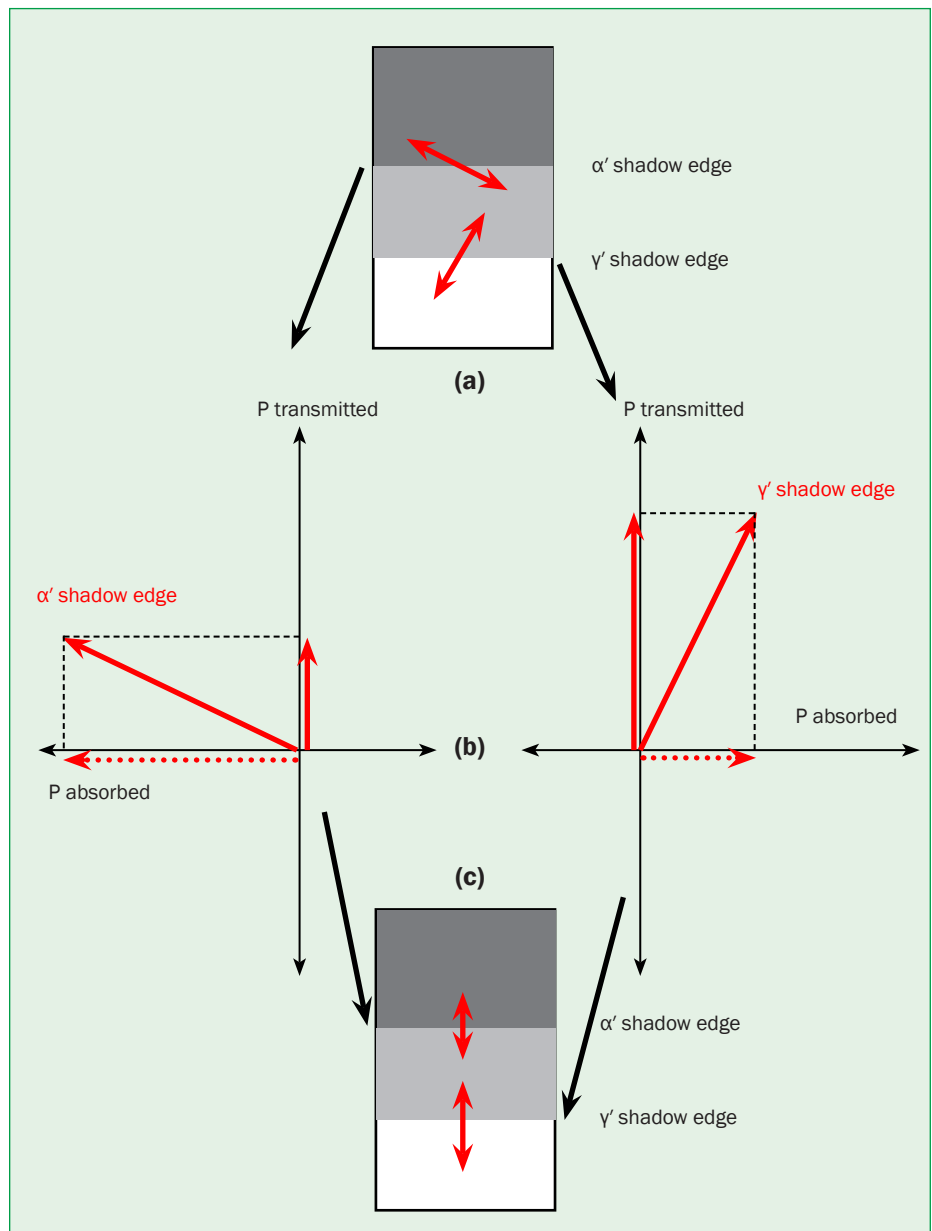
Figure 2: The intensity of the transmitted ray depends on the angle between vibration directions of the polarizing filter and the incoming ray. The decrease in this angle is reflected in the increased intensity of the transmitted ray.

ray are exactly perpendicular to each other, then the incoming ray is totally absorbed.

> When a polarizing filter is rotated on the refractometer's eyepiece, the strength of the image of a shadow edge of an anisotropic gemstone changes from zero to the maximum for every 90° rotation.

In the field of view of a refractometer, two shadow edges are usually observed during the rotation of anisotropic gemstones. In *Figure 3* they are marked γ′ and α′; their vibration directions change during the rotation of a gemstone on the refractometer.

Without the polarizing filter, the shadow edges are visible in different

Figure 3: (a) Observation without the polarizing filter. Both shadow edges have similar intensities.
(b) Light rays of shadow edges are divided into two components in the polarizing filter. One is absorbed, the other is transmitted.
(c) Two shadow edges coming to the eye now have different intensities and are polarized parallel to the axis of the refractometer.

Use of the polarizing filter to improve observations of the shadow edges on the refractometer
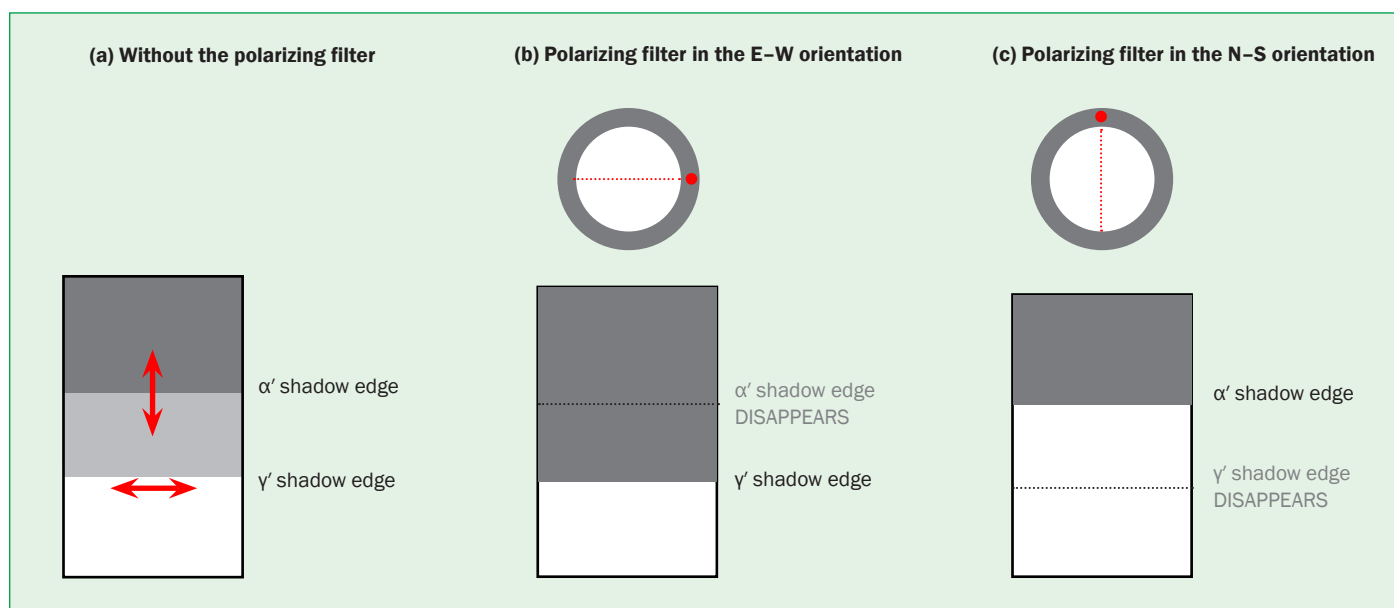

Figure 4: The use of the polarizing filter to bring one shadow edge to the extinction position. The other shadow edge may appear sharper and enable more accurate readings. (a) Observation without the polarizing filter. Both shadow edges are seen with similar intensity. Red arrows indicate the vibration directions of the shadow edges. (b) Po larizing filter is inserted and rotated until α′ shadow edge disappears. (c) Polarizing filter is inserted and rotated until γ′ shadow edge disappears.

positions in the field of view of the refractometer during the rotation of the gemstone. They indicate different refractive indices but, generally, they are seen as two lines with similar intensities. What the human eye does not see is that they are polarized and that their vibration directions are perpendicular to each other (*Figure 3a*).

When the polarizing filter is inserted, then the shadow edges are seen in exactly the same positions on the scale but their intensities change because their vibration directions are at different angles to the polarizing filter (see *Figure 3b*). The human eye may notice the change in intensities of the shadow edges but cannot see that their vibration directions are now parallel to each other (*Figure 3c*) as they travel through the air to the eye.

When the polarizing filter is rotated and the vibration direction of one shadow edge becomes exactly parallel to the polarizing filter, it is seen at maximum intensity. The other shadow edge is then not seen at all.

The use of the polarizing filter produces better contrast because it eliminates one shadow edge and a grey zone between the shadow edges (see *Figure 4*).

- Without the filter we see two shadow edges: dark area/α′ shadow edge/grey area/γ′ shadow edge/light grey area (*Figure 4a*).
- When the filter is inserted and rotated so that one shadow edge becomes invisible, we see a single shadow edge: dark area/shadow edge/light grey area (*Figures 4b and c*).

B. The correct use of the polarizing filter to increase sensitivity of observations on the refractometer

When two shadow edges are very close or if we wish to increase the sensitivity with which they are seen, the polarizing filter can be used to bring one shadow edge to extinction. The other shadow edge may then be seen with better contrast and enable a more accurate reading.

The best practice is first to rotate a gemstone on the refractometer and observe any changes without the filter. If needed, the polarizing filter is then inserted and rotated to bring one, and then the other, shadow edge to extinction.

The procedure is straightforward:
1. Two shadow edges are observed first without the polarizing filter.
2. The filter is then set on the eyepiece and rotated until one shadow edge is invisible. Reading on the scale of the position of the other shadow edge may become easier.
3. After this, the filter is rotated 90° until the other shadow edge is invisible and the refractive indexof the now visible shadow edge can be read.

C. Incorrect procedures can lead to serious error in determination of the optic character and the optic sign of biaxial gemstones.

In some literature or equipment instructions, the measuring procedure is presented in a very simple and attractive form, for example: "Turn the gemstone gradually without readjusting the polarizing filter." It seems impossible that such a simple procedure may lead to a serious error in identification, but in some circumstances it can.

As mentioned above, rotation of a gemstone is accompanied by rotation of the vibration directions of the shadow

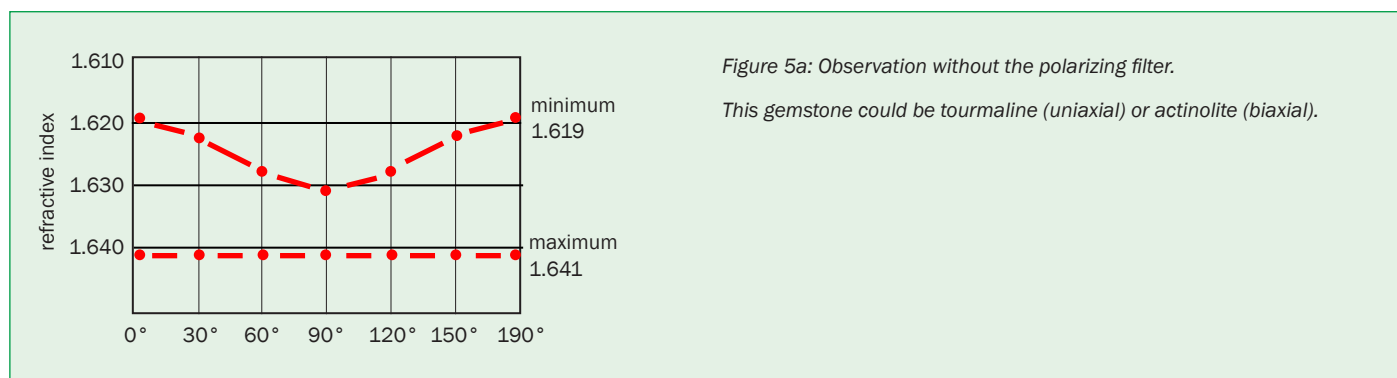Use of the polarizing filter to improve observations of the shadow edges on the refractometer

Figure 5a: Observation without the polarizing filter.

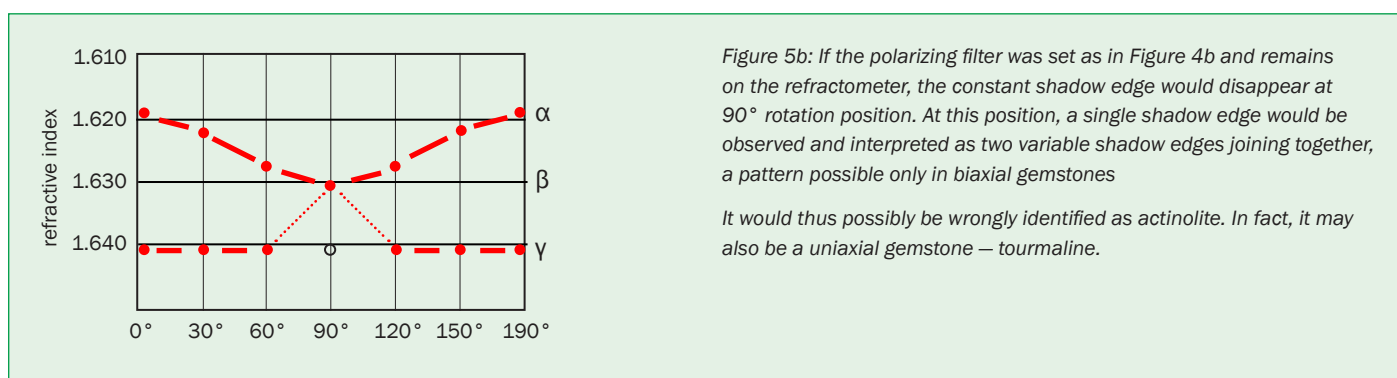*This gemstone could be tourmaline (uniaxial) or actinolite (biaxial).*

Figure 5b: If the polarizing filter was set as in Figure 4b and remains on the refractometer, the constant shadow edge would disappear at 90° rotation position. At this position, a single shadow edge would be observed and interpreted as two variable shadow edges joining together, a pattern possible only in biaxial gemstones

It would thus possibly be wrongly identified as actinolite. In fact, it may also be a uniaxial gemstone — tourmaline.
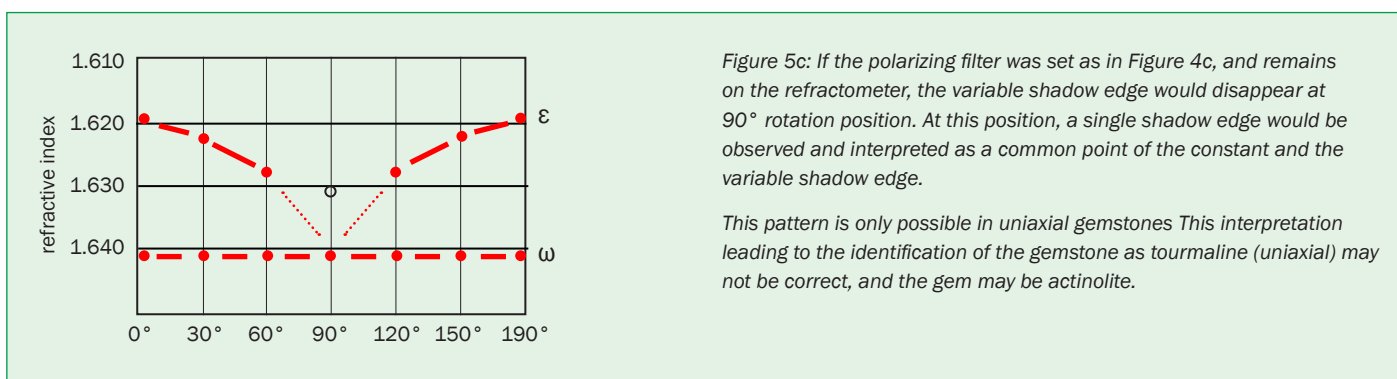

Figure 5c: If the polarizing filter was set as in Figure 4c, and remains on the refractometer, the variable shadow edge would disappear at 90° rotation position. At this position, a single shadow edge would be observed and interpreted as a common point of the constant and the variable shadow edge.

This pattern is only possible in uniaxial gemstones This interpretation leading to the identification of the gemstone as tourmaline (uniaxial) may not be correct, and the gem may be actinolite.

edges. If the polarizing filter stays in one orientation during rotation of a gemstone, sooner or later the vibration direction of one shadow edge will become perpendicular to the polarizing filter. This shadow edge will disappear and a single shadow edge will be observed. This may lead to an incorrect determination of the optic character *(Figure 5)* or to an incorrect determination of β *(Figure 6)* and, consequently, to incorrect determination of the optic sign in biaxial gemstones.

Wrong determination of optic character

A very common pattern of the movement of the shadow edges during the rotation of an anisotropic gemstone on

the refractometer consists of one variable and one constant shadow edge that do not meet (see *Figure 5a*). This pattern can be observed in uniaxial gemstones and in biaxial gemstones if the facet being measured has a particular orientation of the optical elements and the facet.

Keeping the polarizing filter in the same orientation during the rotation of a gemstone on the refractometer, may result in the extinction of one of the two shadow edges just at the critical rotation position (90° in *Figure 5*). *Figures 5b* and *5c* show situations which would lead gemmologists to think that they had observations which are only possible in uniaxial gemstones or which are only possible in biaxial gemstones. In fact, such an error can be caused by wrong use

of the polarizing filter bringing one of the shadow edges to extinction.

Wrong determination of the principal refractive index β

The most common pattern of the movement of the shadow edges during the rotation of biaxial gemstones on the refractometer consists of two variable shadow edges that do not join. Only the maximum principal refractive index γ and the minimum principal refractive index α can be determined *(Figure 6a)*.

Where the facet of a biaxial gemstones has a particular orientation of the optical elements (the optic axis is parallel to the facet) a different pattern can be observed: two variable shadow edges which join during the rotation. At this

Use of the polarizing filter to improve observations of the shadow edges on the refractometer
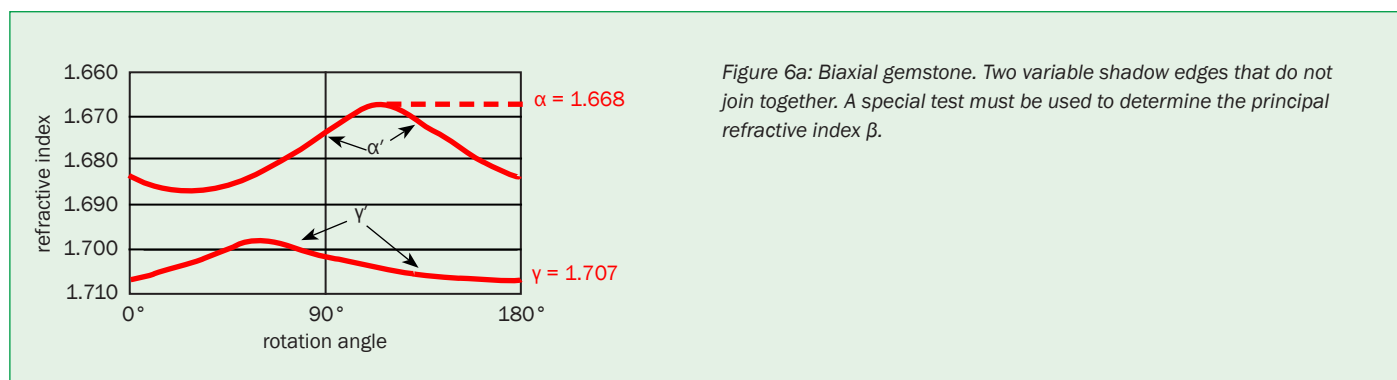

Figure 6a: Biaxial gemstone. Two variable shadow edges that do not join together. A special test must be used to determine the principal refractive index β.

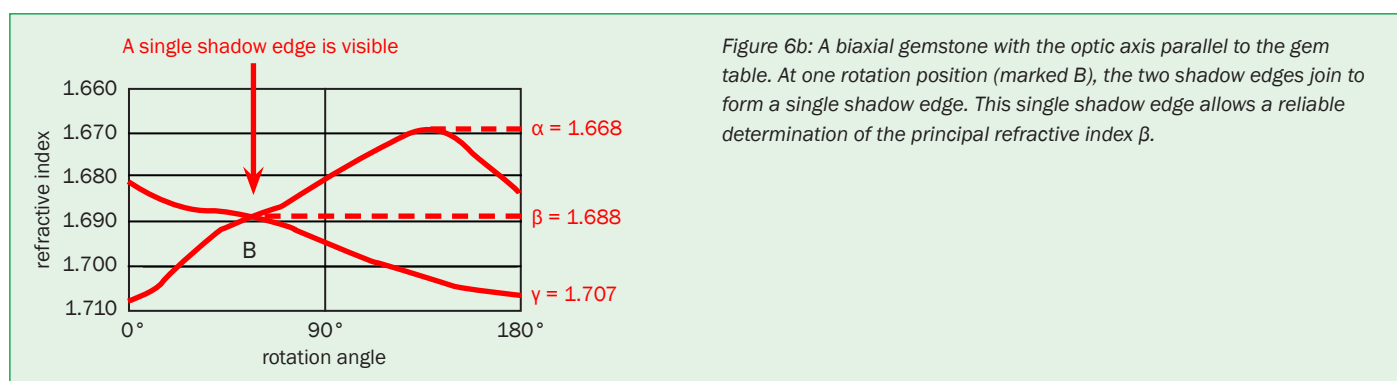Figure 6b: A biaxial gemstone with the optic axis parallel to the gem table. At one rotation position (marked B), the two shadow edges join to form a single shadow edge. This single shadow edge allows a reliable determination of the principal refractive index β.
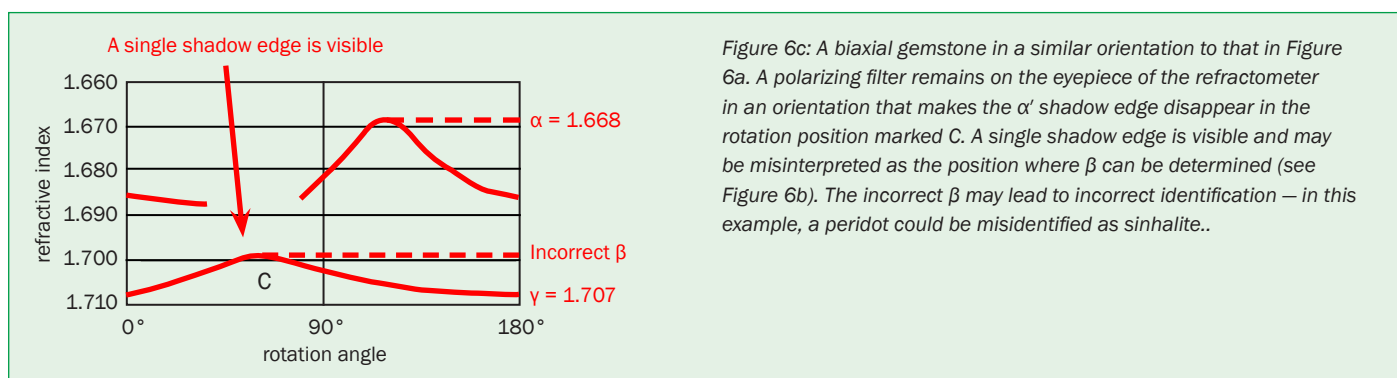

Figure 6c: A biaxial gemstone in a similar orientation to that in Figure 6a. A polarizing filter remains on the eyepiece of the refractometer in an orientation that makes the α′ shadow edge disappear in the rotation position marked C. A single shadow edge is visible and may be misinterpreted as the position where β can be determined (see Figure 6b). The incorrect β may lead to incorrect identification — in this example, a peridot could be misidentified as sinhalite..

rotation position, a single shadow edge is observed and allows reliable and accurate determination of the principal refractive index β *(Figure 6b)*.

However the same observation – a single shadow edge – can be observed at some stage in rotation of a gem with the common biaxial pattern *(Figure 6a)* if the polarizing filter is left on the eyepiece and the vibration direction of one, or the other, shadow edge becomes perpendicular to the polarizing filter. This shadow edge will disappear and a single shadow edge is seen and may lead to the wrong determination of the principal refractive index β.

This wrong determination of β can lead to incorrect determination of the optic sign and, eventually, to wrong identification of a gemstone (see *Figure 6c)*.

These two examples show the importance of always following the correct procedure for the use of the polarizing filter. The polarizing filter must be adjusted every time a gemstone is rotated on the refractometer. However, the best practice is to use the polarizing filter when needed to increase the sensitivity of observation and to remove it immediately after.

The Authors

Darko B. Sturman
Curator Emeritus, Royal Ontario Museum, Toronto, Ontario, Canada

Duncan Parker FGA FCGmA
Harold Weinstein Ltd, Gemmological Laboratory, Toronto, Ontario, Canada

Abstracts

Diamonds

Diamond formation from CaCO$_3$ at high pressure and temperature.

L. Bayarjargal (bayarjargal@kristall.uni-frankfurt.de), T.G. Shumilova, A. Friedrich and B. Winkler. *European Journal of Mineralogy,* **22**(1), 2010, 29–34.

From a study by micro-Raman spectroscopy of the decomposition of CaCO$_3$ by laser-heated diamond-anvil cell experiments at 9–21 GPa up to 4000 K, it is indicated that calcite decomposes into CaO+O$_2$+C across the whole pressure range at temperatures around 3500 K, initially forming graphite nanoparticles of ~3–11 nm. These graphite particles may aggregate and transform into ~20 nm diamonds if the sample is annealed in the diamond stability field. It is concluded that diamond can be crystallized directly from carbonatitic melts by the decomposition of CaCO$_3$ at high pressures and temperatures, and that phase diagrams showing a decomposition to CaO+CO$_2$ in the *P–T* range need to be re-evaluated.   R.A.H.

The Wittelsbach-Graph and Hope diamonds: not cut from the same rough.

E. Gaillou (asteriee@yahoo.fr) W. Wang, J.E. Post, J.M. King, J.E. Butler, A.T. Collins and T.M. Moses. *Gems & Gemology,* **46**(2), 2010, 80–88.

The Wittelsbach-Graff and the Hope, two of the world's most famous blue diamonds, share similarities in history, colour and phosphorescence, but distinct differences in their luminescence emission and internal strain patterns demonstate that these two type IIb diamonds did not originate from the same crystal. Their overall resemblance and Indian origin, however, suggest that they formed in similar geological settings.   R.A.H.

Gemmologie Aktuell (Gemmological news).

C.C. Milisenda. *Gemmologie. Z. Dt. Gemmol. Ges.,* **59**(3/4), 2010, 65–70.

A cross section of a diamond was submitted because it had been thought to be synthetic. The diamond showed grey-brown star- and cross-like growth structures representing undulating, non-planar cuboid growth features which only occur in natural diamonds.

          E.S.

Lab notes.

T.M. Moses and S.F. McClure (Eds). *Gems & Gemology,* **45**(4), 2009, 288–95.

Items include a 1.49 ct Fancy deep brown-orange diamond that owes its colour to laboratory radiation.   R.A.H.

Lab notes.

T.M. Moses and S.F. McClure (Eds). *Gems & Gemology,* **46**(1), 2010, 48–57.

Notes are given on a cut diamond with rare green fluorescence and a 6.46 ct Fancy intense blue HPHT-treated type IIb diamond.   R.A.H.

Morphology and defects of diamond grains in carbonado: clues to carbonado genesis.

V.A. Petrovsky, A.A. Shiryaev, V.P. Lyutoev, A.L. Sukharev and M. Martins. *European Journal of Mineralogy,* **22**(1), 2010, 35–47.

Paramagnetic and non-paramagnetic defects in grains of diamond from Brazilian carbonado indicate that many of the specimens of carbonado studied were annealed under mantle conditions, although for a relatively short time. Diamond grains show various morphological forms with low degrees of dissolution; these include re-entrant apices and incomplete growth layers on faces. It is suggested that micron-sized single crystals of diamond of predominantly octahedral and cubo-octahedral shape grew under conditions of decreasing carbon supersaturation. The temperature decrease is a plausible driving force for crystallization. During the second stage of carbonado formation, mass crystallization of diamond occurred; the necessary C supersaturation was probably caused by crystallization of other minerals, leading to a decrease in the volume and/or constitution of the parent solution.   R.A.H.

Possible "sister" stones of the Hope diamond.

S.D. Sucher (scott@museumdiamonds.com), S.W. Attaway, N.L. Attaway and J.E. Post. *Gems & Gemology,* **46**(1), 2010, 28–35.

The recent discovery of a lead cast of the French Blue, the precursor of the Hope, has provided a more accurate model of the Hope diamond, which disappeared in 1792. Computer models of the French Blue and its parent stone, the Tavernier Blue, were used to determine whether other diamonds might have been created when the Tavernier was cut into the French Blue, or when the latter was cut to produce the Hope. It is demonstrated that it was not feasible for other significant diamonds to have been created during any recutting.
          R.A.H.

Gems and Minerals

Demantoid from Val Malenco, Italy: review and update.

I. Adamo, R. Bocchio, V. Diella, A. Pavese, P. Vignola, L. Prosperi and V. Palanza. *Gems & Gemology,* **45**(4), 2009, 280–7.

New data are presented for demantoid from Val Malenco in northern Italy, including results from electron microprobe, LA-ICP-MS and UV-Vis-NIR and mid-IR

Abstracts (continued)

spectroscopy. These garnets are shown to be almost pure andradite (> 98 mol %, RI > 1.81, SG 3.81–3.88) All 18 samples studied contained 'horsetail' inclusions characteristic of their geological origin in serpentinite. The coloration of this demantoid is controlled by the contents of Fe and Cr, the latter being the major influence.   R.A.H.

Sächsischer Amethyst.

W. BECK. *Lapis.,* **35**(2), 2010, 23–8.

Amethyst of near ornamental quality is described from sites in Saxony, Germany.   M.O'D.

The Kagem emerald mine, Kafubu area, Zambia.

S.C. BEHLING and W.E. WILSON. *The Mineralogical Record,* **41**(1), 2010, 59–67.

Emeralds from the Kagem mine are found in a pegmatite field and may occur with interpenetrant twins of quartz. M.O.D.

Röntgenamorph und lichtkristallin — Optische Eigenschaften opaliner Materialien.

R. GOLDBERG AND H.J. SCHÖPE. *Gemmologie. Z. Dt. Gemmol. Ges.,* **59**(1/2), 2010, 19–34. 4 photographs, 7 diagrams, bibl

Opaline materials like natural precious opals are made up of spherical colloidal particles in a three-dimensional structure with lattice constants in the wavelength range of visible light. But unlike precious opals, close packing of the silica particles is not obligatory; this group includes structures made of chemically different particles with variable packing density as well as bidisperse arrays. A diffraction theory is presented to explain the observations, taking into account the scattering behaviour of the spherical particles.   E.S.

Bastnäsite-(Ce) and parisite-(Ce) from Mt. Malosa, Malawi.

A. GUASTONI (alessandro.guastoni@unipd.it), D. KONDO and F. NESTOLA. *Gems & Gemology,* **46**(1), 2010, 42–7.

Large (up to 20 cm) brownish orange crystals of bastnäsite-(Ce) interlayered with opaque yellow-brown parisite-(Ce) occur associated with aegirine and microcline in alkaline pegmatites on Mt Malosa, southern Malawi. Small parts of some of the crystals are suitable for cutting as gems. The gemmological and chemical properties of these rare-earth carbonates are presented.   R.A.H.

Hibonite: a new gem mineral.

T. HAINSCHWANG (thomas.hainschwang@gemlab.net), F. NOTARI, L. MASSI, T. ARMBRUSTER, B. RONDEAU, E. FRITSCH and M. NAGASHIMA. *Gems & Gemology,* **46**(2), 2010, 135–8.

A 0.23 g orangy-brown crystal yielding a 0.39 ct step-cut stone and a 0.71 g crystal were characterized by IR spectroscopy, XRD and SEM/XRF as hibonite. This material had RI 1.79–1.81, SG 3.84, H 7½–8 and was reputed to be from Myanmar.   R.A.H.

Gemmologische Kurzinformationen. Zuchtperlen mit zerbrochenem Überzug.

H.A. HÄNNI. *Gemmologie. Z. Dt. Gemmol. Ges.,* **59**(3/4), 2010, 106–8. 3 photographs, bibl.

Drilling of South Sea cultured pearls sometimes gives rise to fissures on the surface. The pearls mostly contain classical beads from freshwater shells which have a layered structure. If the direction of the drilling coincides with the layering, the core may split. Cultured pearls with a thin coat are particularly vulnerable.   E.S.

Zuchtperlen mit neuem Kernmaterial.

H.A. HÄNNI, M.S. KRZEMNICKI and L.E. CARTIER. *Gemmologie. Z. Dt. Gemmol. Ges.,* **59**(1/2), 2010, 35–46. 15 photographs, 1 table, bibl.

Different materials have been used as cores for cultured pearls, mainly shell from Mississippi bivalves. As a new option for beads in cultured pearls, baroque-shape shell beads as well as Chinese freshwater cultured pearls have been found to serve this purpose. Experiments with freshwater cultured pearls of 6.5 mm have been carried out with marine *Pinctada maxima* and with *Pinctada margaritifera* oysters. After 13 months 200 pearls were harvested. Natural pearls have also been used as nuclei, the material being either non-nacreous, brown or of an unpleasant appearance; these are difficult to identify as the radiographic structure of the natural cores are masking these cultured pearls.   E.S.

Gemmologische Kurzinformationen. Hypersthen aus Sri Lanka.

U. HENN. *Gemmologie. Z. Dt. Gemmol. Ges.,* **59**(1/2), 2010, 51–2. 3 photographs, bibl.

Gem-quality hypersthene shows remarkable golden-brown wavy zones due to lamellar twinning. Physical properties and chemical composition are given.   E.S.

Gemmologische Kurzinformationen. Aventurisierender Feldspat (Sonnenstein) aus Tansania.

U. HENN. *Gemmologie. Z. Dt. Gemmol. Ges.,* **59**(1/2), 2010, 52–4. 2 photographs, 1 table, bibl

Gem feldspars occur in the Meto hills, northwest of Arusha, near the Kenyan border. They show typical physical and chemical characteristics of oligoclase feldspar. The aventurescent effect is caused by tabular hematite inclusions.   E.S.

Gemmologische Kurzinformationen. Tourmaline aus dem Kongo.

U. HENN. *Gemmologie. Z. Dt. Gemmol. Ges.,* **59**(3/4), 2010, 111–13. 5 photographs, 1 graph, bibl.

Tourmalines from the Democratic Republic of Congo show green to blue-green to greenish-blue colours caused by divalent iron. Some crystals have distinct colour zoning showing green and greenish-blue segments. Typical capillary fluid inclusions can be observed.   E.S.

Ein Beitrag zum Thema Onyx.

U. HENN, T. HÄGER and C.C. MILISENDA. *Gemmologie. Z. Dt. Gemmol. Ges.,* **59**(3/4), 2010, 83–94. 17 photographs, 1 graph, bibl.

In contrast to earlier regulations, recent CIBJO nomenclature requires specific disclosure on the dyeing of chalcedonies and agates. In the trade most onyx is dyed. In addition to the traditional sugar treatment, black in chalcedonies can be induced by the use of cobalt-bearing substances such as cobalt nitrate or cobalt chlorite, which can be detected by XRF analysis. Natural coloured quartz aggregates or onyx can be obtained from India, Brazil and South Africa. The Brazilian specimens are fibrous aggregates coloured by natural organic carbon. Samples from India and South Africa are grained polycrystalline aggregates and take a weaker polish. Their dark colour is due to iron, manganese and titanium oxides.   E.S.

Abstracts (continued)

Short gemmological notes. Emerald green muscovite as a gemstone.

J. Hyršl. *Gemmologie. Z. Dt. Gemmol. Ges.,* **59**(3/4), 2010, 109–11. 4 photographs, bibl.

Muscovite belongs to the mica group and is generally thought too soft (hardness 2.5–3) to be suitable for jewellery. It also has perfect cleavage. In 2009 a new emerald-green rough appeared from Tanzania, first offered as emerald, then zoisite, but proved to be muscovite. About 10 rough pieces and 15 cut stones were examined; the faceted pieces weighed between 0.25 and 1.25 ct. Under the Chelsea Colour Filter the stones showed red; Cr lines were seen with a spectroscope. Two other examples of muscovite are mentioned; one is a carving of a green monkey from Peru examined in 2009, which proved to be muscovite; the other are some cabochons on the base of a rock crystal vessel in St. Vitus cathedral in Prague which were previously thought to be emeralds.   E.S.

Short gemmological notes. Barite from Alenquer, Brazil.

J. Hyršl, R. Scholz and K. Krambrock. *Gemmologie. Z. Dt. Gemmol. Ges.,* **59**(3/4), 2010, 103–5. 3 photographs, 1 graph, bibl.

A new source of rough baryte in Alenquer in the state of Para, Brazil, started to produce in 2009. It occurs there in loose crystals always free of matrix rock. Nothing is known of its geological context. The crystals are usually 2–5 cm across, rarely over 10 cm long, weighing a few hundred grams. They are very transparent which is rare in baryte from other parts of the world. Most crystals are colourless, very light yellow or smoky, often with thin parallel blue zones near the rim of some crystal faces. A few cut stones, the largest weighing 375 ct, were examined in more detail.   E.S.

Gem News International.

B.M. Laurs (Ed.) (blaurs@gia.edu). *Gems & Gemology,* **45**(4), 2009, 296–311.

Items mentioned include cut stones of yellow grossular whose only inclusions are colourless crystals of apatite, an 83.45 ct transparent phenakite from Nigeria, transparent and bright blue sodalite reportedly from a locality near the Badakhshan lapis lazuli mines in Afghanistan and pink-to-red Cu-bearing tourmaline from Nigeria.   R.A.H.

Gem News International.

B.M. Laurs (Ed.) (blaurs@gia.edu). *Gems & Gemology,* **46**(1), 2010, 58–72.

Items noted include brownish-yellow cut andradites (0.30-1.58 ct) from western China, strings of beads of coarse-grained lepidolite from Mozambique, a cat's-eye rhodonite (6.93 ct) from Brazil showing good chatoyancy, cut green diopsides (5.93 and 6.50 ct) from Ihosy, Madagascar, a 2.16 ct brownish-orange sapphire coloured due to Be-diffusion, and an amazing decorative prayer rug (106 x 60 cm) with 27,104 gemstones (including 1242 diamonds, 4580 emeralds, 1888 rubies and 9668 yellow sapphires) with all the gems in perfect alignment and arranged in attractive patterns (reportedly it took five years to gather and cut all the gemstones and another five years to assemble them in the final tapestry).   R.A.H.

Gem News International.

B.M. Laurs (Ed.) (blaurs@gia.edu). *Gems & Gemology,* **46**(2), 2010, 147–62.

Descriptions are given of large (up to 11.2 cm) crystals of kunzite from the Pala district of California, scallop pearls containing calcite prisms, fine sapphire and ruby from eluvial deposits at Montepuez in northern Vietnam, green gemmy titanite from the Shigar valley area of northern Pakistan, tsavorite and other green garnets from Afghanistan, a 5.43 ct synthetic Ca-Nb-Ga garnet, serpentine doublets sold as pietersite, and an antique pendant with a 7.50 ct lead-glass-filled ruby.   R.A.H.

Gemstone enhancement and its detection in the 2000s.

S.F. McClure, R.E. Kane and N. Sturman. *Gems & Gemology,* **46**(3), 2010, 218–40.

Advances in technology during the first decade of this century and the increasing demand for lower-priced gem materials both contributed to the proliferation of such developments as the diffusion treatment of corundum and beryllium, the diffusion of copper into feldspar, and the heat treatment of diamond, ruby and sapphire. The gemmological research laboratories have done their best to keep up with these treatments and the jewellery trade has struggled to cope with their disclosure. These developments are summarized, as are the methods used to identify the various enhancements. R.A.H.

Gemmologie Aktuell (Gemmological news).

C.C. Milisenda. *Gemmologie. Z. Dt. Gemmol. Ges.,* **59**(3/4), 2010, 65–70.

Some precious opals weighing between 1 and 13 ct from the Wollo province in Ethiopia were investigated. Due to high porosity the samples increased in weight significantly when immersed in water.

An interesting colourless scapolite was submitted for identification. When exposed to UV for five minutes, the colourless stone turned blue, but faded within a few seconds after removal from UV.

A faceted, translucent to opaque brown stone weighing 1.06 ct said to be from Myanmar was submitted and was found to be baddeleyite, zirconium oxide, used in the production of CZ.

Other specimens described include a faceted yellow milarite from Namibia, faceted bright yellowish-green titanite (sphene) from Madagascar, colourless faceted kurnakovite from California and a colourless transparent strontianite from California.   E.S.

Spessartin: Vom Sammlerstein zum Topseller.

C.C. Milisenda, Th. Lind and U. Henn. *Gemmologie. Z. Dt. Gemmol. Ges.,* **59**(1/2), 2010, 3–18. 18 photographs, 2 tables, 7 diagrams, bibl.

Spessartine garnets, first found in the Spessart mountains in Bavaria, Germany, in 1832, followed by other locations, were comparatively rare until a new source was found in Namibia in 1992. These stones were tangerine-orange and became known as mandarin garnets. This article compares the physical and optical properties of spessartines from Ramona in California, Namibia, Pakistan, Nigeria, Tanzania and other occurrences.   E.S.

Alpine pink fluorite.

T.P. Moore. *The Mineralogical Record,* **41**(1), 2010, 9–52.

A thorough survey of ornamental pink fluorite from Alpine sites. Includes a comprehensive bibliography.   M.O'D.

Lab notes.

T.M. Moses and S.F. McClure (Eds). *Gems & Gemology,* **45**(4), 2009, 288–95.

Items include a colourless cat's-eye phenakite and a 9.28 ct blue sapphire

Abstracts (continued)

which had been diffusion treated with both Ti and Be.   R.A.H.

Lab notes.

T.M. Moses and S.F. McClure (Eds). *Gems & Gemology,* **46**(1), 2010, 48–57.

Notes are given on a jadeite bangle with remarkable transparency due to having been impregnated with a polymer with an RI very close to that of the host, and a watermelon tourmaline in which a feldspar crystal had interrupted crystal growth, creating growth tubes which have a dramatic effect on the pleochroic colours.   R.A.H.

Lab notes.

T.M. Moses and S.F. McClure (Eds). *Gems & Gemology,* **46**(2), 2010, 140–6.

Items noted include a 14.20 ct green sapphire treated by beryllium diffusion and a 17.02 ct red oval modified brilliant which was identified as a heated natural spinel.   R.A.H.

Andradite from Antetezambato, North Madagascar.

F. Pezzotta [fpezzotta@yahoo.com], *Mineralogical Record*, **41**(3), 2010, 209-29

Near the village of Antetezambato situated in Antsiranana Province in North Madagascar a relatively new deposit of andradite garnet has been yielding not only gem quality varieties of demantoid and topazolite, but also some of the world's finest andradite mineral specimens. Mining activity is challenged by the fact that the productive area is located in a mangrove swamp, which at high tide is flooded by 50–80 cm of sea water every day. Prior to initial reports of andradite in 2006 (erroneously called green tourmaline, green zircon and green sapphire), the only other confirmed occurrence of green andradite was at Mount Bezavona in 1922. In 2008, the identity of the material was confirmed by a gemmological laboratory and by April of 2009 rumours of the find brought thousands of miners, buyers, and brokers to the previously sparsely inhabited area.

The author describes the extreme mining conditions, unstable political situation and ongoing problems with corruption which make the mining of andradite in the region very difficult and dangerous, if not at times impossible. He details the geology of the area and the genesis of the andradite, stating that it "is the first important mineral and gemstone deposit formed by contact metamorphism of the Permian-Mesozoic sediments to be discovered in Madagascar". The absence of titanium in the sedimentary rocks accounts for the demantoid and andradite varieties, rather than the more common titanium-rich melanite variety. Fossil shells and corals have been found replaced by garnet and quartz and forming the matrix for demantoid crystals. An overview of the history, nomenclature, properties and chromophores of andradite varieties is followed by a description the wide range of crystal specimen types seen at this locality. Note is made of a colour-change variety found at Antetezambato which shows greenish yellow in daylight and reddish yellow in incandescent light, as well as an unusual bluish hue observed in some green crystals visible only under daylight conditions. Other significant mineral specimens found at the site include quartz, calcite, stilbite-Ca, pyrite and probable wollastonite (as inclusions). E.A.S.

Play-of-color opal from Wegel Tena, Woolo province, Ethiopia.

B. Rondeau (benjamin.rondeau@univ-nantes.fr), E. Fritsch, F. Mazzero, J.-P. Gauthier, B. Cenki-Tok, E. Bekele and E. Gaillou. *Gems & Gemology,* **46**(2), 2010, 90–105.

A newly discovered opal deposit is reported from the village of Wegel Tena in northern Ethiopia. The material is mostly white, but with some brown opal, fire opal and white opal with high quality play-of-colour opal. The opals are found in a specific Oligocene volcanic sequence of alternating basalt and ignimbrite. Their properties are consistent with those of opal-CT. They become transparent when soaked in water, showing a remarkable hydrophane character. The white opals from this deposit contain an elevated content of Ba of 82–226 ppm. A Raman spectrum is shown; TEM reveals a microstructure of nanospheres ~ 170 nm in diameter.   R.A.H.

Montebrasit in Edelsteinqualität: ein seltener Fund aus Brasilien.

J. Schnellrath, R. Scholz, K. Krambrock, C.C. Milisenda and A.M. de Figueiredo Epaminondas. *Gemmologie. Z. Dt. Gemmol. Ges.,* **59**(3/4), 2010, 95–102. 2 photographs, 1 map, 5 graph, bibl.

Amblygonite and montebrasite are rarely found in the trade. Most gem-quality specimens are often collectively known as amblygonite. The samples examined come from a mine 16 km north of Galileia in Minas Gerais, Brazil, amongst them an exceptionally large, faceted, light greenish specimen weighing 185.65 ct. Physical and chemical analysis showed that these samples were hydroxyl-rich montebrasite.   E.S.

Alexandrite von Minaçu, Goias, Brasilien: ein primäres Vorkommen.

R. Schultz-Güttler, K.-J. Petersen Jr and U. Henn. *Gemmologie. Z. Dt. Gemmol. Ges.,* **59**(3/4), 2010, 71–82. 16 photographs, 2 maps, 1 table, 1 graph, bibl.

The alexandrites found in Minaçu, Brazil, are mostly small stones, yielding cut specimens of between 0.05–0.15 ct. They have many inclusions and the colour change ranges from weak to definite, mainly from blue-green in daylight to violet to orange-yellow in artificial light. It is a primary occurrence which is rare in Brazil. The mother rock is a mica schist mainly composed of biotite, muscovite and quartz.   E.S.

Gem localities of the 2000s.

J.E. Shigley, B.M. Laurs, A.J.A. Janse, S. Elen and D.M. Dirlam. *Gems & Gemology,* **46**(3), 2010, 188–216.

During the past decade there were impressive discoveries of diamonds and coloured gemstones, but a decline in sales due to high development costs, environmental considerations, and a downturn in the global economy. The 'locality of origin' took on increasing importance for some coloured stones such as ruby, sapphire, emerald and copper-bearing tourmaline. The geographic sources of diamonds and coloured stones are reviewed and the production areas that were commerically important during the years 2001–2010 are each discussed. Maps of most of the important gem-producing areas in the world are included in an accompanying (folded) wall chart.   R.A.H.

Chrysoprase and prase opal from Haneti, central Tanzania.

J.E. Shigley, B.M. Laurs and N.D. Renfro.

Abstracts (continued)

Gems & Gemology, **45**(4), 2009, 271–9.

Commercial quantities of gem-quality chrysoprase and green prase opal (Ni-bearing chalcedony and common opal, respectively) have been recovered from altered serpentinite deposits near Haneti, Tanzania. The largest mine, on top of Iyobo Mountain, has been actively exploited for two decades. Chrysoprase can be distinguished from prase opal by its higher RI (~ 1.55 vs ~ 1.45) and SG (~ 2.60 vs ~ 2.11). Chrysoprase is the main product of the mine, which shows a good potential for continued production.   R.A.H.

Ruby and sapphire production and distribution: a quarter century of change.

R. Shor and R. Weldon. *Gems & Gemology,* **45**(4), 2009, 236–59.

During the past 25 years, the market for corundum gems has been transformed from one of medium to high prices to one encompassing nearly all price ranges. This transformation was brought about by the discovery of several large deposits and the development of treatment processes that enhanced the colour and clarity of very large amounts of previously non-commercial ruby and sapphire. More recently, however, controversial treatments have undermined confidence and prices in some material, while political events and press scrutiny have affected the supply chain for rubies and sapphires from such localities as Myanmar and Madagascar.   R.A.H.

An era of sweeping change in diamond and colored stone production and marketing.

R. Shor and R. Weldon. *Gems & Gemology,* **46**(3), 2010, 166–87.

Since the start of the twenty-first century new markets for gems and distribution have emerged around the world as a result of economic forces and political pressures. De Beers abandoned its role as a single-channel seller, creating a competitive diamond market. Political pressures in Madagascar and a ban on gem exports from Myanmar disrupted supply channels for ruby and sapphire. A new class of well-informed customers who value ethically-, socially- and environmentally-friendly products are making their demands known in the gemstone business.   R.A.H.

New occurrence of fire opal from Bemia, Madagascar.

M. Simoni (rsimoni@tin.it), F. Caucia, I. Adamo and P. Galinetto. *Gems & Gemology,* **46**(2), 2010, 114–21.

The investigation of 22 gem opals from a new volcanic deposit near Bemia, south eastern Madagascar, by classical gemmological, SEM-EDS, powder XRD, LA-ICP-MS and by both Raman and IR spectroscopy techniques is reported. None showed any play-of-colour, but exhibited a wide variety of hues, including those typical of fire opal, due to Fe-rich inclusions. These microcrystalline samples consist of opal-CT or opal-C. Their RIs and SGs are higher than those of typical fire opals from elsewhere, allowing their ready distinction.   R.A.H.

The Clay Canyon variscite mine, Fairfield, Utah.

W.E. Wilson. *The Mineralogical Record,* **41**(4), 2010, 321–49.

A classic site for ornamental and even gem quality variscite is described.   M.O'D.

Instruments and Techniques

Developments in gemstone analysis techniques and instrumentation during the 2000s.

C.M. Breeding, A.H. Shen, S. Eaton-Magaña, G.R. Rossman, J.E. Shigley and A. Gilbertson. *Gems & Gemology,* **46**(3), 2010, 241–257.

Advances in gem treatment and synthesis technology, together with the discovery of new gemstone deposits, led to the need for improved techniques in gem identification, and to the development and widespread use of chemical microanalysis techniques such as LA-ICP-MS, luminscence spectroscopy and X-ray imaging, together with the development of nanoscale analysis. Innovations in laser mapping and computer modelling of the appearance of diamond rough and faceted stones changed the way gemstones are cut and the manner in which they are graded by gem laboratories.   R.A.H.

Cutting diffraction gratings to improve dispersion ("fire") in diamonds.

A. Gilbertson, B. Gudlewski, M. Johnson, G. Maltezos, A. Scherer and J. Shigley. *Gems &*

Gemology, **45**(4), 2009, 260–70.

A new microlithography process developed to create high-resolution diffraction grating patterns on portions of certain facets can improve the dispersion of light and hence the amount of 'fire' in a diamond. These nanocut plasma-etched diamonds are identifiable under magnification by the presence of small, unpolished-looking areas on the facets where the grating pattern has been created. Round brilliant-cut diamonds showing such patterns will be classified by the GIA Laboratory as modified round brilliants: as such, they will be given colour and clarity grades, but not a cut grade.   R.A.H.

Confocal micro-Raman spectroscopy: a powerful tool to identify natural and synthetic emeralds.

Le T.-T. Huong (letth@vnu.edu.vn), T. Häger and W. Hofmeister. *Gems & Gemology,* **46**(1), 2010, 36–41.

The examination of more than 300 natural and synthetic emeralds from various sources by confocal spectroscopy demonstrated that this technique can identify the different types of water in the beryl channel sites, making it possible to determine whether an emerald is natural or synthetic. This approach may also be able to provide information about the geographic origin or synthesis of the stone.   R.A.H.

X-ray computed microtomography applied to pearls: methodology, advantages and limitations.

S. Karampelas, J. Michel, M. Zheng-Cui, J.-O. Schwarz, F. Enzmann, E. Fritsch, L. Leu and M.S. Krzemnicki. *Gems & Gemology,* **46**(2), 2010, 122–7.

X-ray computed tomography reveals the internal features of pearls in great detail, and can distinguish between some of the natural and cultured pearls that are difficult to separate using X-radiography. The disadvantages include a long measurement time, high cost of instrumentation and only being able to image one pearl at a time.   R.A.H.

X-ray computed microtomography: distinguishing natural pearls from beaded and non-beaded cultured pearls.

M.S. Krzemnicki (gemlab@ssef.ch), S.D.

Abstracts (continued)

Friess, P. Chalus, H.A. Hänni and S. Karampelas. *Gems & Gemology,* **46**(2), 2010, 128–34.

The distinction of natural from cultured pearls using X-ray computed microtomography [preceding abstract] has shown this technique to be a powerful tool for pearl identification, including its ability to distinguish between natural pearls, beaded and non-beaded cultured pearls.

R.A.H.

Synthetics and Simulants

A new type of composite turquoise.

G. Choudhary (gtl@giepcindia.com). *Gems & Gemology,* **46**(2), 2010, 106–13.

The examination of pink, purple-pink, yellow-green and blue specimens of dyed and/or stabilized turquoise revealed that all these specimens were composites of pieces of turquoise bonded together. The purple-pink and yellow-green samples were bonded with a coloured polymer, and the blue ones had a colourless polymer. The gemmological properties are listed, together with EDXRF and FTIR analyses; the reactions of these materials with the solvents acetone and methylene chloride are also discussed.

R.A.H.

Synthetischer Feueropal — "MexiFire®".

U. Henn, K. Wehr and C.C. Milisenda. *Gemmologie. Z. Dt. Gemmol. Ges.,* **59**(1/2), 2010, 47–5. 2 photographs, 1 table 1 graph, bibl.

The synthetic fire opals are produced in India and marketed under the name 'MexiFire®'. They have a lower RI and density than natural fire opals and can also be identified by chemical analyses and infrared spectroscopy.

E.S.

Color alteration in CVD synthetic diamond with heat and UV exposure: implications for color grading and identification.

R.U.A. Khan (riz.khan@DTC.com), P.M. Martineau, B.L. Cann, M.E. Newton, H.K. Dhillon and D.J. Twitchen. *Gems & Gemology,* **46**(1), 2010, 18–26.

In response to heat (>450°C) and UV exposure, some cut and faceted synthetic pale-coloured diamonds grown by chemical vapour deposition exhibit large, reversible changes in colour. Conversely, a darker colour is shown by samples following exposure to UV radiation. Both types of change returned to their initial (stable) colour when they were illuminated for >30 minutes with a standard daylight lamp, but did not do so when kept in the dark. These non-permanent changes might affect the apparent colour grade of a CVD synthetic diamond.

R.A.H.

Lab notes.

T.M. Moses and S.F. McClure (Eds). *Gems & Gemology,* **46**(2), 2010, 140–6.

Items noted include a 1.05 ct CVD synthetic diamond graded as G which developed strong pink fluorescence when exposed to strong UV radiation.

R.A.H.

Strongly colored pink CVD lab-grown diamonds.

W. Wang (wwang@gia.edu), P. Doering, J. Tower, R. Lu, S. Eaton-Magana, P. Johnson, E. Emerson and T.M. Moses. *Gems & Gemology,* **46**(1), 2010, 4–17.

Samples of 19 faceted pink diamonds (0.3–0.7 ct) grown in the laboratory by Apollo Diamond Inc. using CVD methods were examined and their colour and clarity grades were found to be comparable with those of top-quality natural pink diamonds. A combination of optical centres similar to those seen in previously studied in pink-to-red diamonds that had been exposed to HPHT annealing, irradiation and further annealing at relatively low temperatures, were found. These pink CVD products can be distinguished from natural and treated-colour natural diamonds by a combination of fluorescence colour, growth zoning and absorption featres in the IR and UV-Vis regions.

R.A.H.

Abstractors

R.A. Howie – R.A.H.   M. O'Donoghue – M.O'D.   E.A. Skalwold – E.A.S.   E. Stern – E.S.

Book reviews

Studies on Agate. Microscopy, spectroscopy, growth, high temperature and possible origin.
Terry Moxon, 2009. Terra Publications, Doncaster, S. Yorks. pp 102. Paperback. ISBN 978-0-9528512-1-9. £20.00

This is Terry Moxon's second book on agates and is more wide ranging than his first which dealt with agate microstructures and possible origins. This one is intended for lapidary workers and mineral collectors who are keen to learn more about agate occurrence and genesis and at the scientifically-orientated general public. The prime aim is to introduce the reader to some of the scientific techniques that have been used to examine agate over the last twenty years. Has he been successful? To a degree — yes. Without doubt this is the best book covering the major problems associated with agate genesis. Other recent books on agates focus on agate beauty and worldwide occurrences whilst largely avoiding the thorny questions.

However, the content is incongruously couched in language on a variety of levels. Initially it gives the impression of "I'm not quite sure what kind of book I am" but it quite quickly moves into the research scientist mode with a basic science preamble. This may be a little daunting for some readers but their persistence will be rewarding.

This 96 page book is divided into nine chapters:

Chapter 1 Agates: occurrence, regions and hosts. Deals briefly with the varieties of microcrystalline quartz and types of agate. The majority of the chapter comprises brief descriptions of around 30 regions worldwide including the age of the deposits. It is rather superficial and does not compare well with recent 'Coffee Table' books that depict beautiful agate from all over the world.

Chapter 2 Optical microscopes and photomicroscopy: This chapter covers sample preparation and equipment and describes the simple techniques used to create many of the images in the book. Rather surprisingly about half of this chapter is devoted to superficial coverage of dyeing, structural features, pigmentation and interpretation that bear little relationship to the theme of the chapter.

Chapter 3 Electron microscopy. Chapter 3 begins with an historical review of the electron microscope imaging techniques. Twenty images using electron microscopy techniques are presented and their features described. There is sometimes poor correlation between the images and their descriptive text such that the reader may find it difficult to relate the description to the illustrated feature. More use of arrows pointing to the features would have helped overcome this as would have better captions. To aid clarity and ease of understanding the whole aspect of linking text, captions and images could have been better. Nevertheless the features are fascinating albeit that the interpretation is limited.

Chapter 4 X-ray diffraction. Basic descriptions of powder X-ray diffraction are given and the application of the technique to crystallite size, phase identification and their relationship to age is discussed.

Chapter 5 Visible, infrared and Raman spectroscopy. The basic principles of each spectroscopy method are described. Usefully the various forms of silica described in the book are defined in this chapter but there are omissions. However as one reads through the book some of these omitted terms are defined. It would have been helpful to have all the described terms together and to have extended this to cover all the silica phases mentioned including their relationships (for example the relationship between colloidal silica and sol). To have had this at the outset would have been beneficial.

Spectroscopy investigations cover: identifying the effect of metal ions on silicic acid and colloidal silica; identifying water and hydroxyl groups in agate; and identifying moganite in agate.

Chapter 6 High temperature and pressure studies. This chapter begins with a brief simple introduction to reaction kinetics and then concentrates on experimental work on water loss at elevated temperature, the relationship between age and water content, the type of water (both free water and as silanol) and the implication for crystallite coarsening and linked moganite reduction. The diagrams complement the text discussion.

Chapter 7 Cathodoluminescence (CL). A short basic overview of cathodoluminescence and its methodology when applied to agate begins the chapter. The nature of chemical bonding is also discussed as a precursor to understanding defects, largely water-related Si-O-'X' bonds, in the crystal structure in agate. Figures associated with this are adequate without reaching high levels of clarity. Age-related changes in type and number of defects using CL are discussed.

Chapter 8 Agate from Cumbria, England, and the Pilbara Craton, Australia. Discussion in this chapter centres on the thermal history of these deposits employing the techniques of X-ray diffraction, infrared spectroscopy, Raman spectroscopy, cathodoluminescence and specific gravity determination. This case study takes the findings in the other chapters and applies them to these deposits to explain anomalies.

Chapter 9 Agate genesis. Explaining agate genesis is the Holy Grail of agate research. The author states that the origin of agate still remains an enigma and poses the five fundamental questions that need yet to be answered in order to solve the problem of agate genesis. He reviews

Book reviews (continued)

current research and thinking on these and presents the pros and cons of several possible explanations.

The analytical equipment generated images are useful and instructive whilst the colour images of agates are at best adequate with poor focus. Fortunately this latter aspect is not a crucial aspect of the book. The overall impression is that of an unsophisticated approach to imaging and the book would benefit from better images and annotations.

Readers will find the bibliography rewarding. The index however is rather sparse.

For anyone who has pondered over the paradoxical situation presented by the apparent simplicity of agate chemistry, the complexity of agate structures, agate abundance worldwide and agate occurrence in a variety of different rocks, this book offers, if not an answer, both a satisfying and at the same time tantalising journey into the science of agate genesis. For agate enthusiasts, *Studies on Agate* is a must-have item. For others this could be the beginning of a lasting quest for knowledge about this fascinating material, or dismissed (even though the science is often at a basic level), as a 'boffins book'.

Brian Jackson

Russian Alexandrites.

Karl Schmetzer, 2010. Schweizerbart Science Publishers, Stuttgart. pp 141, over 200 colour illustrations. Hard Cover. ISBN 978-3-510-65262-4. €34.80 (USA $49.90).

Having been able to facilitate the study of alexandrite specimens in the Natural History Museum collections with renowned gemmologist and author Dr Karl Schmetzer, it was with eager anticipation that I received his new book *Russian Alexandrites*. With contributions from George Bosshart, Marina Epelboym, Dr Lore Kiefert and Anna-Kathrin Malsy, the book seeks to be an all encompassing work on this valuable variety of chrysoberyl; the authors' intentions being made clear in the short introduction whereby they state that although much has been written on alexandrite, there is a paucity of data concerning inclusions, microscopic features and indicators of provenance.

My first impression of the book is one of quality, with a simple but elegant frontispiece of an alexandrite crystal group in both daylight and incandescent light. The book is slightly larger format at 275x215 mm, is superbly produced, and beautifully illustrated with over 200 coloured figures, photographs, maps and diagrams.

The introduction gives a summary of the geological setting of the Uralian deposits and recent mining activity including photographs of Schmetzer and Kiefert's visit to the Malysheva mine in 2007. Chapter 2 follows with a historical overview of the Tokovaya area, and whilst the author notes that this has been the subject matter of numerous publications beforehand, this is an excellent summary. Chapter 3 describes in great detail the discovery, naming and historical use of Russian alexandrite. This chapter can be regarded as the definitive chronology of Russian alexandrite, the author having excelled in bringing together a wealth of information that includes historical literature, family archives, published reports, illustrated portraits and discussions of the more famous specimens which includes emerald as these two gem varieties are so closely associated in the deposits in the Urals. Chapter 4 gives a brief overview of Russian alexandrites in mineralogical Museums and in the trade, the author having comprehensively studied over 400 alexandrite crystals, crystal groups and gemstones from major European and Russian museums and private collections. This leads us into chapters 5 and 6 which are closely linked. Chapter 5 on morphology and twinning is extensively illustrated with photographs of alexandrite crystals. The chapter is so 'photo rich' that it gives the impression of being able to personally browse the holdings of those great collections. I particularly liked how these images are compared to equivalent crystal drawings by the author who has colour-coded the faces to make it easy to distinguish the different forms and development of complex twinning. Chapter 6 looks at mineralogical and gemmological properties with beautifully illustrated sections on typical microscopic features such as twinning and inclusions. Chapter 7 discusses the chatoyant effects of alexandrite and chrysoberyl, and although Russian cat's-eyes are discussed, the chapter also includes sections on Sri Lankan material. Chapter 8 is very short

at only three pages, but discusses the comparison of growth patterns of Russian, other natural and synthetic alexandrites. Chapter 9 discusses the colorimetric data of Russian alexandrite and yellowish green to green chrysoberyl using the CIELAB colour space model, with interesting discussion as to the practical application of colorimetry in provenance and nomenclature studies. Chapter 10 looks at trace element and locality determination of Russian alexandrites using LA-ICP-MS. As a relatively recent and increasingly important technique used in gemmology, I was pleased to see a short but concise summary of the principles of the application itself.

Aside from the appendix of seven tables of data, transcription of names, historical timetable, and index, the exhaustive research that the author has undertaken is reflected in an extremely useful and comprehensive reference list.

Overall, *Russian Alexandrites* is an excellent scholarly work and is the choice for anyone looking for a wealth of information on this most enigmatic of gem varieties. Indeed, it is one of the best 'single species' volumes ever published. There is more to this book than the title suggests, especially in the later chapters where comparisons and references to chrysoberyl and alexandrites from other localities including synthetics are made. The book is well laid out and is notable for its beautiful and relevant illustrations. This is a book for historians, enthusiasts, mineralogists, gemmologists and researchers and with its low price is an essential buy for any reference collection.

Alan Hart

Proceedings of the Gemmological Association of Great Britain and Notices

Gem-A Events

Gem-A Conference: Gemmology and the Gem Market: Micro and Macro

Gem-A Conference speakers and presenters: (left to right) Andrew Cody, Richard Drucker, Michael Krzemnicki, James Riley, Maggie Campbell Pedersen, Rui Galopim de Carvalho, Michael Hügi, Crhistopher P. Smith and Professor Andy Rankin.

The 2010 annual Conference, held on Sunday 7 November at the Hilton London Kensington Hotel, looked at gems from both gemmological and marketing perspectives, and in detail as well as giving the wider picture. Speakers included Andrew Cody, Rui Galopim de Carvalho, Christopher P. Smith, Michael Hügi, Michael Krzemnicki, Maggie Campbell Pedersen and Richard Drucker.

During the breaks delegates had the opportunity to browse through the latest books and instruments from Gem-A Instruments and to view displays including those by Maggie Campbell Pedersen on organics, the Institute of Registered Valuers, the Scottish Gemmological Association, Richard Drucker with *The GemGuide* and the GemGuide Appraisal Software, and Gem-A Education with samples of glass-filled rubies.

The day concluded with a dinner held at the Hilton followed by a disco.

A programme of events and workshops was arranged to coincide with the Conference. These started on Saturday 6 November with a one-day seminar held at the Gem-A headquarters by Ted Themelis entitled 'An update on the heat treatment of ruby and sapphire'. On Monday 8 November at Goldsmiths' Hall in the City of London, John Benjamin gave a one-day seminar entitled From Medieval to Modernism: a thousand-year tour of international jewellery design'. This was followed in the evening by the Graduation Ceremony at Goldsmiths' Hall (see below). On Tuesday 9 November Michael Hügi presented a half-day workshop on photomicrography. This was followed in the afternoon by a guided tour of the Crown Jewels at the Tower of London with David Thomas. The final event was Gem Discovery Club with guest speaker Marijan Dundek entitled 'The magic world of diamonds'.

A full report of the Conference and events was published in the Winter 2010 issue of *Gems & Jewellery*.

Proceedings of the Gemmological Association of Great Britain and Notices

Conference Sponsors and Supporters:

The Association is most grateful to the following for their support:

MAJOR SPONSORS

Marcus McCallum FGA, London
w: www.marcusmccallum.com

T.H. March, Insurance Brokers
w: www.thmarch.co.uk

SUPPORTER

Apsara
w: www.apsara.co.uk

We would also like to thank **dg3 Diversified Global Graphics Group** for sponsoring the leaflets and delegate badges for the conference. Visit their website at www.dg3.com

Nature's Treasures 3

A seminar organized jointly by Gem-A, the Mineralogical Society, the Russell Society and Rockwatch, was held on Sunday 12 December 2010 at the Flett Theatre, Natural History Museum, London SW7.

Short talks on a variety of subjects from mining the oceans to meteorites, were presented by William Burgess, Ron Callender, Maggie Campbell Pedersen, Doug Garrod, Fred Mosselmans, Caroline Smith and Peter Treloar.

During the lunch break, delegates had the opportunity to view displays by Gem-A, Leica, Marcus McCallum, The Mineralogical Society, RockWatch, The Russell Society, Richard Tayler and Andy Tindle. Harold Killingback displayed the 'White Flag' agate featured in the Autumn issue of *Gems & Jewellery* and Ron Callender gave a demonstration of gold panning.

Graduation Ceremony

On Monday 8 November the Graduation Ceremony and Presentation of Awards was held at Goldsmiths' Hall in the City of London. Professor Andy Rankin, President of the Gemmological Association, presided and Rui Galopim de Carvalho, founder of LABGEM in Lisbon, Portugal, presented the awards and gave the address.

Following the presentations to the graduates, the first members to be awarded Fellowship status in recognition of their high level of expertise and who had made a significant contribution to the field of gemmology for no less than ten years were presented with their Fellowship dilpomas. They were Dr Douglas Nichol of Wrexham, North Wales, Christopher P. Smith of New York and Mary Burland of Gem-A, London.

A certificate was awarded to Evelyne Stern, who retired from the Gem-A Council in 2010, recognizing her contribution to diamond education in the Association.

In his address, Rui Galopim de Carvalho stressed the importance of the Gem-A graduates to continue their education by learning as much as possible about gemmology. Addressing the graduates, he said: "Yours is an exciting and rapidly developing field which provides the background for a fascinating career and participation in a worldwide community of like-minded people."

The ceremony was followed by a reception for graduates and guests.

A report of the Graduation Ceremony was published in the October issue of *Gems & Jewellery*.

Photo courtesy of Photoshot
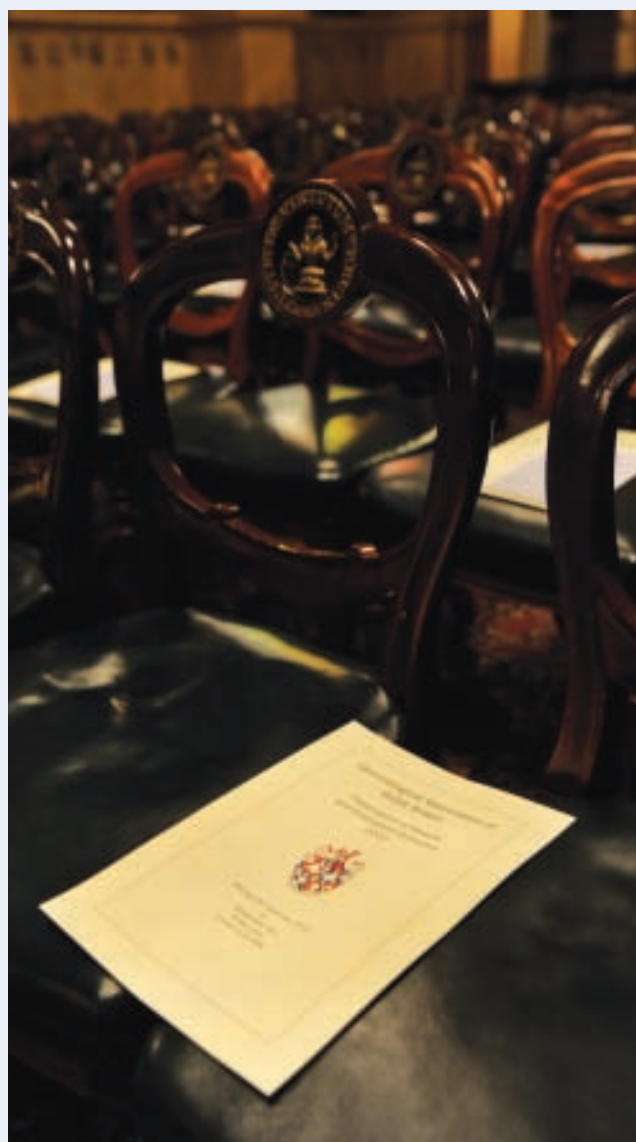
Proceedings of the Gemmological Association of Great Britain and Notices

Gem-A Awards

Gem-A Examinations were held worldwide in January and June 2010. In the Examinations in Gemmology 209 students qualified in the Diploma Examination, including seven with Distinction and 18 with Merit. In the Foundation in Gemmology Examination 349 qualified. In the Gem Diamond Examination 98 qualified, including 21 with Distinction and 20 with Merit.

The **Christie's Prize for Gemmology** for the best candidate of the year in the Diploma Examination was awarded to **Louise Dennis** of Halesowen, West Midlands.

The **Anderson Bank Prize** for the best set of theory papers in the Diploma in Gemmology examination was awarded to **Chen Suoyi** of Beijing, P.R. China.

The **Read Practical Prize** for excellence in the Diploma Practical Examination, named in memory of Peter Read, was sponsored for 2010 by DeeDee Cunningham of Toronto, Canada. The Read Practical Prize was awarded to **Leung Ka Yee Ainsley** of Hong Kong.

In the **Foundation Certificate in Gemmology** examination, the **Anderson Medal** for the candidate who submitted the best set of answers which, in the opinion of the Examiners, were of sufficiently high standard, and the **Hirsh Foundation Award** for the best candidate of the year, were awarded to **Robin Hansen** of Warminster, Wiltshire.

In the **Gem Diamond Diploma** examination, the **Bruton Medal**, awarded for the best set of theory answer papers of the year, and the **Deeks Diamond Prize** for the best candidate of the year, were awarded to **Ben Wen** of Wuhan, P.R. China.

The **Dominic Mok Diamond Practical Prize** for excellence in the Diamond Practical Examination, is sponsored by Dominic Mok from AGIL, Hong Kong. The Dominic Mok Diamond Practical Prize was awarded to **Sheung Mei Tang** of Hong Kong

The Tully Medal was not awarded.

The names of the successful candidates are listed below.

Examinations in Gemmology

Gemmology Diploma

Qualified with Distinction
Chen Suoyi, Beijing, P.R. China
Dennis, Louise, Hasbury, Halesowen, West Midlands
Orsini, Paolo, Alessandria, Italy
Perosino, Lorenzo, Novi Ligure, Italy
Wang Shang Bai, Beijing, P.R. China
Yan Xiao-Xuan, Beijing, P.R. China
Zhang Rui, Beijing, P.R. China

Qualified with Merit
Benard, Guillaume, Montreal, Quebec, Canada
Cai Jia, Beijing, P.R. China
Cheng Lian, Wuhan, Hubei, P.R. China
Chunxia Shen, Chengdu, Sichuan, P.R. China
Fox, Karen Elizabeth, Toronto, Ontario, Canada
Grocholska, Katherine Rose, Highbury, London
Han Yi, Baotou, Inner Mongolia, P.R. China
Hart, Alan D., Beckenham, Kent
Jia Xiaodan, Beijing, P.R. China
Lau King Suen, Shau Kei Wan, Hong Kong
Lemaire, Alisson, Drummondville, Quebec, Canada

Li Yan, Beijing, P.R. China
Lian Guo, Shanghai, P.R. China
Liu Na, Beijing, P.R. China
Masselot, Joelle, Geneva, Switzerland
Nicolai, Namaste, Cardiff, Glamorgan
Tsai Min-Chieh, Taipei, Taiwan, R.O. China
Zhu Jiachen, Beijing, P.R. China

Qualified
Aderhold, Bryan C., Ridgewood, New Jersey, U.S.A.
Andersson, Lina, Sundbyberg, Sweden
Arpino, Delphine, Viroflay, France
Aung Ko Ko, Yangon, Myanmar
Austin, Megan, Rocklea, Queensland, Australia
Bailey, Sarah, London
Beale, Sioned Ann, Lapworth, Solihull, Warwickshire
Berezovsky, Florence Paulette Marie, Zurich, Switzerland
Bonnin, Romain Claude Michel, Montreal, Quebec, Canada
Borenstein, Guy, Pardes-hana Karkur, Israel

Proceedings of the Gemmological Association of Great Britain and Notices

Bright, David, Riverside, Missouri, U.S.A.
Brown, Sandra Jane, Birmingham, West Midlands
Byrne, Ruth, South Woodford, Essex
Cederferm, Magdalena, Märsta, Sigtuna, Sweden
Cederholm, Jenny, Farsta, Sweden
Chatagnier, Pierre Yves, Saint Albin, Vareilles, France
Chatzipanagiotou, Ioannis Tzannis, Athens, Greece
Chen Shifeng, Beijing, P.R. China
Cheung Yuk King, New Territories, Hong Kong
Choi Chi Ho Jim, Tuen Mun, Hong Kong
Chun Lv, Xiamen, Fujian, P.R. China
Chunnong Du, Nanning, Guangxi, P.R. China
Cooper, Amy S., Las Vegas, Nevada, U.S.A.
Cox, Rebecca Jane, York
Dan, Wang, Beijing, P.R. China
Davis, Natasha, Northwood, Middlesex
De Gaetano, Antonella, Genoa, Italy
Delerholm, Peter, Enskede, Sweden
Deng Lei, Guangzhou, Guangdong, P.R. China
Deng Xiansong, Guilin, Guangxi, P.R. China
Dimitrakopoulos, Charalabos, Athens, Greece
Du Liuyin, Beijing, P.R. China
Duraffourg, Valerie, Belle Fontaine, France
Evans, Charles I., Camden, London
Evans, Daniel Raymond, Brisbane, Queensland, Australia
Evans, Rachel, London
Falah, Jamal, Concord West, New South Wales, Australia
Fang Yixiang, Yichang, Hubei, P.R. China
Gerez, Ingrid Kintgen, Wasquehal, France
Gokani, Anooj, Leicester
Goubert, David, Villeneuve Les Avignon, France
Gowans-Poli, Julie, London
Graham, Lisa J., Tunbridge Wells, Kent
Guenin, Nathalie, Sainte Foy, Quebec, Canada
Haifei Chen, Qixing District, Guilin, P.R. China
Hammond, Ross, Hackney, London
Harnois, Dominique Marie, Paris, France
Hell, Martine Svitlana, Hedalen, Norway
Ho Yue Yau, Tsuen Wan, Hong Kong
Huang Binli, Wuhan, Hubei, P.R. China
Huang Ting, Tianyang, Guangxi, P.R. China
Huang Yisheng, Shanghai, P.R. China
Hui Hang Chung, Marilyn, Hong Kong
Huijbrechts, Thomas N., Schoorl, The Netherlands
Iozzino, Vittorio, Genoa, Italy
Jia Liu, Beijing, P.R. China
Jia Lu, Wuhan, Hubei, P.R. China
Joannou, Christina Maria, Ilford, Essex
Kang Yanan, Wuhan, Hubei, P.R. China
Kapoor, Kushagra, New Delhi, India
Krontira, Sofia, Athens, Greece
Kuklinski, Frank, Niebull, Germany

Lai Yuen Wan, Eva, Hong Kong
Lai Siu Kwong, New Territories, Hong Kong
Lai Xiaojing, Guilin, Guangxi, P.R. China
Lawson, Charles Peter Grahame, Indooroopill, Brisbane, Australia
Lee Ka Chun, New Territories, Hong Kong
Lee Wai Yin, Kitty, New Territories, Hong Kong
Leon, Virginie, Marseille, France
Leung Ka Yee Ainsley, New Territories, Hong Kong
Li Dongmei, Beijing, P.R. China
Li Dongyi, Shenzhen, Guangdong, P.R. China
Li Lingyun, Yining, Xinjiang, P.R. China
Li Pufu, Nanning, Guangxi, P.R. China
Liao Chengwen, Luoding, Guangdong. P.R. China
Lili Wan, Wuhan, Hubei, P.R. China
Liu Hongjie, Beijing, P.R. China
Liu Sui Chung, New Territories, Hong Kong
Liyan He, Nanxiong, Guangdong, P.R. China
Lo Wai Yee Bibian, New Territories, Hong Kong
Loeb, Nicolas, Paris, France
Logan, Peter M., Coventry, West Midlands
Lung Mei Ting, May, Shatin, Hong Kong
Luo, Helen Rong, North York, Ontario, Canada
Lust, Nathalie, Les Pennes Mirabeau, France
Lynch, Anne Lynette, Nundah, Queensland, Australia
Ma Hui, Beijing, P.R. China
Ma Yan Ting, Tsim Sha Tsui, Hong Kong
Maclean, Victoria E.F., London
McKeown, Julia, Oldbury, West Midlands
McNiven, Adrian, London
Manuelli, Piero Alberto, Genoa, Italy
Matthews, Emma, Sunninghill, Berkshire
Meikle, Alastair Murray Scott, London
Meng Yan, Beijing, P.R. China
Mi Ying, Hu, Shannxi, P.R. China
Michaelides, Emma, Enfield, Middlesex
Midwinter-Porter, Holly, London
Mo Qian, Guilin, Guangxi, P. R. China
Mohammad, Aamir, Oldham, Lancashire
Mulrooney, Rosalyn, London
Myint Tun @ Stephen Yan, Yangon, Myanmar
Neuyen Thi Thuy Nea, Terry, Montreal, Quebec, Canada
Ng Wing Yan, New Territories, Hong Kong
Ngao Mei Wan, New Territories, Hong Kong
Ning Peiying, Yulin, Guangxi, P.R. China
Noble, Frances, Wendover, Buckinghamshire
Ntsanga Olivier, Robert Rahardahy, Antananarivo, Madagascar
O'Cock, Sabrina Alice Palmer, London
Paige Anderson, Denise, London
Palo, Markus Karl, Malmberget, Sweden
Petit, Gregory, Le Plessis-Robinson, France

Proceedings of the Gemmological Association of Great Britain and Notices

Petropoulou, Alexia, Athens, Greece
Picard, Chloe, Vessy, Switzerland
Po Pui Chun, Tuen Mun, Hong Kong
Pons, Thierry, Ambohidratrim, Madagascar
Pradat, Thierry, Francheville, France
Raherinirina, Haingo Hasina, Antananarivo, Madagascar
Ramoisy, Nathalie, Boulogne-Billancourt, France
Rocchiero, Loredana, Genoa, Italy
Rowe Rawlence, Emily, London
Sawas, Jeremy, Montreal, Quebec, Canada
Seyue Tang, Guilin, Guangxi, P.R. China
She Lisheng, Shanghai, P.R. China
Shen Yi, Shanghai, P.R. China
Shi Huadan, Shanghai, P.R. China
Sim Tam Yuk, North Point, Hong Kong
Song Yanchun, Beijing, P.R. China
Soubiraa, Guillaume, Marseille, France
Stefani, Eleni, Ilioupoli, Athens, Greece
Sujun Liu, Urumqi, Xinjiang, P.R. China
Sukhdev, Bhavna, Gandhinagar, India
Sun Ruo Zhen, Roslyn, Birmingham, West Midlands
Sun Tian-qi, Qinhuangfao, Hebei, P.R. China
Tamboise, Capucine, Paris, France
Tian Menghan, Beijing, P.R. China
Ting Zhang, Fuan, Fujian, P.R. China
Tong Siu Kuen, Ma On Shan, Hong Kong
Trolle, Natascha, Copenhagen, Denmark
Tsai, Emma, Barcelona, Spain
Tsai Su-Fen, Shanghai, P.R. China
Verma, Dheeraj, Palwal, India
Vodyanova Hitzi, Elena, Athens, Greece
Wan Ching Yi, New Territories, Hong Kong
Wang Jingyuan, Shenzhen, Guandong, P.R.China
Wang Lei, Shanghai, P.R. China
Wang Ping, Qiangjiang, Hubei, P.R. China
Wang Ting, Beijing, P.R. China
Wang Xiawen, Guilin, Guangxi, P.R. China
Wang Xu, Shanghai, P.R. China
Wangwei He, Guilin, Guangxi, P.R. China
Watanabe, Yoshiko, Minamitsuru-gun, Yamanashi Pref., Japan
Westley, Penny, Hagley, Worcestershire
Wetherall, Alan, Hitchin, Hertfordshire
Wong, Phyllis, London
Wong Fung Ha, Christine, New Territories, Hong Kong
Wong Yee Man, Quarry Bay, Hong Kong
Wu Yu, Urumqi, Xinjiang, P.R. China
Xi Zhang, Guilin, Guangxi, P.R. China
Xia Xiyue, Guilin, Guangxi, P.R. China
Xiaoxue Duan, Wuhan, Hubei, P.R. China
Xiaoyi Wu, London

Xie Tian Qi, Beijing, P.R. China
Xie Yan, Shanghai, P.R. China
Xue Qin, Shanghai, P.R. China
Yang Bei, Taizhou, Jiangsu, P.R. China
Yapa Abeywardena, Jayani Madhavi, Colombo, Sri Lanka
Ye Hui, Ningbo, Zhejiang, P.R. China
Yi Yang, Guilin, Guangxi, P.R. China
Yin Yi-Ming, Beijing, P.R. China
Yin Yiqing, Shanghai, P.R. China
Yu Tao, Guilin, Guangxi, P.R. China
Yuan Heng Yi, Beijing, P.R. China
Yue Xuan, Jia, Beijing, P.R. China
Yunhai Huang, Luchuan, Guangxi, P.R. China
Zerillo, Jocelyn, Marseille, France
Zhang Kai, Shanghai, P.R. China
Zhang Peng, Beijing, P.R. China
Zhang Yi, Beijing, P.R. China
Zhangrui Ouyang, Liuzhou, Guangxi, P.R. China
Zhao Xin, Guilin, Guangxi, P.R. China
Zhi Yingxue, Jia Shan, Zhejiang, P.R. China
Zhou Chuan-Peng, Beijing, P.R. China
Zhu Peini, Wuhan, Hubei, P.R. China

Foundation Certificate in Gemmology

Qualified
Alliaume, Nicole, Moustiers St. Marie, France
Alvarez, Andrew, Cheltenham, Gloucestershire
Andriamaro, Manitra, Antananarivo, Madagascar
Andriamboavonjy, Rasamuel Heriniaina, Antananarivo, Madagascar
Antonucci, Andrea, Stockholm, Sweden
Arda, Basak, Geneva, Switzerland
Arpino, Delphine, Viroflay, France
Aung, Ei Ei San, Yangon, Myanmar
Aye Thin Thin, Yangon, Myanmar
Bai Jing, Beijing, P.R. China
Bakahi, Chekeba, Marseille, France
Balasubramaniam, Subanthini, Rugby, Warwickshire
Bane, Jonathan William, South Yorkshire
Bell, Nicola, Birmingham, West Midlands
Benard, Guillaume, Montreal, Quebec, Canada
Bernau, Eric, Vinsobres, France
Biaggiotti, Frazione Carpreno, Genoa, Italy
Bonnin, Romain Claude Michel, Montreal, Quebec, Canada
Bordenave, Mathilde, Montreuil sous Bois, France
Bradley, Tineke Monica, Langport, Somerset
Bratek, Elizabeth Jane, Romford, Essex
Butterworth, Gareth John, York

Proceedings of the Gemmological Association of Great Britain and Notices

Cafaro, Patrice, Vitrolles, France
Cahill, Anna, Brighton, East Sussex
Callandreau, Alexandra, Paris, France
Cappelli, Antonella, Genoa, Italy
Cassanelli, Alice, Modena, Italy
Ceroux, Jean Jacques, Chanteix, France
Chan Chi Wai, Dick, NewTerritories, Hong Kong
Chan Chui Wan, Annabel, Tsuen Wan, Hong Kong
Chan Hsin-Ju, Taipei, Taiwan, R.O. China
Chan Miu Yee, New Territories, Hong Kong
Chan Yuen Ping, Aberdeen, Hong Kong
Chaplin, Letitia, Ipswich, Suffolk
Chauhan, Harbinder, Leicester
Chen Chih-Chieh, Taichung, Taiwan, R.O. China
Chen Haifei, Qixing, Guilin, P.R. China
Chen Jie, Shanghai, P.R. China
Chen Qian Zheng, Beijing, P.R. China
Cheung Shui Ling, Sai Wan Ho, Hong Kong
Chit, Wathon, Yangon, Myanmar
Choi Min Seok, Seoul, South Korea
Chu Siu Ming, Joanna, Hong Kong
Chun Lv, Xiamen, Fujian, P.R. China
Coldham, Terrence Stewart, Sydney, New South Wales,
    Australia
Collot, Jocelyne, Montesson, France
Condon, Rebecca, New Barnet, London
Cooper, Euan Douglas, Grange Park, London
Coquillette, Ghislaine, Meudon, France
Davies, Christine, Birmingham, West Midlands
Davis, Natasha, Northwood, Middlesex
de Gaspe Beaubien, Isabelle, Montreal, Quebec, Canada
de Lussanet de la Sablonière, Monique E., The Hague,
    The Netherlands
De Vismes, Raphaele, Versailles, France
Di Gegorio, Giuseppe, Spadafora, Messina, Italy
Diamond, Marcia Jane, London
Dingley, Stacey M., Oakham, West Midlands
Du Chunnong, Nanning, Guangxi, P.R. China
Dudun, Svetlana, Dagenham, Essex
Dutton, Mark, Bexhill-on-Sea, East Sussex
Edvardsson, Lena, Herrljunga, Sweden
Evans, Eibhlin Ide, Skelmersdale, Lancashire
Fachidou, Soumela-Melina, Athens, Greece
Fang Jun, Shanghai, P.R. China
Fernando, Expedith Mothilal, Colombo, Sri Lanka
Fernebrand, Mats, Helsingborg, Sweden
Fu Jiaping, Gulin, Guangxi, P.R. China
Gao Shijia, Shanghai, P.R. China
Gao Yujie, Beijing, P.R. China
Ginsberg, Max, Borehamwood, Hertfordshire
Gokani, Anooj, Leicester

Golechha, Dinesh Kishore, Raipur, India
Goma, Rosemichelle, Hendon, London
Gowans-Poli, Julie, London
Graham, David B., Lincoln, Massachusetts, U.S.A.
Grammenidis, George, Vrilissia, Athens, Greece
Grishin, Phillipe, Kings Langley, Hertfordshire
Gu Jialu, London
Guo, Lian, Shanghai, P.R. China
Guo Yongquan, Xiamen, Fujian, P.R. China
Hallikas, Minna, Helsinki, Finland
Hansen, Robin, Warminster, Wiltshire
Hao Yudi, Beijing, P.R. China
Hardy, Sarah, Stockton-on-Tees, County Durham
Harper-Roberts, Amy, Stratford-upon-Avon, Warwickshire
He Liyan, Nanxiong, Guangdong, P.R. China
He Yiting, Beijing, P.R. China
Heilio, Saara, London
Ho Yuen Yan, Karen, New Territories, Hong Kong
Huang Mengyao, Beijing, P.R. China
Huang Rong, Beijing, P.R. China
Huang Ting, Tianyang, Guangxi, P.R. China
Huang Yisheng, Shanghai, P.R. China
Huang Yuan, Beijing, P.R. China
Huang Yunhai, Luchuan, Guangxi, P.R. China
Hunt, Glynis, Andover, Hampshire
Hutchinson, Fiona, Albourne, West Sussex
Ikeuchi, Mototeru, Edogawa-ku, Tokyo, Japan
Ivancic, Ivan, Colombo, Sri Lanka
Jain, Sanjay, Karnataka, India
Jheng Jin-Bao, Hsin Juang City, Taiwan, R.O. China
Jiang Baoxin, Shanghai, P.R. China
Jiao Yongling, Beijing, P.R. China
Jin Wei, London
Jing Chen, Beijing, P.R. China
Jokinen, Tiina, Tampere, Finland
Kapetanaki, Sofia-Dagkmar, Glyfada, Greece
Karimzadeh, Leyla, London
Katsof, Erika, Montreal, Quebec, Canada
Kaye, Charlotte Jane, Hungerford, Berkshire
Keiko, Kamijima, Nishi-Tokyo City, Tokyo, Japan
Keskitalo, Riikka, Vantaa, Finland
Keverne, Alice, Bradford-on-Avon, Wiltshire
Kikkawa, Tomomi, Kofu City, Yamanashi Pref., Japan
Killick, Tracy, Edgbaston, West Midlands
Kim Chul Gyoon, Gyeonggi-Do, South Korea
Kim Kyung Sook, Kyungsangnam-do, South Korea
Kirkham, Sally Louise, Birmingham, West Midlands
Kirsi, Kettunen, Jarvenpaa, Finland
Kuklinski, Frank, Niebull, Germany
Kulmie, Ahmed, London
Kuo Chi, Tseung Kwan O, Hong Kong

Proceedings of the Gemmological Association of Great Britain and Notices

Kuo Yi Yi, Taipei, Taiwan, R.O. China
Kyaw Soe Htet, Yangon, Myanmar
Lahtinen, Tiina, Oitti, Finland
Lai Sok Leng, Kowloon, Hong Kong
Lai Wing Lam, Tseung Kwan O, Hong Kong
Lai Xiaojing, Guilin, Guangxi, P.R. China
Lai You-Lin, Erik, Birmingham, West Midlands
Lam Kwok Yee, Teresa, New Territories, Hong Kong
Lam Yu Ha, Wanchai, Hong Kong
Lau Yue Bong, James, North Point, Hong Kong
Le Bagousse, Laure, Boulogne-Billancourt, France
Le Morvan-Damour, Helene, Paris, France
Lee, Alix, Rognes, France
Lee Jin Sook, Gyeonggi-Do, South Korea
Lee Lai Chun, Loletta, Mid-Levels West, Hong Kong
Lee Mei-Hui, Sanchong City, Taiwan, R.O. China
Lee, Sealim, London
Lee Sun Hee, Deajon, South Korea
Lemaire, Alisson, Drummondville, Quebec, Canada
Leung Chun Kit, Kowloon, Hong Kong
Leung Suet Lin, Kowloon, Hong Kong
Leung Yin Chun, Jeannie, Kowloon, Hong Kong
Li Pufu, Nanning, Guangxi, P.R. China
Li Shanshan, Wulumuqi, Xinjiang, P.R. China
Li Shuang, Beijing, P.R. China
Li Ye, Shanghai, P.R. China
Liang Wei, Yulin, Guangxi, P.R. China
Liao Chengwen, Luoding City, Guangdong, P.R. China
Liao Mengyuan, Guangxi, P.R. China
Lin Chen-Chi, Kowloon, Hong Kong
Lin Jing, Beijing, P.R. China
Liu Di, Guilin, Guangxi, P.R. China
Liu Tian Tian, Birmingham, West Midlands
Liu Yuan, Guilin, Guangxi, P.R. China
Li-Yan Hu, Taipei, Taiwan, R.O. China
Loeb, Nicolas, Paris, France
Lortie, Dominique, Montreal, Quebec, Canada
Lowther, Joan, London
McDonaugh, Robert Francis, London
McIver, Samantha, Solihull, West Midlands
McKenzie, Troy, Greenslopes, Queensland, Australia
McNiven, Adrian, West Kensington, London
Mahmood Zadeh, Saghi Tamara, Montreal, Quebec, Canada
Maiko, Kawasaki, Minami-Tsuru-Gun, Yamanashi Pref., Japan
Mailly, Caroline, Versailles, France
Maki, Jarkko, Lampaala, Finland
Mallia, Rachel, London
Mandrali, Alexia, Athens, Greece
Marcus, Caroline Rose, Oxford
Masselot, Joelle, Geneva, Switzerland

Maurice, Francois, Chambery, France
Mayer, Helen, London
Menard, Georges-Etienne, Saint Hyacinthe, Quebec, Canada
Meng Caizhen, Nanning, Guangxi, P.R. China
Meunier, Delphine, Barcares, France
Miles, Fiona Christina, Wimborne, Dorset
Mkogian, Elen, Thessalonika, Greece
Mo Qian, Guilin, Guangxi, P.R. China
Modi, Upaasna, Golders Green, London
Mohler, Anja, London
Morris, Susan L., Columbia, California, U.S.A.
Mowbray, Caroline, Barnes, London
Musasa, Yves Mbala, Sutton, Surrey
Myint, Yinmon, Yangon, Myanmar
Naylor-Leyland, Jessica, London
Neurauter, Amy Lynn, New York, U.S.A.
Ng Tsz Hong, Kowloon, Hong Kong
Ng Wan Yuen Eoroy, Kowloon, Hong Kong
Nguyen Thi Thuy Nga, Terry, Montreal, Quebec, Canada
Ning Peiying, Yulin, Guangxi, P.R. China
Norrgard, Anna, Helsinki, Finland
Ntsanga, Robert, Antananarivo, Madagascar
Nussenblatt, Fabio, Castelletto Molina Asti, Italy
Oderda, Dr. Gianluca, Vesenaz, Switzerland
O'Reilly, Erin, Montreal, Quebec, Canada
Orton, Christine, Bradford-on-Avon, Wiltshire
Otten, Anthony John Hubert, London
Ouyang Zhangrui, Liuzhou, Guangxi, P.R. China
Owen, Cheryl Mae, Erdington, West Midlands
Palliyaguruge, Lalaka Sanjeewa, Battaramulla, Sri Lanka
Papalekakou, Despoina, Korydallos, Athens, Greece
Parry, Tessa Pryce, Ardington, Oxfordshire
Patel, Farzin, Karachi, Pakistan
Paupinat, Jacques, La Ciotat, France
Perkkio, Maria, Helsinki, Finland
Pfeifer, Annelisse, Ripon, North Yorkshire
Philippou, Alexia, London
Picard, Chloe, Vessy, Switzerland
Pik Shan Fan, Kowloon, Hong Kong
Pino, Orazio, Sestri Levante, Italy
Pogorzelski, Didier, Nice, France
Pons, Thierry, Ambohidratrimo, Madagascar
Porter, Niall, Ballinaclash, Co. Wicklow, Rep. of Ireland
Powers, Christopher J., San Antonio, Texas, U.S.A.
Powers, Jennifer I., San Antonio, Texas, U.S.A.
Qi Weihong, Birmingham, West Midlands
Qiu Xiao Fang, London
Quan Jie, Guangzhou, Guangdong, P.R. China
Raherinirina, Haingo Hasina, Antananarivo, Madagascar
Ramoisy, Nathalie, Boulogne-Billancourt, France
Ramstadius, Michael, Casino, New South Wales, Australia

Proceedings of the Gemmological Association of Great Britain and Notices

Ratnayake, Dayanthi, Colombo, Sri Lanka

Redmond, Sarah, Weybridge, Surrey

Ren Xiaoxue, Beijing, P.R. China

Reynaud, Lucy Claire Charlton, Singapore

Richards, Nick, Weston-Super-Mare, Somerset

Rimal, Helena Kirstiina, Kokola, Finland

Roach, Fay, Norwich, Norfolk

Robinson, Kate, West Didsbury, Greater Manchester

Robinson, Laura J., Tipton, West Midlands

Robson, Thomas, Birmingham, West Midlands

Rodriguez, Faritza, London

Rossetto, Franck, Les Pennes Mirabeau, France

Rudzinske, Skirma, Bristol

Sawas, Jeremy, Montreal, Quebec, Canada

Schildt, Sebastian, Stockholm, Sweden

Schuch, Vanessa Elizabeth Maria, Delft, The Netherlands

Seifert, Magdalena R., Edgbaston, West Midlands

Sequino, Francesco, Naples, Italy

Seto, Kuriko, Tokyo, Japan

She Lisheng, Shanghai, P.R. China

Shen Lida, Xiamen, Fujian, P.R. China

Shenoi, Anita, Longhope, Gloucestershire

Sheridan, Meghan E., Upper Montclair, New Jersey, U.S.A.

Shevchenko, Olga, Montreal, Quebec, Canada

Shmukler, Boris, Chandler, Arizona, U.S.A.

Smart, Jacqui, Cupar, Fife

Smith, Stephen Gibson, Newcastle Upon Tyne, Tyne and Wear

Smither, Susannah, London

Sohm Reubi, Felicitas, Chaoyang, Beijing, P.R. China

Song Jia, Gulin, Guangxi, P.R. China

Spetas, Paula, Oslo, Norway

Strikker-Hemmink, Johanna Aaltje Hendrika, De Lutte, The Netherlands

Su Shi Zhen, Beijing, P.R. China

Sun Hongmeng, Beijing, P.R. China

Sun Ruo Zhen, Roslyn, Birmingham, West Midlands

Sy, Dicken, New Territories, Hong Kong

Tamboise, Capucine, Paris, France

Tang Pik Yin, Kowloon, Hong Kong

Tang Seyue, Guilin, Guangxi, P.R. China

Tang Sheung Mei, Dominic, Kowloon, Hong Kong

Tang Yik Hei, NewTerritories, Hong Kong

Tanzini, Diletta, London

Tatlow, Emily Louise, Guilford, Surrey

Tempe, Li, Hericourt, France

Tew, Timothy David, Atlanta, Georgia, U.S.A.

Tha Nyein Yu, Yangon, Myanmar

The Khanh Linh, Vien, Strasbourg, France

Thiebaud, Mandy, Paris, France

Tian Menghan, Beijing, P.R. China

Timms, Ashley, Brisbane, Queensland, Australia

Tin Zaw Win, May, Yangon, Myanmar

To Siu Lun, Kowloon, Hong Kong

Tong Ching Man Yucca, Kowloon, Hong Kong

Tong Siu Han, New Territories, Hong Kong

Toure, Abdoul Alim Herimandresy, Toamasina, Madagascar

Tseng Kuei Yu, Taipei, Taiwan, R.O. China

Tsoi Wai Yee, Joyce, Kowloon, Hong Kong

Tu Hui-Min, Taipei, Taiwan, R.O. China

Turner, Brian, Bitton, Bristol

Valasmo, Hannu, Vantaa, Finland

Van Kolck, Nubar Francois William, Bray Park, Queensland, Australia

van Rossum, Wilhelmina F.J., The Hague, The Netherlands

Vazzana, Franck, Cosnes Et Romain, France

Verdoorn-De Vrede, Veronica Chantal, Dordrecht, The Netherlands

Vining, Robert Arthur Charles, London

Von Allmen, Andrea, Munsingen, Switzerland

Vorilhon, Alix, Antananarivo, Madagascar

Voulgaridis, Konstantinos, London

Walker, Katharine, London

Waltert Bigler, Rebecca, St Legier, Switzerland

Wan, Qiaoxi, Beijing, P.R. China

Wang Jinlan, Guilin, Guangxi, P.R. China

Wang Kun, Qi County, Shanxi, P.R. China

Wang Man, Taipei, Taiwan, R.O. China

Wang Ming Ying, Beijing, P.R. China

Wang Zi, Beijing, P.R. China

Wangwei He, Guilin, Guangxi, P.R. China

Watson, Abigail, Eynsham, Oxfordshire

Weng Xiaofan, Beijing, P.R. China

Weyers, Stefanus, Brandhof, Bloemfontein, South Africa

White, Lucy, Virginia Water, Surrey

Whiting, Marielle, Salisbury, Wiltshire

Wijesinghe, Jagath, Ipswich, Suffolk

Williams, Debbie Jane Louise, Quinton, West Midlands

Willmott, Karra Jane, Croydon, Surrey

Wilson, Claire E., Bristol

Win Htet Naung, Yangon, Myanmar

Win Yu Hlaing, Yangon, Myanmar

Windeyer, Patricia Annette, Brisbane, Queensland, Australia

Wohland, Laura, Parsippany, New Jersey, U.S.A.

Wolff, Ella Sakura, Fenham, Tyne and Wear

Wong Shuk Ching, New Territories, Hong Kong

Wong Yick Chung, New Territories, Hong Kong

Woodcock, Olga Faye, Basingstoke, Hampshire

Wu Yi, Beihai, Guangxi, P.R. China

Wu Yi-Hong, Taipei, Taiwan, R.O. China

Proceedings of the Gemmological Association of Great Britain and Notices

Xu Yanran, Beijing, P.R. China
Xu Ying, Shanghai, P.R. China
Yan Yun, Xuhui, Shanghai, P.R. China
Yanase, Tomohiro, Toyota-City, Aichi Pref., Japan
Yang Shuo, Auckland, New Zealand
Yang Xi, Beijing, P.R. China
Yat, Richard, New Territories, Hong Kong
Ye Hui, Ningbo, Zhejiang, P.R. China
Ye Xiaohan, Guangzhou, Guangdong, P.R. China
Ye Xiecai, Wenzhou, Zhejiang, P.R. China
Yeung, Kwok Li, Kowloon, Hong Kong
Yi Shuihan, Birmingham, West Midlands
Yi Yang, Guilin, Guangxi, P.R. China
You Shu-Lin, Taipei, Taiwan, R.O. China
Yu Jinping, Beijing, P.R. China

Zdeb, Robert, London
Zhang Di, Beijing, P.R. China
Zhang Hui, Beijing, P.R. China
Zhang Linlin, Qinyang, Henan, P.R. China
Zhang Ting, Fuan, Fujian, P.R. China
Zhang Xi, Guilin, Guangxi, P.R. China
Zhang Xiaochen, Shanghai, P.R. China
Zhang Xiaofan, Dalian, Liaoning Province, P.R. China
Zhang Yinghui , Dudley, Worcestershire
Zhang Yiwen, Beijing, P.R. China
Zhao Yang , Beijing, P.R. China
Zheng Yan , Beijing, P.R. China
Zhou Nanbin , Beijing, P.R. China
Zhu Xiao Li, Beijing, P.R. China

Gem Diamond Diploma Examination

Qualified with Distinction
Afshar, Brett, Islington, London
Blagg, Natalie, London
Cha, Erman, Wuhan, Hubei, P.R. China
Chatzipanagiotou, Ioannis Tzannis, Athens, Greece
Chrismas, Jacqueline, Godalming, Surrey
Guoting Wang, Beijing, P.R. China
Jingyi Shi, Beijing, P.R. China
Jones, Camilla, Huddersfield, West Yorkshire
Min-Chieh Tsai, Taipei, Taiwan, R.O. China
Ngan Yin Ying, Kowloon, Hong Kong
Norris, Eddi, London
Poore, Sarah, Worthing, West Sussex
Stephenson, Elizabeth, Poole, Dorset
Tyrrell, Siobhan Ann, Walthamstow, London
Watson, John Richard, Berkhamsted, Hertfordshire
Wen Ben, Huangshi, Hubei, P.R. China
Woo Ka Yin, Agnes, Kowloon Bay, Hong Kong
Xiang Li, Beijing, P.R. China
Xiong Yanian, Zhujiang Newtown, Guangzhou, P.R. China
Young, Stephanie Lynne, Chalfont St. Peter, Buckinghamshire
Yu-Han Chen, Taipei, Taiwan, R.O. China

Qualified with Merit
Chai Yuet, Viola, Taikoo Shing, Hong Kong
Dimitrakopoulos, Charalabos, Athens, Greece
Hong Jun Chen, Beijing, P.R. China
Horn, Chandra Leah, Montreal, Quebec, Canada
Ip King Lun, Howard, Kowloon, Hong Kong

Li Dongsheng, David, Guilin, Guangxi, P.R. China
Lilley, Samantha, Hanwell, London
Lin Yu Chi, Taipei, Taiwan, R.O. China
Mengying Luo, Guangzhou, Guangdong, P.R. China
Miao Yu, Chengdu, Sichuan, P.R. China
Mitchell, Shirley D., Windsor, Berkshire
Preston, Paula, Blackheath, London
Qiushi Cui, Xuzhou, Jiangsu, P.R. China
Sanders, Jacqueline, Towcester, Northamptonshire
Tang Sheung Mei, Dominic, Kowloon, Hong Kong
Thomas, Jade, London
Wan Sai Man, New Territories, Hong Kong
Welsh, Simon Ian, Erdington, West Midlands
Xue Long Li, Beijing, P.R. China
Yee Man Mak, New Territories, Hong Kong

Qualified
Amrit, Paveet, Northolt, Middlesex
Asplund, Jan Olof, Kiruna, Norrbotten, Sweden
Chan Bik Ki, Icarus, Kowloon, Hong Kong
Chan Ka Yee, Carrie, Stanley, Hong Kong
Chang Hsiao Huei, Westmount, Quebec, Canada
Chong Yim Mui, Cristy, Tseung Kwan O, Hong Kong
Cote, Angela Marie, London
Delerholm, Peter, Enskede, Sweden
Dowding, Lucy Jane, St Andrews, Fife
Evans, Charles I., London
Fong Kwok Shui, Charlotte, Southgate, London
Fu Han Yao, Glasgow, Lanarkshire
Gong Ying, Yujiashan, Wuhan, P.R. China
Graham, Lisa J., Tunbridge Wells, Kent

Proceedings of the Gemmological Association of Great Britain and Notices

Hell, Martine Svitlana, Hedalen, Norway
Huang Shih-Jung, Taipei, Taiwan, R.O. China
Jeon Seon Yeong, London
Jinglin Wang, Hubei, Wuhan, P.R. China
Kong Wai San, Nw Territories, Hong Kong
Kwan Shingyan, Zhujiang Newtown, Guangzhou, P.R. China
Kwok Wing Hong, Kowloon, Hong Kong
Lai May Wah, Kennedy Town, Hong Kong
Lam Pui Kwan, Kowloon, Hong Kong
Lam Ting Yan, New Territories, Hong Kong
Lau Wai Keung, Leslie, New Territories, Hong Kong
Leung Suet Kuen, Lam Tin, Hong Kong
Li Han Geng, Beijing, P.R. China
Li Yuen, Hong Kong
Liu Wing Chi, New Territories, Hong Kong
Lui Ah Wing, Joyce, New Territories, Hong Kong
Luo Hong, Shihezi, Xinjiang Province, P.R. China
McNiven, Adrian, West Kensington, London
Mei Sze Wong, Hang Hau, Hong Kong
Mohammad, Aamir, Oldham, Lancashire
Mok Yan Yan, Nadia, Kowloon, Hong Kong
Naito, Ayako, Taito-ku, Tokyo, Japan

Partner, Robert Leslie, Cropston, Leicestershire
Partridge, Jennifer Anne, Plymouth, Devon
Poon Pak Kei, New Territories, Hong Kong
Redmond, Sarah, Weybridge, Surrey
Reynolds, Eva, Cheltenham, Gloucestershire
Sahni, Harcharan Singh, Stourbridge, West Midlands
Segurado, Taynara Leao, Glasgow, Lanarkshire
Share, Rebecca Louise, Kingswinford, West Midlands
Spenser, Sarah, London
Tse Ping, New Territories, Hong Kong
Tsui Yu Ying, Loretta, North Point, Hong Kong
Walas, Monika Magdalena, London
Wall, Jonathan Martin, Stourbridge, West Midlands
Wang Hao Shi, Beijing, P.R. China
Watson, James Alexander, Northwood, Middlesex
Wong Chiu Yung, Belinda, Kowloon, Hong Kong
Wong Chun, Jordan, Hong Kong
Xu Lingna, Zhujiang Newtown, Guangzhou, P.R. China
Yee Man Yuen, Ma On Shan, Hong Kong
Zaleszczyk, Alicja, London
Zeng Yuhua, Paty, Zhujiang Newtown, Guangzhou, P.R. China

Membership

During 2010, the Council approved the election to Membership of the following:

Fellowship and Diamond Membership (FGA DGA)
Ho Yue Yau, Tsuen Wan, Hong Kong. 2010/2007
Lee Wai Yin, Kitty, Hong Kong. 2010/2008
McNiven, Adrian, West Kensington, London. 2010/2010
Partridge, Jennifer Anne, Plymouth, Devon. 2008/2010
Tidd, Lauren Elizabeth, Birmingham, West Midlands. 2009/2008

Fellowship
Aboosalih, Najeema Shahin, Colombo, Sri Lanka. 2009,
Aderhold, Bryan C., Ridgewood, New Jersey, U.S.A. 2010
Andrianarimanana, Maminirina, Antananarivo, Madagascar. 2005
Arentsen, Ernst, Noordwolde, The Netherlands. 1999
Berezovsky, Florence Paulette Marie, Zurich, Switzerland. 2010
Blagg, Natalie, London. 2009
Brown, Sandra Jane, Birmingham, West Midlands. 2010
Cederholm, Jenny, Farsta, Sweden. 2010
Cederferm, Magdalena, Märsta, Sigtuna, Sweden. 2010

Chatagnier, Pierre Yves, Vareilles, France. 2010
Chatzipanagiotou, Ioannis Tzannis, Athens, Greece. 2010
Chen Shifeng, Beijing, P.R. China. 2010
Close, Helen Selby, North Yorkshire.1996
Davis, Natasha, Northwood, Middlesex. 2010
De Gaetano, Antonella, Genoa, Italy. 2010
Dimitrakopoulos, Charalabos, Athens, Greece. 2010
Duraffourg, Valerie, Belle Fontaine, France. 2010
Falah, Jamal, Concord West, New South Wales, Australia. 2010
Gokani, Anooj, Leicester. 2010
Gowans-Poli, Julie, London. 2010
Guenin, Nathalie, Sainte Foy, Quebec, Canada. 2010
Harnois, Dominique Marie, Paris, France. 2010
Hart, Alan D., Beckenham, Kent. 2010
Joannou, Christina Maria, Ilford, Essex. 2010
Lau King Suen, Shau Kei Wan, Hong Kong. 2010
Lee Ka Chun, New Territories, Hong Kong. 2010
Liu Sui Chung, New Territories, Hong Kong. 2010
Lo Wai Yee Bibian, New Territories, Hong Kong. 2010
Loke Hui Ying, Singapore. 2009
Lovering, Paula, Central Otago, New Zealand. 1985,
Luo, Helen Rong, North York, Ontario, Canada. 2010
Lynch, Anne Lynette, Nundah, Queensland, Australia. 2010

Proceedings of the Gemmological Association of Great Britain and Notices

McKeown, Julia, Oldbury, West Midlands. 2010
Man, Camus, Sai Wing Yuen Long, Hong Kong. 2009
Manuelli, Piero Alberto, Genoa, Italy. 2010
Masselot, Joelle, Geneva, Switzerland. 2010
Matthews, Emma, Sunninghill, Berkshire. 2010
Mohammad, Aamir, Oldham, Lancashire. 2010
Mulrooney, Rosalyn, London. 2010
Ng Fei Yeung, Kowloon, Hong Kong. 2010
Ngao Mei Wan, New Territories, Hong Kong. 2010
Nicolai, Namaste, Cardiff, Glamorgan. 2010
O'Cock, Sabrina Alice Palmer, London. 2010
Palo, Markus Karl, Malmberget Sweden. 2010
Po Pui Chun, Tuen Mun, Hong Kong. 2010
Than Tin Kyaw, Yangon, Myanmar. 1997
Thomas, Ian William, Chermside West, Queensland, Australia. 1978
Tissa, V.G. Samith Madhawa, Colombo, Sri Lanka. 2009
Walters, George, London. 1964
Wang Jingyuan, Shenzhen, Guandong, P.R. China. 2010
Westley, Penny, Hagley, Worcestershire. 2010
Woolgar, Michael, Gillits, South Africa. 1971
Xu Zhao, Richmond, British Columbia, Canada. 2009
Zaleszczyk, Alicja, London. 2008

Diamond Membership (DGA)

Chan Ka Yee, Carrie, Stanley, Hong Kong. 2010
Haymes, Richard, Caterham, Surrey. 2009
Kwok Wing Hong, Kowloon, Hong Kong. 2010
Leung Suet Kuen, Lam Tin, Hong Kong. 2010
Poon Pak Kei, New Territories, Hong Kong. 2010
Tachiveyi, Brian, Birmingham, West Midlands. 2009
Wan Sai Man, New Territories, Hong Kong. 2010
Wong Chun, Jordan, Hong Kong. 2010

Associate Membership

Acharya, Rakesh, Bickley, Kent
Adcock, Kathryn, Wimborne, Dorset
Akester, Penelope, London
Algie, Joanne, Auckland, New Zealand
Alsvold-Torndahl, Rebecca, Skanor, Sweden
Antonucci, Andrea, Stockholm, Sweden
Arredondo, David, Geneva, Switzerland
Atkova, Atkova, London
Brianceau, Boris, Saint-Julien, France
Chambers, Ann, Cranbrook, Kent
Clutterbuck, Guy, London
Coldham, Terrence Stewart, Sydney, New South Wales, Australia
Conrey, Keith, Evergreen, Colorado, U.S.A.
Dudun, Svetlana, Dagenham, Essex
Duncan, Colleen, Aberdeen
Elliott, Paul, Woodville, South Australia, Australia
Elliott, Yvonne, London
Field, Stephen, Beckenham, Kent

Finn, Emma, Singapore
Gadsdon, Corin, Truro, Cornwall
Gibson, Antonia, Stockholm, Sweden
Godfroy, Ariane, London.
Goldhill, Richard, Bushey Heath, Hertfordshire
Hammerstein, Quirine, Geneva, Switzerland
Healy, Marilyn, Grange, Queensland, Australia
Hutchinson, Fiona, Albourne, West Sussex
Ikeuchi, Mototeru, Edogawa-ku, Tokyo, Japan
Jian-Zibaee, Shadi, London
Kalvig, Per, Copenhagen, Denmark
Keiko, Kamijima, Nishi-Tokyo City, Tokyo, Japan
Kendirci, Rebecca, Stone, Staffordshire
Kikkawa, Tomomi, Kofu City, Yamanashi Pref., Japan
Knutsen, Annmari Ellilia, Oslo, Norway
Kon, Keiko, Taito-ku, Tokyo, Japan
Konishi Mika, Kawasaki City, Kanagawa Pref., Japan
Kotsatos, Kristi, Houston, Texas, U.S.A.
Kruger, Louise, London
Lally, Joanne Claire, Southampton, Hampshire
Leblanc, Delphine, Hoboken New Jersey, U.S.A.
Lee, Jeffrey, Totnes, Devon
Lemeshkro, Natalie, London
Li, Richard, Taoyuan, Taiwan, R.O. China
McCallum, Neil Keith, Martinborough, New Zealand
McIntyre, Andrew, New South Wales, Australia
Maiko, Kawasaki, Yamanashi Pref., Japan
Mariko, Murakami, Osaka City, Osaka, Japan
Millen, Laura, North Chailey, East Sussex
Mousavi Pak, Niloofar, Tehran, Iran
Newlands, Sarajane, Bickley, Kent
O'Sullivan, Lauren, Glenside, Pennsylvania, U.S.A.
Palmieri, Donald A., New York, U.S.A.
Parkinson, Janine, Cambridge
Pimlott, Sandra, Adelaide, South Australia, Australia
Pradat, Thierry, Francheville, France
Quaintance, Katherine, Birmingham, West Midlands
Rambaran, David, Palm Springs, California, U.S.A.
Ratnayake, Dayanthi, Colombo, Sri Lanka
Roditi, David, London
Rust, Brigitte, Bonn, Germany
Seaman, Laura, Rugby, Warwickshire
Seto, Kuriko Setagaya-ku, Tokyo, Japan
Shavdia, Praful, Northwood, Middlesex,
Smith, Billy, Colchester Essex
Smith, Christopher P., New York, U.S.A.
Smith, Stephen Gibson, Newcastle upon Tyne, Tyne and Wear
Sørensen, René, Vibourg, Denmark
Staruch, Barbara, New Malden, Surrey
Sundheim, Jennifer, Southampton, Hampshire
Tew, Timothy David, Atlanta, Georgia, U.S.A.
Torretta, Janice, Glen Spey, New York, U.S.A.

Proceedings of the Gemmological Association of Great Britain and Notices

Van Der Wolf, Nicole, Dublin, Republic of Ireland
Van Molendorff, Steffan, Woking, Surrey
Verwijk, Moira, Toronto, Ontario, Canada
Webb, Linda, Staines, Hertfordshire
White, Margot, Nailsworth, Gloucestershire
Winski, Jacqueline, Dunfermline, Fife
Woodrow, Gillian, Wokingham, Berkshire
Yanase Tomohiro Toyota-City, Aichi Pref., Japan
Yoshio, Kinoshita, Osaka City, Osaka, Japan
Yukiko, Horie, Chofu City, Tokyo, Japan

Gold Corporate Membership

Anchorcert, Birmingham, West Midlands
Aubrey Gems Ltd., Tunbridge Wells, Kent
Bentley & Skinner, London
Blacklock Jewellery, Durham
Borro Ltd, Oxford
Bramwells Jewellers, Durham
Brufords of Exeter Ltd, Exeter, Devon
Chamade Antiques, London
Davidsons the Jewellers Ltd, Newcastle upon Tyne, Tyne and Wear
Denhams (Leicester) Ltd, Leicester
Fraser Hart Ltd, Borehamwood, Hertfordshire
F. Hinds, Uxbridge
R. Holt & Co. Ltd, London
Lucas Rarities Ltd, London
MacIntyres of Edinburgh, Edinburgh
Onecaratonline Ltd., Orpington, Kent,
Pravin A Pattni Ltd t/a Minar Jewellers, London
David Richards Jewellers Ltd., Ruddington, Notts., Nottinghamshire
Safeguard Quality Assurance Ltd, Birmingham, West Midlands
Searle & Co Ltd., London
John Taylor FGA DGA FNAG, Chislehurst, Kent
A.E. Ward & Son, London
G.F. Williams & Co., London

Corporate Membership

Pearl Magpie, London
Sarajane Newlands, Bickley, Kent
L. & G. Webb Gemstones, Staines, Surrey

Transfers

Associate Membership to Fellowship (FGA)

Borenstein, Guy, Pardes-hana Karkur, Israel. 2010
Bright, David, Riverside, Missouri, U.S.A. 2010
Burland, Mary Ann, London
Evans, Charles I., London. 2010
Evans, Daniel Raymond, Brisbane, Queensland, Australia. 2010
Fox, Karen Elizabeth, Toronto, Ontario, Canada. 2010

Graham, Lisa J., Tunbridge Wells, Kent. 2010
Hell, Martine Svitlana, Hedalen, Norway. 2010
Kapoor, Kushagra, New Delhi, India. 2010
Michaelides, Emma, Enfield, Middlesex. 2010
Nichol, Douglas, Wrexham, North Wales
Paige Anderson, Denise, London. 2010
Pradat, Thierry, Francheville, France. 2010
Smith, Christopher P., New York
Trolle, Natascha, Copenhagen, Denmark. 2010
Wetherall, Alan, Hitchin, Hertfordshire. 2010
Wong, Phyllis, London. 2010

Associate Membership to Diamond Membership (DGA)

Delerholm, Peter, Enskede, Sweden. 2010
Huang Shih-Jung, Taipei, Taiwan. R.O. China. 2010
Mitchell, Shirley D., Windsor, Berkshire. 2010
Norris, Eddi, London. 2010
Segurado, Taynara Leao, Glasgow, Lanarkshire. 2010

Fellowship to Fellowship and Diamond Membership (FGA DGA)

Amrit, Paveet, Northolt, Middlesex. 2010
Blagg, Natalie, London. 2010
Chang Hsiao Huei, Westmount, Quebec, Canada. 2010
Chatzipanagiotou, Ioannis Tzannis, Athens, Greece. 2010
Chrismas, Jacqueline, Godalming, Surrey. 2010
Dimitrakopoulos, Charalabos, Athens, Greece. 2010
Evans, Charles I., London. 2010
Graham, Lisa J., Tunbridge Wells, Kent. 2010
Hell, Martine Svitlana, Hedalen, Norway. 2010
Horn, Chandra Leah, Montreal, Quebec, Canada. 2010
Li Dongsheng, David, Guilin, Guangxi, P.R. China. 2010
Lilley, Samantha, Hanwell, London. 2010
Mohammad, Aamir, Oldham, Lancashire. 2010
Naito, Ayako, Taito-ku, Tokyo, Japan. 2010
Partner, Robert Leslie, Cropston, Leicestershire. 2010
Poore, Sarah, Worthing, West Sussex. 2010
Preston, Paula, Blackheath, London. 2010
Sanders, Jacqueline, Towcester, Northamptonshire. 2010
Share, Rebecca Louise, Kingswinford, West Midlands. 2010
Tyrrell, Siobhan Ann, Walthamstow, London. 2010
Watson, John Richard, Berkhamsted, Hertfordshire. 2010
Woo Ka Yin, Agnes, Kowloon Bay, Hong Kong. 2010
Young, Stephanie Lynne, Chalfont St. Peter, Buckinghamshire. 2010
Zaleszczyk, Alicja, London. 2010

Diamond Membership to Fellowship and Diamond Membership (FGA DGA)

Huijbrechts, Thomas N., Schoorl, The Netherlands. 2010/2007
Lai Siu Kwong, New Territories, Hong Kong. 2010/2005

Proceedings of the Gemmological Association of Great Britain and Notices

Gifts and Donations to the Association

The Association is most grateful to the following for their gifts and donations for research and teaching purposes:

Asia Gems, London, for a selection of cut gemstones.

Maggie Campbell Pedersen FGA, London, for *Amber views opinions*, a copy of the *Bilingual Newsletter of the International Amber Association* and pieces of natural and dyed bamboo coral.

Marijan Dundek, Noble Gems International, London, for his book *Diamonds*.

Gemmological Instruments Ltd, London, for copies of *Exotic Gems* by R. Newman, *Ruby, Sapphire and Emerald Buying Guide* by R. Newman, *Diamond Cuts in Historic Jewellery* by H. Tillander and *Photoatlas of Inclusions in Gemstones* Volume 3 by E. Gubelin and J.I. Koivula.

Steven L. Jordan FGA DGA, Biggleswade, Bedfordshire, for a selection of synthetic gemstones.

Cynthia Mendis FGA DGA, Ottawa, Canada for a selection of diamond simulants and a sample of synthetic diamond grit.

Damian J. Miles, Okehampton, Devon, for 20 sillimanite cat's-eyes.

Pravins, London, for a large selection of gem material.

Jean-Claude Rufli FGA and Lisbet Rufli FGA, Swedish Gemmological Association, Stockholm, Sweden, for cut samples of synthetic rutile and YAG.

Helen Serras-Herman MFA FGA, Rio Rico, Arizona, U.S.A., for sapphire crystals from Philipsburg, Montana, pieces of tumbled polished turquoise, a string of tumbled 'sugarcane' emerald from Brazil, two copies of *Cameos Old and New* and a signed copy of *Phenomenal Gems* by Fred and Charlotte Ward

Trevor Simson, Abingdon, Oxfordshire, for two pieces of lead glass filled ruby.

Thomson Gems, London, for selections of opals and cultured pearls.

Jason Williams, G.F. Williams, London, for a selection of cut stones including rubies and sapphires.
.

Monetary donations were gratefully received from:

Raed Mustafa Al-Hadad FGA, Abu Dhabi, U.A.E.
Vincenzo De Michele, Milan, Italy
Masao Kaneko FGA, Tokyo, Japan
Edward F.G. Nealon, Perth, Western Australia
Ng Mei Hang DGA, Hong Kong
Robert L. Rosenblatt FGA, Salt Lake City, Utah, U.S.A.
Moe Moe Shwe FGA, Singapore
Paul Louis Siegel FGA, Rocky Point, New York, U.S.A.
Nancy Warshow FGA DGA, Nairobi, Kenya

Special thanks go to **Professor Johnny Lu,** Founder of the Jewelry institute of America, New York, U.S.A., for a substantial contribution towards the cost of Chinese translation of the Gem-A Gemmology course notes.

Annual General Meeting

The Annual General Meeting was held during International Jewellery London in The Whitehall Room, Earls Court 2, London W14 8UX, on Sunday 5 September 2010. The meeting was chaired by James Riley the Chairman of the Council. The Annual Report and Accounts were approved. James Riley was re-elected and Richard Slater and Landy Palmer elected to serve on the Council. Jason Williams retired from the Council in rotation and did not seek re-election; Evelyne Stern resigned. Peter Dwyer-Hickey was re-elected to serve on the Membership Liaison Committee. Hazlems Fenton were re-appointed as auditors for the year.

Subscriptions 2011

The membership subscriptions for 2011 are £90.00 for UK members and £95 for those in Europe and overseas. re-appointed as auditors for the year.

Proceedings of the Gemmological Association of Great Britain and Notices

Obituary

Dr Kurt Nassau
(1927–2010)

It is with deep sadness that we record the death of Dr Kurt Nassau who died on 18 December 2010. Born in Austria in 1927, Dr Nassau was educated in England gaining BSc Hons in Chemistry and Physics at the University of Bristol. He served in the US army as a medical researcher at Walter Reed hospital before earning a PhD in Physical Chemistry from the University of Pittsburgh.

In 1959 Dr Nassau joined AT&T Bell Laboratories at Murray Hill, New Jersey, where he earned a worldwide reputation for his research in crystal growth and structure. He retired as Distinguished Research Scientist in 1989.

Dr Nassau was awarded an Honorary Fellowship of the Gemmological Association of Great Britain in 1992 in recognition of his extensive contributions to understanding in the field of gemmology.

Dr Nassau was predeceased by his wife, Julia.

Remembrances

Many members posted tributes and shared their memories of Dr Nassau on Gem-A's MailTalk. Following is a selection of those received.

Dr Nassau was a good friend who always exhibited to a marked degree the true spirit of hospitality and generosity. I was fortunate enough to experience this first hand when I met him in 1976.

Kurt was my host for several days both at his home and in his workplace at the Bell Research Laboratories, Murray Hills, New Jersey. It was an unbelievable privilege to have him introduce me to the Bell research teams and show me through the extensive facilities. He explained and demonstrated many aspects of their ongoing solid state research. He also allowed me to examine numerous synthesized crystals, many of them unique at that time, together with an extensive collection of stones that had been faceted from these materials.

Farewell Kurt, you will be sadly missed.

Arthur Thomas FGA, Gauteng, South Africa

Kurt Nassau was such a knowledgeable man and so willing to share that knowledge. He was a good friend of my dad [Antonio Bonanno], and one of the few people with whom I could share stories — he shared some wonderful anecdotes with me after dad's death … Kurt Nassau's death is another tragic loss.

With great sadness.

Antoinette Matlins, Woodstock, VT, USA

Though I didn't know Dr Nassau personally, I still feel a great loss. His work touched so many people I am sure; I for one appreciated his patient correspondence a few years ago with regard to the Usambara effect and colour-change — I wished I had kept up that correspondence, but got too busy and now that connection is lost. I am sitting here at work now, staring at his books on my desk and contemplating some of the dedications within — always to his wife Julia: "...Love is not love, which alters when it alteration finds" (William Shakespeare) and another: "For all knowledge and wonder (which is the seed of knowledge) is an impression of pleasure in itself" (Francis Bacon). In our own work, Dr Bassett and I very frequently refer to his text *The Physics and Chemistry of Color* and I often steer interested people to that wonderful book or the short version published in the *American Mineralogist,* 1978, **63**, 219-29 (www.minsocam.org/msa/collectors_corner/arc/color.htm). The answers to things we thought we might ask him sometime are probably somewhere in there or his many papers — what a great legacy.

Elise Skalwold FGA, Ithaca, New York, USA

Proceedings of the Gemmological Association of Great Britain and Notices

George Harrison Jones
(1924–2010)

George was born in Liverpool, educated at Liverpool Collegiate School and went on to Liverpool University to gain a first degree in chemistry. He then worked for a chemical company whilst studying as an external student for his doctorate in organic chemistry, which he was awarded in 1949. He then joined the staff of Mars Ltd, the confectioners, as a chemist. Early in his career at Mars, the then Government offered scholarships to promising young scientists/engineers to study in America (and encouraged by Mars to take up this offer) George spent nearly two years at Cornell University studying the 'technical aspects of manufacturing operations'. He returned to Mars and spent the rest of his career with the firm, retiring at managerial level in 1982.

George's interest in gemmology blossomed in the 1960s, and he gained his FGA (with distinction) in 1970. However he was a practical man and he became known to the British gemmological fraternity as a consummate lapidary. He excelled in cutting gemstones, usually finished with his distinctive faceted girdles. He also fashioned cabochons, including a magnificent suite of jade-like scapolites from remote localities in the Shetlands discovered by British Geological Survey geologists. His lapidary skills extended to the fashioning of table coasters from fossilized palm wood to producing spheres of rocks and minerals on a rig of his own design. He also produced optical components for a firm of gemmological instrument makers. These tasks were a labour of love – he never sought nor expected financial reward.

George gave yeoman service to the Gemmological Association. He was appointed as an examiner for the FGA diploma in 1975 and became Chief Examiner in 1993, retiring in 1999. He was a major player in the revision of the course notes for the FGA diploma in the 1980s. George supported the Association Education staff greatly with his painstaking attention to detail, great scientific integrity and wonderful dry sense of humour.

As a boy he always had a sense of community and he joined the Boy Scouts in his early teens. He was appointed a District Commissioner for the movement in the 1960s. He was a keen gardener, but ill health forced him to give up both gardening and his beloved lapidary hobby.

George is survived by his wife Anne whom he married in 1947. They had three children Nigel, Rosamund and Diana, but tragically Nigel died from pneumonia at the early age of sixteen. They have two grandchildren.

E. Alan Jobbins

Deidre Kay Alejo FGA (D.1990), Central, Hong Kong, died on 22 April 2010.

Norman H. Harding FGA (D.1934 with Distinction), Haywards Heath, West Sussex, died on 14 December 2009.

Sylvia Gwendoline Hyde FGA (D.1950), Tixover, Stamford, Lincolnshire, died in June 2010 aged 88. Mrs Hyde was the winner of the Rayner Prize in the Preliminary Gemmology Examinations in 1949.

Raymond George Lee FGA (D.1962), Torquay, Devon, died in 2010.

Thea McDonald FGA (D.1949 with Distinction), Edinburgh, Lothian, died in 2010.

Anthony William Round FGA (D.1975), Ewell, Surrey, died in 2010.

Carol Anne Lesley Saxton FGA DGA (D. 1993 with Distinction), Alton, Hampshire, died on 27 February 2010.

Daniel Taylor FGA DGA (D.2005), Leeds, Yorkshire, died in 2010.

Wilhelm Jacobus E. Van Deijl FGA (D.1969), Bellville, South Africa, died in 2010.

Patricia Joan Walker FGA DGA (D.1969), London, died in 2010.

Lizanne Welch FGA (D.1991), Taunton, Somerset, died in 2010.

Gem-A

THE GEMMOLOGICAL ASSOCIATION OF GREAT BRITAIN

Supercharge your career

Open Distance Learning Courses in Gemmology enrolling now

A strong knowledge of gemstones and diamonds will increase customer confidence and boost your sales. Gain that knowledge by studying with the world's longest established educator in gemmology. Graduates may apply for Fellowship of the Association enabling them to use the initials FGA after their name.

Study gemmology from your own home or workplace with comprehensive course notes, and online coursework and study groups*. You will also receive a selection of instruments and stones to help you with your studies. Additional instruments and books can be purchased from Gem-A's extensive range.

* Access to a computer with an internet connection essential.

Foundation Certificate in Gemmology
Start dates: 2 August 2011 (six-month programme) and 5 September 2011 (nine-month programme)
Course fees: £1725 (or £1995 to include the London three-day practical workshop) payable in instalments

Diploma in Gemmology (open only to Foundation Certificate holders)
Start date: 12 September 2011 (nine-month programme)
Course fees: £1925 (or £2495 to include the London five-day practical workshop) payable in instalments

Full details at **www.gem-a.com/education.aspx** or call 020 7404 3334

The Gemmological Association of Great Britain
27 Greville Street (Saffron Hill entrance), London EC1N 8TN
tel: 020 7404 3334 fax: 020 7404 8843 email: information@gem-a.com
UK Registered Charity No. 1109555

Contents

Cover Picture: Alexandrite trillings from the Ural mountains, which form part of the Koksharov collection at the Natural History Museum, London. The faces are labelled with Miller indices in different colours, allowing twinning and twin boundaries to be easily recognized. The samples measure approximately 3.5 x 4.5 cm (top) and 6.5 x 6.5 cm (the two photographs below, which give different views of the same stone). The photographs were taken by Karl Schmetzer during a visit to the Natural History Museum and are featured on page 60 of his book *Russian Alexandrites*. (See book review by Alan Hart of the Natural History Museum of *Russian Alexandrites* by Karl Schmetzer, page 113.) Courtesy of Schweizerbart Science Publishers, Stuttgart, Germany, www.schweizerbart.de/9783510652624

The Gemmological Association of Great Britain